Characterization of Aluminium and its Alloys by means of Analysis of passive, pitting and galvanic Behaviour in Contact with CFRP by Electrochemical Noise and Polarization Methods

Dissertation

zur Erlangung des akademischen Grades

Dr. rer. nat.

eingereicht an der

Mathematisch-Naturwissenschaftlich-Technischen Fakultät

der Universität Augsburg

von

Oruethai Jaiboon

Augsburg, Dezember 2014

Erstgutachter: Prof. Dr. Siegfried R. Horn

Zweitgutachter: Prof. Dr. Armin Reller

Tag der müdlichen Prüfung: 18.02.2015

TABLE OF CONTENTS

Chapter I: Introduction..... 1

Chapter II: Literature Review..... 4

Chapter III: Theoretical Background..... 17

Chapter IV: Experimental Set-ups and Results..... 38

1. Electrochemical Noise (EN) Measurement..... 38
   - 1.1) Noise behaviour of Al with Al reference electrode..... 38
   - 1.2) Noise behaviour of Al with NiO (oxidised wire) reference electrode..... 48
   - 1.3) Noise behaviour of NiO (oxidised wire) with C reference electrode..... 52
   - 1.4) NiO (oxidised wire) reference electrode testing 55
   - 1.5) Effect of surface area on noise behaviour of pure aluminium 57
   - 1.6) Time evolution of noise behaviour in long term measurement..... 61
   - 1.7) Noise behaviour of aluminium alloys..... 65
   - 1.8) Galvanic behaviour of aluminium partially sputtered with carbon..... 71
   - 1.9) Galvanic behaviour of aluminium with sputtered with gold 74
   - 1.10) Noise behaviour of aluminium when coupled with graphite in deionised water..... 79
   - 1.11) Noise behaviour of aluminium when coupled with graphite in NaCl solution..... 82
   - 1.12) Effect of surface area ratio on galvanic behaviour..... 87
2. Open circuit potential (OCP) and Polarization Measurement..... 89
   - 2.1) Pitting behaviour of pure aluminium when coupled with Cu or CFRP..... 89
   - 2.2) Scan rate testing..... 92
   - 2.3) Characterising aluminium oxide surface by Tafel slope analysing..... 94
   - 2.4) Scan rate testing: Comparison with commonly used scan rate of 600mV/h..... 95
   - 2.5) Long term passivation..... 99
   - 2.6) Passive behaviour: Effect of spontaneous oxide film..... 100
   - 2.7) Passive behaviour: Different surface treatments..... 102
   - 2.8) Passive behaviour: Time dependent activation..... 106
   - 2.9) Passive behaviour: Quality of passive layer..... 107
   - 2.10) Passive behaviour: Oxygen concentration in solution..... 109
   - 2.11) Pitting behaviour in NaOH (pH 12)..... 111
   - 2.12) Pitting behaviour in H_2O (pH 7)..... 115
   - 2.13) Dynamic current signal on constant anodic polarization in pitting and non-pitting regions..... 118
   - 2.14) Pitting behaviour in pure tap water..... 121

2.15) Effect of aeration on active/passive behaviour 122
2.16) Pitting behaviour in low NaCl concentration range..... 124
2.17) Pitting behaviour in HCl..... 128
2.18) Pitting behaviour: Effect of pH value and chloride concentration 132
2.19) Corrosion behaviour in Nitric acid (HNO_3)..... 135
2.20) Pitting behaviour in acidic chloride solution..... 137
2.21) Pitting behaviour in basic chloride solution..... 141
2.22) Comparison of activation process in different solutions..... 146
2.23) Pitting behaviour: Effect of surface finish in NaCl solution..... 148
2.24) Passive behaviour: Effect of surface finish in deionised water..... 151
2.25) Evolution of oxide film surface: Effect of surface finish in NaCl..... 153
2.26) Evolution of corrosion behaviour with time of pure aluminium in NaCl solution..... 154
2.27) Comparing passive layer: growing in water and modified in NaCl solution..... 157
2.28) Passive behaviour of aluminium alloys in deionised water..... 160
2.29) Pitting behaviour of aluminium alloys in NaCl solution..... 161
2.30) Electrochemical behaviour of CFRP in NaCl solution..... 169
2.31) Galvanic behaviour of aluminium alloys coupled with CFRP in NaCl solution..... 171
2.32) Galvanic behaviour: Effect of surface area ratio..... 181
2.33) Galvanic behaviour: Effect of solution's pH..... 182
3. Surface Analysis..... 188
3.1) Surface Morphology of Aluminium/CFRP joints after long time immersion..... 188

Chapter V: Discussion..... 194

Chapter VI: Conclusion..... 205

Appendix: Measurement table..... 208

Reference..... 216

Acknowledgement..... 220

Curriculum Vitae..... 221

CHAPTER I

INTRODUCTION

The recent trend in structural component for automotive and aerospace applications is aimed to improve weight saving since the structural weight has significant effect on their performance and fuel consumption. In order to achieve the weight saving, the lightweight material is needed for structural components. Moreover, the safety requirement must also be preserved while minimizing the weight of structural components. Therefore, material with high specific strength is required for high performance structure [1, 2].

Aluminium and carbon fibre reinforced polymer (CFRP) are competing materials for lightweight structural applications. Both materials have their own advantages and disadvantages. Aluminium is lightweight and ductile but poor fatigue strength while CFRP exhibits high strength and stiffness to weight ratio but poor impact and residual strength. Therefore the idea of combination of these two materials forming hybrid structural materials was born. This hybrid material consists of fibre reinforced composite (e.g., CFRP) bonded with metal (e.g., aluminium). For this hybrid material, the key advantages of each material are combined while their disadvantages are avoided. This hybrid material possesses excellent fatigue, impact and residual strength characteristics and also exhibit high specific strength and stiffness. Therefore this hybrid material is increasingly used in high performance structures [3-5].

In practical aerospace and automotive applications, the hybrid material of Aluminium/CFRP joint is exposed to a variety of environments such as deicing fluid, salt spray, urine and etc.,. The exposure leads to the change in durability and mechanical properties of this hybrid joint. The changes are the result of degradation of CFRP and corrosion of aluminium [6, 7]. Therefore the utilization of Aluminium/CFRP joint requires additional consideration to ensure its long term performance during exposure to environment. It was found that fibre reinforced polymer (FRP) material typically exhibits excellent corrosion resistance and chemical attack [8]. However, aluminium may be influenced by long term exposure to aggressive environment, thus corrosion of aluminium is one of the major factors affecting long term service ability of the hybrid material.

Aluminium usually possesses excellent corrosion resistance because it forms a thin, compact passive oxide film on its surface. However, when exposed to an aggressive environment such as chloride ions-containing solutions, pure aluminium and aluminium alloys are attacked by localised corrosion especially pitting corrosion due to the local breakdown of passive oxide film by the aggressive anions [9, 10]. The corrosion behaviour of pure aluminium and aluminium alloys in solution depends on several parameters such as solution condition (pH, type and concentration of aggressive anions, concentration of oxygen etc.) and structure and composition of oxide layer, which are influenced by mechanical and heat treatment, on aluminium surface [11].

A major concern regarding the use of this hybrid material is the possibility of galvanic corrosion between aluminium and carbon of CFRP. As carbon fibre is very noble and aluminium is a very active anodic metal, galvanic coupling is possibly formed when aluminium is in electrical contact with carbon in the presence of electrolyte. If the galvanic coupling takes place, uniform galvanic corrosion of aluminium may occur. Therefore, current can flow from anodic metal (e.g., aluminium) to cathodic material (e.g., carbon fibre). This means carbon fibre of CFRP is protected while aluminium suffers greater corrosion with increasing rate [8]. Moreover, the combination of CFRP to aluminium may also significantly change the corrosion behaviour of aluminium due to the difference in physical and chemical properties between aluminium and CFRP [7, 12]. Therefore the ability to detect the corrosion of aluminium component of this hybrid material would greatly increase the confidence in the use of this high performance structure.

Although corrosion of aluminium has been widely analysed by electrochemical techniques, there is only a little bit attention toward corrosion of Aluminium/CFRP joint. Therefore the main objective of this research is to investigate the possibility of the use of electrochemical methods to study the corrosion behaviour of hybrid Aluminium/CFRP joints. The electrochemical methods used in this research include the electrochemical noise (EN), the open circuit potential (OCP) and the potentiodynamic polarization measurements. In order to discuss corrosion behaviour of hybrid Aluminium/CFRP joint, the electrochemical behaviour (active, passive and pitting behaviour) of aluminium need to be understood first. Therefore the first part of this research is to examine the EN behaviour of pure aluminium and aluminium alloys in chloride solution and to determine if EN measurement can be used to analyse the corrosion behaviour of

aluminium as other electrochemical methods. The analysis of EN data is mainly performed in time domain, including the noise resistance. After that the EN method is adapted to study the corrosion of pure aluminium when coupled with graphite, which is the nobler material than aluminium. The second part of this research is to study the effect of pH of solution, aeration, chloride ions concentration especially at relatively low concentrations, and surface finish on the corrosion behaviour of pure aluminium and aluminium alloys by OCP and potentiodynamic polarization measurements with relatively low scan rate. The effect of long term immersion on corrosion behaviour of pure aluminium is as well studied here using the anodic polarization curve. It is not only corrosion behaviour of aluminium that is individually studied, but also CFRP in the same solution. After that the possible use of the potentiodynamic polarization method to predict the corrosion behaviour of hybrid Aluminium/CFRP joint when immersed in solution is reported. Although NiO (oxidised wire) is not commonly used as a reference electrode, the potentials in this research are measured against NiO (oxidised wire) electrode since it is flexible for our measurement set-ups. In the last part of this research, the hybrid Aluminium/CFRP joints are fabricated and then immersed in chloride solution. After long term immersion, the surface morphologies of aluminium components are investigated under digital microscopy. In the discussion, the correlations of corrosion behaviour and corrosion parameters of aluminium metal and Aluminium/CFRP joint from different methods are discussed.

CHAPTER **II**

LITERATURE REVIEW

Zhang et al. [13] in 2007 discussed the corrosion mechanism of AZ91D (Mg, Al, Zn, Mn) magnesium alloy during immersion in alkaline 0.05M NaCl solution (pH12) in term of EN and polarization data. It was found from anodic polarization measurement that the corrosion resistance of AZ91D apparently deteriorated with immersion time and its corrosion behaviour change during immersion in solution from anodic dissolution behaviour at 200s to passive behaviour at 6.5h. For better understanding of corrosion behaviour of magnesium alloy AZ91D, EN measurement was performed. For immersion time less than 1.5h, the periodic transients of positive or negative potential noise coupled with a positive or negative current noise shift respectively were detected, this indicated that anodic dissolution undertook on surface of AZ91D. For immersion time from 1.5h to 3h, the slow transient overlapped by fast transient appeared. The fast transient was characterized as a potential drop coupled with simultaneously current rise, inferring that (metastable) pitting corrosion attacked the surface of AZ91D alloy. For the immersion time from 3h to 7h, the slow transient overlapped by fast transient on potential noise was detected while no obvious fluctuation on current noise was observed, revealing that protective film of MgH_2 was formed and localised corrosion rarely undertook on AZ91D alloy. Moreover, the analysis of EN data by means of noise resistance (R_n), power spectrum density (PSD) calculated by Fast Fourier transform(FFT) and energy distribution plot calculated by fast wavelet transform as well give the useful information about the dominant corrosion process of AZ91D alloy.

Lafront et al. [14] in 2005 studied the electrochemical evolution of localized corrosion on magnesium alloy AZ91D and AJ62X (Mg, Al, Sr, Mn) in basic NaCl solution (pH12) by Scanning reference electrode technique (SRET). The result showed that many dense pitted areas were generally observed. Theses dense pitted areas have been confirmed to associate with a short pit lifetime or metastable pits. The short lifetime of a pit gave a less depth of the pit. On the other

hand only a few classical pits are observed. These classical pits are associated with a longer pit lifetime. This suggested that the deeper pits also could exist on the surface of magnesium alloy.

Breslin et al. [15] in 2000 investigated the possibility to use the electrochemical noise analysis to study the activation of pure aluminium in an indium-containing solution. The potential and current noises of pure aluminium in acidified 0.5M NaCl solution (pH1.6) with and without 0.005M of $In_2(SO_4)_3$ were compared to study the effect of indium on corrosion behaviour of aluminium. The EN data were performed in time domain. It was found that the presence of indium accelerated the dissolution of aluminium with a greatly higher current and more electronegative potential. Much larger current fluctuations and less potential fluctuations are as well observed for aluminium in indium-containing solution. For solution in the absence of indium, the frequency of pit nucleation increased with time. On the other hand, for the solution in the presence of indium it was impossible to determine the number of individual metastable pitting events because the general-like dissolution occurred on the aluminium surface. The current peaks (I_{peak}) in the solution in the presence of indium (10μA) were considerably higher than that in solution in the absence of indium (2.5μA). The pit growth time (t_g), which was defined as the time period between the onset and the point where the current reaches maximum (I_{peak}), in the absence of indium was about 5s while in the presence of indium was about 10s. The rates of pit propagation were also calculated and it was found that the rate of pit propagation in the presence of indium was approximately two times higher than in the absence of indium. The visual examination of the surface showed that significantly larger pits were formed in the presence of indium. The noise resistance in the solution in the absence of indium was approximately 500 times higher than in the presence of indium. Moreover, the analysis of EN data in the frequency domain and spectral impedance were both consistent with that from the EN analysis in the time domain. These all results clearly showed the noise measurement, especially current noise, provided a lot of information about pitting corrosion of aluminium and the presence of indium in solution exerted an activating effect on pure aluminium.

Sasaki et al. [16] in 2004 mentioned that the corrosion behaviour of aluminium in chloride ions-containing solution are different from metastable pitting corrosion of stainless steel so that the model for metastable pitting corrosion of stainless steel cannot be applied to pitting corrosion of aluminium. At the beginning, the electrochemical transients during pitting corrosion of aluminium were similar to those of metastable pitting corrosion of stainless steel.

However there were characteristic transitions in electrochemical noise transients. After the transitions, potential and current showed vigorous fluctuation and their baselines disappeared. This indicated that the mechanisms that control the pitting corrosion process in aluminium altered after the transitions. In their study, they tried to verify pitting corrosion characteristics of aluminium in 0.05M NaCl solution by EN measurement. They found that there were 2 characteristic transitions of electrochemical noise. Before the first transition, only isolated metastable pitting events were detected on aluminium surface. The first transition took place when one pit continued to propagate, producing vigorous fluctuations in current and potential. After a pit on aluminium surface become inactivated, pitting can be reactivated at the same site. This implied that the pitting site on aluminium after first transient didn't fully repassivate, as metastable pitting of stainless steel, but remain susceptible for further activation. On the other hand, when a metastable pit on stainless steels repassivate, the site didn't reactivate again. The second transition occurred when more than one active pit propagate on the surface at the same time, causing vigorous fluctuation with relatively higher amplitude. The growing pit could supply the higher cathodic current, by hydrogen evolution reaction at the bottom of the pits, to the newly formed pit compared to passive surface. This meant that the communication between the pits was easier than with passive surface, indicating much lower polarization resistance of pits than the passive film. For the frequency domain analysis, the magnitude spectra of current transient before the first transition showed a small and smooth decay without prominent spike while after the first transition, it showed a small and continuous spikes between 0.1 and 1Hz. After the second transition, peaks at 87, 69 and 2.4mHz were observed, probably representing electrochemical interaction between the active pits. Moreover, Sasaki et al. [17] also mentioned in 2002 that the predominant anodic reaction of aluminium in 0.05M NaCl is aluminium dissolution and cathodic reactions are hydrogen reduction within the pit and oxygen reduction at the passive surface.

Cheng et al. [18] in 2003 investigated the electrochemical potential noise of pure aluminium, AA2024 (Al, Cu, Mg, Mn) and AA7075 (Al, Zn, Mg, Cu) in 3%wt NaCl solution. It could be shown that amplitude of potential noise of AA2024 was larger than AA7075 while that of pure aluminium was negligible. The EN of both AA2024 and AA5052 was attributed to the heterogeneous structure of their surface morphology because the alloying elements could form constituent particles. Every constituent particle and its vicinal matrix on the surface of AA2024 and AA7075 would form micro-galvanic corrosion cell. When micro-galvanic cell took place, the

current would flow between constituent particle (cathode) and its adjacent matrix (anode). This caused the re-distribution of electrical charge between anodic and cathodic area, therefore a fluctuation in potential (potential noise) was detected. The more the number of micro-galvanic cell, the higher the amplitude of potential noise would be. Moreover, the amplitude of potential noise of AA2024 and AA7075 decreased with immersion time, indicating the reduction of corrosion rate with immersion time. However after extremely long immersion of 38 day the potential noise's amplitude of AA2024 increased, due to the increase of micro-galvanic cell on the enlarged surface area by corrosion. Unlike heterogeneous structure of AA2024 and AA7075, the microstructure of pure aluminium was homogeneous. The pitting corrosion mechanism of pure aluminium may be the breakdown of passive film. Therefore only long term fluctuation, or low frequency of potential noise, was detected

Arrieta et al. [19] in 2004 investigated the effect of specimen's surface area on magnitude of electrochemical potential noise of aluminium alloy (AA1100, AA2024 and AA5052) in chloride ions-containing solution. It was found that a large number of events were detected from all three aluminium alloys and the individual noise event tended to follow the pattern of metastable pitting corrosion as would be mentioned in the theoretical background. The frequency of events decayed with exposure time. The magnitude of the noise events of all aluminium alloys decreased with increasing surface area. This implied the corresponding increase in interfacial admittance by increasing surface area. Moreover, this experimental result was consistent with the prediction of simplified model which assumed that the rate of random generation of similar independent pitting corrosion event was only proportional to the surface area.

Gouveia-Caridade et al. [20] in 2004 examined the influence of pH and the presence of 0.1M acetate buffer on corrosion behaviour of aluminium in 0.1M KCl solution by OCP, EN and impedance measurement. It was found from OCP measurement that immediately after immersion aluminium in solution, formation of aluminium oxide could occur on the surface in all types of solution. After that in unbuffered KCl solution (pH5.4), oxychloro complex could be formed, resulting in thinning of the oxide film before stabilisation. On the other hand, the presence of acetate ions and acetic acid molecules in buffered KCl solution with pH 5.4 and 4.3 resulted in fluctuations of OCP, which could be attributed to cycles of localised formation/dissolution of aluminium oxide. This implied that the corrosion was more uniform in

unbuffered than buffered solution. For the EN measurement, the potential and current noise in buffered solution with pH 4.3 showed much larger amplitude than in unbuffered and buffered solution with pH 5.4. Moreover, the transients of fast current rise followed by a slower recovery, which was characteristic of metastable pitting corrosion, were detected only in buffered solution with pH 4.3, meaning that metastable pitting corrosion only occur in this solution. The analysis of EN data in time domain showed that corrosion rate was lower in more acid buffered solution with pH4.3 whereas the analysis of EN data in frequency domain and impedance data showed that aluminium was faster corroded in this solution. A possible explanation for this difference was given by the presence of metastable pits, which is a localised phenomenon, on the surface of an electrode in more acidic buffered solution (pH4.3). For the analysis of EN data in time domain, the corrosion rate, which is equivalent to noise resistance, is only valid for uniform corrosion. Therefore it can be concluded that the presence of acetate buffer increased the corrosion rate of aluminium due to the localised formation/dissolution of aluminium oxide and the presence of metastable pits on the surface of aluminium.

Klapper et al. [21] in 2010 investigated the effect of cathodic process (oxygen reduction reaction) on EN signal arising from metastable pitting corrosion on stainless steel. The EN signal from different dissolved oxygen concentrations in solution was compared. It was found that the shape of the individual transient change with increasing dissolved oxygen concentration in solution. This was due to the fact that the increase of oxygen concentration results in a stronger consumption of electrons at the oxide/solution interface of stainless steel. Therefore it was concluded that not only anodic dissolution reaction but also cathodic reduction reaction could influence the shape of EN signal on stainless steel. It was found that the quantity and amplitude of EN signals could be reduced by a stronger cathodic process due to the corresponding electron consumption on the same stainless steel electrode. The EN signal from pitting corrosion was only measurable because cathodic process was inhibited on stainless steel electrode through the passive layer and subsequently the electrons flow to counter electrode to be recorded. The more stable the passive layer, the stronger the cathodic reaction on stainless steel was inhibited. If the cathodic process on stainless steel was not hindered enough, the reduction of the EN signal can occur.

It was mentioned in [22] that the aluminium oxide film formed in solution can reach 1000 times (about 5,000nm) thicker than the film formed in air. This oxide layer is found to be stable

under atmospheric conditions. In acid and basic solution, the solubility of aluminium oxide is enhanced so that aluminium corrodes with high rate. Moreover, the presence of chloride ions in solution accelerates the corrosion of aluminium especially pitting corrosion. Therefore, by rising and lowering the pH of solution as well as by addition of chloride ions can suppress the passivation, or formation of passive film, of aluminium. At pitting potential, the formed passive oxide layer is replaced by unstable salt layer which easily undergoes dissolution above pitting potential. Therefore, Mazhar et al. [22] in 2001 studied the effect of pH and chloride ion on passivation and corrosion of Al-Si alloy when immersed in deaerated sulphate solution. It was found that Al-Si alloy was attacked by localised corrosion while pure aluminium only exhibited general corrosion and Al-Si alloy corroded more rapidly due to the formation of galvanic coupling cell in the alloy. With increasing HCl concentration, the corrosion potential of Al-Si shifted to more positive value due to the decrease in pH of solution. In neutral sulphate solution (pH7), the corrosion rate increased at first with increasing chloride ion concentration then reduced for concentration higher than 0.1M due to synergistic effect of chloride and sulphate ion to slow down the attack. In basic sulphate solution (pH10), corrosion rate increased with increasing chloride ion concentration, but these corrosion rates have been lower than in the absence of chloride ions. This can be attributed to the reduction in alkalinity at the electrode surface due to the displacement of hydroxide ions by chloride ions. In acidic sulphate solution (pH2) corrosion rate also increased with increasing chloride ions concentration and the pitting corrosion was accelerated due to the positive charge on oxide surface at low pH, this led to attraction of chloride ions (negative charge) and subsequent attack of the oxide film. Therefore, it was concluded that both pH and chloride ions concentration played an important role in pitting corrosion of Al-Si alloy.

Van Gheem at al. [11] investigated the effect of oxygen concentration and pH on corrosion behaviour of AA1050 (Al, Fe, Si) in chloride, sulphate and perchlorate solutions by OCP and polarization measurement as well as SEM observation. It was found that when exposed to all types of solution, AA1050 alloy was attacked by microgalvanic corrosion due to the cathodic character of precipitates compared to aluminium matrix but only in chloride and perchloride solution, AA1050 exhibited crystallographic pitting corrosion at steady state or pitting corrosion at corrosion potential. Comparison of the polarization curves of AA1050 and pure aluminium in NaCl solution showed that they had different corrosion potentials but the same pitting potential. This meant it was not the presence of alloying influencing the pitting corrosion but the presence

of anions in the solution. It was also found that the oxygen concentration in solution and pH of solution can determine whether aluminium exhibited passive behaviour or pitting corrosion at corrosion potential.

Many corrosion experiments of aluminium in alkaline solution were reviewed in [23] and it was found that the corrosion rate of aluminium depended on pH, temperature, flowing velocity of solution and the exposure time. The corrosion rate may also be changed by changing the composition of the aluminium metal by alloying as well as the addition of organic and inorganic ions, such as chloride ions and inhibitors, into solution. Moreover, silicate was an effective inhibitor, with efficiency of inhibition almost 100%.

Lampeas and Koutsoukos [9] in 1994 tried to investigate the intrinsic effect of hydrogen ions activity on corrosion characteristics of aluminium by using a pH controller and addition of standard acid and basic solutions to keep pH of solution at the desired value during the measurement. This was due to the fact that pH of solution was varied during the polarization measurement, which may lead to the misleading results concerning the corrosion behaviour of aluminium. It was found that pH of solution shifted to more alkaline values during the cathodic polarization, while to more acidic value during anodic polarization. It can be concluded that the change in pH of solution was dominated by the redox reaction on working electrode. The cathodic reduction produced the hydroxide ions and the anodic oxidation subsequently produced hydrogen ions. The polarization curves in neutral solution (pH 7) of constant pH exhibited larger passive region and more positive pitting potential than initial adjusted pH. The corrosion rate obtained in constant pH solution was also found to be different with the initially adjusted pH. Moreover, they also found that the corrosion was influenced by concentration of NaCl, aeration and temperature.

Emergül and Aksüt [24] in 2000 characterised the electrochemical interface of pure aluminium in strong alkaline solution of NaOH by using polarization and impedance techniques. From polarization curves, passive film could be formed on aluminium surface in basic solution. The surface film was proposed to be a duplex structure of an inner anhydrous layer and outer hydrate layer with the degree of hydration depending on potential and hydroxide ion concentration. The thickness and the chemical composition of surface film were as well affected by scan rate of polarization. The microscopy revealed the anhydrous layer on surface of aluminium to be porous-like structure. The increase in hydroxide ion concentration and anodic

overpotential led to the enlargement of the pores, which was due to the increasing rate of aluminium dissolution. The impedance measurement suggested that with increasing hydroxide ion concentration, the anhydrous layer was thinner with the larger pore and the hydrate layer was thicker. Moreover, the surface film thickened dependently with increasing potential.

Branzoi et al. [10] in 2000 studied the influence of different aggressive anions on electrochemical behaviour of aluminium in 1M sodium nitrate solutions by polarization measurement. The corrosion behaviour was qualified by the kinetic parameters such as pitting potential, the protection potential, passive region range and repassivation range. It was found that the proper scan rate was in the range of 15-0.1mV/s where the scan rate as low as possible was more suitable. The addition of aggressive anions led to an extensive localised corrosion and the aggressivity of the anions arranging from the strongest to the weakest were chloride, thiodie, acetate and sulphate. It was mentioned that the primary corrosion process of aluminium in neutral solution was the formation of *hydroxo-complexes* (e.g., gelatinous alumina). Then this gelatinous aluminium transfer into pseudoboehmite, boehmite and finally bayerite. The aggressive anions in the solution were chemically bonded to these *oxo*- and *hydroxo-complexes* to form the *aniono –complexes* at different site of surface. These *aniono-complexes* were soluble so that they were transported from the surface. The passive layer was continually renewed by dissolution of metal and formation of *oxo*-and *hydroxo complexes*. Therefore the action of aggressive anions on pitting corrosion of aluminium was to aid the dissolution of aluminium via the formation of *aniono-complexes*. Moreover, ammonium rhodanide can be used as the pitting corrosion inhibitor of aluminium

Vijh [25] in 1968 examined the electrolytic hydrogen evolution reaction (h.e.r.) on aluminium covered with “spontaneous” oxide film in buffered acetate solution of pH5.5. The spontaneous oxide film was acquired by exposure the electrode to air for a few days or to distilled water for several days. It would be predicted from DC resistance that the thickness of spontaneous barrier oxide layer was about 6Å if this layer composes of amorphous Al_2O_3. When immersed this electrode in the buffered acetate solution at 55 ˚C, the oxide layer of Al_2O_3 became a protective, nonbarrier, hydrate oxide layer with the thickness of less than 2000 Å. It was found that the observed cathodic Tafel slopes were bigger than $2.3 \times 2\mathrm{RT/F}$, which is equal to 0.118V at room temperature for hydrogen evolution. The increased Tafel slope was due to the presence of surface films, which supposed to be semiconducting.

Moon and Pyun [26] in 1997 examined the corrosion mechanism of pure aluminium under cathodic polarization in acidic, basic and neutral solution. They found that the cathodic corrosion aided the dissolution of pure aluminium, by the attack of hydroxide ions produced from reduction water during cathodic polarization, only in neutral solution. In the case of acidic solution, the cathodic corrosion didn't take place due to no hydroxide produced during cathodic polarization. Whereas in basic solution high concentration of hydroxide ions in solution was responsible for the high corrosion rate, irrespective of applied cathodic current. It was also found that the aluminium oxide film can be formed spontaneously on aluminium surface even under cathodic polarization in all solution. Therefore, the cathodic corrosion of pure aluminium included the simultaneous formation of oxide film at aluminium/oxide interface and dissolution of aluminium oxide at oxide/solution interface.

It was mentioned in [27] that when anodic polarization was applied to valve metals such as aluminium, development of anodic oxide layers took place on their surfaces which led to the increase of corrosion resistance. Moon and Pyun [27] in 1998 investigated the growth mechanism of anodic oxide layer on pure aluminium in acidic and alkaline solution by using impedance spectroscopy and a beam deflection technique. The result indicated that thickness of the anodic oxide film increased with increasing film formation potential. In acidic solution, field-assisted dissolution of anodic oxide film at the oxide/solution interface caused the generation of aluminium vacancies, which involved the direct injection of aluminium ion from oxide film into solution. This suggested that the movement of only oxygen vacancies through oxide film that accounted for the growth of anodic oxide film in acid solution. However in alkaline solution, aluminium vacancies were generated through adsorption of water on oxide film surface, resulting in the formation of anodic oxide layer. This suggested that the movement of both aluminium vacancy and oxygen vacancy contribute to the growth of oxide film in alkaline solution. Moreover, it was found that the oxygen evolution can occur on aluminium in NaOH at potentials of $15V_{SCE}$.

Munoz and Bessone [28] in 1999 analysed the specific effect of chloride ion on the pitting initiation and pit growth on aluminium in non aqueous chloride media by cyclic polarization method with low scan rate of 0.001V/s and AC impedance method. It was found that the pitting potential was close to the potential of zero charge (pzc). When the potential exceed the pzc, the electric field induced the immigration of aggressive anions (Cl^-) toward the metal/oxide

interface especially at the imperfection sites. The appearance of the wide hysteresis and SEM image confirmed the existence of the salt film. The formation of salt film at the initial stage gave rise to the transport limiting condition for further anodic dissolution of aluminium. The anodic current was found to decrease with successive cyclic polarization, due to the sealing of the initiated pitting sites by the salt film. The initiated pit can grow only at potential more positive than the potential at maximum current of the hysteresis curve, which is close to pzc. This was attributed to the enrichment of aggressive anions inside the pits at more positive potential than pzc. Whereas if potential was more negative than pzc, the adsorption of chloride ions was not favoured so that pit growth was stopped. Moreover, the ClO_4^- can act as pitting inhibitor of aluminium.

Lin and Hebert [29] in 1994 mentioned that they have already found the growth of an *oxyhydroxide* or *hydroxide* surface film during cathodic polarization in 0.1M HCl. This film growth didn't take place by precipitation of solution, but by the direct electrochemical reaction. As the film growth at cathodic potential was limited by high resistance of oxide film, the original film must undergo a structural transformation. Therefore in their present work, they tried to measure electrochemical conductor properties of aluminium before, during and after constant cathodic polarization in HCl solution by using the electrochemical quartz crystal microbalance in order to investigate the electrochemical behaviour of aluminium during cathodic polarization. It was found that during cathodic polarization, the surface film transformed from high field electrical conductor (oxide) to an ohmic conductor (hydroxide), and then began to grow. The result suggested that even the cathodic potential prevented aluminium oxidation at the metal/oxide interface, the large positive film overpotential drove aluminium ion (Al^{3+}) to transport out through the film. Consequently, the aluminium ions concentration near metal/oxide interface reduced with time. In order to preserve electrical neutrality, the movement of protons compensated the depletion of aluminium ions. The protons were transferred to oxide ions near the metal/oxide interface, and then form hydroxide ions. Therefore the film composition near metal surface changed from hydrate aluminium oxide to aluminium hydroxide, reducing the cathodic overpotential to zero. At this point, oxidation of aluminium began and film growth initiated. Moreover, this hydroxide film has porous structure due to the partial dissolution from the oxide/solution interface into the acidic solution.

It was mentioned in [30] that the presence of intermetallic phases in the aluminium alloys can produce the alkaline pits since they possess higher potential than matrix. The intermetallic phases act as cathodes and provoke the anodic dissolution in the surrounding matrix. These alkaline pits can be formed below the pitting and repassivation potential. Therefore Aballe et al. [30] in 2000 studied the corrosion process of alloy AA5083 (Al-Mg) when immersed in aerated 3.5%wt NaCl solution for 30 days. It was found that only alkaline pits, which were hemispherical shaped, were produced due to the presence of Al(Mn,Fe,Cr) intermetallic phase from the first day of exposure and the oxide film was also observed on the surface of alloy from tenth day of exposure. The oxide film developed in area and in thickness with time, but it cannot prevent the alkaline pitting corrosion. Under cathodic polarization treatment, alkaline pitting corrosion with more intense was observed, whereas under anodic polarization treatment the crystallographic pitting corrosion was observed without alteration to intermetallic phase. Therefore it was deduced that there was no relationship between the intermetallic phase and formation of crystallographic pitting corrosion. The addition of $CeCl_3$ as an inhibitor blocked the effect on the cathodic area and prevented the increase in pH so that no alkaline pitting corrosion occurred on the aluminium surface. Moreover, it was found that the alkaline pits could also occur in distilled water, indicating that the existence of chloride ions may accelerated the alkaline pitting corrosion but it wasn't a prerequisite.

Aballe et al. [31] in 2004 studied the influence of the surface finish on corrosion behaviour, including the type and intensity of corrosion attack, of aluminium alloy (AA5083) in aerated NaCl solution by using the weight loss, linear polarization, electrochemical noise techniques as well as optical and scanning electron microscopy. The degree of surface finish was controlled by means of wet grinding with SiC papers with average abrading grit size of 15 to 68μm. It was concluded by their former study that AA5083 prepared from SiC with abrading grit size of 30 μm when exposed to aerated NaCl solution, the localised alkaline corrosion (LAC) occurred at the surrounding area of Al(Mn,Fe,Cr) cathodic precipitates. While the formation and growth of oxide layer took place in the matrix zone. Their current results have shown that the degree of surface finish didn't affect the type of corrosion attack, which was always LAC. It was also found that the corrosion susceptibility increased with decreasing grit size of abrading SiC particle on SiC paper due to the increase in density of surface precipitates. Moreover, the polarization curves showed that the different surface finish only produced change in the corrosion potential but not in the

pitting potential, indicating that the degree of surface finish didn't influence the nucleation of crystallographic pits.

It was mentioned in [32] that AA2024 is one of the material for aerospace application because it possesses high strength to weight ratio and damage tolerance. However, their susceptibility to corrosion is high due to their heterogeneous microstructure. Therefore Lacroix et al. [32] in 2012 simulated galvanic coupling between the matrix and S-Al_2CuMg particles in AA2024 by Al-Cu/Al-Cu-Mg model alloy couple in order to understand the corrosion behaviour of AA2024 in sulphate solutions. The polarization and local impedance spectroscopy (LEIS) measurements were performed on the individual alloy and on the model alloy couple. It was found that the Al-Cu, which represented the matrix, was passivated while the Al-Cu-Mg alloy, which represented the S-Al_2CuMg particles, underwent localised corrosion. Moreover after Al-Cu/Al-Cu-Mg model alloy couple immersed in sulphate solution, the Al-Cu-Mg alloy was more pitting corroded close to the interface between Al-Cu and Al-Cu-Mg. This revealed the galvanic corrosion on AA2024.

Ahmad et al. [33] in 2001 evaluated the corrosion performance of Al-Mg alloy with addition of 0.1-0.3 %wt Sc in 3.5%wt NaCl solution by means of weight loss, polarization measurement and microstructure examination. The additions of Sc to Al-Mg alloy increased the strength of scandium-free alloys due to the presence of small Al_3Sc precipitates. The result showed that for all samples the corrosion rate decreased with exposure time due to the formation of a duplex protective film. By adding 0.1-0.15 %wt Sc, the corrosion rate slightly increased, however the corrosion rate was still better than other conventional aluminium alloy in similar environment. The pitting potential of Al-Mg-Sc alloy shifted to more positive values compared to scandium-free alloy and other conventional aluminium alloys. Morphology of pits also confirmed that the Al-Mg-Sc alloy offer a good resistance to pitting corrosion, suggesting that the small size of Al_3Sc particle was not sufficient to influence the pitting corrosion.

Su et al. [34] in 2002 compared the corrosion behaviour of aluminium alloys when brazed with Al-Si-Cu-based filler metals and traditional Al-12Si filler metal by using polarization and immersion tests in 3.5%wt NaCl solution. This measurement was conducted due to the fact that the bond strength increases from 67MPa by using traditional Al-12Si filler metal to 147MPa by using this Al-Si-Cu filler metal. During the polarization test, the potential was first held at more cathodic potential for 5 min to remove any oxide film. It was found that the Al-Si-Cu filler metals

possessed higher corrosion current density and strong pitting tendencies than Al-12Si filler metals. More severe galvanic corrosion, which occurred at the butt joint region between AA6061 and the filler metals, was detected from the case of AA6061/ Al-Si-Cu brazement due to that the larger difference in corrosion potential between AA6061 and Al-Si-Cu based filler metals. However AA6061/Al-12Si created more extensive corrosion regions due to the wider butt joint area.

Tavakkolizadeh and Saadatmanesh [35] in 2001 investigated the possibility and intensity of galvanic corrosion between steel and CFRP in deicing solution and sea water. The galvanic corrosion rate of steel and CFRP were assessed by means of polarization and galvanic corrosion test. The results showed that the galvanic corrosion occurred when there was a direct contact between CFRP and steel. As CFRP was nobler than steel, the corrosion rate of steel highly increased by about 13 times faster when coupled with CFRP. Moreover, it was also found that the galvanic corrosion rate of steel/CFRP coupling system was related to the solution in use, the thickness of epoxy coating on carbon fibre and types of solvent to remove the sizing agents from the surface of carbon fibre.

Tucker et al. [7] in 1990 investigated the degradation mechanism of galvanic coupling between graphite fibre composite and metals in sea water. The metals used in their study were AA2014, commercially pure grade aluminium, and 316stainless steel. The visual examination showed that the galvanic coupling between titanium and graphite fibre composite didn't induce degradation of both titanium and composite. The stainless steel exhibited the change in corrosion behaviour from non-corroding to localised corrosion with no change on composite when coupled with graphite fibre composite. On the other hand, uncoated AA2014 still exhibited active corrosion when coupled with graphite fibre composite, but the composite exhibited degradation by the formation of blister due to the higher tendency for aluminium to corrode than stainless steel. This resulted in the faster cathodic oxygen reduction on composite when couple with aluminium. The higher concentration of species which can diffuse into composite created the formation of blister. Therefore it was clear that strong galvanic corrosion induced blister in composite material.

It was mentioned in [8] in 2005 that the use of non-conductive layer (e.g., GFRP sheet or epoxy film) between the CFRP and steel and the use of water resistant sealant on the metal surface can protect hybrid material of steel/CFRP against galvanic corrosion.

CHAPTER III

THEORETICAL BACKGROUND

The theoretical background is mainly based on [36].

1. Aluminium

Aluminium is lighter than all common metals. Its low density of 2.70g/cm^3 is nearly 3 times less than that of steel. It is not only lightness, but also a very good resistance to atmospheric corrosion that makes aluminium and its alloys widely used in many applications.

2. Corrosion of metal

Corrosion can be defined as a deterioration of metal's properties under the influence of surrounding environment. The metal's properties include appearance, surface aspect and mechanical properties. Under normal environmental conditions, most of metals such as iron, steel, titanium, aluminium and their alloys are attacked by corrosion except the very noble metals such as gold and platinum that are immune against corrosion.

The corrosion of metal is the result of at least 2 simultaneous electrochemical reactions between a metal and aqueous phase.

1. The oxidation reaction of metal: $\mathrm{M} \rightarrow \mathrm{M}^{n+} + \mathrm{ne}^-$

The oxidation of metal at anode forms metal ions (M^{n+}) that are released into solution (figure 1, left). This creates a flux of electrons within the metal. This oxidation reaction results in the anodic current ($\mathrm{i_a}$) that flows from metal to solution. Electrons that are liberated by oxidation flow through cathode where they are consumed by reduction reaction of an ion or molecules presenting in the aqueous solution.

2. The reduction reaction of an ion presenting in the aqueous solution: $\mathrm{X}^{n-} \rightarrow \mathrm{X} + \mathrm{ne}^-$

The reduction reaction transforms ions or molecules, by taking up electron, into another chemical species (figure 1, right). This reduction reaction creates the flux of electrons within the

metal in the direction from metal to solution, resulting in the cathodic current (i_c) flowing from solution to metal.

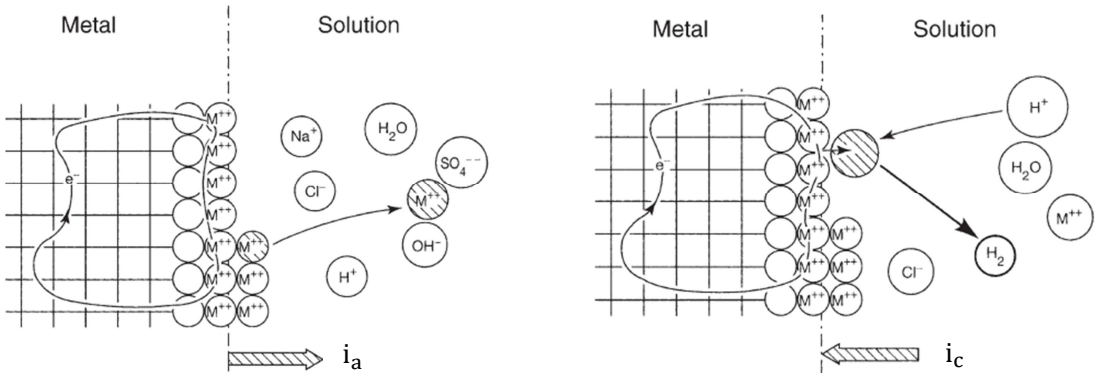

Figure 1: Electrochemical reactions at the metal/solution interface: (left) oxidation reaction and (right) reduction reaction (Modified after [36]).

When metal is plunged into the solution, many anodic oxidation and cathodic reduction reactions simultaneously occur at the metal/solution interface. The electrical currents from all electrochemical reactions are dependent on the potential difference between metal and solution. Under conditions of natural corrosion, where there is no external electric current or potential, the system formed by metal and solution establishes an open electrical circuit. In this open electrical circuit, the anodic current equal to cathodic current ($\sum I_a = \sum I_c$) therefore the net current is zero.

3. Corrosion of aluminium

For corrosion of aluminium, oxidation of aluminium metal forms trivalent cation and a loss of 3 electrons.

Oxidation of aluminium: $Al \rightarrow Al^{3+} + 3e^-$

The released electrons are captured by a simultaneous reduction reaction of ions presenting in the solution. The primary cathodic reduction reaction is hydrogen evolution which is the reduction of proton in acidic solution. While in basic solution the reduction of water will take place.

Reduction of proton in acidic solution: $2H^+ + 2e^- \rightarrow H_2$

Reduction of water in basic solution: $2H_2O + 2e^- \rightarrow H_2 + 2OH^-$

When dissolved oxygen gas is presenting in the solution, reduction of dissolved oxygen is also possible:

In basic or neutral solution: $O_2 + 2H_2O + 4e^- \rightarrow 4OH^-$

In acidic solution: $O_2 + 4H^+ + 4e^- \rightarrow 2H_2O$

Therefore the total corrosion of aluminium in solution is the sum of two electrochemical reactions, oxidation and reduction (of proton):

Total corrosion of aluminium: $Al + 3H_2O \rightarrow Al(OH)_3 + \frac{3}{2}H_2$

The corrosion of aluminium results in the formation of alumina $Al(OH)_3$. Alumina is insoluble in water and precipitates as a white gel. In addition, corrosion of aluminium releases a large volume of hydrogen gas which can cause the catastrophic consequence.

The valves metals such as titanium and aluminium exhibit high corrosion resistance due to their passivity. Their passive oxide films typically exhibit asymmetric conductivity that blocks anodic dissolution of metal except at high applied voltage. This oxide film can be grown by anodic polarization. Passivation of aluminium is always spontaneous [37]. When aluminium plunge into oxidising media such as air and water, oxide layer will immediately formed.

Formation of aluminium oxide film: $2Al + \frac{3}{2}O_2 \rightarrow Al_2O_3$

Aluminium is one of the easiest metals to oxidise but aluminium is a very stable metal in the oxidising media because the oxide film of aluminium is continuous and uniform therefore this protective oxide film can protect aluminium from further corrosion.

The oxide film of aluminium is colourless and composes of 2 superimposed layers with a total thickness of 4 to 10nm.

- The inner barrier layer:

This layer is in contact with aluminium metal. Aluminium oxide in this layer is compact and amorphous therefore this layer possesses dielectric properties. This layer is formed very fast within a few milliseconds.

- The outer porous layer:

This layer grows on the top of the first layer by the reaction with external environment, probably by hydration. The hydration transforms the barrier layer film into bayerite or boehmite depending on the temperature. This layer is porous and less compact than the first layer. The final thickness of this layer will not be achieved before several weeks or even months, depending on the physicochemical conditions.

It was mentioned that the corrosion rate of aluminium in solution is controlled by the outer porous layer and depends on its thickness. Therefore the corrosion rate of aluminium depends on 3 reactions:

- The dissolution rate of the outer layer
- The conversation of the barrier layer into bayerite or boehmite
- The formation of the barrier layer from the metal

Moreover, the alloying metal and additives in aluminium metal also influence on the rate of formation and the surface properties of this oxide film.

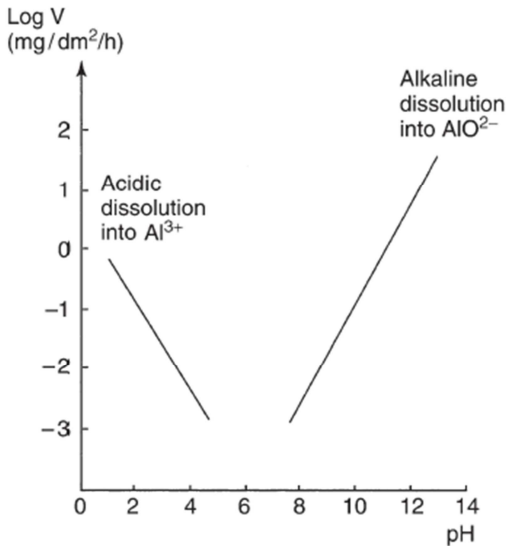

Figure 2: Dissolution rate of alumina in solution as a function of pH [36].

As aluminium is valve metal, the corrosion of aluminium is dependent on the stability of spontaneous oxide film covered on the metal surface. This oxide film is most stable in the pH range of 6.5 to 7.5, making aluminium extremely useful only for environment conditions where

aggressive solution is more or less neutral. In neutral environment, aluminium oxide is compact and thermodynamic stable as well as good adherence to the aluminium surface so that aluminium oxide can be a good protective layer. However, dissolution rate of aluminium oxide depends on the pH values of solution (figure 2). The dissolution rate of aluminium oxide is higher in acidic and alkaline solution, meaning that aluminium oxide is amphoteric. Therefore aluminium oxide layer can be dissolved in acidic or alkaline solution. Moreover, it is not only pH of solution that affects the dissolution rate of aluminium, but also the nature of the acid and base dissolved in solution.

4. Type of corrosion on aluminium

Many different types of corrosion can occur on aluminium but in this research only uniform (generalised) corrosion and pitting corrosion will be mentioned.

4.1 Uniform corrosion:

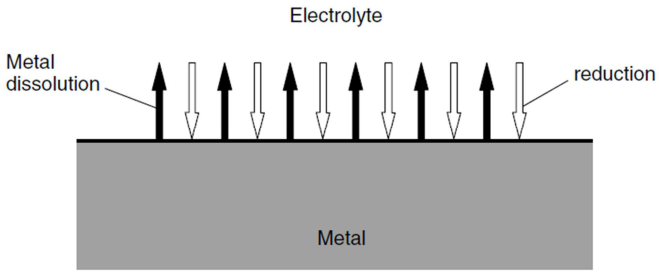

Figure 3: Uniform corrosion of metals [38].

Uniform corrosion, or homogeneous corrosion, is defined as a corrosion process with a uniform dissolution rate of metal over entire surface area. This type of corrosion results in a uniform and continuous reduction of metal thickness. As corrosion composed of at least 2 partial reactions such as dissolution of metals and reduction of ions or molecules presenting in solution, the dissolution and reduction reactions are evenly distributed over the entire surface and the rate of anodic metal dissolution should be equal at all places during the uniform corrosion as shown in figure 3. The distance between the metal dissolution and reduction should be really small and the locations of these reactions will continuously and randomly shift across the surface of metal [38]. The uniform corrosion of aluminium is found especially in strong acidic and alkaline solution where the solubility of oxide film is high. In these solutions, dissolution rate of

aluminium oxide is higher than its formation rate. The rate of uniform corrosion can be easily measured by mass loss, quantity of released hydrogen gas and polarization measurement.

4.2 Pitting corrosion:

The passive oxide layer can protect metals against the environmental degradations. However, the presence of aggressive anions leads to the breakdown of passive film and formation of pits, by so called pitting corrosion. The pitting corrosion is one of the localised forms of corrosion and characterised by the formation of irregularly shaped holes on the surface of metal. Diameter and depth of the pits are dependent on several parameters related to metal, solution and service condition in use. All halide ions act as aggressive anions but chloride ions is the most important because its presence in most of technical environments such as seawater and deicing salt. Almost all metals and alloys are susceptible to pitting corrosion [38].

5. Pitting corrosion of aluminium

Like other valves metals, aluminium is very resistant against uniform corrosion in neutral solution, which basically covers all natural environments such as surface water, seawater and moist air, due to the formation of passive oxide film. However if these nearly neutral solutions contains aggressive anions, pitting corrosion can occur because of the localised breakdown of the passive film [38]. A large number of pits are formed on its surface. Most of these pits are described as metastable pits which do not propagate but repassivate after a very short period of growth. The other pits keep on growing for long time to form stable pits with larger depth. These stable pits result in high corrosion damage. The stable pits are considered to be a subset of metastable pit therefore in order to predict when stable pits will develop, it is important to determine when metastable pits generate and subsequently the possibility of growing from metastable pits to stable pits.

Pitting corrosion is a very complex phenomenon. Even nowadays, its corrosion mechanism is still remains controversial. Pitting corrosion is characterized by 2 stages:

5.1. Initiation stage:

As the presence of aggressive anions in solution, the aggressive anions are adsorbed on the spontaneous oxide film and then absorbed chloride ions transport through the oxide film by means of oxygen vacancies or migrate to the film/metal interface by the defect in passive film

such as inclusion and voids. The incorporation of chloride ions into the oxide film may lead to the formation of chloride ions-containing complexes at the film/solution interface [Ref.39]. In neutral and acid solution, transitional *chloride complexes* ($AlCl_n^{(n-3)-}$) are formed while *oxo-*, *hydroxo-* and *chloro- complexes* are formed in basic solution [22]. These chloride ions-containing complexes have higher solubility than compared to aluminium oxide film. Therefore, the dissolution of oxide film is possible. At the weak points of oxide film, the locally breakdown of oxide film take place and subsequently form micorcracks with a few nanometres wide. This results in the initiation of pit. For metastable pitting corrosion, the opening of the initiated pits is covered by osmotic pressure in solution, possibly resulting in mixture of solution inside and outside the pit. This can cause concentration of metal chloride in the pits below critical value for active dissolution inside the pits, leading to repassivation [39]. Among all anions, chlorides ions have a highest tendency to penetrate into the spontaneous oxide layer because chlorides ions are small and very mobile. The chloride ions may replace oxygen atoms in the network of oxide film, leading to the decrease of film's resistivity. This facilitates the release of aluminium into solution.

5.2. Propagation stage:

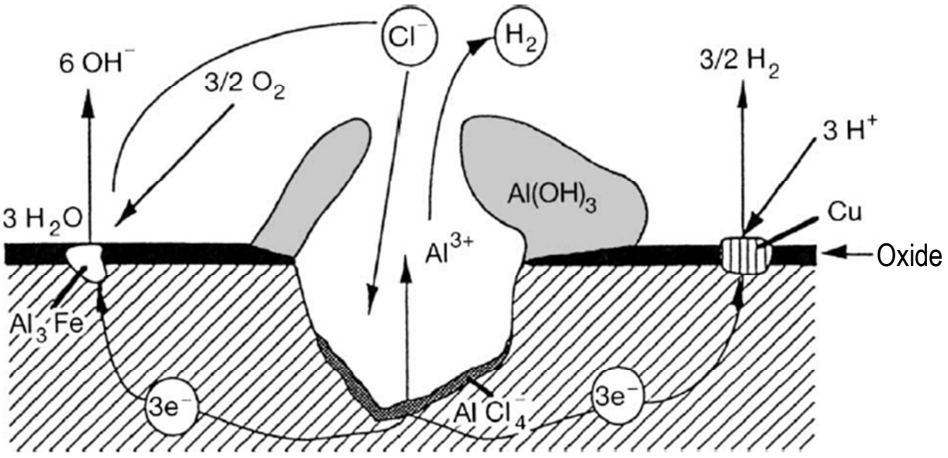

Figure 4: Pitting corrosion mechanism of aluminium [36].

The initiated pitting sites are anodic with respect to the oxide film area surrounding the pits. The initiated pits will continue to propagate according to the anodic metal oxidation at the pits bottom. In open circuit conditions, the anodic dissolution is electrical compensated by the cathodic reaction usually taking place outside the pits (figure 4):

Anodic oxidation at the pit's bottom: $Al \rightarrow Al^{3+} + 3e^-$

Cathodic reduction outside the pits: $2H^+ + 2e^- \rightarrow H_2$ or $O_2 + 2H_2O + 4e^- \rightarrow 4OH^-$

If the anode is stable and localised, corrosion reaction continue digging the microcrack (initiated pits). This results in the growing of the initiated pits.

The formation of $Al^{3+}$by dissolution of aluminium metal at the pit's bottom creates the electric field that can shifts Cl^- ions towards the pit's bottom. In order to electrical neutralisation of solution, the aluminium chlorides ($AlCl_4^-$) is formed at the pit's bottom. Then the hydrolysis of aluminium in aluminium chlorides occurs according to the reaction:

Hydrolysis of aluminium in aluminium chlorides: $Al^{3+} + 3H_2O \rightarrow Al(OH)_3 + 3H^+$

This causes the acidification of the solution at the pit's bottom to pH less than 3. The solution becomes very aggressive, leading to the autopropagation of the pits. The formed aluminium hydroxide will be pushed to the opening of the pits. Moreover, the formation of OH^-ions and the consumption of H^+ions by cathodic reduction outside the pits will locally lead to the excess of OH^-ions, thus alkalisation of local medium. The high concentration of Al^{3+} at the pit's bottom can diffuse towards the pit's opening and meet the medium which is more and more alkaline by result of cathodic reduction. According to reaction above, $Al(OH)_3$ is the precipitated at the pits opening.

Therefore the overall reaction of pitting corrosion of aluminium is

$$2Al + 3H_2O + \frac{3}{2}O_2 \rightarrow 2Al(OH)_3$$

As the equation above, the corrosion product is aluminium hydroxide ($Al(OH)_3$) which is commonly called alumina. Alumina is a gelatinous white gel and adheres well to the metal's surface. The accumulation of corrosion product at the pit's opening will progressively block the entry of the pits. Therefore the exchange of ions, especially chloride ions, is blocked. This slows down and finally stops the pitting corrosion.

Unlike uniform corrosion, the intensity and rate of pitting corrosion cannot be measured by mass loss and released hydrogen gas because the very deep and isolated pits lead to an only small mass loss.

6. Pourbaix Diagram

As pH is a very important parameter for corrosion of metal, Pourbaix diagram is generated based on thermodynamics to represent the equilibrium conditions in potential/pH space [Ref.38]. Pourbaix diagram, or potential-pH diagram, indicates the region of the stable phase for each chemical species as a function of pH (for chemical reaction) and as a function of the potential (for electrochemical reaction). Therefore Pourbaix diagram is a very useful tool for predicting corrosion behaviour of metal. Generally, there are 3 regions in Pourbaix diagram:

- Corrosion:
  In this region, the dissolved cation or oxy-anion is stable phase. For most of the metals, the corrosion region is at the acid and base ends of diagram.
- Passivation.
  In this region insoluble oxide or hydroxide are stable phase. The oxide and hydroxide is formed on the metal surface, resulting in the decrease in corrosion rate of the metals to very low values. Most metals exhibit passivation in the mid-pH range.
- Immunity:
  In this region, metal is the stable phase therefore corrosion is thermodynamically unfavoured. The immunity region is typically at low potentials.

The Pourbaix diagram of aluminium in figure 5 shows that aluminium metal is stable only at low potentials (immunity region). The passivation region ranges between pH4 to pH 8.5, in which solubility of aluminium oxide is low (see figure 2). In the passivation region, oxide Al_2O_3 is formed and can be modified to hydroxide $Al(OH)_3$ and oxyhydroxide $AlOOH$. Corrosion regions of aluminium take place in acidic or alkaline solutions. In acidic solution, aluminium metal and its oxide dissolve to Al^{3+}, while in alkaline solution, they dissolve as $AlO_2{}^-$ [40] or $Al(OH)_4{}^-$[38].

In the presence of a substance in solution such as chloride ions and the presence of alloying element in metal, Pourbaix diagram is revised. The Pourbaix diagram of aluminium alloy (AA5086) in seawater is shown on the figure 6. This Pourbaix diagram is plotted based on the measurement result.

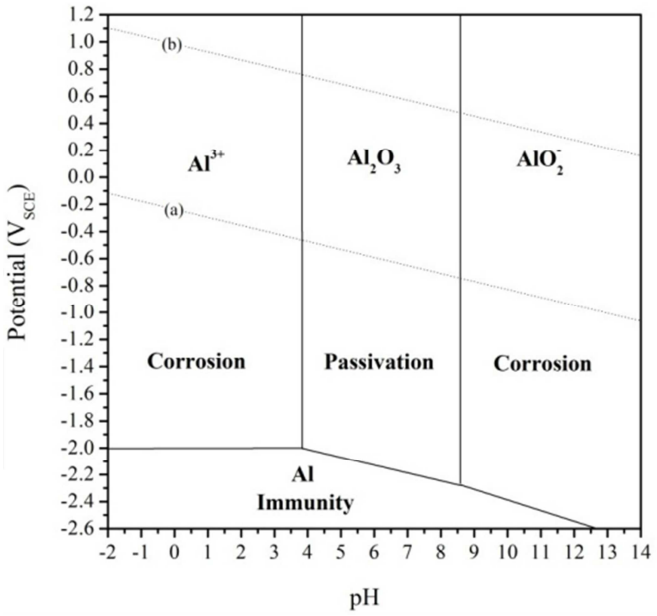

Figure 5: Potential-pH diagram of aluminium in water [40].

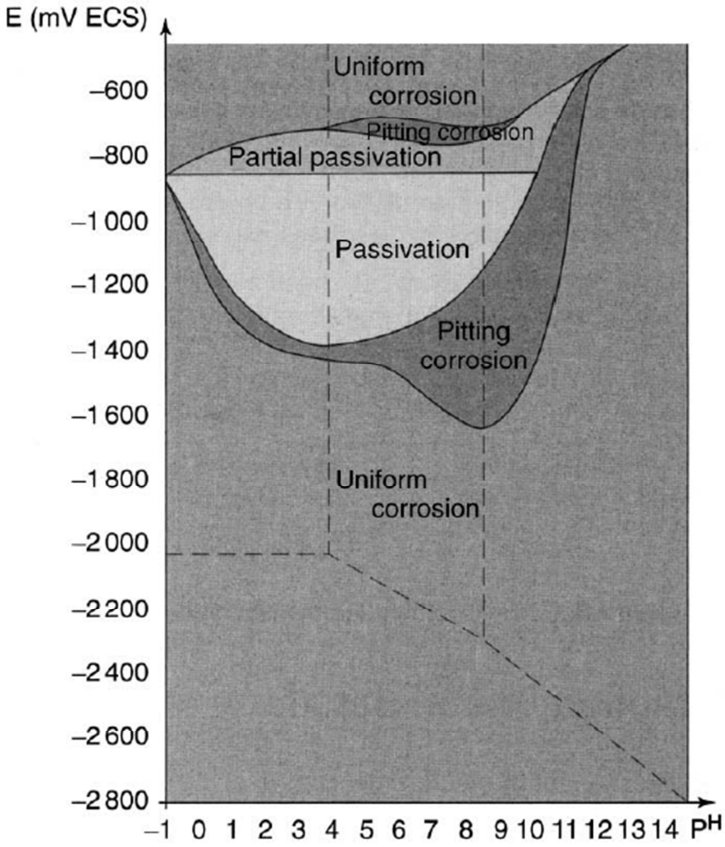

Figure 6: Experimental potential-pH diagram of 5086 in the presence of chloride ions [36].

As Pourbaix diagrams are constructed purely from thermodynamic data, it can only be used to determine possible reaction of metal when immersed in a solution but it provides no information about kinetics such as corrosion rate.

7. Galvanic Corrosion

Galvanic corrosion occurs when two dissimilar materials are in direct contact in a conducting liquid medium. Corrosion of one metal is greatly accelerated while the other metal is not corroded or it may even be protected. The appearance of galvanic corrosion is really characteristic. Unlike dispersed pitting corrosion, galvanic corrosion is highly localised in the contact zone with the other material. In order for galvanic corrosion to take place, all 3 conditions must simultaneously meet:

- Dissimilar types of materials
- presence of an conductive liquid medium or the electrolyte
- Electrical continuity between the two materials.

Galvanic corrosion works like battery built from 2 electrodes of 2 dissimilar metals. One metal electrode acts as cathode where reduction reaction takes place and another one acts as the anode where oxidation reaction takes place. These electrodes are plunged into electrolyte. The electrolyte can provide an ionic junction between the electrodes to transport electrical current by the movement of ions. The two electrodes are externally linked by electrical circuit to circulate electrons. The example of galvanic cell between zinc and copper is shown in figure 7.

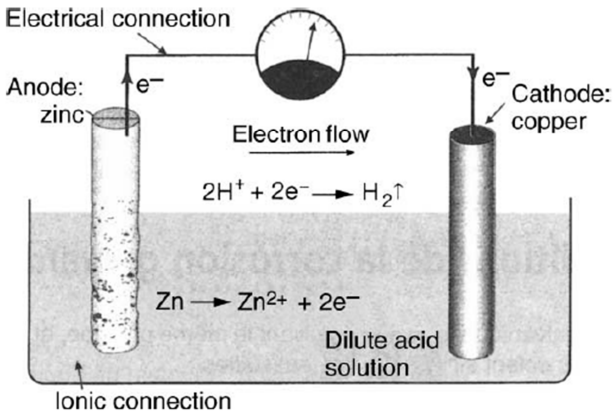

Figure 7: Principle galvanic cell between zinc and copper [36].

The galvanic corrosion between zinc and copper occurs according to 2 electrochemical reactions:

Anodic oxidation at the zinc electrode: $\mathrm{Zn} \rightarrow \mathrm{Zn}^{2+} + 2\mathrm{e}^{-}$

Cathodic reduction on the copper electrode: $2\mathrm{H}^{+} + 2\mathrm{e}^{-} \rightarrow \mathrm{H}_2$

The net reaction is

$$\mathrm{Zn} + 2\mathrm{H}_2\mathrm{O} \rightarrow \mathrm{Zn(OH)}_2 + \mathrm{H}_2$$

This cell will produce electricity whilst consuming zinc metal by forming zinc hydroxide.

In many applications, aluminium is commonly assembled with other materials due to technical and economic reasons. From the galvanic series in table 1, aluminium is more electronegative than most common metal. Therefore when in contact with more electropositive (nobler) material in solution, aluminium acts as the anode and undergoes galvanic corrosion.

GALVANIC SERIES
In Flowing Seawater

Alloy		*Voltage Range of Alloy vs. Reference Electrode**
Magnesium	**Anodic or Active End**	-1.60 to -1.63
Zinc		-0.98 to -1.03
Aluminum Alloys		-0.70 to -0.90
Cadmium		-0.70 to -0.76
Cast Irons		-0.60 to -0.72
Steel		-0.60 to -0.70
Aluminum Bronze		-0.30 to -0.40
Red Brass, Yellow Brass, Naval Brass		-0.30 to -0.40
Copper		-0.28 to -0.36
Lead-Tin Solder (50/50)		-0.26 to -0.35
Admiralty Brass		-0.25 to -0.34
Manganese Bronze		-0.25 to -0.33
Silicon Bronze		-0.24 to -0.27
400 Series Stainless Steels**		-0.20 to -0.35
90-10 Copper-Nickel		-0.21 to -0.28
Lead		-0.19 to -0.25
70-30 Copper-Nickel		-0.13 to -0.22
17-4 PH Stainless Steel †		-0.10 to -0.20
Silver		-0.09 to -0.14
Monel		-0.04 to -0.14
300 Series Stainless Steels ** †		-0.00 to -0.15
Titanium and Titanium Alloys †		+0.06 to -0.05
Inconel 625 †		+0.10 to -0.04
Hastelloy C-276 †		+0.10 to -0.04
Platinum †	**Cathodic or Noble End**	+0.25 to +0.18
Graphite		+0.30 to +0.20

* These numbers refer to a Saturated Calomel Electrode.
** In low-velocity or poorly aerated water, or inside crevices, these alloys may start to corrode and exhibit potentials near -0.5 V.
† When covered with slime films of marine bacteria, these alloys may exhibit potentials from +0.3 to +0.4 V.

Table 1: Galvanic series of metals in flowing seawater [41].

The relative position of two materials in galvanic series only indicates the possibility of galvanic corrosion when there is a high difference in potential. The intensity or the rate of galvanic corrosion is not related to the difference in potential between these two materials. The intensity of galvanic corrosion depends on several factors such as nature of electrolyte (e.g. their conductivity), polarisation phenomena, surface ratio between two materials, their distance, and temperature.

As carbon or graphite is a very noble or electropositive material while aluminium is a very active or electronegative material (see table 1), the galvanic coupling is possibly formed between carbon and aluminium in the presence of electrolyte. It was found that the contact between carbon fibre reinforced polymer (CFRP) and aluminium leads to severe galvanic corrosion of aluminium in the contact zone. In addition, the local change of pH by the release of OH^- ions during galvanic corrosion of aluminium may damage composite material.

8. Corrosion testing method

Corrosion is not an instantaneous phenomenon and the real-time corrosion testing may be a slow or fast process, depending on the metal, the solution and the form of corrosion. Therefore in order to reduce the waiting time for testing results, the accelerated corrosion test, such as the solution with high concentration of NaCl, is used in the laboratories. Certain corrosion testing methods are commonly used such as the mass loss and volume of released hydrogen gas. However theses two methods are only valid for uniform corrosion. Since the uniform corrosion on aluminium is extremely low and when corrosion occurs it always develops as pitting, the mass loss and hydrogen gas method cannot be used as indicator for corrosion of aluminium. Electrochemical techniques, such as open circuit potential (OCP), polarization and electrochemical noise measurement are also the most popular method for corrosion analysis since the computer-controlled potentiostat are now relatively inexpensive and its software for experimental control, data collection and data analysis is very easy to use.

8.1) Open circuit potential (OCP) measurement:

OCP measures the potential of metal with respect to a reference electrode when no potential or current being applied to the metal. The OCP can be used to classify metals with respect to each other, such as noble or active metal, which is useful to predict galvanic corrosion when two metals are in electrical contact as mentioned earlier. Moreover the OCP can shift with time if

the surface of metal changes [38] so that the evolution with time of OCP can also give useful information about the evolution of corrosion and passivation phenomena of metal under study.

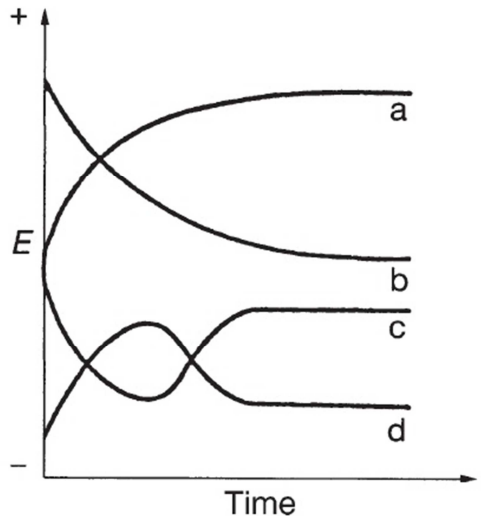

Figure 8: Typical evolution curves with time of OCP [36].

The 4 classical evolutions with time of OCP in figure 8 are:

- **Curve a** is defined as the potential become more and more noble. This indicates the passivation of metal.
- **Curve b** is defined as the potential becomes less and less noble, indicating the attack of the metal.
- **Curve c** is defined as the potential drops and then increases. This indicates the attack of metal followed by passivation.
- **Curve d** is defined as the potential rise and then decrease. This indicates the formation of passive oxide film followed by its modification.

8.2) Polarization measurement :

The polarization is related to the measurement of current (i) as a function of the voltage or potential (E) applied to the metal under study. The polarization method is often used to obtain some kinetic information of corrosion such as the corrosion potential ($\mathrm{E_{cor}}$), the corrosion current ($\mathrm{i_{cor}}$), polarization resistance ($\mathrm{R_p}$) and especially corrosion rate ($C.R$). For potentiodynamic polarization measurements, the driving force such as potential is scanned at a

fixed scan rate and the net charge in the reaction rate, which is current, is measured [42]. The polarisation curve of aluminium in solution is the sum of two electrochemical reactions (see figure 9):

For the cathodic curve, reduction of H^+ions may take place: $3H^+ + 3e^- \rightarrow \frac{3}{2}H_2$

For the anodic curve, oxidation of aluminium takes place: $Al \rightarrow Al^{3+} + 3e^-$

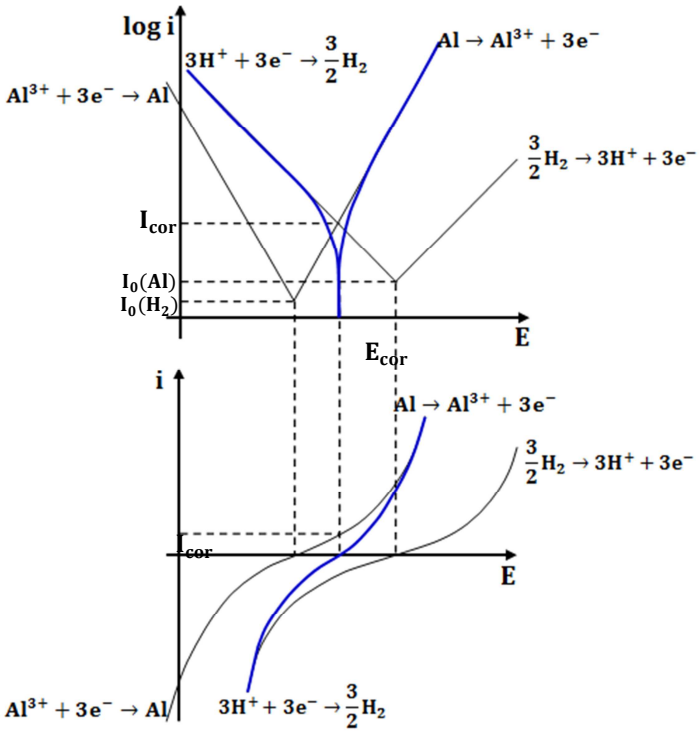

Figure 9: Model of polarization curves (blue line) of aluminium in acidic solution (Modified after [36]).

The typical scan rate of potentiodynamic polarization is in range of 0.1 to 1mV⁄s. However, slower scan rate is preferred to determine nearly steady state behaviour.

According to the Butler-Volmer equation, the current density of reaction is often controlled by the transfer charge across the interface [38].

Butler-Volmer equation : $$i = i_{cor}\exp\left[\frac{\alpha_a z_a F(E-E_{cor})}{RT}\right] - i_{cor}\exp\left[\frac{\alpha_c z_c F(E-E_{cor})}{RT}\right]$$

Where α is the charge transfer coefficient, F is Faraday's constant, R is gas constant, z is charge number and T is temperature [38]. For system under activation control (or charge transfer

control) and the overpotential ($\eta = E - E_{cor}$) is higher than 50mV, a Tafel behaviour, which is a linear relationship between potential and the log of the current density, will be observed. Therefore, corrosion rate of a metal can be determined by Tafel extrapolation. Potentiodynamic polarization for Tafel extrapolation experiment typically often starts at a potential of 250mV below OCP and scan in noble direction to a potential of 250mV above OCP. During polarization, a zero-current potential, where the sum of anodic and cathodic reaction rates is zero, is defined as corrosion potential (E_{cor}). This corrosion potential might be different from OCP measured before polarization due to reactions that occur during the polarization. The linear region of polarization in anodic and cathodic reactions is called the Tafel slope for anodic and cathodic reaction. Once these Tafel slopes have been established, it is possible to extrapolate the point where anodic and cathodic reaction rates are equivalent. The potential and current at this point are the corrosion potential (E_{cor}) and corrosion current (i_{cor}). According to faraday's law, the corrosion rate is direct proportional to corrosion current density. It must be noted that this corrosion rate is only valid for uniform corrosion.

The potentiodynamic polarization not only provides information about corrosion rate, but also about the behaviour of metal over a wide range of potential in positive direction of corrosion potential, or in anodic polarization [38]. The various regions of metals behaviour are labelled in figure 10.

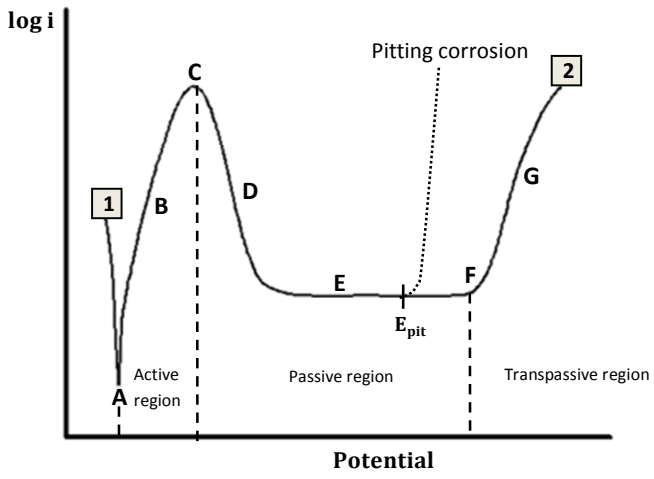

Figure 10: Theoretical anodic polarization curve (Modified after [42]).

From figure 10, the polarization starts from point **1** and scans upward through corrosion potential to a termination at point **2**. The corrosion potential locates at point **A**. As the potential

increases further, we move to region **B**, which is the active region. In this region, metal dissolution takes place. Point **C** is known as passivation potential, where the active/passive transition takes place. As the applied potential increase further, the current decreases with increasing potential (region **D**) until the low passive current is reached (region **E**). The decrease in current is a result of the formation of a thin protective passive film so that this region is called a passive region. At very high potential of point **F**, which is sometime termed the breakaway potential), the current start to rapidly increase again. The increase of current in Region **G**, which is transpassive region, is associated with the oxygen evolution on electrode surface. For some system such as aluminium in solution with the presence of aggressive anions like chloride, the sudden increase in current may occur at relative lower potential within the passive region, due to the localised breakdown of passive film or pitting corrosion by chloride ions [38, 42]. The least positive potential at which pits can form is called pitting potential (E_{pit}). The E_{pit} - E_{cor} is the extent of passive region on polarization curve and give the information about the susceptibility to pitting corrosion [28].

Moreover, the potentiodynamic polarization is also the most electrochemical techniques for studying the evolution of localised corrosion of metal by cyclic polarization. The cyclic polarization typically starts at the corrosion potential and scans upward in anodic direction until pass through the pitting potential, after that the scanning direction is reversed (figure 11).

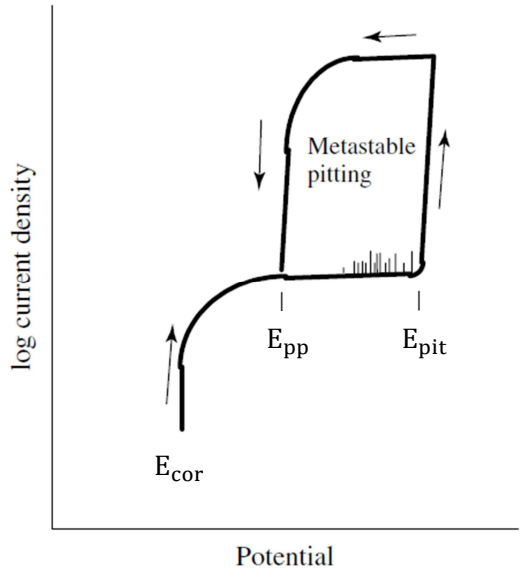

Figure 11: Cyclic polarization curve of system exhibiting localised corrosion (Modified after [38]).

In figure 11, the corrosion potential (E_{cor}) is much lower than pitting potential (E_{pit}), so that the material exhibit spontaneously passive behaviour at the corrosion potential and no active region is observed during anodic polarization. As potential approaches pitting potential, it is not common to detect the noisy current transient which is the sharp increase of current followed with sudden decrease caused by the initiation and death of the metastable pits, respectively. Metastable pits are the initiated pits that grow for short period of time and then repassivate. At pitting potential, the current continue to increase due to the stable pits formation. After the scanning direction is reverse, hysteresis is observed. The positive hysteresis exhibits that during reverse polarization, the initiated pits will tend to grow but not initiate at potential below pitting potential. Until the protection potential (E_{pp}) is reached, which is defined as the intersection of the forward and reverse anodic polarization curves, the repassivation of localised corrosion takes place so that current returns back to passive current. This means no propagation of pits occurs below E_{pp} [10]. The difference between E_{pit} and E_{pp} has been considered to have relationship to susceptibility to pitting corrosion of material [38].

8.3) Electrochemical Noise (EN) measurement:

Since 1968 when Iverson observed the potential fluctuation between platinum and various metal and suggested that these fluctuation were directly related to corrosion process, the spontaneous fluctuation of potential and current have been widely used for characterization of corrosion phenomena on metal. The fluctuation of potential and current during electrochemical processes in media are called electrochemical noises (EN). It was suggested that local corrosion is the principal source of EN data therefore the analysis of EN data could be used to monitor the corrosion activity. The EN measurement offers some advantages compared to the other common electrochemical techniques [13, 14, 18] such as:

1. EN is a completely non-perturbative technique. Unlike polarization measurement that measures the response of the system to an external applied perturbation, the electrochemical noise measures the inherent noise of the system. Therefore the advantage of electrochemical noise is that there is no need to polarize the system from its natural condition. This makes the electrochemical noise measurement a promising technique for corrosion monitoring in the field.
2. EN is able to instantaneously register and monitor the rate of the corrosion process.

3. EN can provide more information of localized corrosion than conventional techniques.

Moreover, it was confirmed by some researchers that the electrochemical noise data are in a good agreement with electrochemical parameters from polarization and impedance techniques [14]. Therefore, many analysis methods for analyzing the EN data have been developed.

Generally, EN is classified into potential noise and current noise. The potential noise is measured as the fluctuation in potential difference between working electrode and reference electrode or two nominally identical working electrodes. The current noise is measured as a current flow between two nominally identical working electrodes using a zero resistance ammeter (ZRA). It was found that the fluctuations of corrosion potential in free corroding system will give the information about the heterogeneous corrosion process and the fluctuation in current follows the intensity of the actual corrosion rate of the system [18].

The electrochemical noise related to the mechanisms of pitting corrosion of stainless steel are better understood than that of pitting corrosion of aluminium [17]. It is generally accepted that the electrochemical noise of stainless steel in chloride ions-containing solution below pitting potential is ascribed to the evolution of metastable pitting corrosion. The metastable pitting event includes initiation, propagation and repassivation after a short period of growth. During metastable pitting event, the open circuit potential (OCP) of stainless steel rapidly drops due to the anodic growth of the pit, followed by a relatively slower cathodic recovery after repassivation of the pit as shown in figure 12

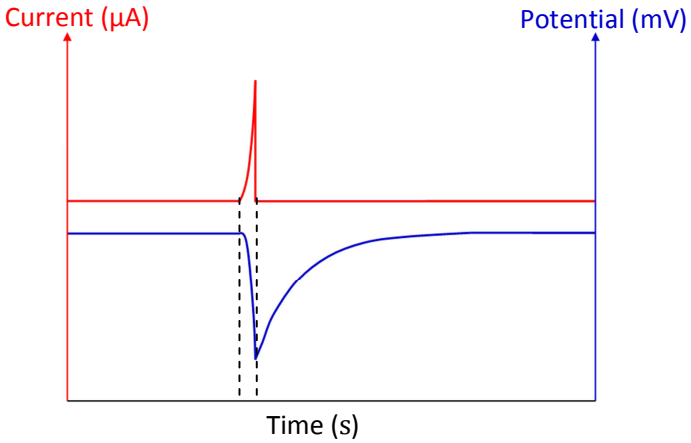

Figure 12: Idealized potential and current noise pattern under open circuit potential of metastable pitting event (Modified after [43]).

During pit's growth, the cathodic current comes from the discharging of passive film's capacitance. And after repassivation, where the potential slowly recovers, the capacitance is recharged by a cathodic oxygen reduction reaction [16]. The event of metastable pitting corrosion may be observed taking place individually or as superimposed events if they occur frequently enough. The anodic event of metastable pitting covering the period from pit birth to pit death can be short-lived of approximately 1 second [15]. However, the electrochemical potential noise at OCP of aluminium show different features, indicating the mechanism during pitting corrosion is different from metastable pitting corrosion of stainless steel.

The analysis of EN data can be carried out in both time and frequency domains. In the time domain, the most interesting parameter is the noise resistance (R_n). The R_n is defined as the ratio of the standard deviation of potential noise to that of current noise:

Noise resistance: $$R_n = \frac{\sigma_E}{\sigma_i}$$

This noise resistance has been found to associate with polarization resistance (R_p) from polarization measurement and the ratio $1/R_n$ is in direct proportional to the instantaneous corrosion rate [43]. The noise data also can be transformed into the frequency domain using fast Fourier transform algorithm (FFT) and fast wavelet transform algorithm (FWT) [13].

8.4) The exposure testing:

The exposure testing, which is the non-electrochemical technique, of sample to service or accelerated environment is widely used [38]. The samples are simultaneously exposed in environmental condition. After the exposure, the samples are evaluated by other techniques such as the surface morphology analysis by digital microscopy.

9. Aluminium Alloys

Alloying elements such as copper, magnesium, manganese, silicon and zinc are added to wrought alloys in quantities up to 7% by mass. Wrought aluminium alloys are divided into 8 alloy series by main alloying element (table 2). The alloying elements determine the common properties of alloys therefore the alloys belonging to the same series exhibit a set of common properties such as mechanical properties (corrosion resistance and etc.). Only 3 series of aluminium alloys will be mentioned in this current research (e.g., 2000, 5000 and 6000).

Mode of hardening	Series	Alloying element	Concentration range (%)	Additives	Mechanical strength R_m (MPa)
Strain hardening	1000	None		Cu	50–160
	3000	Manganese	0.5–1.5	Mg, Cu	100–240
	5000	Magnesium	0.5–5	Mn, Cr	100–340
	8000	Iron and silicon	Si: 0.30–1 Fe: 0.6–2		130–190
Age hardening	6000	Magnesium and silicon	Mg: 0.5–1.5 Si: 0.5–1.5	Cu, Cr	200–320
	2000	Copper	2–6	Si, Mg	300–480
	7000	Zinc and magnesium	Zn: 5–7 Mg: 1–2	Cu	Without copper 320–350 With copper 430–600
	4000	Silicon	0.8–1.7		150–400

Table 2: Series of wrought alloys [36]

9.1) The series 2000

The main alloying element in this series is copper. The alloys in this series exhibit good mechanical properties, fracture toughness and resistance to crack propagation. The AA2024 with high magnesium content is mainly used in aircraft construction.

9.2) The series 5000

The main alloying element in this series is magnesium. The mechanical properties of alloys in this series increase with increasing magnesium content. However, the alloys rarely contain more than 5% magnesium because above that level, the stability of these alloys is reduced. These alloys have good resistance to corrosion. AA5052 exhibits a good compromise between mechanical resistance, formability, fatigue resistance and corrosion resistance. Therefore it is widely used in many applications such as food cans and vehicle bodies.

9.3) The series 6000

The 2 main alloying elements in this series are magnesium and silicon. The alloys in this series show a good aptitude for hot transformation by rolling, extrusion and forging, a high level of mechanical properties and good resistance to corrosion.

CHAPTER **IV**

EXPERIMENTAL SET-UPS AND RESULTS

1. Electrochemical Noise(EN) Measurement:

The spontaneous fluctuation of potential and current, which is called electrochemical noise, was monitored in order to study the corrosion process on pure aluminium surface.

1.1) Noise behaviour of Al with Al reference electrode

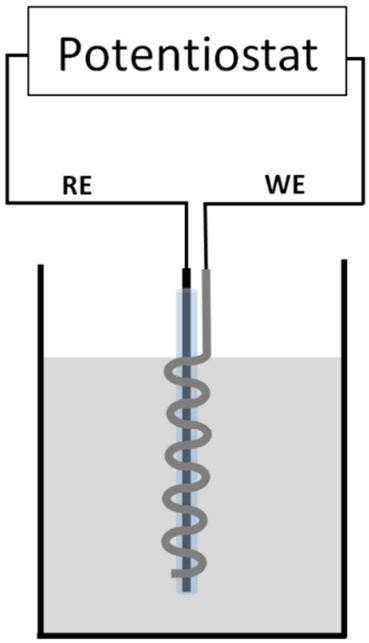

Figure 13: Twist electrode set-up.

The small distance between working electrode (WE) and reference electrode (RE) was essential prerequisite for EN measurement in order to reduce the environmental disturbance. Therefore twist electrode set-up of one working electrode (figure 13) was applied for the EN measurements. For this twist electrode set-up, the reference electrode was firstly wrapped with

tissue to protect the direct contact with working electrode and then the working electrode was tightly twisted around reference electrode. As this twist electrode set-up, the distance between working and reference electrodes was less than 1mm. The testing system wasn't shielded from the disturbance of external signal by faraday cage. All electrochemical measurements were performed using a PGU100PCR potentiostat controlled by personal computer. During the measurement, potential and current signals were simultaneously measured in the open electrical circuit with the sampling interval of 0.1s (or sampling of 10Hz). The data were recorded immediately after the immersion of the electrodes in the solution. All of the EN measurements in this study were carried out at room temperature. The fluctuations of both potential and current signals were analysed in the both time and frequency domain.

As pure aluminium was the material under study and the potential and current variations of aluminium for this measurement set-up was unknown, two pure aluminium wires were used as working and reference electrodes in this first measurement in order to get higher potential and current variations. Firstly, these two electrodes were immersed in tap water for 3 days for the purpose of building up spontaneous oxide layer (passivation). After that NaCl was put into the solution.

It can be seen in figure 14 that generally in tap water, the baseline of potential is clearly defined and only several fluctuations of potential and current signals show up. At the beginning of immersion in tap water, baseline of potential decreases possibly due to the modification or dissolution of air-formed oxide film on the surface of pure aluminium electrode. After short time of immersion this baseline of potential gradually increases with time, implying of the growing of the oxide film on the surface. The fluctuations or noises of potential and current signals in tap water are characterized by single or isolated transients (figure 15). The first isolated transient is observed after immersion in tap water for about 12h, indicating that the Al/Al system in tap water is in complete passive state for 12h before the first localized corrosion attack. During immersion in tap water, a lot of transients are observed. The duration of each isolated transient is in the range of 8s to almost 1h and the magnitude of potential and current fluctuations are in the range of 10 to 89mV and 0.15 to 0.83pA, respectively. The detail of fluctuations, or corrosion transients, of potential and simultaneous current signals in figure 16 and 17 shows that the transients of corrosion event starting with potential drops (negative ΔE) always corresponds with current rises (positive ΔI). On the other hand in the red dashed circle of figure 17 (right)

when the potential rise up, no corresponding current transient is observed. Therefore, it can be interpreted as an artefact. Figure 18 shows other examples of noise from artefact when there is noise in current signal but no corresponding noise in potential signal.

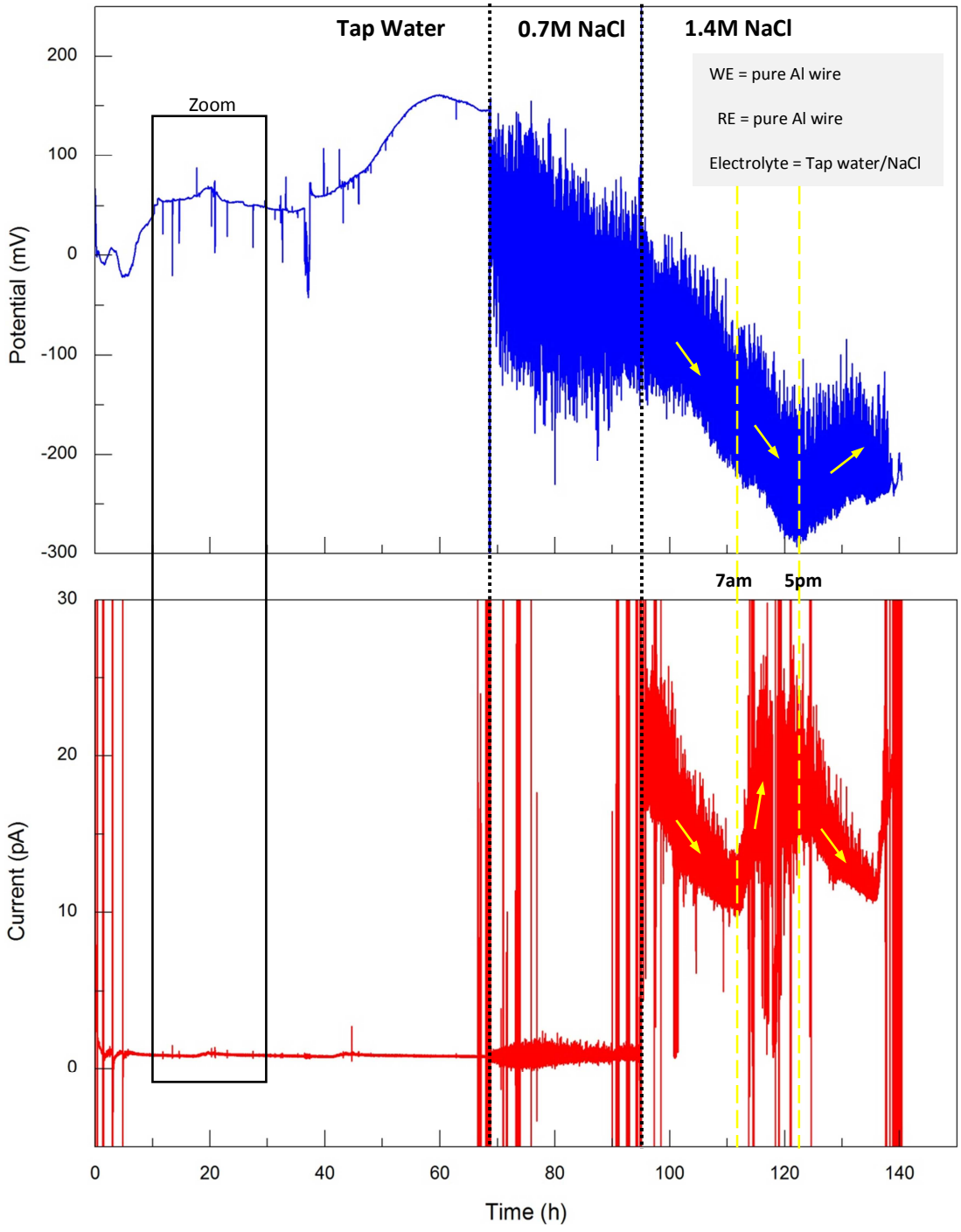

Figure 14: Potential and current signals of Al with Al reference electrode in NaCl solution.

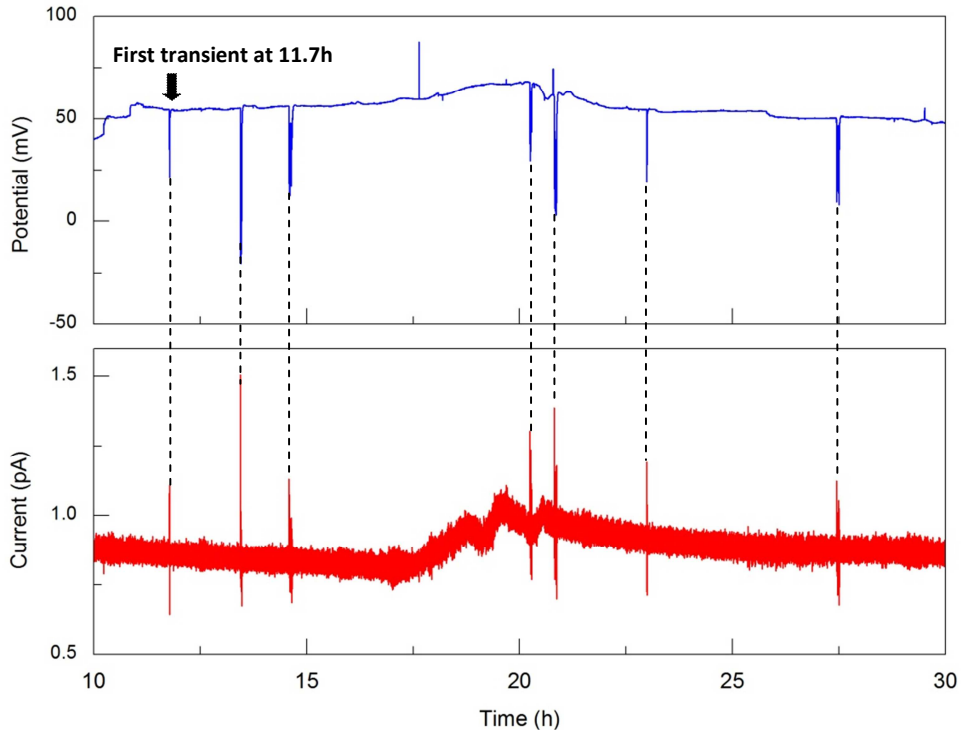

Figure 15: Zoom of potential and current signal in tap water.

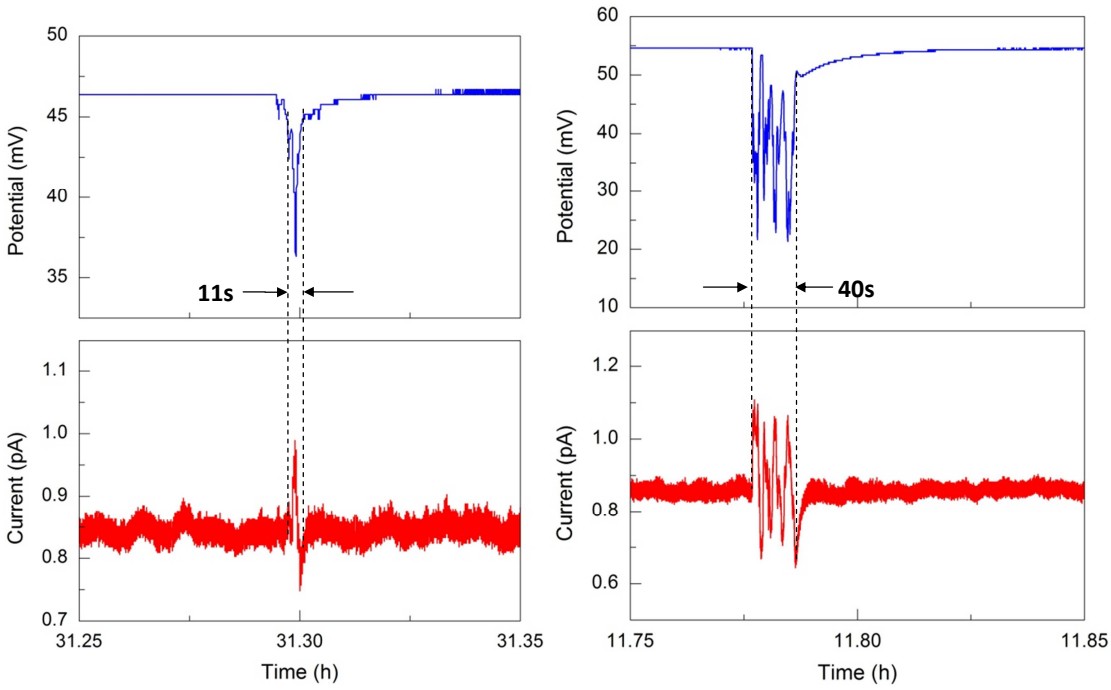

Figure 16: Examples of short-time transients in tap water.

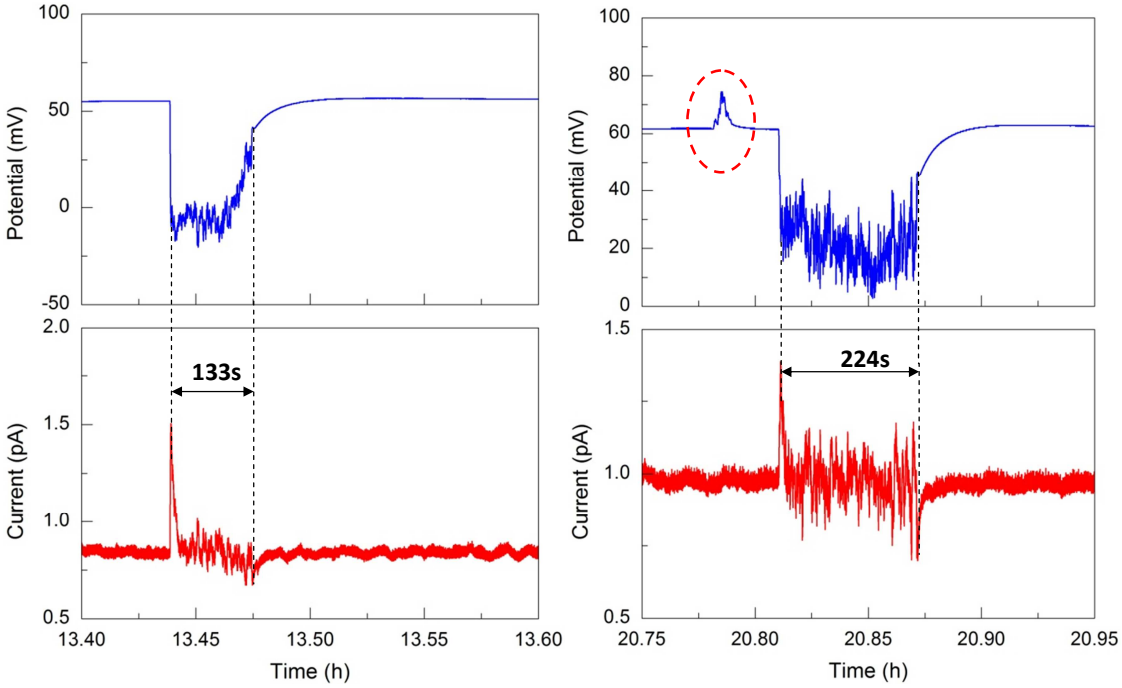

Figure 17: Examples of long-time transients in tap water.

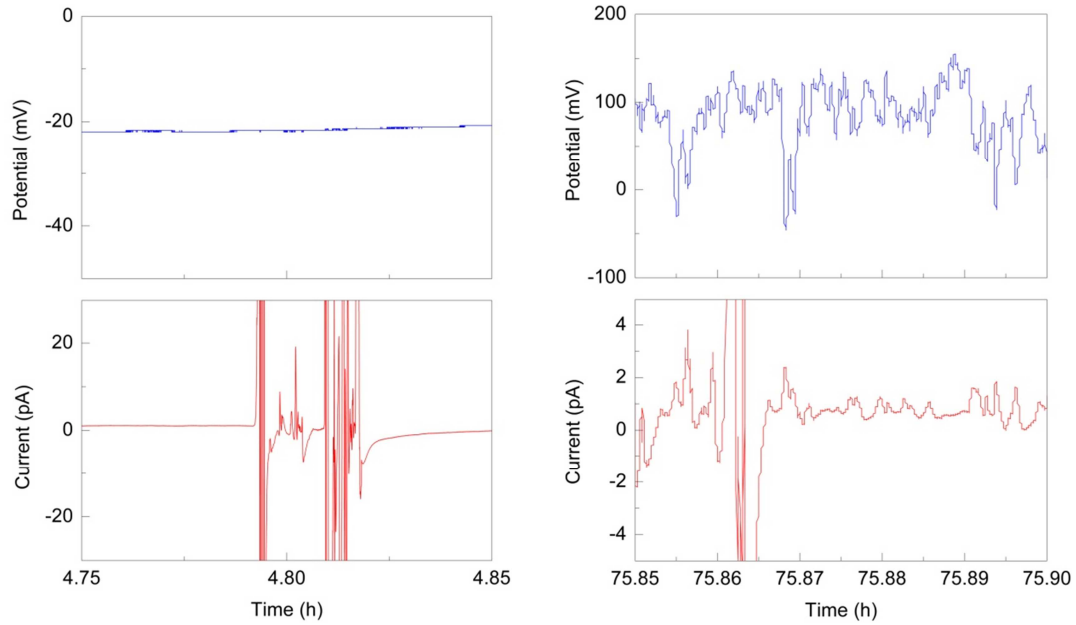

Figure 18: Examples of noise signal from artefact: (left) in tap water and (right) in NaCl solution.

A model of the isolated transient for explanation of pitting corrosion event of pure aluminium in tap water may comprise of 3 stages: pit initiation, pit propagation (or pit growth), and repassivation.

For pit initiation: After breakdown of oxide film occurs on the surface, pit is initiated. Anodic aluminium dissolution is active so that the current rapidly increases in anodic direction (positive ΔI) from the baseline of current signal. During this anodic aluminium dissolution, many electrons left in aluminium metal are stored in the interfacial capacitance, resulting in a shift down of potential (negative ΔV).

Pit Propagation: The initiated pit will continue to propagate by two reactions such as anodic aluminium dissolution at the pit's bottom and cathodic reduction for example hydrogen evolution outside and inside [16] the pits. Therefore the current continues deviating from passive current and the potential will still not return back to passive potential. The relatively small fluctuation during this propagation stage is likely expected because of the fluctuation of mass transport rates into and out of the pits [44].

Repassivation: After the death of the pit (or repassivation), anodic dissolution stops. This results in the rise up of potential and the increase of current from last cathodic spike to passive current. After that the potential will slowly recover back to passive potential reflecting the relatively slow consumption of stored electron by cathodic reactions.

As a relatively short anodic transient, which is a rapid potential drop followed by slower recovery, is the signature character of individual metastable pitting process [43, 44], it can be deduced that:

a) The transient in figure 16 (left) is a result of *one individual metastable pitting event* attacking on the surface.
b) The transient in figure 16 (right) is the combination of many short anodic sub-transient in one transient. It therefore is hypothesized that this transient comes from *superposition of many metastable pits events*.
c) The long-time isolated transients in figure 17 (left and right) show that the fast potential drop and simultaneous current rise are not suddenly followed by slow return back to the passive value, but it keeps fluctuating with relatively small amplitude for some period of time before the recovery. This small fluctuation out of the baselines of potential and current indicate the pit propagation. This pit propagation stage is the longest stage among the 3 stages of pitting corrosion. Thus it can be deduced that these long time isolated transients are the consequence of *one individual growing pit event*.

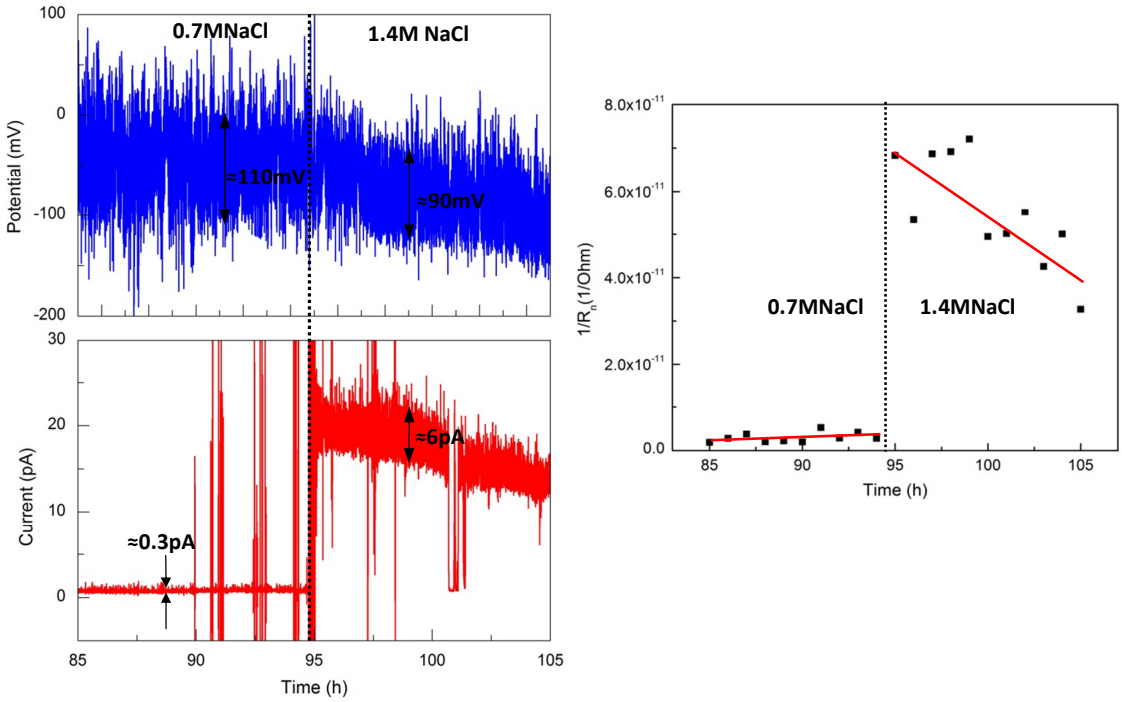

Figure 19: Effect of NaCl concentration on: (left) Noise's Amplitude and (right) noise resistance.

After adding NaCl in tap water, the vigorous fluctuations of both potential and current signals show up (figure 14). This indicates less stability of pure aluminium in NaCl solution than in tap water. The frequency and amplitude of potential and current fluctuations increases and the clearly defined baseline of potential disappears. This implies that a large number of corrosion events take place during the immersion of pure aluminium in NaCl solution. In contrast to the isolated transients in tap water, many overlapping transients are observed in NaCl solution. Therefore, transient isolation for additional shaped analysis is not possible in NaCl solution. Only the trend of overall signals is analysed and the effect of NaCl concentration on corrosion behaviour of pure aluminium is studied here. Figure 19 (left) shows that the average amplitude of potential fluctuations slightly decreases from 55 to 45mV but the average amplitude of current fluctuations largely increases from 0.15 to 3.0pA after the concentration of NaCl in the solution has been increased from 0.7 to 1.4M. This means that the concentration of chloride ions affects the amplitude of potential and current fluctuations. Figure 19 (right) shows the $1/R_n$, which is directly proportional to corrosion rate. Suddenly after adding more NaCl, the corrosion rate of pure aluminium in 1.4M NaCl solution shifts to much higher rate than that in 0.7M NaCl solution. This reflects that the chloride ion concentration in solution strongly influences the corrosion rate of pure aluminium.

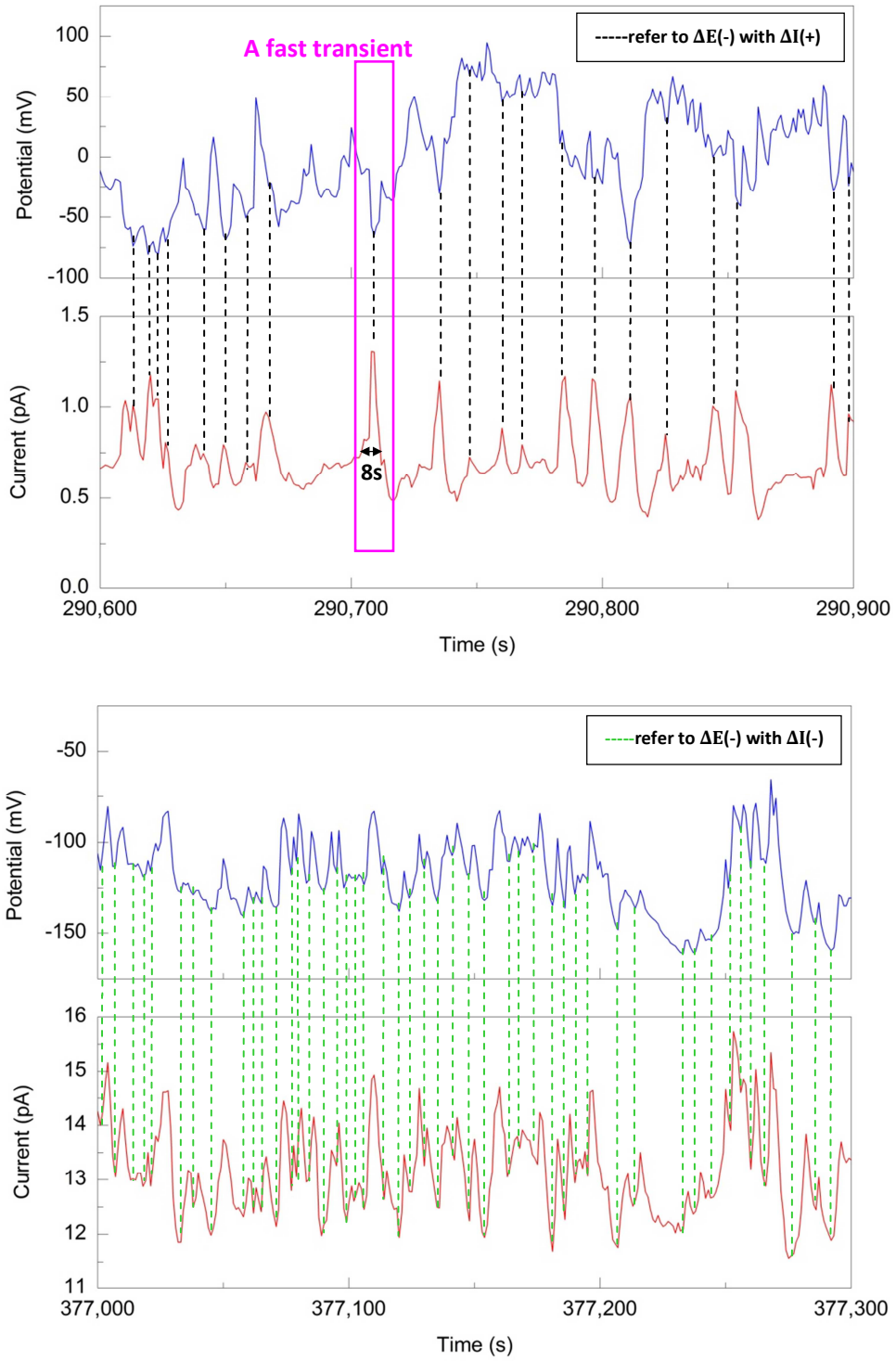

Figure 20: Zoom of potential and current: (top) in 0.7M and (bottom) in 1.4M NaCl solution.

The overlapping transients of potential and current signals in figure 20 reveals that there is a relationship between the fluctuations of potential and current signals and these relationships

change with concentration of NaCl in solution. The observed relationships between potential and current fluctuation is:

a) In 0.7M NaCl solution, most of the transients are characterized as a potential drop (negative ΔV) coupled simultaneously with a short anodic current rise (positive ΔI). According to [13], this implies that pitting corrosion occurs on pure aluminium surface. As each transient lasts less than 20s and the character of these fast transients have been similar to that of metastable pitting as mentioned in [43, 44]. This reflects that the *metastable pitting corrosion* occurs on pure aluminium surface.

b) In 1.40M NaCl solution, the relationship between potential and current fluctuations can be described as a positive or negative potential fluctuation responded to positive or negative current shift, respectively. The overall changes in potential are similar to those in current. According to [13], this phenomenon indicates that *anodic dissolution* takes place on pure aluminium surface as will be analyzed later.

c) The numbers (or frequency) of fast potential transients in 0.7M and in 1.4M NaCl solution are almost identical but the frequency of fast current transient in 1.4M NaCl is higher than in 0.7M NaCl solution. This possibly implies that the corrosion events occur more frequently in solution with higher NaCl concentration.

Generally, various transients indicate different corrosion mechanisms [13]. This means after NaCl concentration of solution increases from 0.7M to 1.4M, the predominant corrosion mechanism of pure aluminium changes from *metastable pitting corrosion* to *anodic dissolution* process. The anodic dissolution process with relatively high current in 1.4M NaCl is induced or accelerated by an increase of chloride ion concentration. This possibly relates to the propagation (or growth) of active pit, which is formerly initiated in 0.7M NaCl. As the amplitude of current fluctuations (figure 20) as well as the corrosion rate (figure 19, right) increases with increasing NaCl in solution, it can be deduced that the amplitude of current fluctuation is direct relation to corrosion rate. Therefore for this twist electrode set-up of one working electrode, the amplitude of current fluctuation can be used as a parameter to compare the corrosion rate of metals.

The total charge passed for fast transient in a pink square (figure 20, top) is calculated by integrating current transient with time ($Q = \int i dt = 10.3 pC$). This charge is a result of the

formation of a metastable pit. From faraday's equation, the charge passed for this fast transient is related to volume of a metastable pit:

$$\text{Volume} = \frac{\text{Charge passed} \times \text{Molecular mass}}{\text{Faraday constant} \times \text{n} \times \text{density}}$$

where molecular mass of aluminium is 26.98g/mol, faraday's constant is 96500C/mol, density of aluminium is 2.7g/cm^3 and charge number of aluminium oxidation is 3. If the metastable pit is assumed to be hemispherical shaped, the pit radius can be calculated by the equation below [45]:

$$\text{Pit radius} = \sqrt[3]{\frac{3 \times \text{volume}}{2\pi}}$$

From the charge of 10.3pC, the calculated radius of metastable pit is about 55nm. This site of metastable pits possibly reactivates again and form larger pit's size. Moreover, it was also mentioned in [45] that the radius of metastable pit should be less than 10µm. This confirms that the transient in a pink square (figure 20, top) is the result of metastable pitting corrosion.

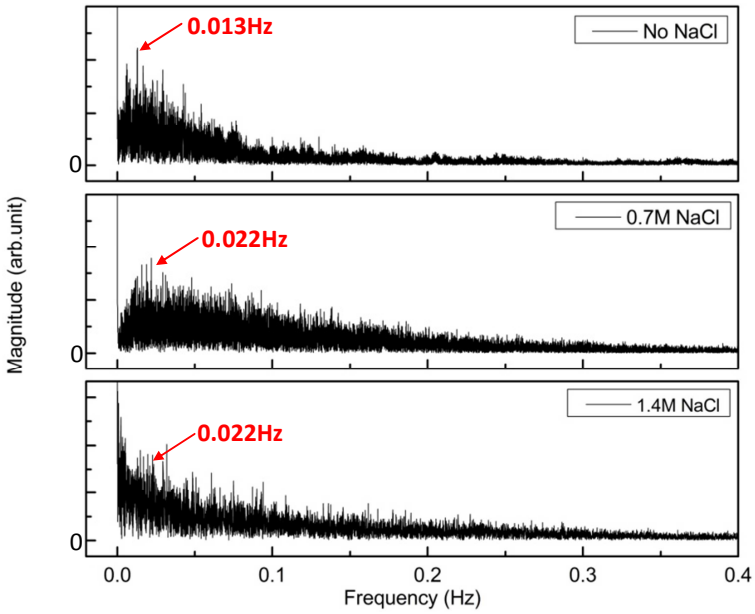

Figure 21: Frequency spectra of current signal.

After remove the baseline signal, the noise data are transferred into frequency domain using fast Fourier transform (FFT). The frequency spectra of current signal changes with increasing

NaCl concentration in solution, but that of potential noise gives no significant information possibly due to its relative higher sensibility. Thus in this research, only the frequency spectra of current are analysed. It is found that in tap water and 0.7M NaCl solution, where metastable pitting corrosion takes place, a peak of frequency distribution of current signal are observed. This peak shifts from frequency 13mHz in tap water to 22mHz in 0.7M NaCl solution. After that when the concentration of NaCl in solution increases from 0.7M to 1.4M NaCl, large frequency distribution is observed and the peak is not clearly seen possibly due to a very high number of corrosion events take place in solution with this high concentration of NaCl.

Therefore, this measurement shows that pure aluminium can be seriously corroded in NaCl solution but much less corroded in tap water.

1.2) Noise behaviour of Al with NiO (oxidised wire) reference electrode

The result from the former measurement shows that the measured current is extremely small but measurable. Therefore in order to monitor the corrosion events taking place on only one electrode (working electrode), NiO (oxidised wire) was used as a reference electrode instead of Al reference electrode. Even through NiO (oxidised wire) is not a commonly used reference electrode, NiO (oxidised wire) reference electrode was applied for this measurement since it can be twist around working electrode. Firstly Al working and NiO (oxidised wire) reference electrodes were spontaneously passivated in tap water for about 2 day and then 0.7M NaCl was added to tap water.

In tap water, the baseline of potential is defined and some fluctuations of potential and current signal are detected (figure 22). Suddenly after adding NaCl to tap water, the fluctuations occur more seriously. This indicates that the Al/Ni system is more stable in tap water than in NaCl solution.

In tap water, the sharply decrease of baseline of potential at the beginning of immersion implies the modification or dissolution of air-formed oxide film. After 2h of immersion, the potential reaches the lowest value and then the baseline of potential sharply increases, indicating formation of passive oxide film. Figure 23 shows, the fluctuations of potential and current occurs simultaneously. The first attacking of corrosion event occurs at 7.5h, after that the

baseline of potential increases with relatively slower rate. After immersion in tap water for 25h (dashed line in figure 22), the baseline of potential nearly disappears owing to the corrosion events seriously occurring on the surface of pure aluminium. In tap water, a lot of transients are observed. The corrosion events last from 15s to more than 4h and the magnitude of potential and current fluctuations of the corrosion transients are in the range of 8 to 188mV and 0.10 to 1.0pA, respectively.

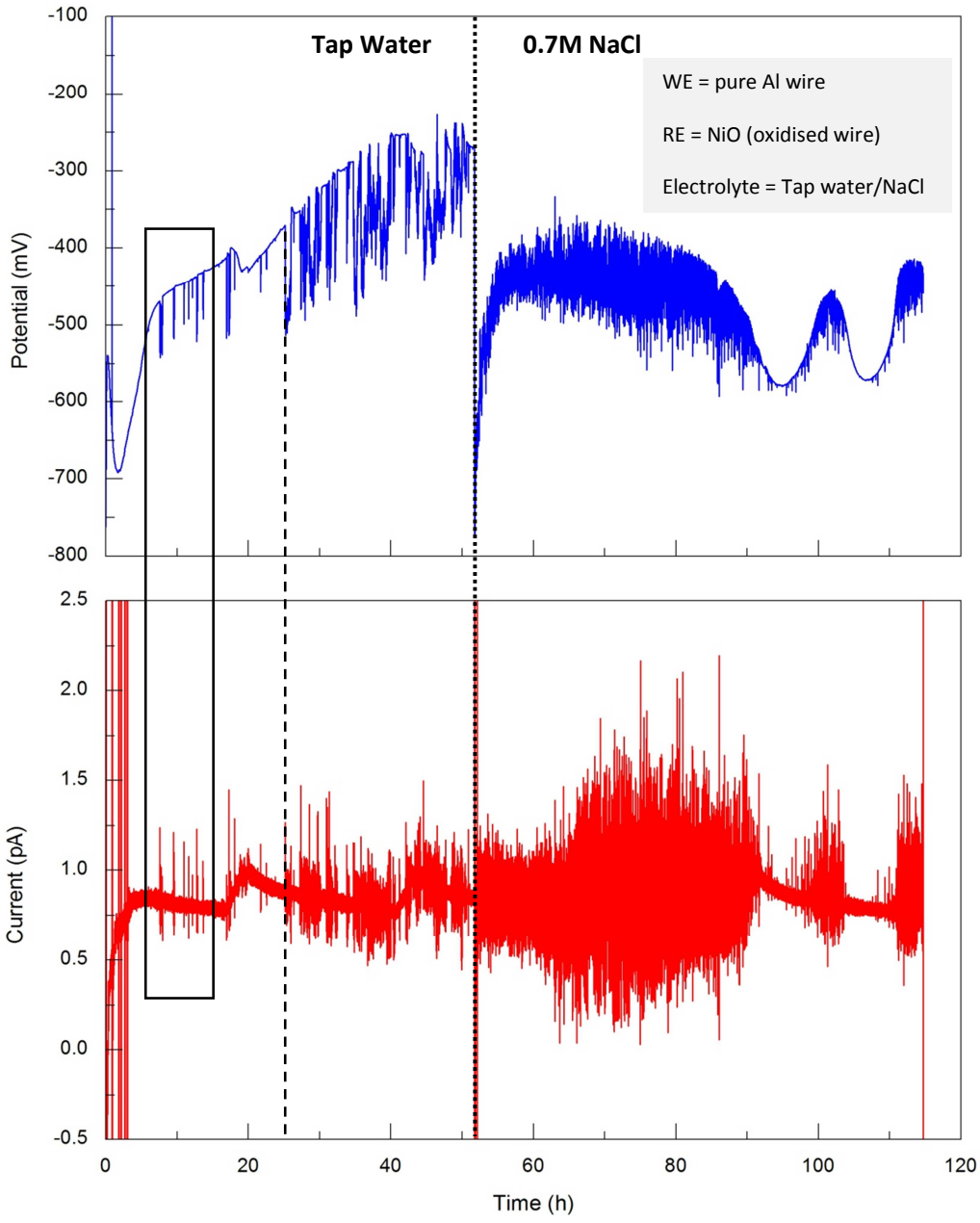

Figure 22: Potential and current signals of Al with NiO reference electrode in NaCl solution.

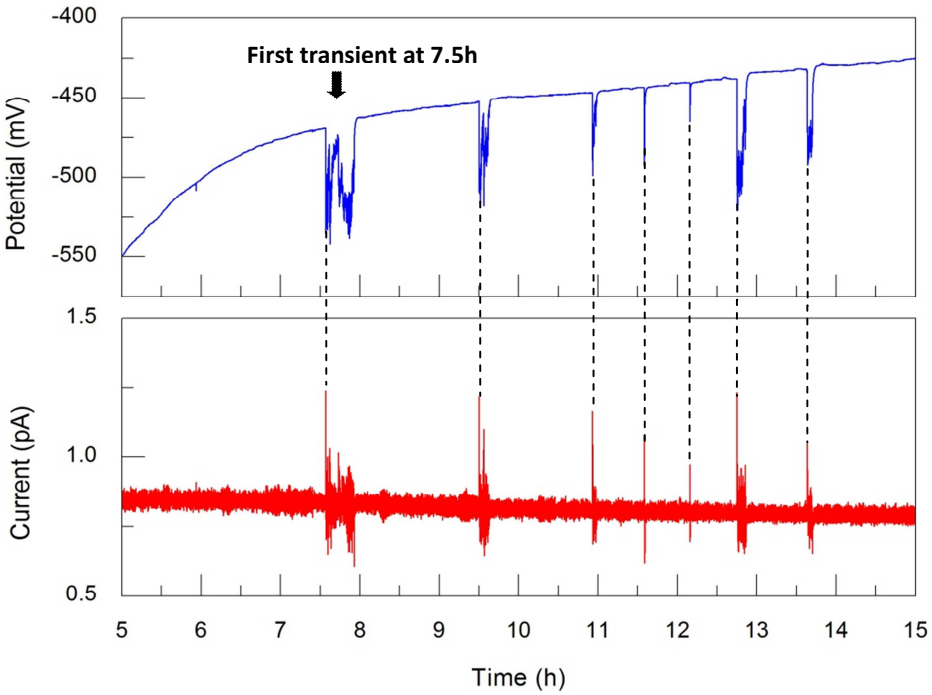

Figure 23: Zoom of potential and current signals in tap water.

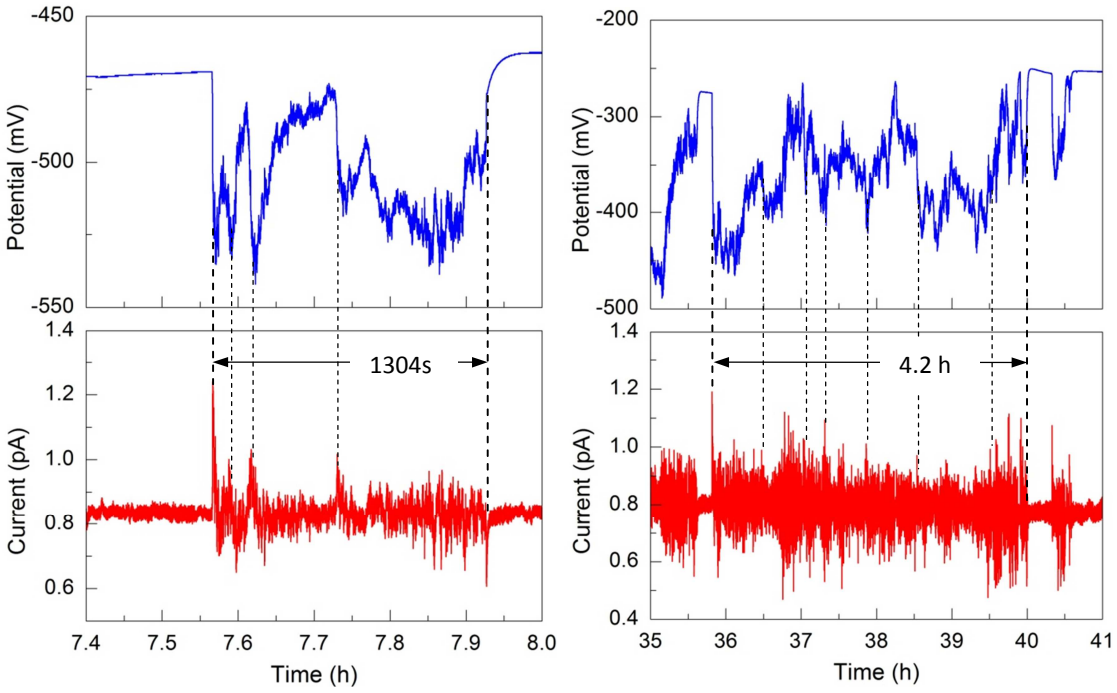

Figure 24: Examples of potential and current transients in tap water.

The potential and current transient in tap water (figure 24) is characterized by a large isolated transient. As the potential of the transient starts with the rapid negative change (negative ΔV)

and the corresponding current starts with anodic current rise (positive ΔI), this can be attributed to pitting corrosion occurring on the surface of pure aluminium. Two possible models may be able to explain the pitting corrosion mechanism of the transients in figure 24:

1. Since each transient takes extremely long time in pit propagation stage which is between pit initiation and pit death (repassivation), this transient may be attributed to *one large growing pit event*.

2. During each transient, the potential gradually returns back to nearly passive potential and then suddenly drops again. This may represent another pit starting suddenly after or during the repassivation of the former pit. The starting of another pit may refer to the initiation of new pit at another pitting site or the reactivation again of the former pitting site. Therefore this transient may be the result of *the overlapping of a few small growing pit and metastable pit events* or *reactivation of a pit to form larger pitting size*.

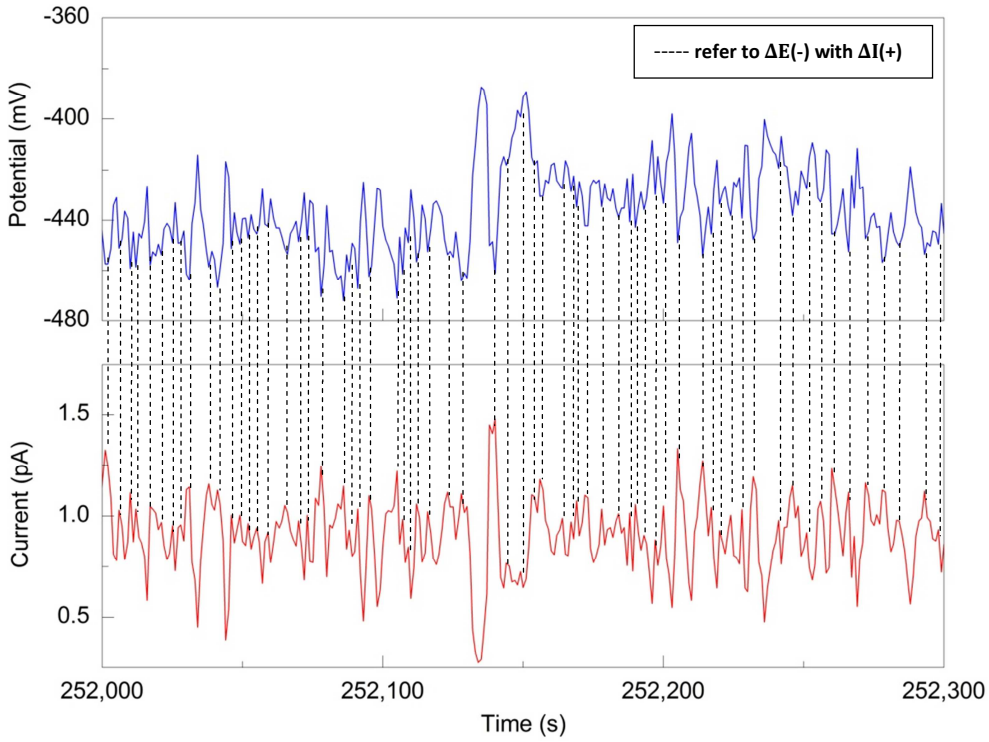

Figure 25: Zoom of potential and current signals in 0.7M NaCl.

After adding NaCl in tap water, overlapping of many transients is observed. Therefore the analysis of transient's shape is not possible. Only the relationship between the fluctuation of

potential and current signals in NaCl solution is studied and shown in figure 25. The transients are characterised as a potential drop (negative ΔV) responded with a simultaneous current rise (positive ΔI). Therefore it can be deduced that these overlapping transients in NaCl solution arise from the overlapping of many pitting corrosion events.

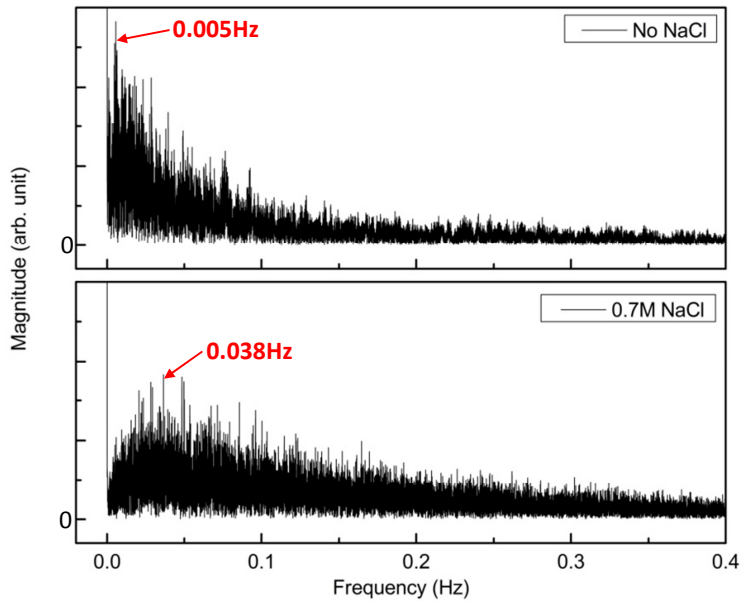

Figure 26: Frequency spectra of current signal.

The frequency spectra of current signal in figure 26 shows, the frequency distribution of current signal changes after adding NaCl in tap water. The frequency spectra in tap water show the highest peak at 5mHz but in 0.7M NaCl, their highest peak shifts to 38mHz.

This measurement shows that Al/NiO system is fairly pitting corroded in tap water and the pitting corrosion is dramatically accelerated in NaCl.

1.3) Noise behaviour of NiO (oxidised wire) with C reference electrode

As mentioned in measurement 1.1 that pure aluminium is surely corroded in NaCl. However it is not certain that for Al with NiO (oxidised wire) system in NaCl solution, only pure aluminium is corroded or both aluminium and NiO (oxidised wire) are corroded. Therefore for this measurement, the corrosion of NiO (oxidised wire) in NaCl solution was verified. In order to verify the corrosion behaviour of NiO (oxidised wire), it was compelled to use as a working

electrode. Since graphite was expected not to corrode in NaCl solution, graphite rod was used as a reference electrode. As fragile graphite, the parallel electrodes set-up with one working electrode (figure 27) was used in this measurement instead of twist electrode set-up. The distance between nickel working electrode and graphite reference electrode was kept to less than 3mm. At the beginning, NiO (oxidised wire) electrode was spontaneously passivated in tap water for 1 day and then 0.7M NaCl was added to tap water.

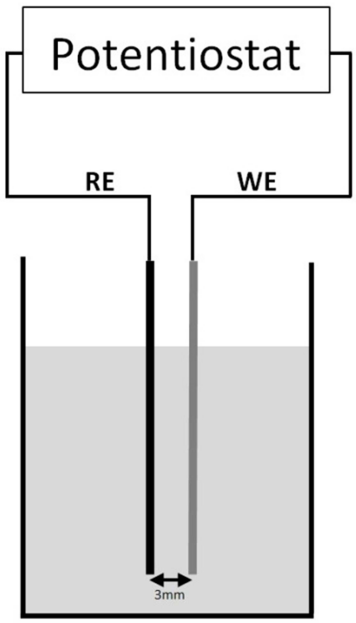

Figure 27: Parallel electrodes set-up.

Compared to Al with Al reference electrode system and Al with NiO (oxidised wire) reference electrode system, the potential and current signals of NiO (oxidised wire) with C reference electrode system in figure 28 are different. It is clearly seen that the fluctuation of potential and current signals in both tap water and especially in NaCl solution are negligible. This implies that no significant pitting corrosion takes place on nickel surface in both tap water and NaCl solution.

In tap water, the baseline of potential slightly decreases with time, implying that the predominant reaction is the modification of air-formed oxide film. While in NaCl solution, the baseline of potential increases with time, implying that passivation predominantly takes place on the surface of NiO (oxidised wire). After adding NaCl to tap water, the fluctuation of current keeps negligible and the amplitude of potential transients are relatively small. Moreover, no

transient of the current rise simultaneously reacting to the potential drop is observed. This confirms that no pitting corrosion occurs on the surface of NiO (oxidised wire) in NaCl solution.

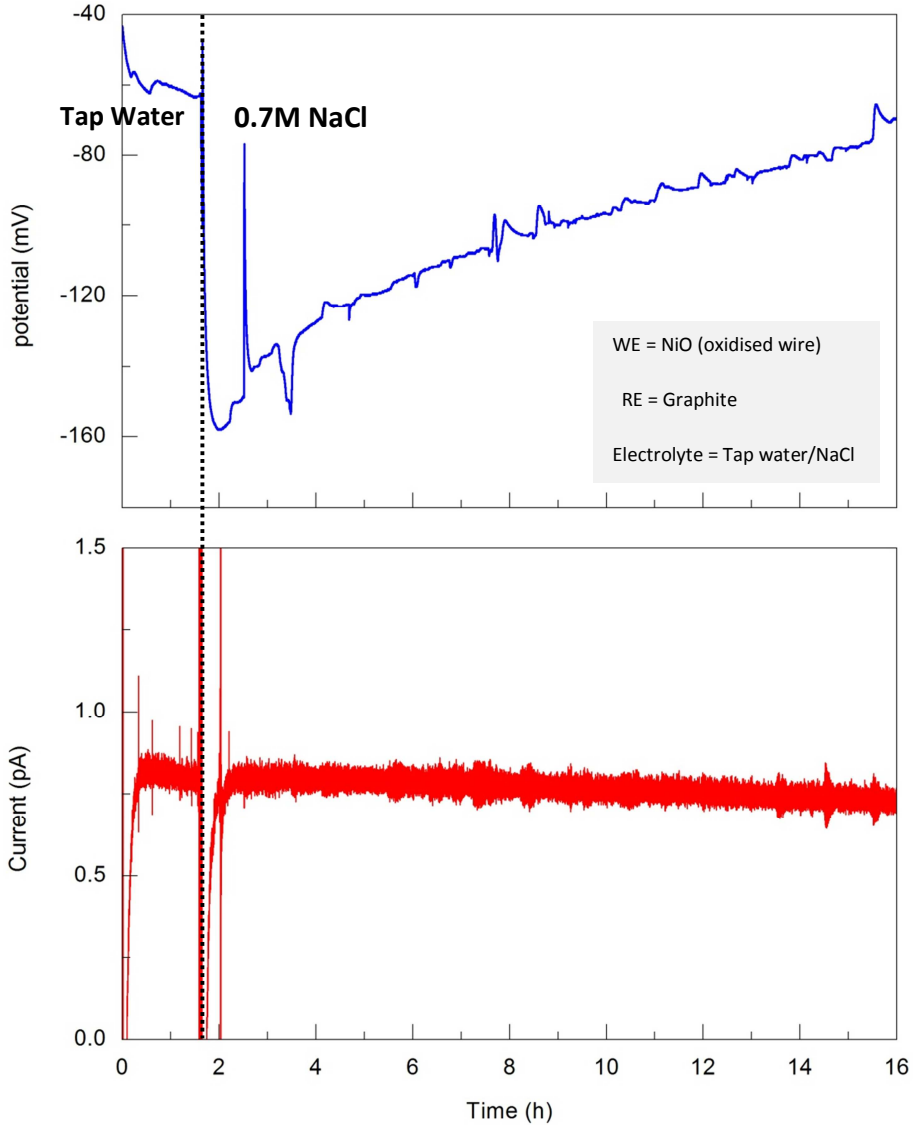

Figure 28: Potential and current signals of NiO (oxidised wire) with C reference electrode in NaCl solution.

This measurement shows that no significant pitting corrosion occurs on nickel and graphite in both tap water and NaCl solution. Therefore NiO (oxidised wire) and graphite can be used as a reference electrode.

1.4) NiO (oxidised wire) reference electrode testing

In this measurement, two NiO (oxidised wires) were used as both working and reference electrodes in order to confirm the proper use of NiO (oxidised wire) as reference electrode. The twist electrode set-up of one working electrode (figure 13) was again applied. At the beginning, these working and reference electrodes were spontaneously passivated in tap water for 1 day and then 0.7M NaCl was put into tap water.

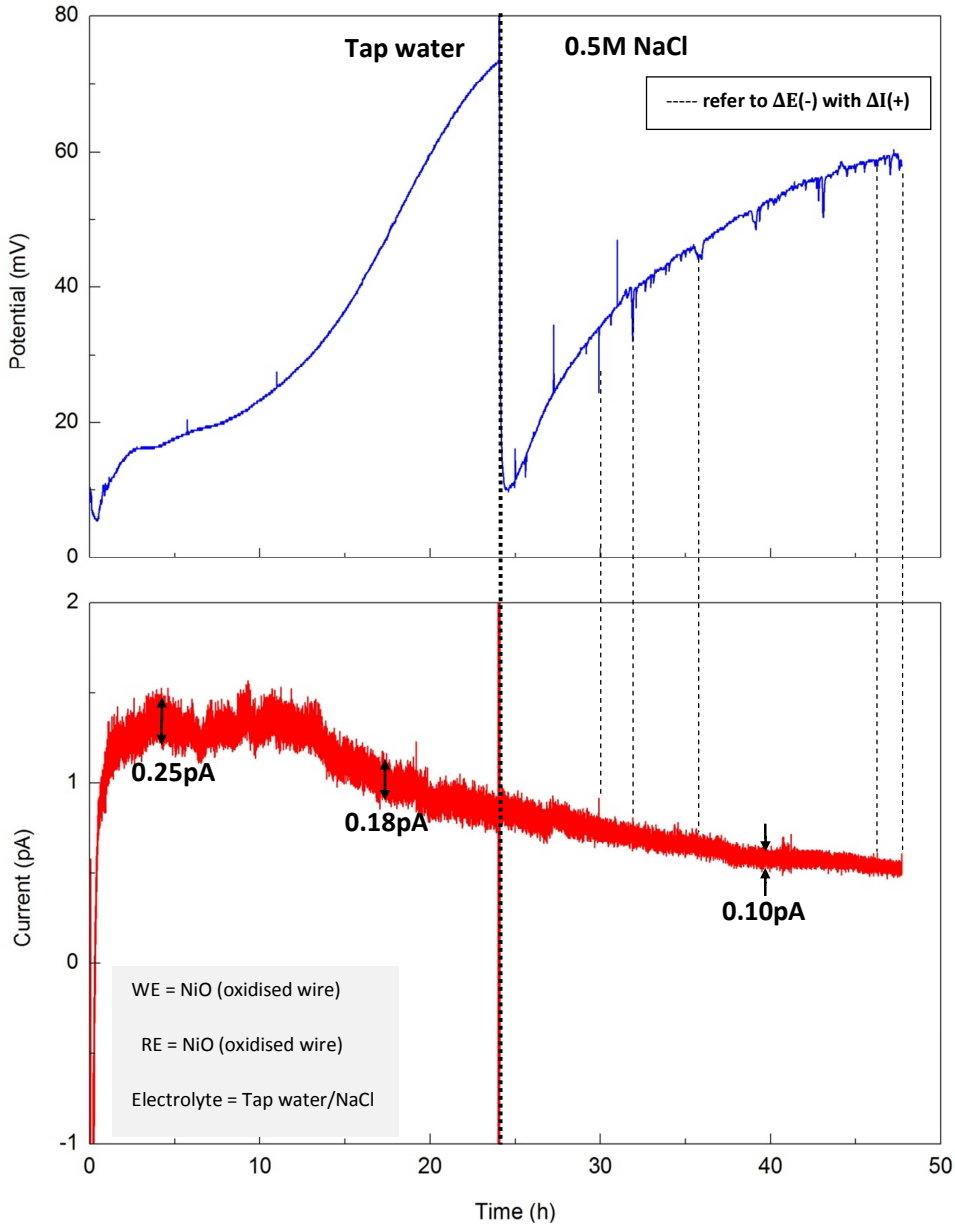

Figure 29: Potential and current signals of NiO (oxidised wire) with NiO (oxidised wire) reference electrode in NaCl solution.

The potential and current signals in figure 29 show that:

a) The current in tap water remains fairly constant at around 1.3pA for around 14h at the beginning and then slowly decreases with time, possibly indicating the formation of oxide film and the decrease of formation rate due to the thickening of oxide film. After adding NaCl to tap water, the current still slowly decreases with time indicating the slow thickening of oxide film even in NaCl solution.

b) No significant fluctuations of potential shows up in tap water and after adding NaCl, serious fluctuation of potential has not still been observed, implying no serious pitting corrosion taking place on NiO in both tap water and NaCl solution. The amplitude of current fluctuations is less than 0.2pA and does not increase at all after adding NaCl in tap water. It even decreases with processing time, confirming that the passive film is thickened with processing time even in NaCl solution. However, a few fast isolated transient is detected in NaCl solution (the black dashed lines in figure 29).

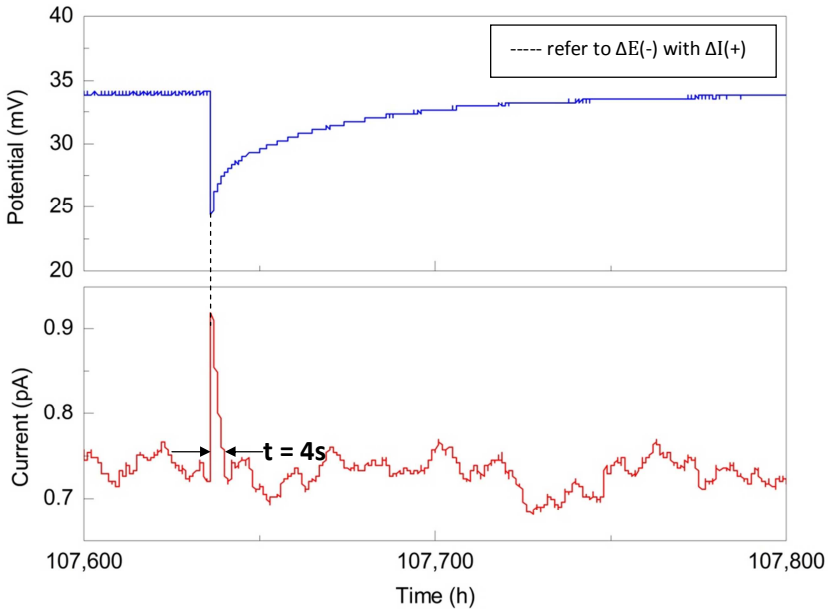

Figure 30: Potential and current signal of fast isolated transient on nickel in NaCl solution.

The fast isolated transient (in figure 30), whenever identifiable, tends to follow the pattern of metastable pitting event. This indicates the attack of metastable pitting corrosion on nickel surface in NaCl solution. However, only a few transients with short time of much less than 10s and small magnitude of less than 10mV for potential and 0.2pA for current are observed.

Therefore it can be deduced that the attacking of metastable pitting corrosion on surface of nickel in 0.5M NaCl is negligible.

Therefore, this measurement confirms that no significant pitting corrosion takes place on NiO in NaCl solution. Therefore this verified the use of NiO as a reference electrode for corrosion characterization.

1.5) Effect of surface area on noise behaviour of aluminium

The objective of this measurement was to study the effect of surface area on potential and current signals of pure aluminium in NaCl solution. Parallel electrodes set-up with one working electrode (in figure 27) was used in this measurement. The aluminium wire and nickel wire were used as working electrode and reference electrode, respectively. Firstly, 8cm of electrodes were spontaneously passivated in tap water for about 1 day and then only 2.5cm of electrodes were immersed in 0.5M NaCl solution for 2 days. After that 0.5M NaCl solution were filled up to get 8cm length of electrodes in 0.5M NaCl solution as shown in figure 31.

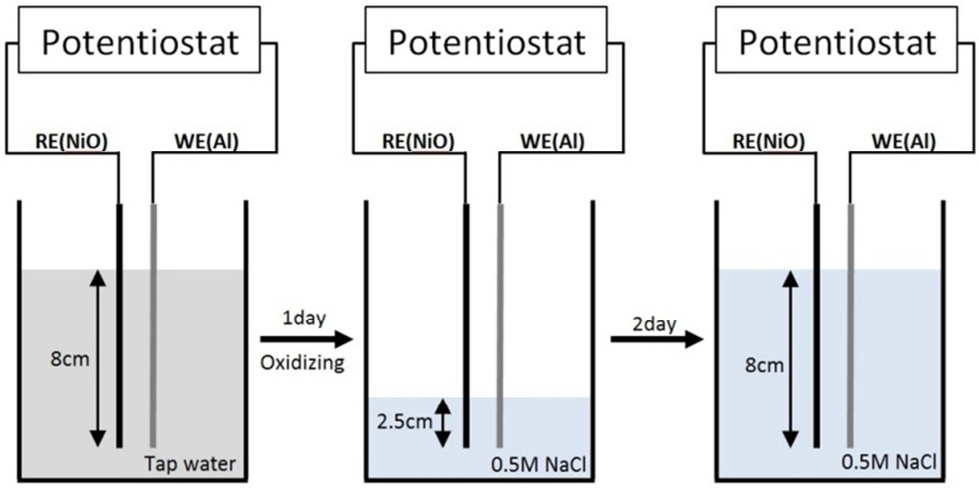

Figure 31: Measurement steps of study the effect of surface area on noise behaviour.

The potential and current signals in figure 32 show that the average amplitude of potential signal decreases from about 32 to 10mV and the average amplitude of current signal decrease from 3.8 to 1.2pA with increasing surface area. Therefore it can be deduced that the amplitude of both potential and current signals depend on the surface area of electrode.

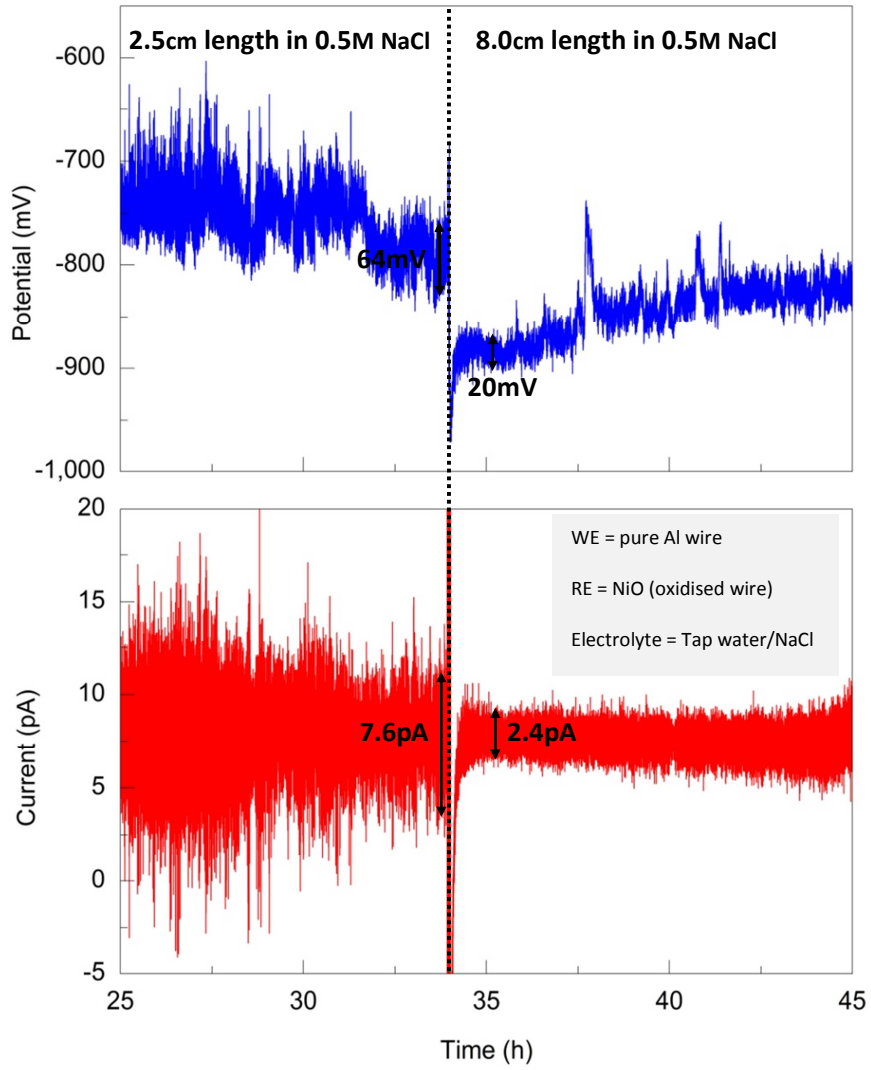

Figure 32: Potential and current signals at different surface areas.

Theoretical background shows that:

During anodic stage after pit initiated, electronic charge left in the metal is stored in interfacial capacitance [19].

From $\Delta V = \frac{Q}{C}$; where ΔV is downward potential step size, Q is the faraday charge equivalent of metal oxidised from anodic dissolution at the pit initiation and C is total interfacial capacitance.

From $C = C_{dl}A_s$, therefore $A_s = \frac{1}{C_{dl}}\frac{Q}{\Delta V}$; where C_{dl} is specific interfacial capacitance, and A_s is surface area of metal/solution interface.

For a given typical value of Q per single pitting corrosion event, ΔV will be expected to decrease with increasing A_S.

It is expected that $A_s \propto \frac{1}{\Delta V}$, therefore $\frac{\Delta V_2}{\Delta V_1} = \frac{A_{s,1}}{A_{s,2}} = \frac{l_1}{l_2}$; where l is the length of aluminium wire immersed in solution.

Applying this equation to result of this measurement, which $\frac{l_1}{l_2} = \frac{8}{2.5} = 3.2\ and\ \frac{\Delta V_2}{\Delta V_1} = \frac{3.2}{10} = 3.2$, it can be seen that the amplitude of potential fluctuation is in agreement with this theoretical background. Therefore it can be deduced that the increase of surface area increases the interfacial capacitance of metal in solution.

The result of this measurement also shows that ($\frac{\Delta V_1}{\Delta I_1} = \frac{32}{3.8} = 8.42 \times 10^{-9}\text{ohms}$) and ($\frac{\Delta V_2}{\Delta I_2} = \frac{20}{2.4} = 8.33 \times 10^{-9}$ ohms). From definition of noise resistance ($R_n = \frac{\sigma_V}{\sigma_I}$), $R_{n,1}$ is nearly equivalent to $R_{n,2}$. This indicates that noise resistance is independent of surface area of electrode. Therefore noise resistance is a better parameter for noise analysis.

The detail of potential and current signals for 100s is shown in figure 33 in order to study the effect of surface area on pitting corrosion event. It can be seen that:

a) The amplitude of both potential and current transients decrease with increasing surface area.

b) For both smaller and larger surface area, the transient is characterized as a potential drop coupled simultaneously with an anodic current upswing. This indicates that the surface of pure aluminium undergo pitting corrosion.

c) The frequency or number of pitting events (the black dashed lines) increases with increasing surface area.

The frequency spectra of current with different surface area in figure 34 shows that the frequency distribution of current signal changes with increasing surface area. For smaller area, the peak of frequency spectra at about 46mHz is clearly seen. However, when the surface area increases, the frequency spectra exhibit a large distribution of the peaks. This may be attributed to an increase number of corrosion events per time with increasing surface area.

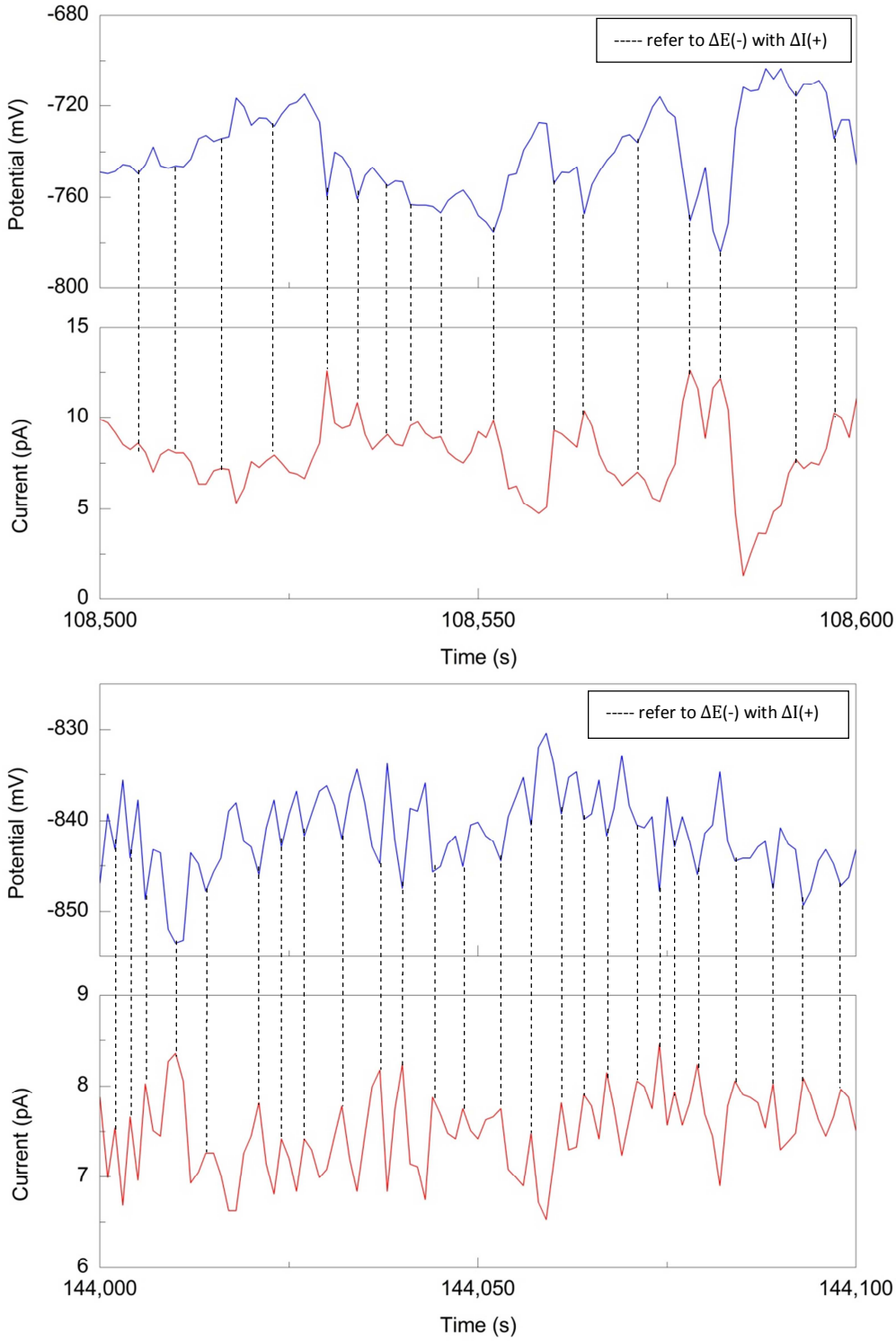

Figure 33: Zoom of potential and current signals for 100s: (top) for smaller area and (bottom) for larger area in 0.5M NaCl solution.

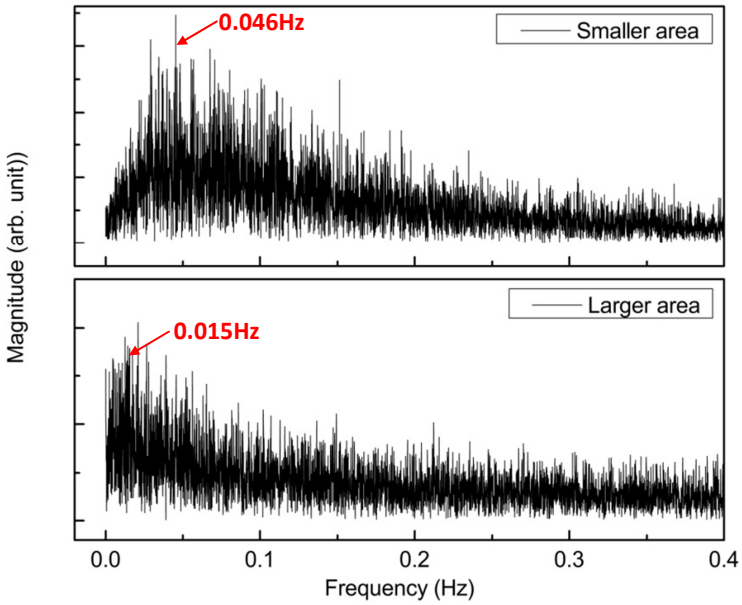

Figure 34: frequency spectra of current at 30h (smaller area) and 40h (larger area).

Therefore this measurement shows that with increasing surface area of pure aluminium in NaCl solution, the corrosion mechanism does not change from pitting corrosion but the frequency and amplitude of corrosion transient change.

1.6) Time evolution of noise behaviour in long term measurement

The objective of this measurement was to investigate the amplitude of potential and current transients of corrosion event as a function of immersion time. The parallel electrodes set-up with one working electrode (figure 27) was still applied for this measurement. Pure aluminium and Nickel wires were used as a working and reference electrode, respectively. Firstly, these electrodes were passivated in tap water for 1 day. After that, 0.5M NaCl was entered into tap water. In order to start with high amplitude, small area of electrodes in solution was required as mentioned in former measurement. Therefore only 5mm of electrodes were immersed in solution. The potential and current signals of pure aluminium in NaCl solution were simultaneously recorded for more than 3 days.

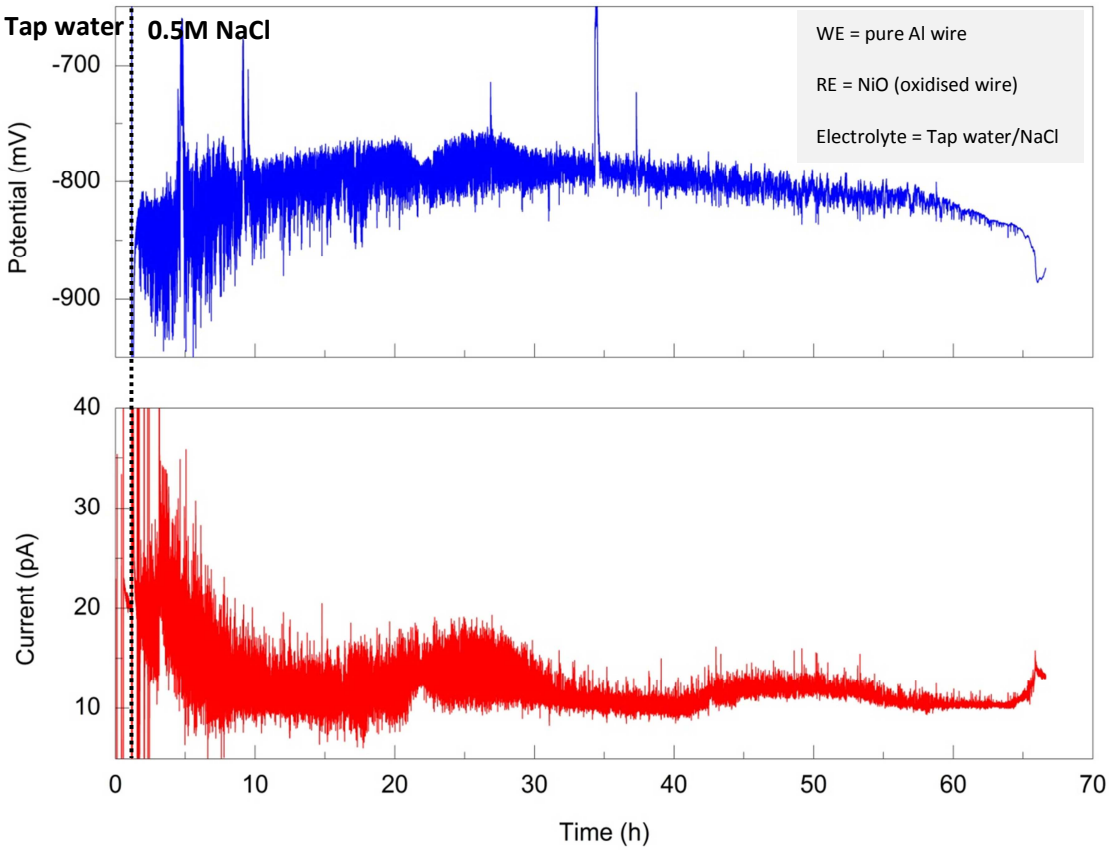

Figure 35: Potential and current signals in long term measurement.

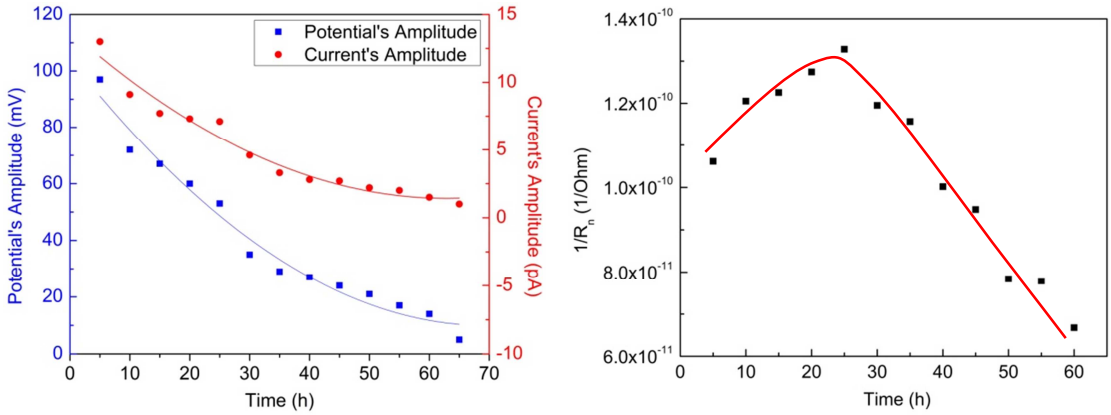

Figure 36: (Left) amplitude of potential and current noises as a function of time and (right) noise resistance of pure aluminium during long immersion time in NaCl solution.

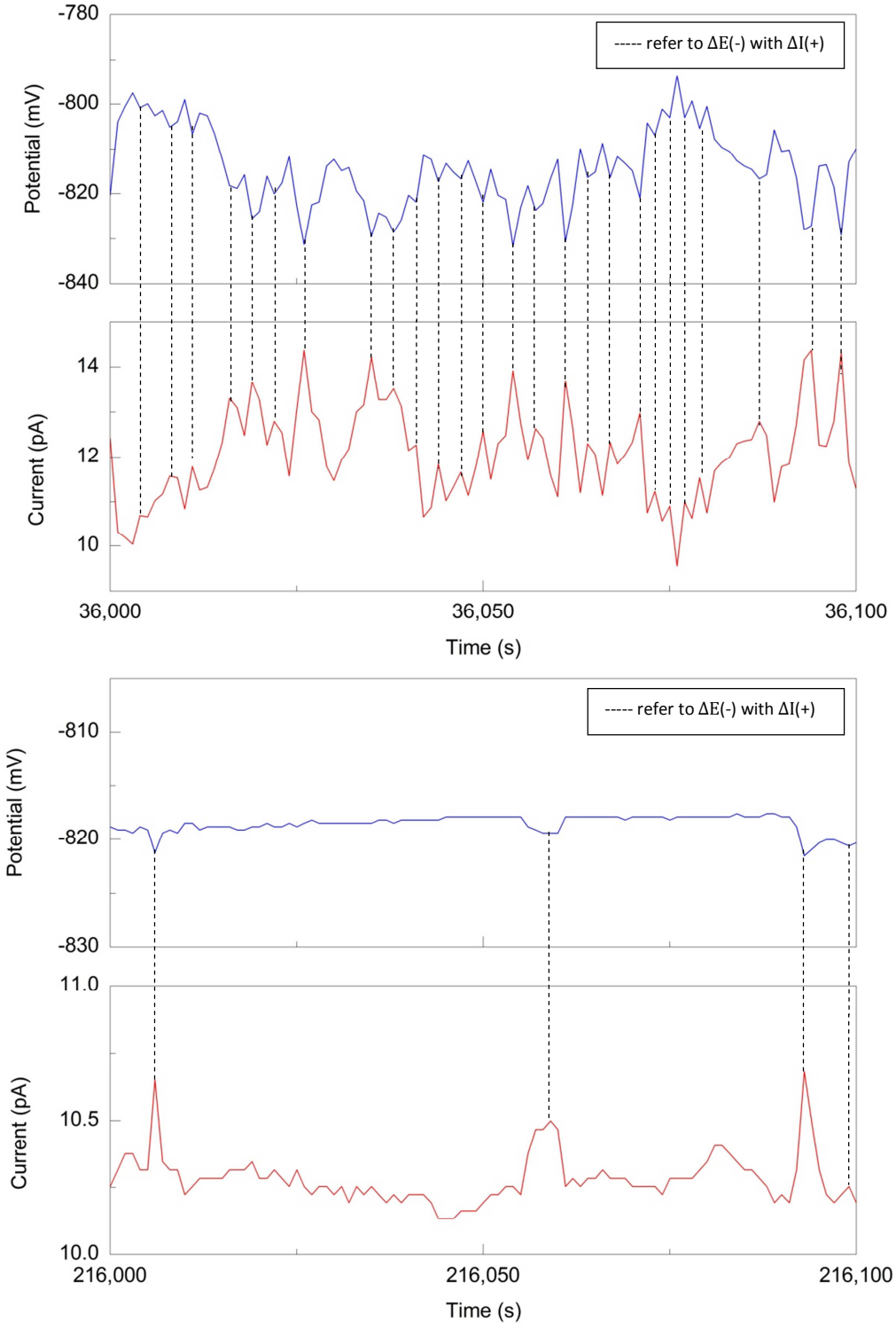

Figure 37: potential and current transients for 100s: (top) at 10h and (bottom) at 60h.

It is clearly seen in figure 35 that the amplitudes of both potential and current fluctuations decrease as the immersion time prolonged. The amplitudes of potential and current as a function of time in figure 36(left) confirms that amplitude of potential and current gradually decrease with time. However, the inverse of noise resistance ($1/R_n$), which is proportional to corrosion rate, in figure 36(right) shows that at the beginning, the corrosion rate slightly increases with the immersion time until reaches the maximum value at immersion time of about 25h. After that when the immersion time prolongs from 30 to 60h, the corrosion rate decreases with time.

The details of potential and current transients at different immersion time in figure 37 shows that:

a) Corrosion transients at both 10h and 60h are characterised by a simultaneous potential drop and anodic current rise, which is the signature of pitting corrosion. This implies that the type of corrosion mechanism of pure aluminium in NaCl solution does not change from pitting corrosion with immersion time in NaCl prolonged.

b) The amplitudes of potential and current fluctuations decrease when the immersion time increases from 10 to 60h.

c) The frequency of pitting transients (black dashed lines) decreases when the immersion time increases from 10 to 60h.

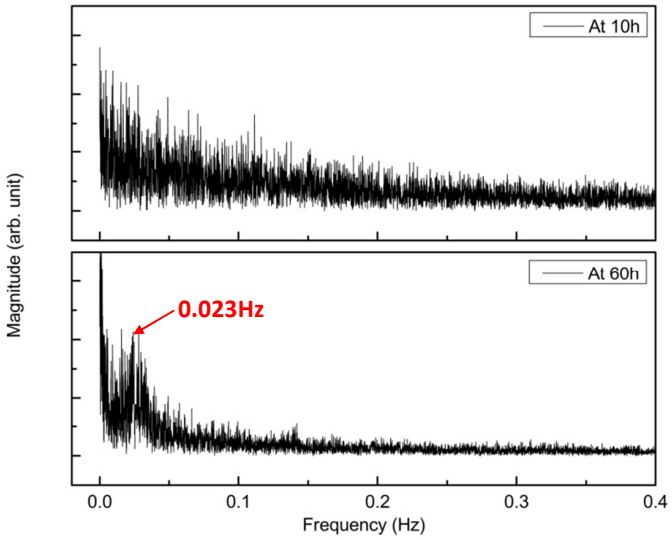

Figure 38: Frequency spectra at different period of immersion time.

The frequency spectra of current signals in figure 38 show that at 10h, the large distribution of peaks is detected. This may be attributed to high number of corrosion event attacking at the beginning of NaCl immersion. After that when the immersion time prolongs to 60h, the peak of frequency distribution shows up at about 23mHz possibly due to the decrease in number of corrosion events with immersion time prolonged from 10h to 60h.

This measurement shows that the tendency to pitting corrosion of aluminium goes to zero with immersion time prolonged.

1.7) Noise behaviour of aluminium alloys

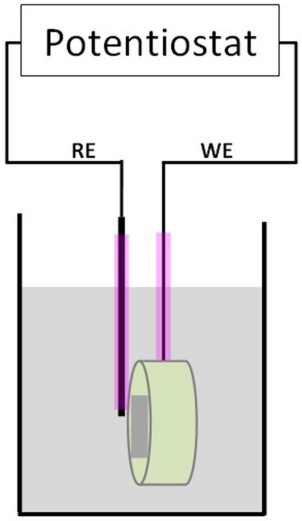

Figure 39: Two electrodes set-up for noise measurement of aluminium alloys.

In this measurement, corrosion behaviour of aluminium alloys such as pure aluminium (Pure Al), AA2024 (Al-Cu alloy), AA5052 (Al-Mg alloy) and AA6061 (Al-Mg-Si alloy) have been studied by EN techniques. The chemical composition of aluminium alloys is presented in table 4. Aluminium alloys have been used as working electrode and NiO (oxidised wire) tip, which is NiO (oxidised wire) covered with insulator except at the tip, have been used as a reference electrode. The two electrodes set-up with one working electrode was applied (figure 39). All samples were cut into 2x2cm square shaped specimens. Then the samples were embedded in the epoxy resin holder allowing a total exposed surface area of 4cm^2. After that they were mechanically abraded by successively 3 silicon carbide papers with abrading grit size of 46, 22 and 15µm, thoroughly

rinsed with plenty of water and dried with air flow. Both NiO wire tip and one sample have been immersed in solution and the NiO wire tip was placed closely to the surface of the sample. Before starting the measurement, solution of 0.5M NaCl was deaerated with N_2 bubbling overnight but during measurement, no N_2 bubbling was injected into the solution in order to reduce disturbance. The testing system was also shielded from external signals by faraday cage. The electrochemical noise measurement started suddenly after immersed the electrodes in the solution. The potential and current signals were monitored for 1h with time interval of 10values/s.

Alloy:	**AA2024**	**AA5052**	**AA6061**
Composition: (%by wt)	Al : Cu : Mg : Mn 93.5 : 4.4: 1.5 : 0.6	Al : Mg : Cr 97.25 : 2.5 :0.25	Al : Mg : Si : Cr 95.8-98.6 : 0.8-1.2 :0.4-0.8 : 0.04-0.35
Named as	Al-Cu alloy	Al-Mg alloy	Al-Mg-Si alloy

Table 4: Chemical compositions of aluminium alloys (Information from Alfa Aesar Company)

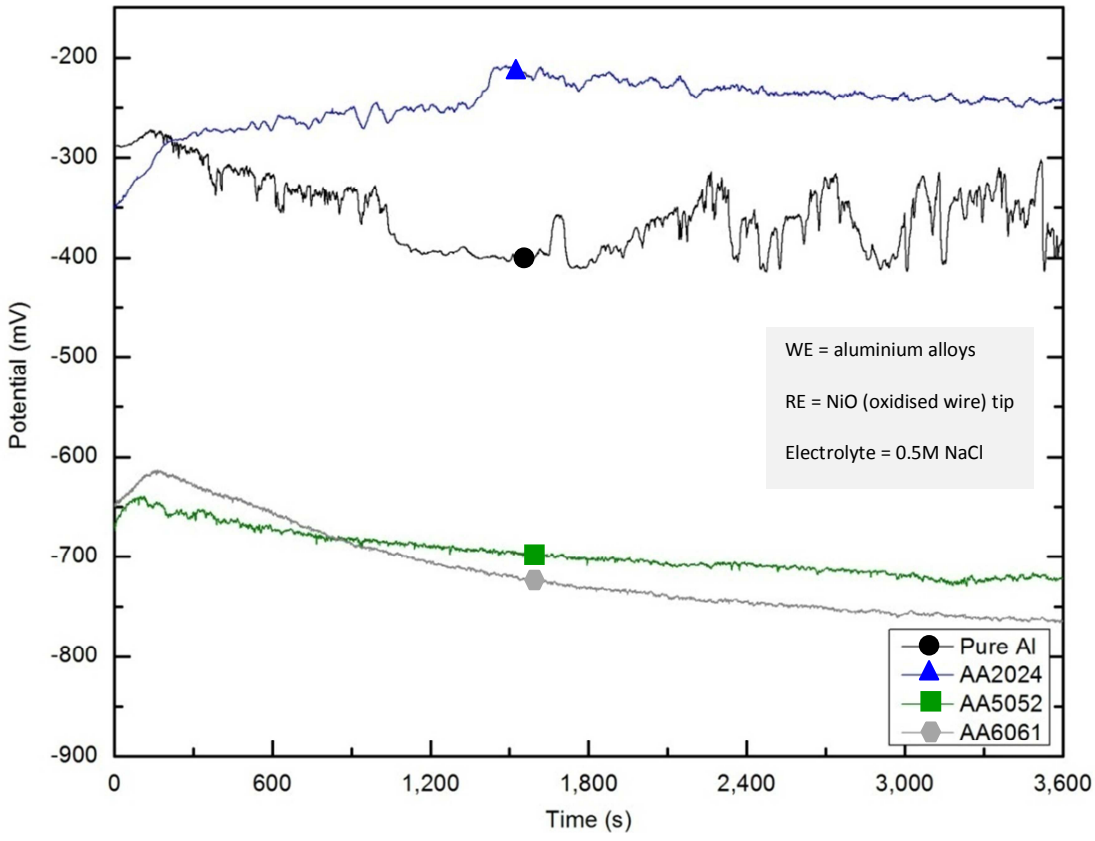

Figure 40: Potential signals of aluminium alloys in 0.5M NaCl solution for 1h.

The potential signals of aluminium alloys in figure 40 and their corrosion parameters in table 5 (appendix) shows that:

a) Potential evolution with time of Pure Al, AA5052 and AA6061 moves towards the negative direction while that of AA2024 moves toward positive direction after the immersion time of 1h in 0.5M NaCl solution.

b) The most distinguished difference of the potential signal of these aluminium alloys is the amplitude of the potential fluctuation (see figure 41). Potential signal of Pure Al exhibits the fluctuation with relatively high amplitude in the range of 50mV and AA2024 shows fluctuation with relatively moderate amplitude. On the other hand, AA5052 and AA6061 exhibit negligible fluctuation with very small amplitude. The amplitude of potential fluctuation ranging from the highest to the lowest are Pure Al, AA2024, AA5052 and AA6061(figure 41).

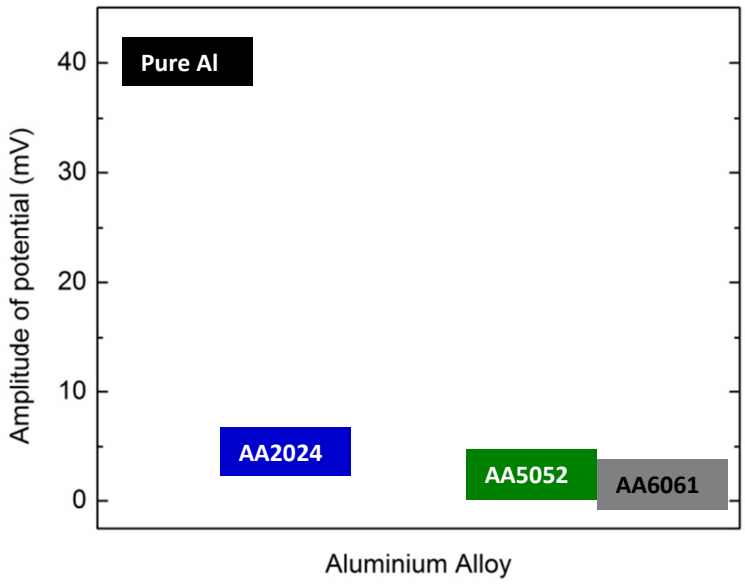

Figure 41: The amplitude of potential signal of aluminium alloys.

The current signals of aluminium alloys in figure 42 shows that unlike potential signal, there are no significant difference of current signal and the amplitude of current fluctuation between aluminium alloys. Therefore amplitude of current fluctuation cannot easily be used to compare the rate of pitting corrosion of aluminium alloys. For better analysis, the relationship between potential and current transients is identified.

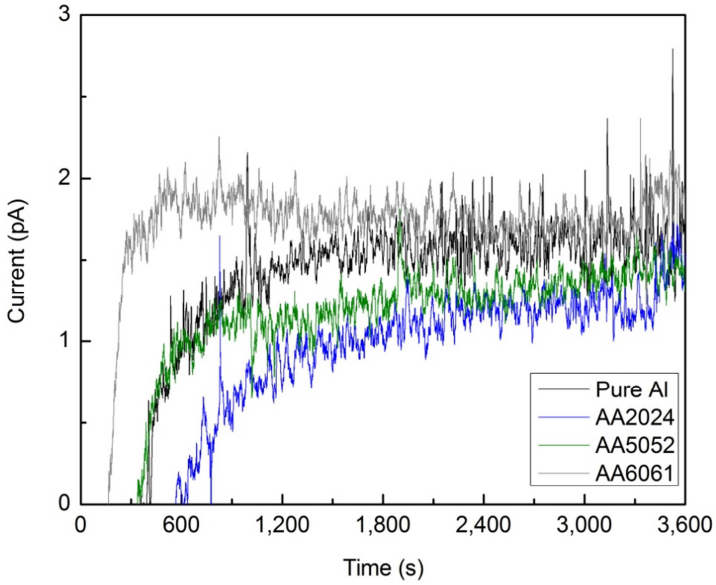

Figure 42: Current signal of aluminium alloys in 0.5M NaCl solution for 1h.

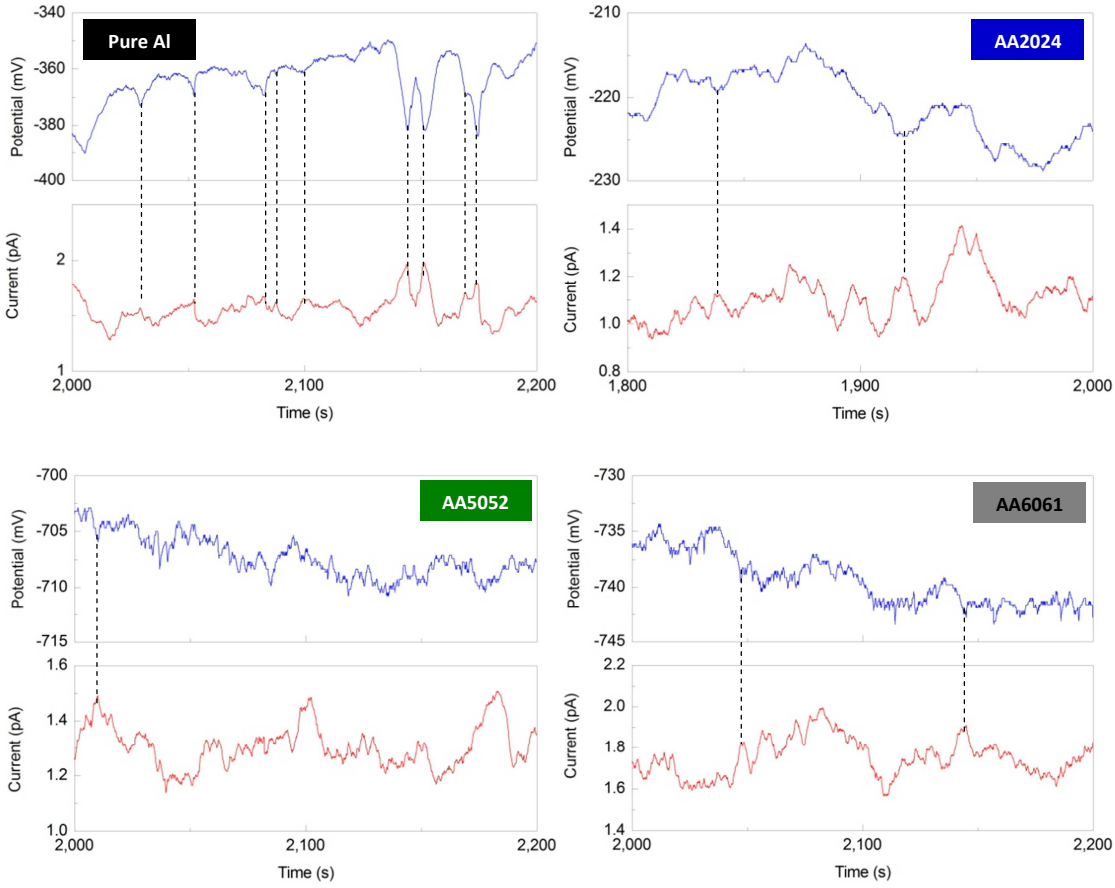

Figure 43: Zoom of potential and current signal of aluminium alloys.

The relationship between potential and current fluctuations in figure 43 shows that:

a) For Pure Al, many metastable pitting transients, which is a potential drop corresponded with a current rise, are easily identified.

b) For AA2024, AA5052 and AA6061, some of the transients are different from the characteristic transient of metastable pitting corrosion. This may imply that the localised corrosion behaviour of aluminium alloy has not been metastable pitting corrosion initiated by the local breakdown of passive oxide film at the weak point.

It was mentioned in [18] that for aluminium alloy, where its surfaces exhibit heterogeneous microstructure, the intermetallic particle and its vicinal matrix will form micro-galvanic cells, leading to the accelerated local corrosion attack in the vicinity of intermetallic particle. However, in this measurement, pure aluminium still undergoes much stronger pitting corrosion attack as pure aluminium exhibits the largest amplitude of potential fluctuation.

In order to verify pitting corrosion on aluminium alloys, surface morphology of all aluminium alloys is analysed. After 1h of electrochemical noise measurement, the aluminium alloys were brought out from the solution, cleaned with plenty of deionised water and dried in an air flow. Then the surface of alloy aluminium samples were analysed by a digital microscope for characterizing the morphology of the pits on the alloy surface. The surface of aluminium alloys in the figure 44 shows that:

a) On the surface of Pure Al, many shallow and small irregular-shaped pits can be seen. The irregular-shaped pits are caused by the local retardation of active dissolution due to a precipitation of oxide and hydroxide at the pitting edges [38].

b) On the surface of AA2024, large numbers of small spherical-shaped pits and some numbers of deep and large spherical-shaped pits with a diameter about 100µm can be seen. The figure 45(left) shows a blurred intermetallic particle in the centre of the corroding pit and the attack of pitting corrosion in its vicinal matrix. Therefore it can be confirmed that micro-galvanic corrosion cell is built on the surface of AA2024. Since the intermetallic phases e.g., Al_2CuMg compound [32] in this AA2000 series is nobler than the aluminium matrix, it acts as cathode and provokes anodic dissolution in the surrounding matrix. When the intermetallic phase disappears, large spherical-shaped

pits can be created. This pit has been called as *alkaline pits*. It was found that this type of pitting corrosion could occur at the potential below pitting potential [30]. It is assumed that figure 45 (right) shows such an alkaline pit. Moreover, figure 45 (left) some crack irradiating from the pit opening is observed, this should be the result of osmotic pressure on passive oxide film during the late stage of pit growth [39].

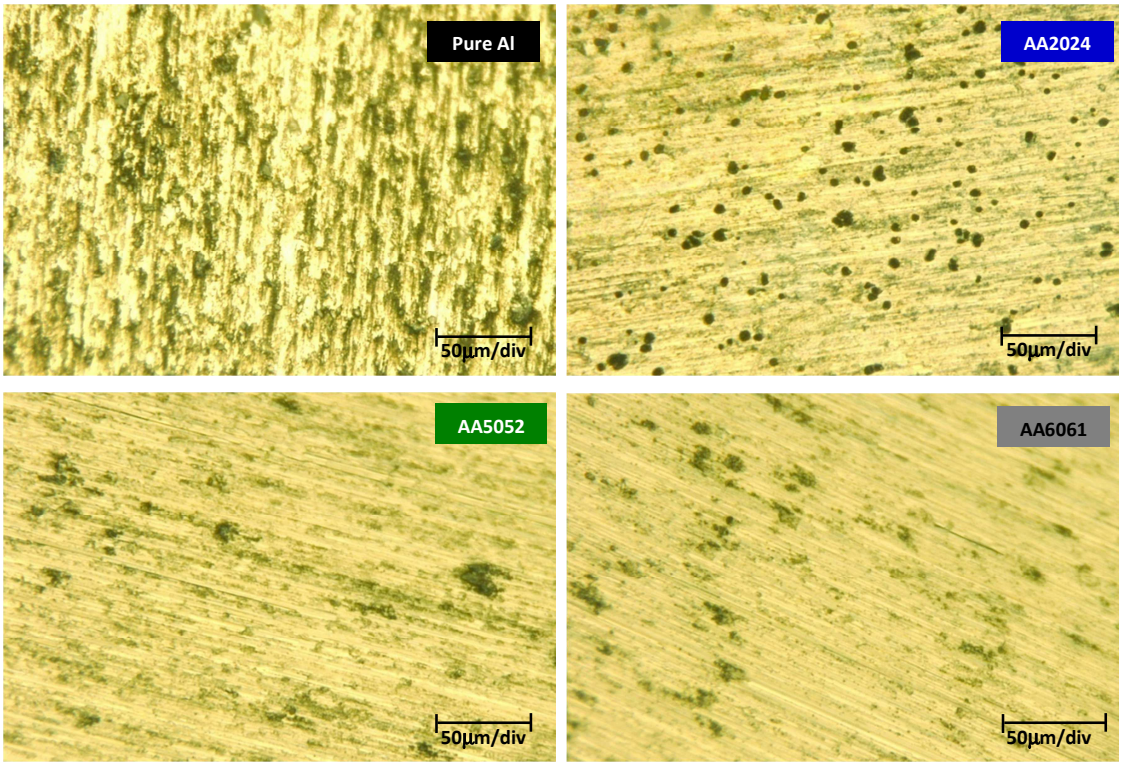

Figure 44: The morphology of pits on surface of aluminium alloys.

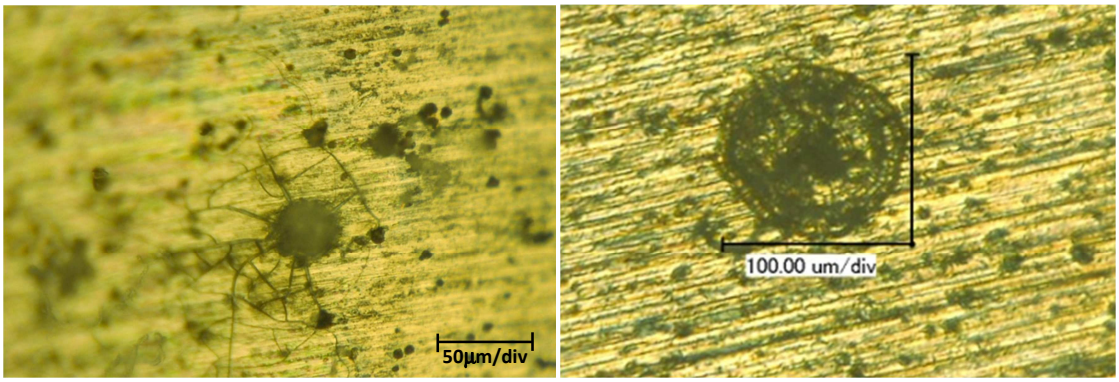

Figure 45: The morphology of large pits on surface of AA2024 at other positions.

c) On the surface of AA5052 and AA6061, only an amount of shallow and small irregular-shaped pits spreads over the entire surface area. This type of pitting character looks similar to that of Pure Al.

The surface morphology shows that Pure Al and AA2024 seriously corrode in 0.5M NaCl, but AA5052 and AA6061 rarely corrode in the same solution. The damage of aluminium alloys' surface ranging from the most to the least are Pure Al, AA2024, and AA6061 or AA5052. This is quite consistent with the amplitude of potential fluctuation. Therefore in this case, it may be deduced that the amplitude of potential fluctuations can be used to compare the rate of pitting corrosion. For this measurement, it is not possible to analyse the frequency spectra because of short measuring time.

This measurement shows that pitting corrosion takes place on surface of pure aluminium, AA2024, AA5052 and AA6061 at OCP.

1.8) Galvanic behaviour of aluminium partially deposited with carbon

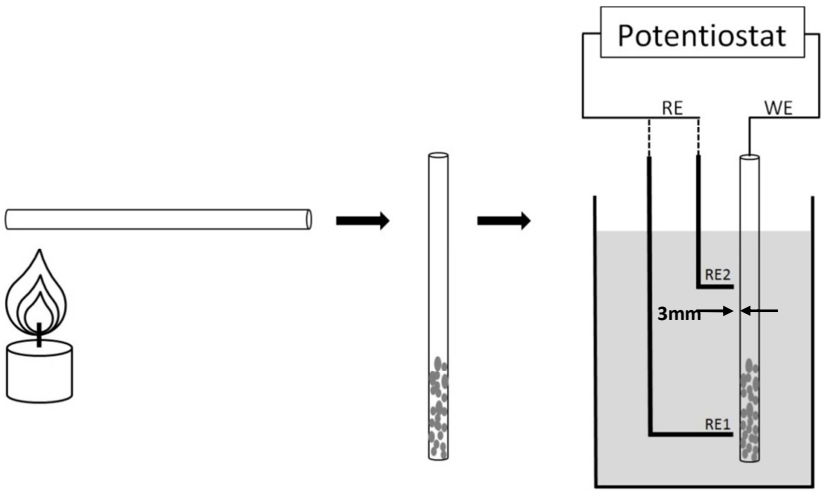

Figure 46: Measurement set-up for analysis of galvanic behaviour of Al partially deposited with C.

The objective of this measurement was to examine the use of the reference electrode position for identification of different pitting corrosion areas for electrochemical noise analysis. As aluminium was material under study, one aluminium wire was used as working electrode. In order to have two different surfaces, one end of the wire was held over fire for short time to

obtain carbon on its surface. This area refers to Al/C surface character. Another end side of wire was used as received which refers to Pure Al surface character. Two NiO (oxidised wires) were used as reference electrodes, which pointed at different surface positions. The reference electrode one (RE1) was pointed at the Al/C surface area and the reference electrode two (RE2) was pointed at Pure Al surface area as shown on figure 46. Since only one reference electrode could connect to potentiostat, during the measurement two reference electrodes could only be used alternatively.

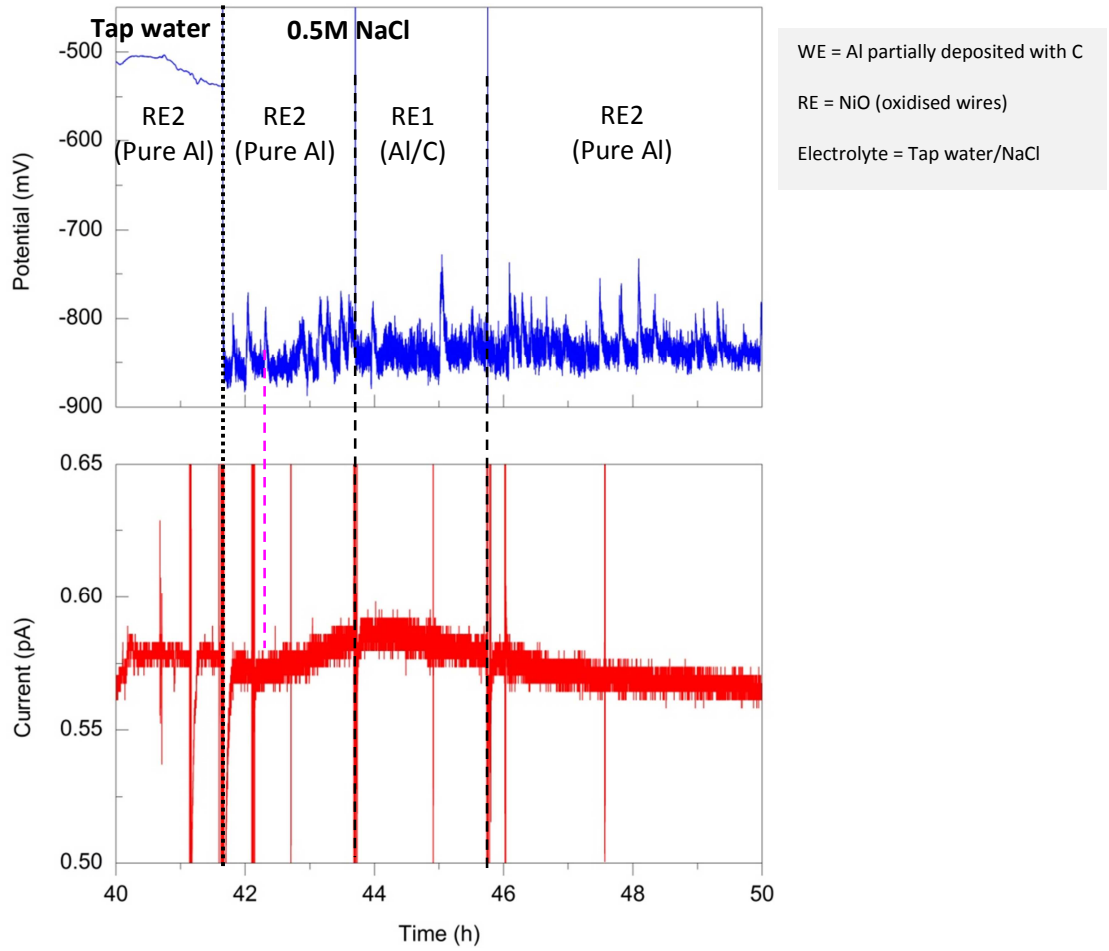

Figure 47: Potential and current signals of Al partially deposited with C.

The potential and current signals from alternative electrode positions during 50h of this measurement in figure 47 shows that:

a) After adding 0.5M NaCl in tap water, the serious fluctuations of potential starts. However, there is no difference of potential and current signals in NaCl solution

between 2 different reference electrodes or their positions. Therefore it can be deduced that no position dependent measurement is possible with this set-up.

b) The measured current is extremely small comparing with former measurement 1.2 and no serious fluctuation is detected. This might be attributed to the galvanic corrosion effect between aluminium and carbon on one working electrode. Pure aluminium acts as anode where anodic oxidation reaction takes place and release electrons. Then these electrons flow to carbon, which in this case acts as cathode, and are consumed by cathodic reduction reactions such as uniform oxygen reduction and hydrogen evolution. Both anodic and cathodic reaction strongly occurs on one working electrode therefore only really small current flow to ammeter in potentiostat, resulting in extremely low measured current.

c) There is no simultaneous transient of potential drop and current rise detected. This might imply that no pitting corrosion taking place on aluminium surface. However, the SEM analysis in figure 48 reveals many pitting sites (examples of pitting site are shown in the red circles). The pitting corrosion only occurs on the surface of aluminium covered with carbon while pure aluminium surface without carbon covered appears intact. This confirms the build up of galvanic coupling cell between aluminium and carbon. Moreover, it is possible that the pitting corrosion mechanism of pure aluminium is superimposed by cathodic reactions of carbon on the working electrode therefore no simultaneous transient of potential drop and current rise is detected.

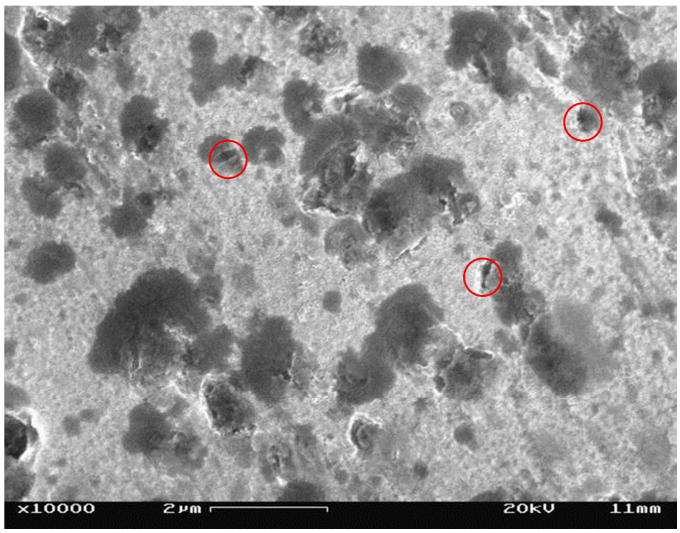

Figure 48: SEM (in lens detector) morphology of Al partially deposited with C.

This measurement shows that position of reference electrode cannot be used to identify pitting corrosion area. Moreover, it reveals that the two electrode set-up with one working electrode cannot be used to characterize the corrosion behaviour of the galvanic coupling electrode by EN measurement.

1.9) Galvanic behaviour of aluminium sputtered with gold

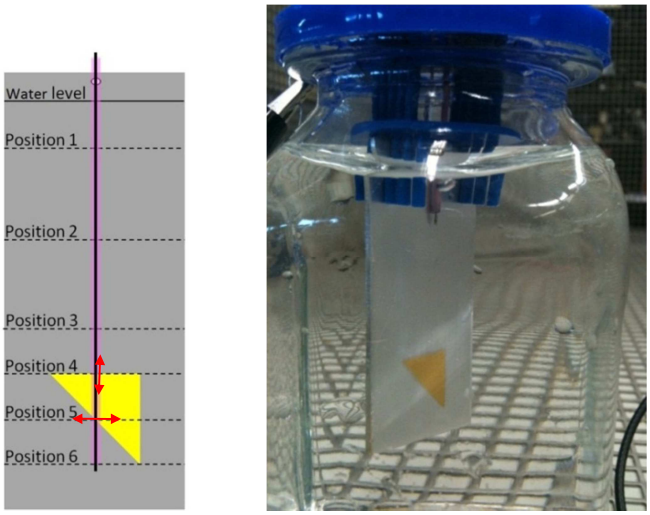

Figure 49: (Left) model and (right) real preparation for analysis of galvanic behaviour of Al sputtered with gold.

The objective of this measurement was still to verify the use of reference electrode position as the identification of pitting corrosion area for EN measurement as measurement earlier, but for this measurement the clearly well defined areas of 2 surface characters on one working electrode was required. Thus, pure aluminium sheet with gold-sputtered area (thickess≈10nm) was used as a working electrode. The surface area of pure aluminium with gold sputtered is referred as Al/Au surface area (yellow area in figure 49) while the surface area of pure aluminium is referred as Pure Al surface area. NiO (oxidised wire) tip was used as reference electrode. Firstly, working and reference electrodes were passivated in tap water for 21h during this period of time reference electrode was positioned at position 1 (figure 49, right) and then 0.5M NaCl were added to tap water. After adding NaCl, reference electrode was moved down from position 1 to 6 and then moved up back to position 1 again step by step every 30 minutes.

At the position 4 and 5, reference electrode's tip was in the asymmetric area of the borderline between Pure Al and Al/Au surface.

It is again that no any significant difference in potential and current signal is detected between different positions of reference electrode. This confirms that the position of reference electrode cannot be used to identify different pitting corrosion area.

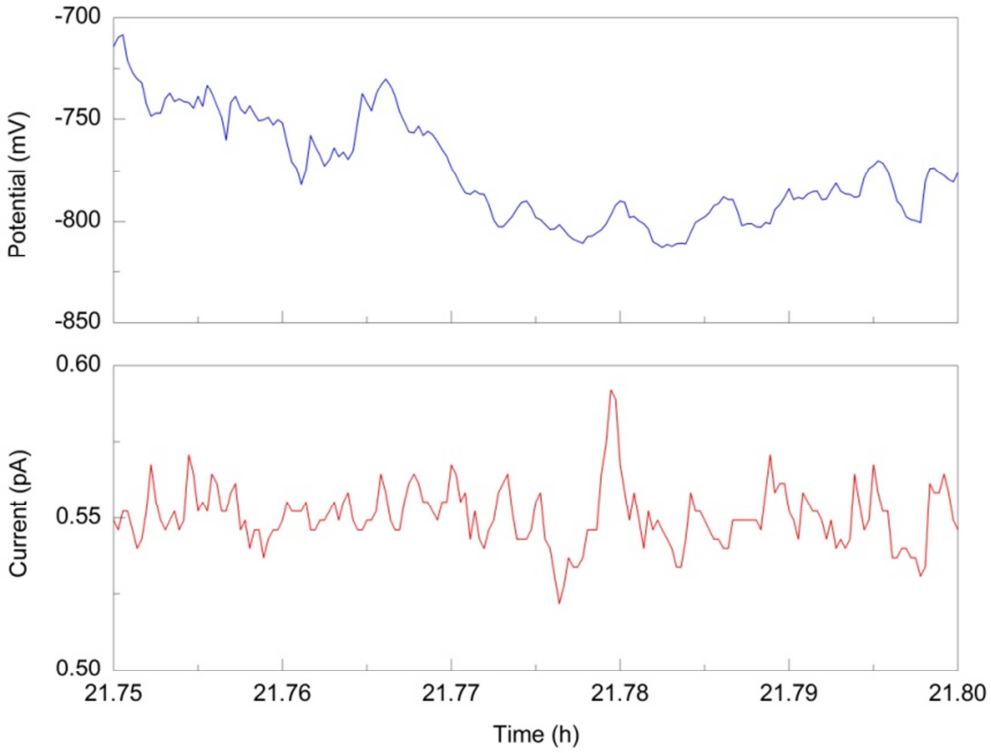

Figure 50: Detail of potential and current signals of pure aluminium with gold sputtered in 0.5M NaCl.

Potential and current signals in figure 50 show that the amplitude of current transients is really small. This implies the build-up of galvanic coupling between aluminium and gold. Moreover, there is no identifiable transient of potential drop coupled simultaneously with current rise. This implies that a possible pitting corrosion mechanism on pure aluminium with gold sputtered is superimposed by other reactions such as uniform oxygen reduction and hydrogen evolution. After the electrochemical noise measurement, the sample was examined by scanning electron microscopy (SEM) and the SEM images in figure 51 shows that Al/Au surface area appears severely pitting corroded while Pure Al surface area appears intact or passive. This mean pitting

corrosion only occurs on pure aluminium in the vicinity of sputtered gold. Therefore this confirms the galvanic coupling effect between pure aluminium and gold of Al/Au surface area. Therefore it can be concluded that the parallel electrode set-up with one working electrode cannot be directly used to study the pitting corrosion behaviour of galvanic coupling electrode.

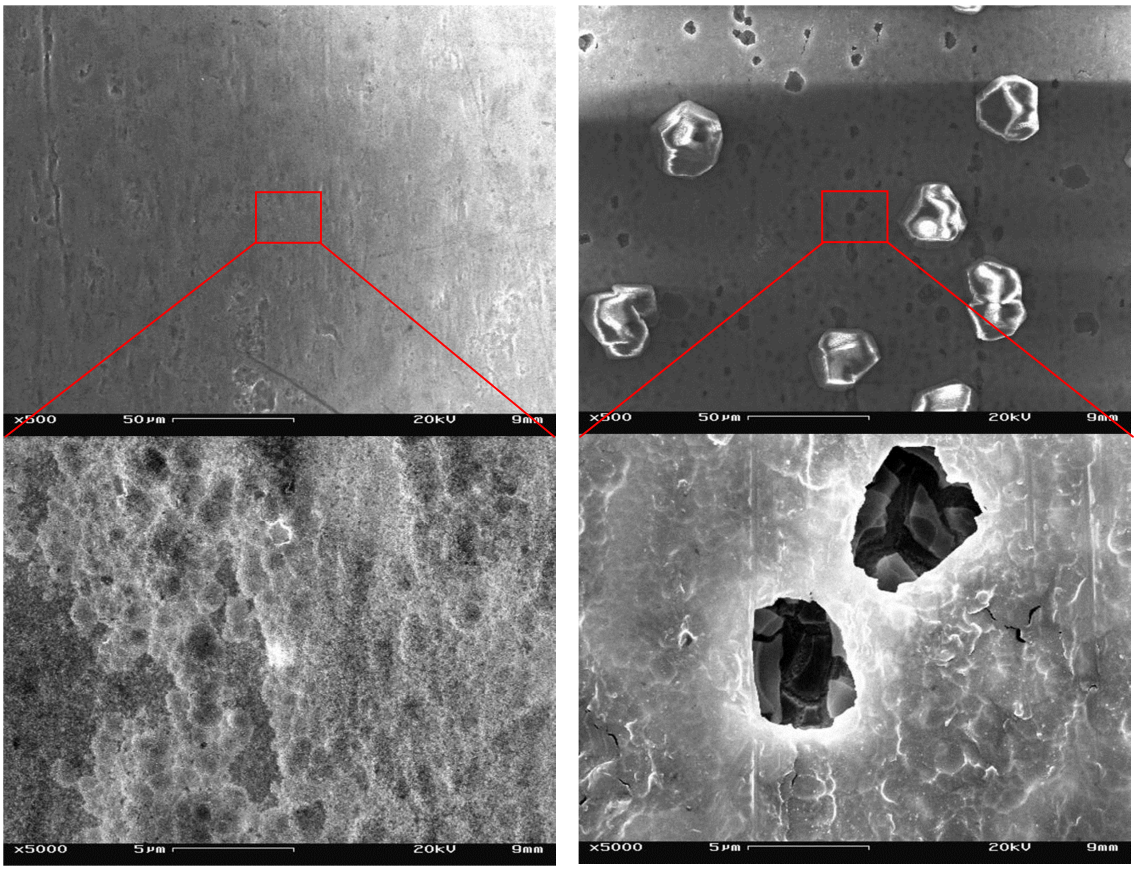

Figure 51: SEM images of aluminium with gold sputtered: (left) Pure Al surface area and (right) Al/Au surface area.

The SEM images in figure 51 show that:

a) For Pure Al surface area or pure aluminium surface without gold sputtered, no any pit is observed.

b) For Al/Au surface area, many pitting sites are detected. The sizes of pits are in the range of 3 -15µm diameter. Moreover, many big particles are also detected on Al/Au surface area, which can be defined by EDX measurement.

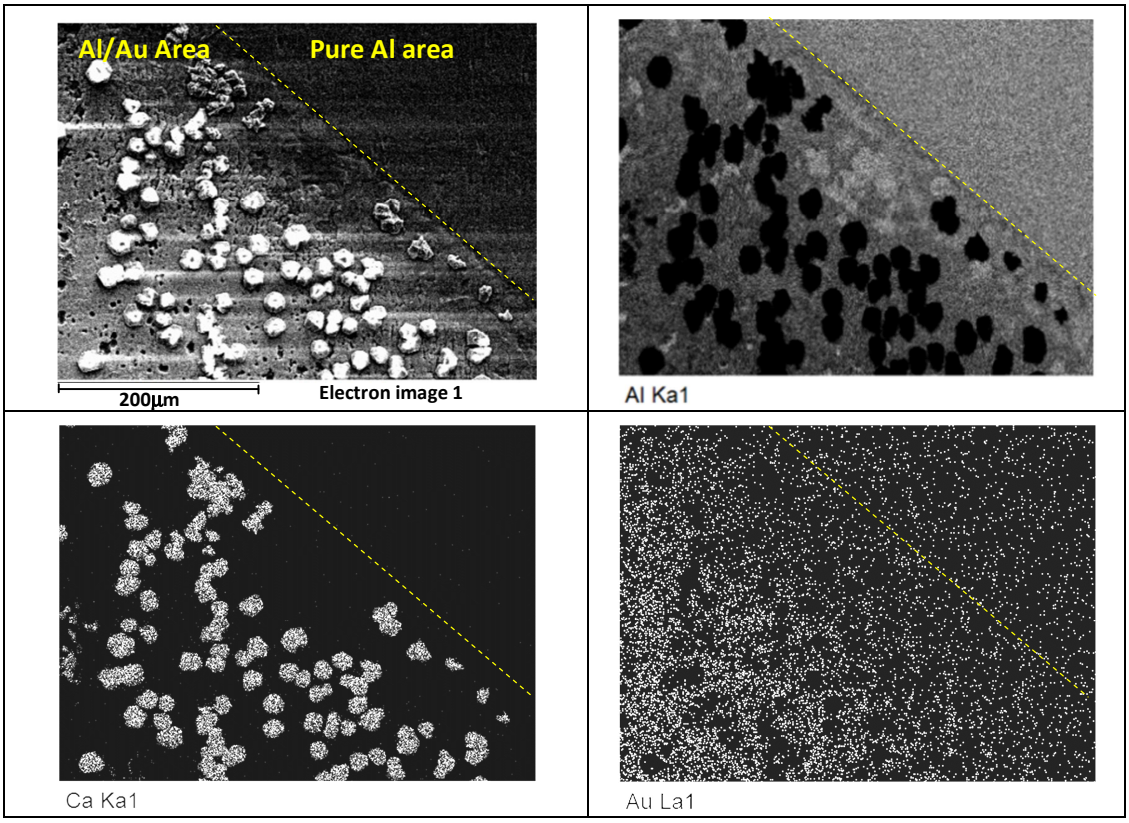

Figure 52a: EDX result on border line between pure Al area and Al/Au area.

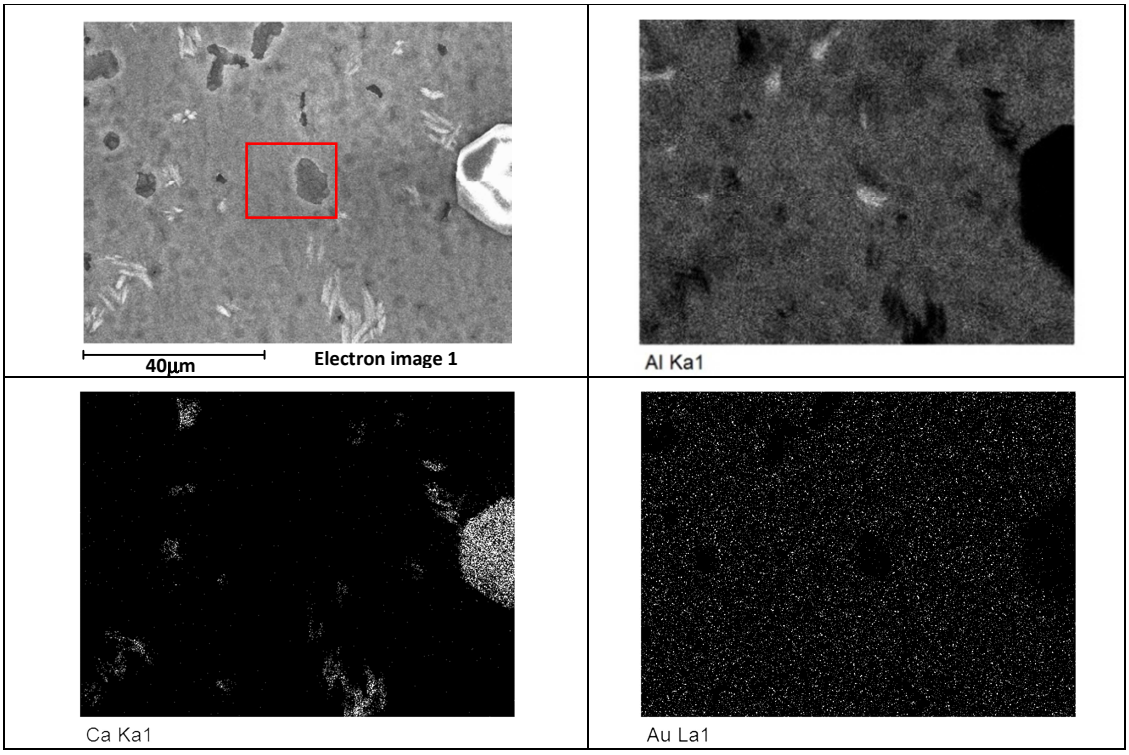

Figure 52b: EDX result on Al/Au area.

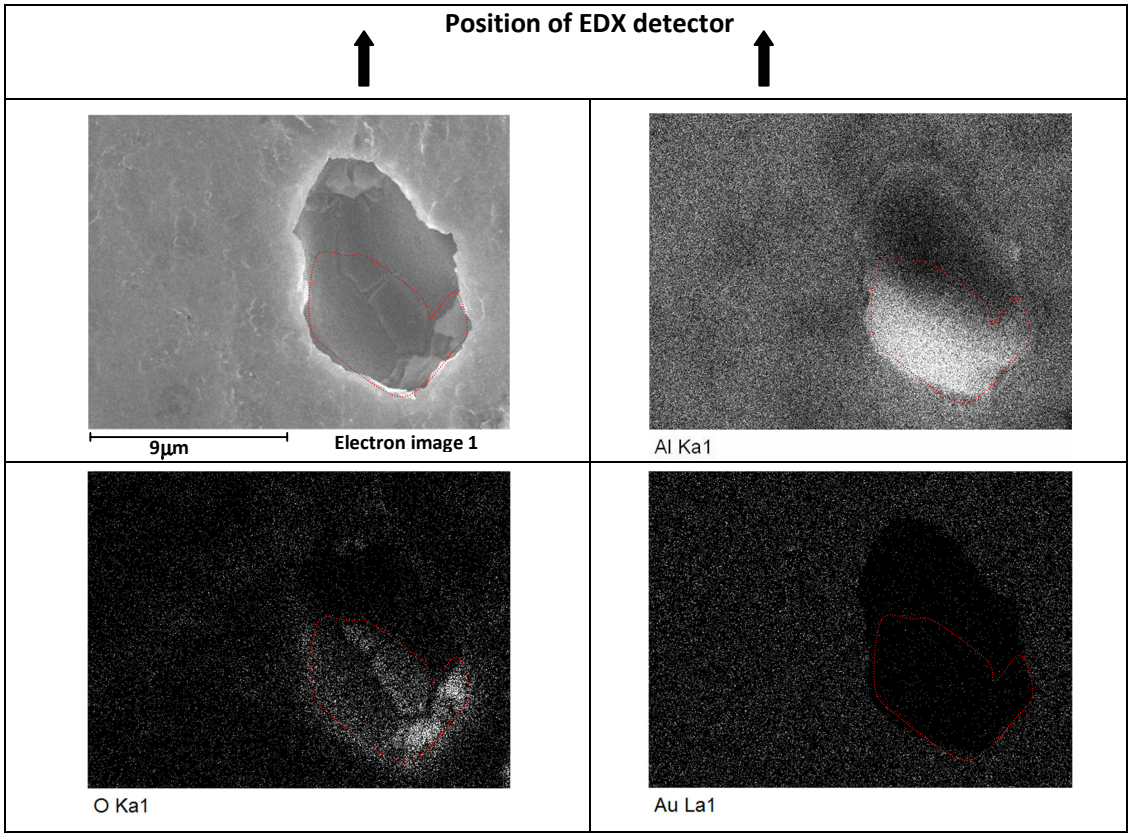

Figure 52c: EDX result of pits in Al/Au area (zoom of pit in Al/Au area from figure 52b).

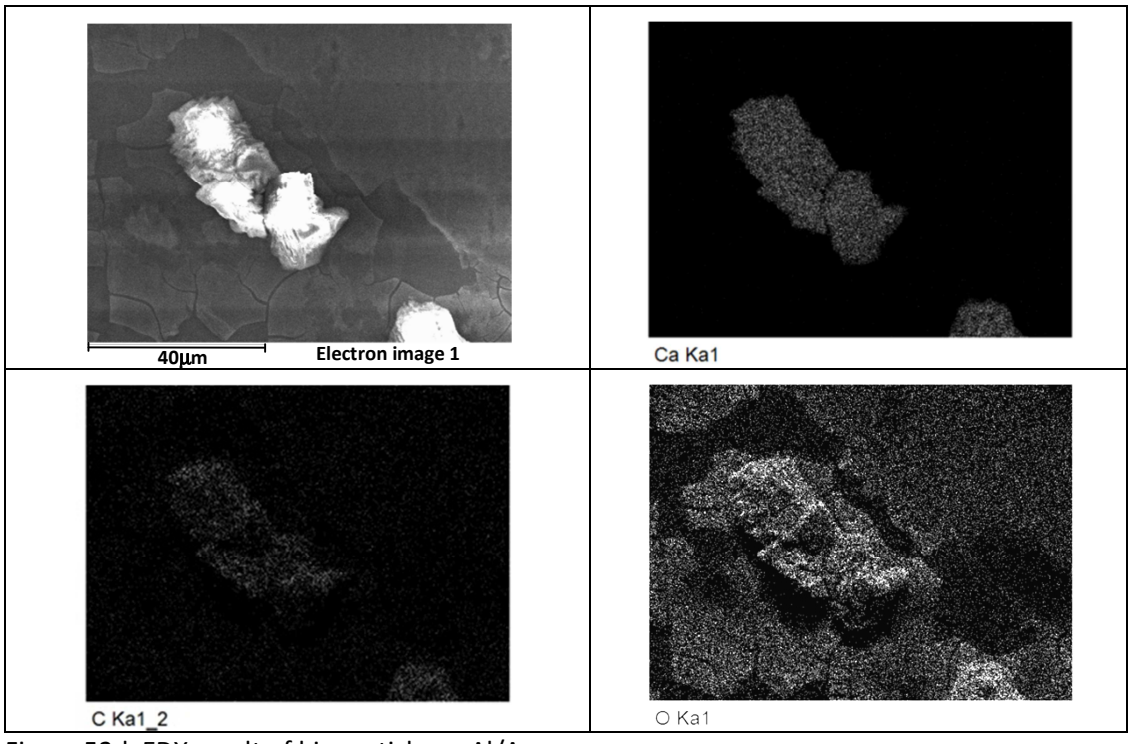

Figure 52d: EDX result of big particle on Al/Au area

EDX results in figure 52a-d show that:

a) Pitting corrosion occurs only on Al/Au surface area (figure 52a).

b) The pit is in the irregular shape with diameter of about 12 μm (figure 52b).

c) Oxygen is detected at the pitting sites (the area in the red dotted line in figure 52c). This implies the partial deposition of Al_2O_3 on the pit's bottom. Due to position of EDX detector, the figure cannot use to specify the rest of the pit's bottom to be active or covered by Al_2O_3.

d) Many big particles observed only on Al/Au area (figure 52d) seem to be calcium carbonate ($CaCO_3$). This can be attributed to the use of natural water for tap water. During polarization in tap water, calcium carbonate ($CaCO_3$) is produced and deposited on aluminium surface, according to the equation below [46]:

$$2Ca^{2+} + 2OH^- + 2HCO_3^- \rightarrow 2CaCO_3 + 2H_2O$$

Therefore, this measurement confirms that galvanic effect between aluminium and more noble metal (such as gold) can induce pitting corrosion to take place on aluminium surface at open circuit potential.

1.10) Noise behaviour of aluminium when coupled with graphite in deionised water

For this measurement, the potential and current signals of pure aluminium when coupled with graphite were studied. As graphite is nobler that aluminium, galvanic cell is built-up when aluminium coupled with graphite in the present of electrolyte. Aluminium will act as anode where anodic dissolution of aluminium takes place and graphite will act as cathode where cathodic reduction takes place. Therefore, there is galvanic current flow between aluminium and graphite. In order to measure the galvanic current and study the galvanic corrosion between aluminium and graphite, the two working electrodes (WE and WE_G) set-up were applied (see figure 53). The Al wire tip, which was pure aluminium wire covered with insulator except at the tip, was used as the WE since the small surface area of aluminium wire was required in order to get high amplitude of signal's fluctuation. The Al wire tip, NiO (oxidised wire) tip and graphite electrode were immersed together in pure deionised water. At the beginning,

the Al and NiO (oxidised wire) tips, which placed closely to each other, were connected to working and reference electrodes of potentiostat, respectively. Both potential and current signals of Al wire tip were measured for about 2h. After that, graphite electrode (WE_G) was connected to WE via zero resistance ammeters (ZRA) of the potentiostat. Therefore the mixed potential of both working electrodes and the current flowing between them were measured.

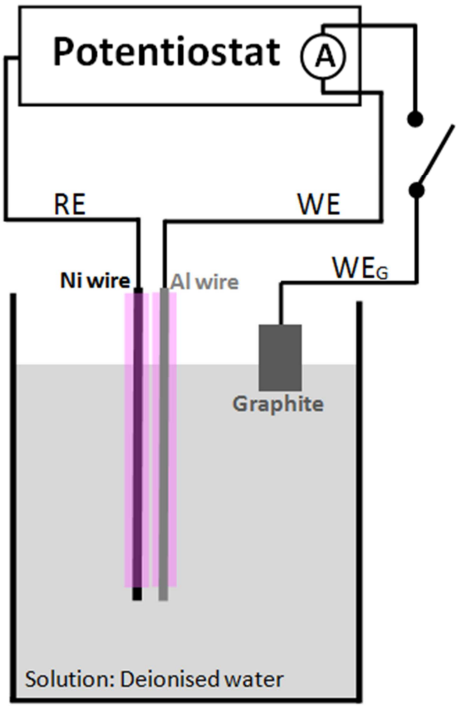

Figure 53: Measurement set-up for EN measurement of pure aluminium when coupled with graphite.

The potential and current signals in figure 54 show that:

a) Without coupled with graphite, the clearly defined baselines of potential and of current of pure aluminium are detected. Generally, the potential of only pure aluminium drifts slowly to noble direction with time and the current is extremely small, lower than 1pA. The potential fluctuation is negligible and the current fluctuates with amplitude less than 0.1pA (figure 55, left). Moreover, no relationship between the potential and current transient is detected. Therefore *pure aluminium in deionised water exhibits only the formation of oxide film with slow rate*.

b) When coupled with graphite, the potential of pure aluminium suddenly increases by 570mV and current suddenly increases from about 1pA to 17.5nA. The increase in current indicates the increase of corrosion rate of pure aluminium, possibly due to the increase in potential of pure aluminium when coupled with graphite. Negligible fluctuation of both potential and current signal is still detected (figure 55, right), indicating that no corrosion occurs in deionised water. Moreover, the current of pure aluminium when coupled with graphite decreases with time. According to measurement 2.13, the decrease of current with time indicates that pure aluminium is in passive region. Therefore it can be concluded that *after coupled with graphite in deionised water, pure aluminium still exhibits passivation or formation of oxide film with increasing rate*.

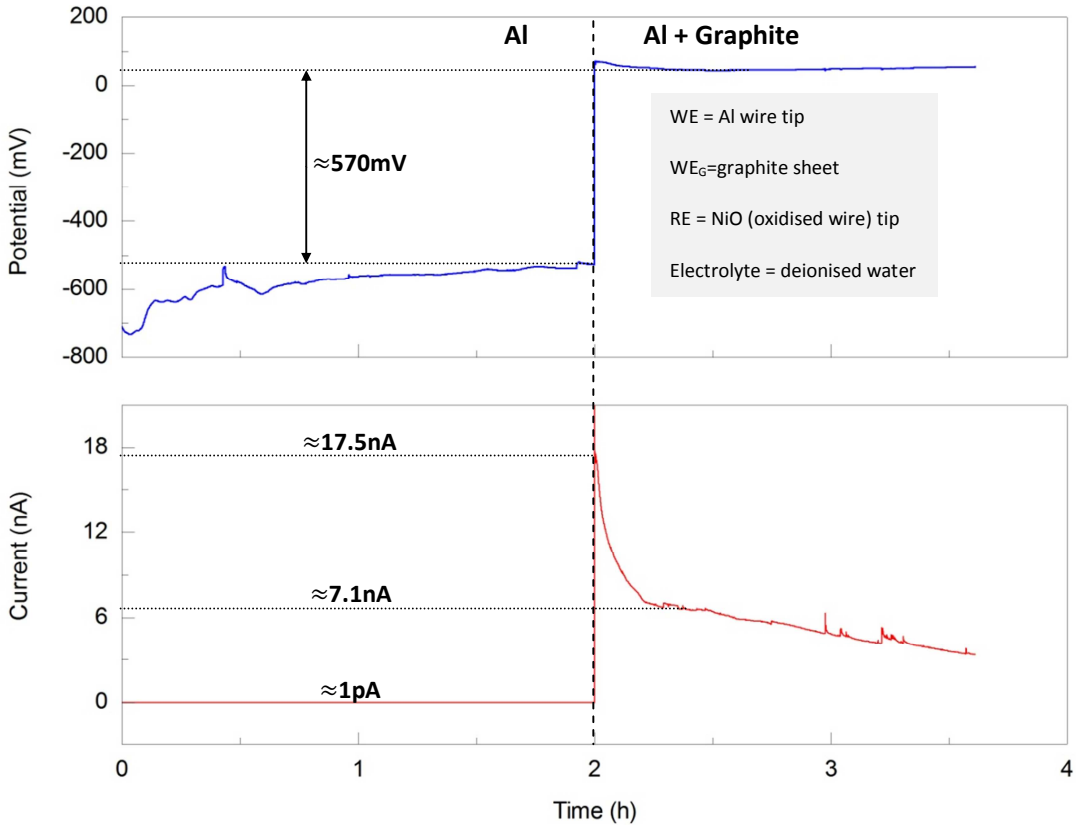

Figure 54: Potential and current of pure aluminium when coupled with graphite in deionised water.

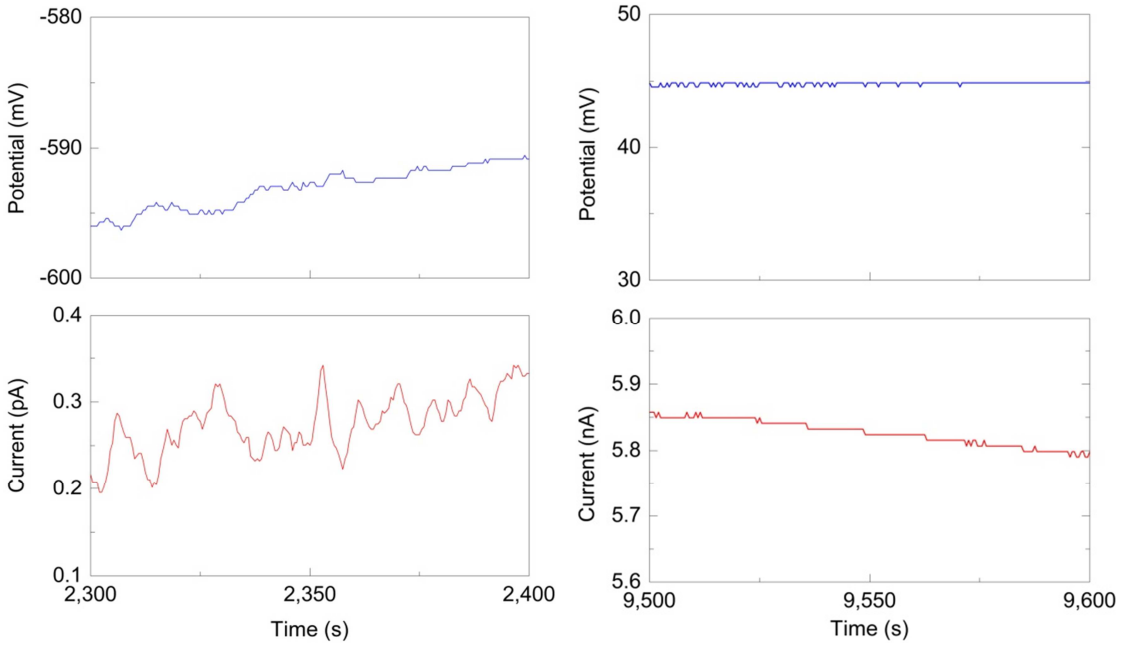

Figure 55: Zoom of potential and current signals of (left) only Pure Al and (right) Pure Al coupling with graphite in deionised water.

Therefore, this measurement shows that after coupled with graphite in deionised water, *corrosion behaviour of pure aluminium does not alter from passivation* (or formation of oxide film) but the passivation rate increases.

1.11) Noise behaviour of aluminium when coupled with graphite in NaCl solution

For this measurement, the set-up was the same as measurement earlier but the solution was changed from deionised water to aggressive solution of 0.001M NaCl in order to study corrosion behaviour of pure aluminium when coupled with graphite in NaCl solution.

The potential and current signals in figure 56 show that:

a) Without coupled with graphite, the baselines of potential and current of pure aluminium are distinctly defined and only 2 short transients, in the pink square, are detected. In general, the potential baseline of only pure aluminium slightly decreases with time, indicating an only slow modification of air-formed oxide film by chloride ions. The observed anodic current is extremely small in the range of only 1pA, indicating nearly no

corrosion process occurring on pure aluminium surface. The short transients of pure aluminium (figure 57) shows the same character as metastable pitting corrosion, which is the potential drop corresponding with a current rise, meaning that only two metastable pitting corrosions occurs on pure aluminium surface when immersed in 0.001M NaCl solution.

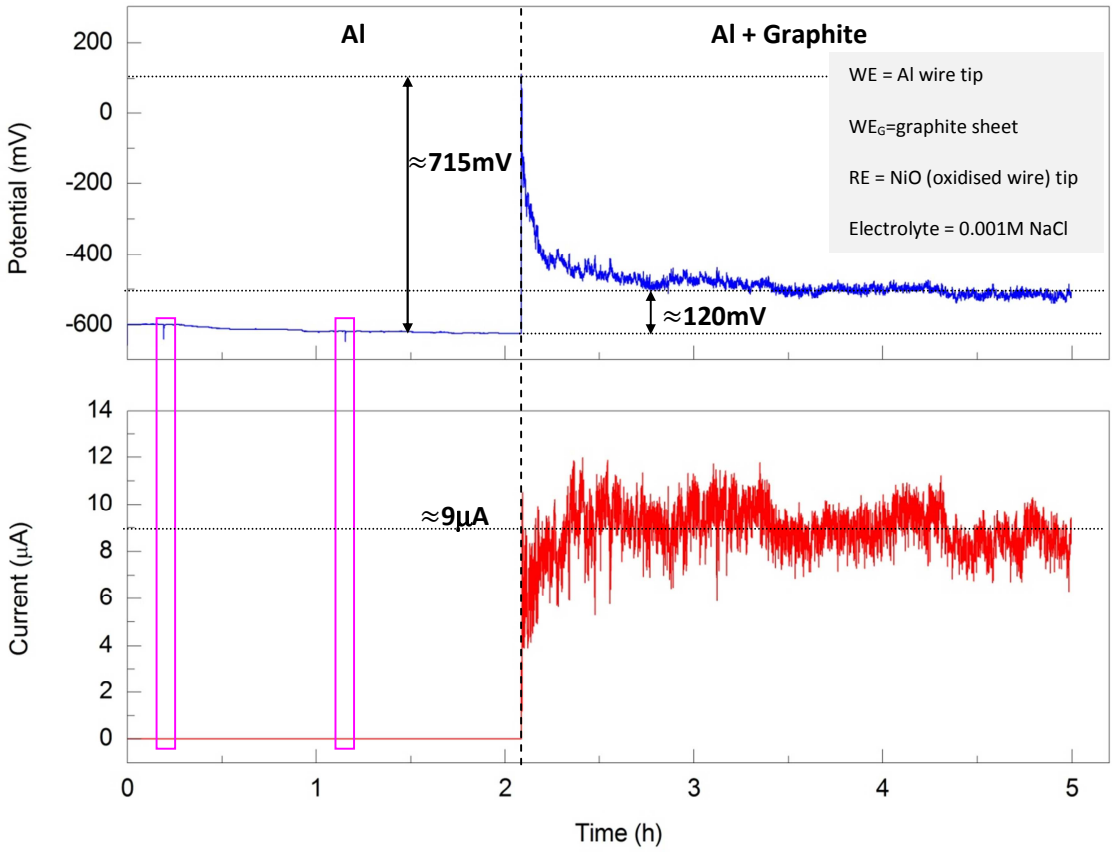

Figure 56: Potential and current signals of pure aluminium when coupled with graphite in 0.001M NaCl.

b) After coupled with graphite, both potential and current signals start fluctuating intensely and their distinct baselines disappear. This indicates that many numbers of pitting corrosion event occur when pure aluminium coupled with graphite. Therefore the stability of pure aluminium reduces when coupled with graphite. Generally, potential of pure aluminium after coupled with graphite suddenly increases by 715mV and then gradually decreases with time. The increase of potential can be attributed to galvanic corrosion. Therefore graphite anodically polarises aluminium. Moreover, current of pure

aluminium after coupled with graphite sharply increases from about 1pA to 9µA. The increase in current indicates the increase of corrosion rate of pure aluminium due to the increase in potential of pure aluminium when coupled with graphite. As aluminium is anodically polarized by graphite, the anodic reaction is accelerated on the pure aluminium surface.

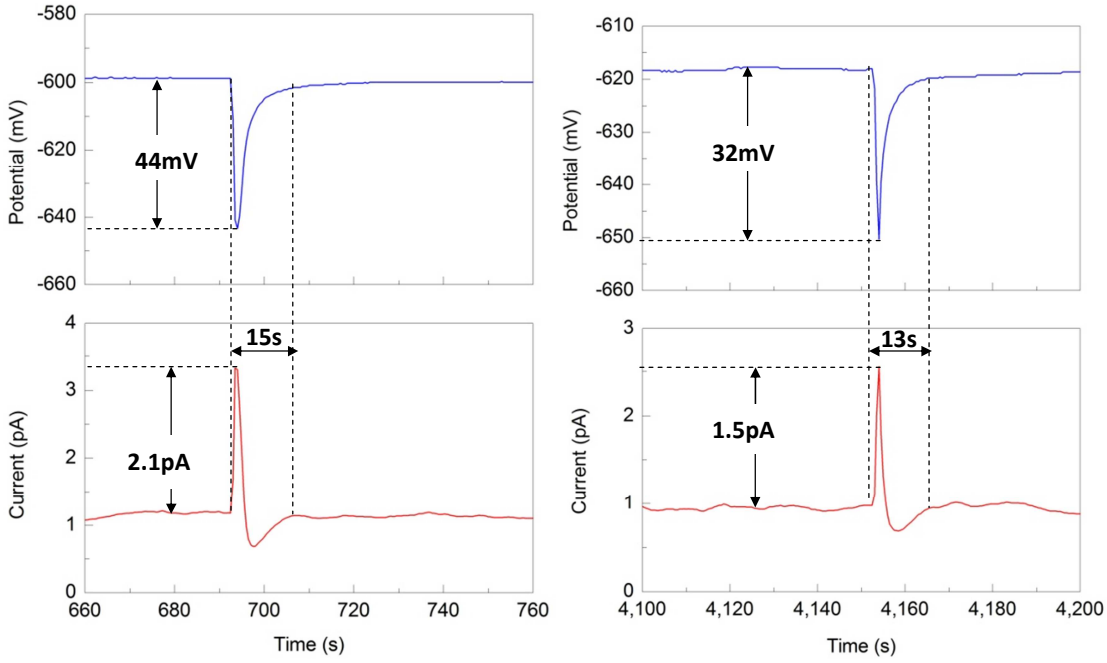

Figure 57: Metastable pitting transients of pure aluminium in 0.001M NaCl.

The metastable pitting transients of pure aluminium in NaCl in figure 57 shows that:

a) As $R_{n,1} = \frac{V_1}{I_1} = \frac{44mV}{2.1pA} \approx 21 \times 10^{-9}ohm$ and $R_{n,2} = \frac{V_2}{I_2} = \frac{32mV}{21.5pA} \approx 21 \times 10^{-9}ohm$, this indicates that noise resistance is constant. Therefore noise resistance is suitable value to compare corrosion rate of metal in solution.

b) Maximal anodic amplitude of current transient much higher than corresponding maximal cathodic amplitude. According to [21], this reflects that the cathodic process is strongly hindered on aluminium surface. This is possibly attributed to the small cathodic surface on pure aluminium, low concentration of oxidizing agents in solution and/or the formation of stable passive layer on aluminium surface.

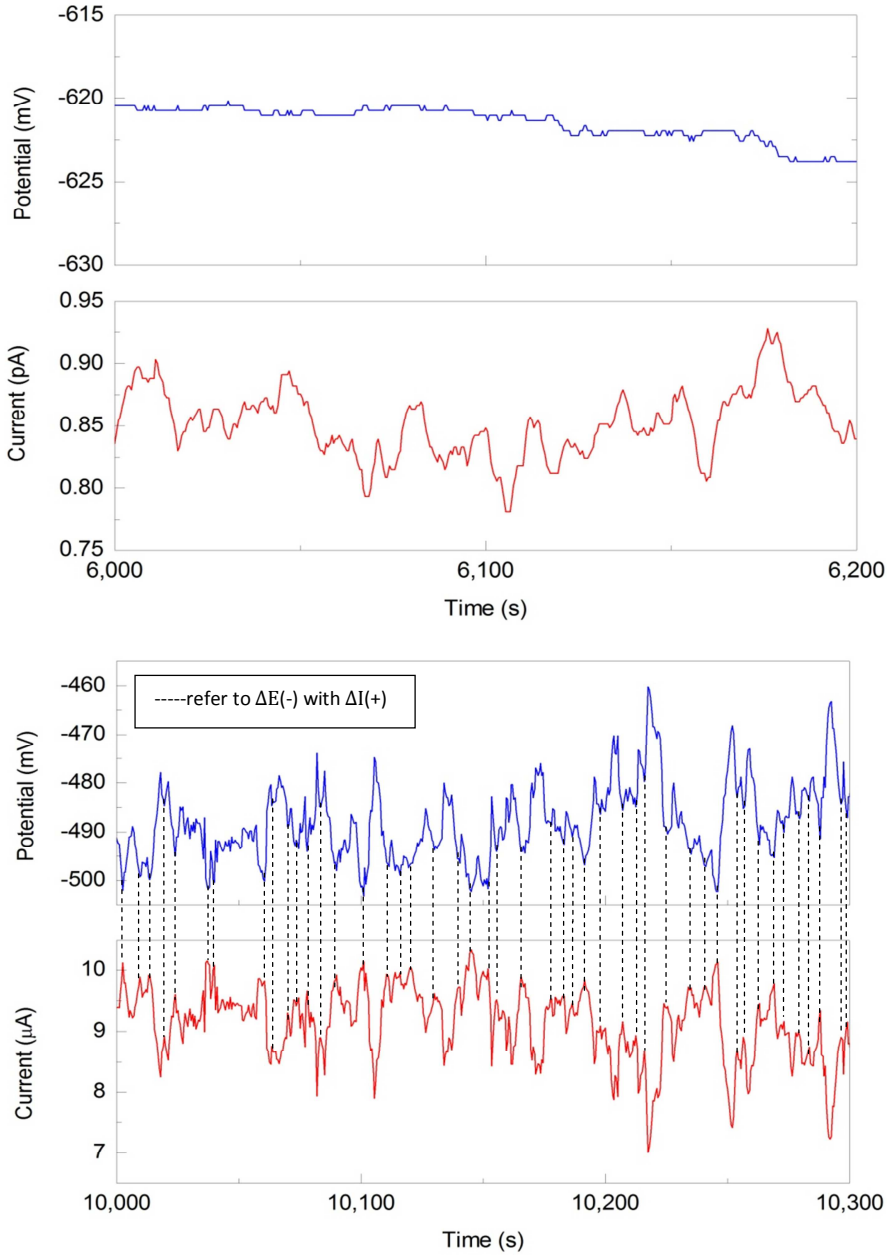

Figure 58: Zoom of potential and current signals of (top) only pure Al and (bottom) pure Al coupled with graphite in 0.001M NaCl.

The observed relationship between potential and current signals in figure 58 shows that:

a) Without coupling with graphite (figure 58, top), the potential and current fluctuations of only pure aluminium show really small amplitude of less than 1mV and 0.1pA, respectively. Moreover, there is no identifiable transient of potential drop coupled

simultaneously with current rise. Therefore it can be deduced that the predominant corrosion mechanism on pure aluminium without coupling with graphite is not pitting corrosion, but only slow *modification of oxide surface* by chloride ions.

b) After coupling pure aluminium with graphite, the transient (figure 58, bottom) can be characterized by potential drops (negative ΔV) coupled simultaneously with short anodic current rises (positive ΔI). This implies that the *pitting corrosion* occurs on the pure aluminium when coupled with graphite.

The serious pitting corrosion of pure aluminium is induced by the increase in potential of pure aluminium from nearly -620 to nearly -500mV after coupled with graphite. Therefore the pitting potential of pure aluminium in solution of 0.001M NaCl seems to lie between -620 and -500mV.

Comparison of potential and current signals of pure aluminium when coupled with graphite in deionised water and in 0.001M NaCl solution, it can be concluded that:

a) In deionised water, the potential of pure aluminium when coupled with graphite increases but the *corrosion mechanism of pure aluminium does not change from formation of oxide film*. This formation of oxide film relates to the potential and current signals that:
    - Potential keeps nearly constant without any fluctuation.
    - Current suddenly increases from nearly 1pA to only 17.5nA and then decrease with time without significant fluctuation.
b) In NaCl solution, the potential of pure aluminium when coupled with graphite increases and the *corrosion mechanism of pure aluminium changes from modification of oxide film to pitting corrosion*. This pitting corrosion relates to the potential and current signals that:
    - Potential evolution with time decreases with serious fluctuation.
    - Current suddenly increases from nearly 1pA to 9µA and keeps fluctuating at constant high current.

This measurement shows that the corrosion behaviour of pure aluminium changes from modification of oxide film in the absence of graphite to pitting corrosion when coupled with graphite in NaCl solution. Moreover, the EN techniques can be used to predict the corrosion behaviour and to estimate the corrosion rate of galvanic coupling system by this two working electrodes set-up.

1.12) Effect of surface area ratio on galvanic behaviour

For this measurement, the effect of surface area ratio of graphite to pure aluminium on potential and current signals of pure aluminium when coupled with graphite in 1M NaCl was studied. The set-up in figure 53 was still applied for this measurement. During the measurement, the surface area of graphite electrode was increased twice from 32mm^2 to 64 mm^2 by inserting more graphite into solution.

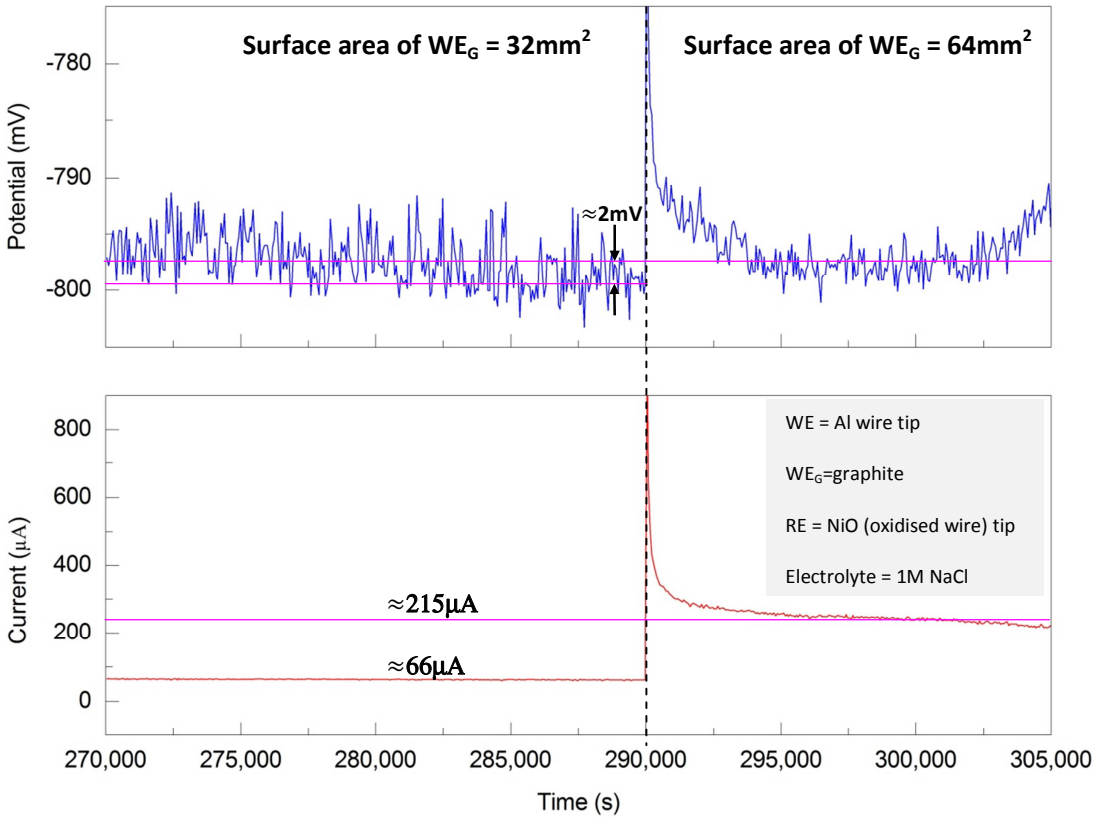

Figure 59: Potential and current signal of pure aluminium when coupled with graphite in 1M NaCl with increasing surface area of graphite.

The potential and current signals in figure 59 show that:

a) The mixed potential of pure aluminium and graphite seems to be nearly constant.
b) Current flowing between pure aluminium and graphite sharply increases from 66 to 215µA with increasing two times of the surface area of graphite. This implies that the corrosion rate of pure aluminium when coupled with graphite increases with increasing surface area of graphite. It is mentioned earlier that when pure aluminium coupled with

graphite, pure aluminium acts as anode and graphite acts as cathode. The increasing surface area of cathode results in the fast consumption of electrons by cathodic reaction on graphite electrode. This possibly leads to the acceleration of anodic reaction of anode to supply more electrons. Therefore it can be said that the increase in surface area ratio of cathode to anode of galvanic coupling results in the increase in corrosion rate of anode.

This measurement shows that when pure aluminium coupled with graphite, the corrosion rate of pure aluminium increases with increasing surface area ratio of graphite to aluminium.

2. Open circuit potential (OCP) and Polarization Measurement:

2.1) Pitting behaviour of pure aluminium when coupled with Cu or CFRP

This measurement was to study the potential of pure aluminium when coupled with copper (Cu) or CFRP in NaCl solution. Prior to measurement, pure aluminium sheet was mechanically polished with abrading SiC particle of 15µm-grit size and rinsed with plenty of deionised water. Then pure aluminium sheet, NiO wire tip and copper plate (or CFRP) were all immersed in 0.05M NaCl solution as shown in figure 60. Firstly pure aluminium sheet and NiO (oxidised wire) tip were connected to working and reference electrode, respectively. After immersion in NaCl for 30 min, pure aluminium sheet was coupled with Cu or CFRP for 30 min and then pure aluminium sheet was uncoupled with Cu or CFRP. During measurement, only OCP was monitored.

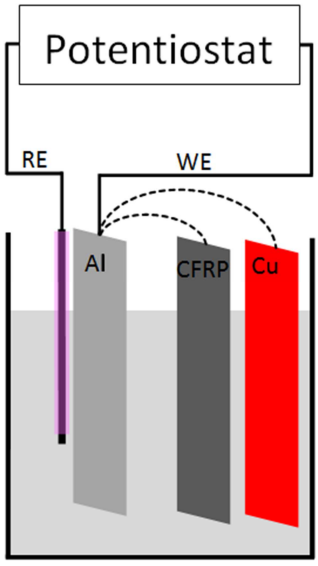

Figure 60: Set-up for OCP measurement of pure aluminium when coupled with Cu or CFRP.

The OCP curve of pure aluminium when coupled with copper in figure 61 shows that:

a) When coupled with copper, OCP of pure aluminium shifts to more positive value by 177mV from potential of pure aluminium in the absence of copper.

b) The step down and subsequent recovery of potential transient (see the red arrows) is observed during the coupling of pure aluminium with copper, indicating the strike of metastable pitting corrosion on pure aluminium surface when coupled with copper.

c) After uncoupled with copper, OCP of only pure aluminium returns back to nearly the same value as before, but noise with higher amplitude shows up. This possibly reflects the growing of the pits initiated during the coupling of pure aluminium with copper.

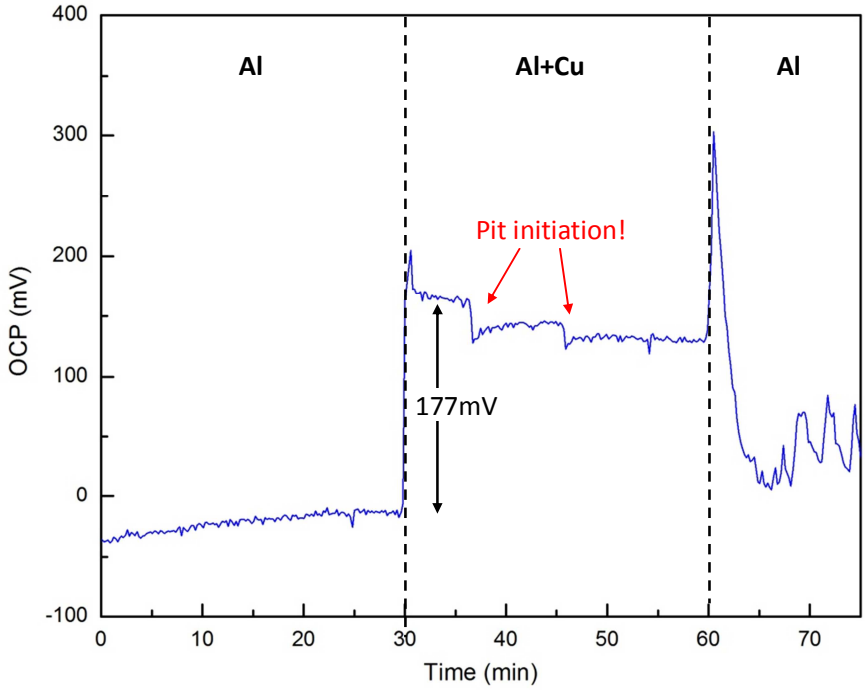

Figure 61: OCP of pure aluminium coupled with copper as a function of immersion time.

The OCP curve of pure aluminium when coupled with CFRP in figure 62 shows that:

a) OCP of only pure aluminium in the absence of CFRP shows no fluctuation.

b) When pure aluminium coupled with CFRP, OCP of pure aluminium sharply increases by 403mV and starts fluctuating. Moreover during the coupling of pure aluminium with CFRP, the OCP of aluminium decreases with time. This combination indicates localised corrosion, such as stable pitting corrosion, occurring on pure aluminium surface.

c) After pure aluminium is uncoupled from CFRP, OCP of pure aluminium shifts down by 200mV to nearly the same potential as before coupled with CFRP. Additionally, no more fluctuation is detected on OCP curve. This reflects that stable pitting corrosion stops suddenly after uncoupled pure aluminium from CFRP.

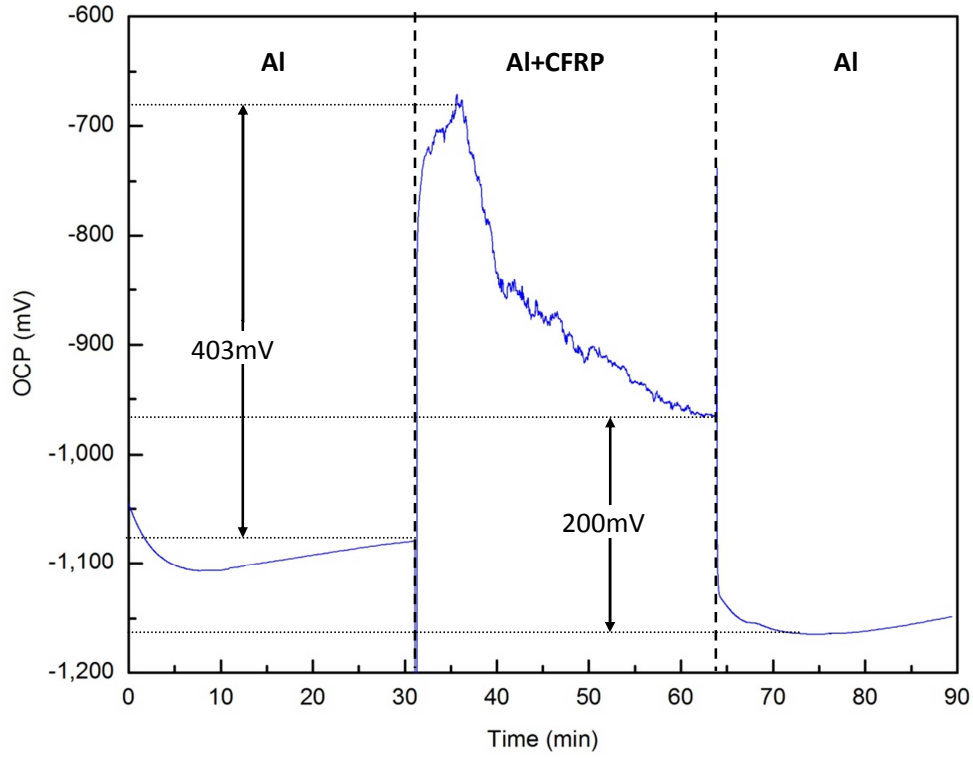

Figure 62: OCP of pure aluminium sheet coupled with CFRP as a function of immersion time.

According to table 1 that copper and carbon (graphite) are in higher galvanic series than aluminium, when aluminium coupled with copper or carbon, galvanic cell is built up between them and copper (or carbon) anodically polarises aluminium. Therefore the potential of pure aluminium increases when coupled with copper or CFRP. Moreover, the pitting corrosion can be induced on pure aluminium surface. It was mentioned in [7] that as pure aluminium is passive metal, it is possible that the increase in potential can accelerate pitting corrosion to occur on surface of pure aluminium. Therefore this measurement verifies the use of OCP technique to predict the galvanic corrosion behaviour between two metals. However the increase in OCP does not say anything about the intensity of corrosion rate of possible galvanic corrosion.

This measurement shows that when pure aluminium coupled with nobler metal such as copper or carbon in CFRP, potential of pure aluminium increases and pitting corrosion can be accelerated on pure aluminium surface.

2.2) Scan rate testing

For this measurement, pure aluminium wire was polarized by potentiodynamic method using different scan rates in order to study the effect of scan rate on polarization behaviour of pure aluminium in tap water. Three electrodes set-up (figure 63) was applied. Pure aluminium wire, NiO (oxidised wire) tip and aluminium sheet were used as working, reference and counter electrodes, respectively. Firstly, electrodes were spontaneously passivated in tap water for 3h. Then potentiodynamic polarisation started from 200mV below the OCP up to 1,200mV above the OCP in noble direction with very low scan rates of 10mV/h and 20mV/h.

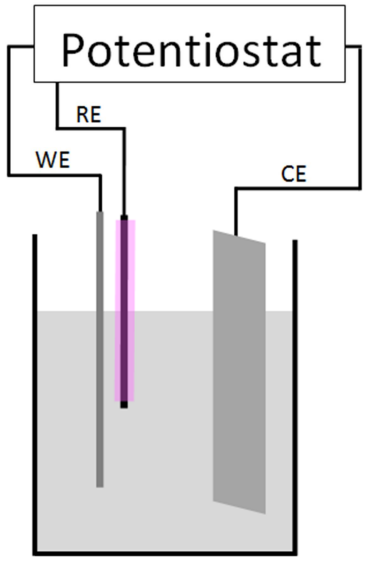

Figure 63: Three electrodes set-up for polarization of pure aluminium wire.

The polarization curves of pure aluminium in tap water with scan rate of 10mV/h and of 20mV/h (in figure 64) are comparable, reflecting that the polarization measurement of pure aluminium wire is reproducible. Moreover, the comparisons of the polarization curves with different scan rate and the corrosion parameters in table 6(appendix) shows that:

a) The passive currents from both scan rates are nearly the same, showing the state of the oxide film in terms of thickness and chemical composition negligibly changes with scan rate. However, the quality of the oxide film may be different.

b) The stable pitting potential decreases from -67 to -88 mV and the passive region range decreases from 1,050mV to 974mV with increasing scan rate from 10 to 20mV/h. The

decrease in pitting potential and passive region range implies that the scan rate have an effect on stable pitting tendencies of pure aluminium. The higher the applied scan rate, the higher the tendencies of pure aluminium to pitting corrosion. This may be attributed to the formation of proper passive oxide film with lower scan rate. With higher scan rate there is not enough time for the formation of proper oxide film whereas with lower scan rate, time needed for formation of proper oxide film is available. This proper passive oxide film demotes the stable pitting corrosion.

c) With lower scan rate of 10mV/h, the metastable pitting corrosion attacks much less seriously on pure aluminium surface than with higher scan rate of 20mV/h. This can also be attributed to the formation of proper oxide film with lower scan rate. The metastable pitting corrosion can occur less seriously on proper oxide film.

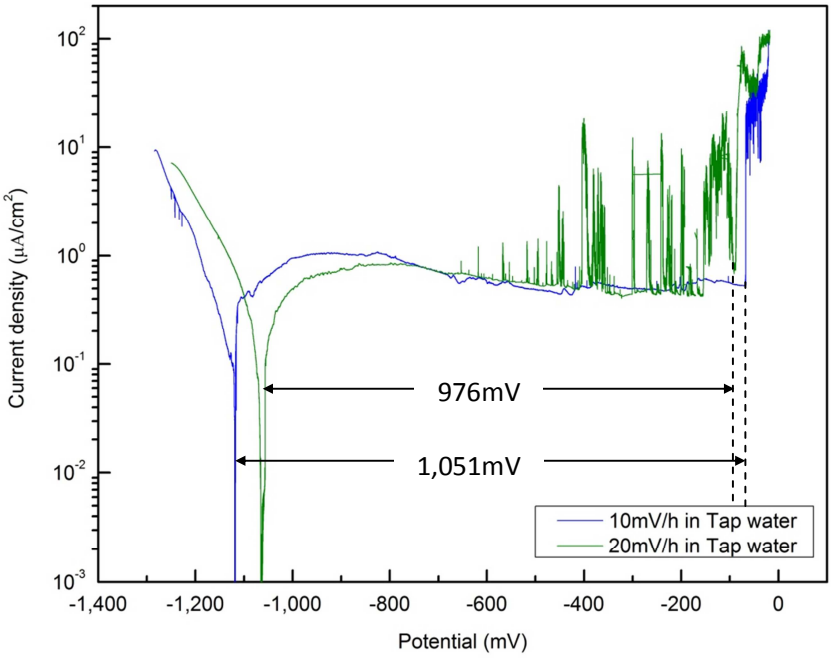

Figure 64: Polarization curves of pure aluminium with different scan rate in tap water.

It may be deduced that with different scan rate, the state of formed oxide film in term of the average thickness and chemical composition has no significant difference. However, the proper oxide film possibly in term of uniform thickness is preferred to form with lower scan rate.

Therefore, this measurement shows that the scan rate of potentiodynamic polarization has a strong effect on metastable pitting corrosion of pure aluminium.

2.3) Characterising aluminium oxide surface by Tafel slope analysing

In order to study the effect of scan rate on other corrosion parameters, Tafel slope analysis was conducted. This measurement used the set-up after measurement 2.2. 0.005M NaCl was added to solution and then the aluminium wire was potentiodynamic polarised from 250mV below the OCP up to 1,200mV above the OCP in noble direction with very low scan rates of 10mV/h and 20mV/h.

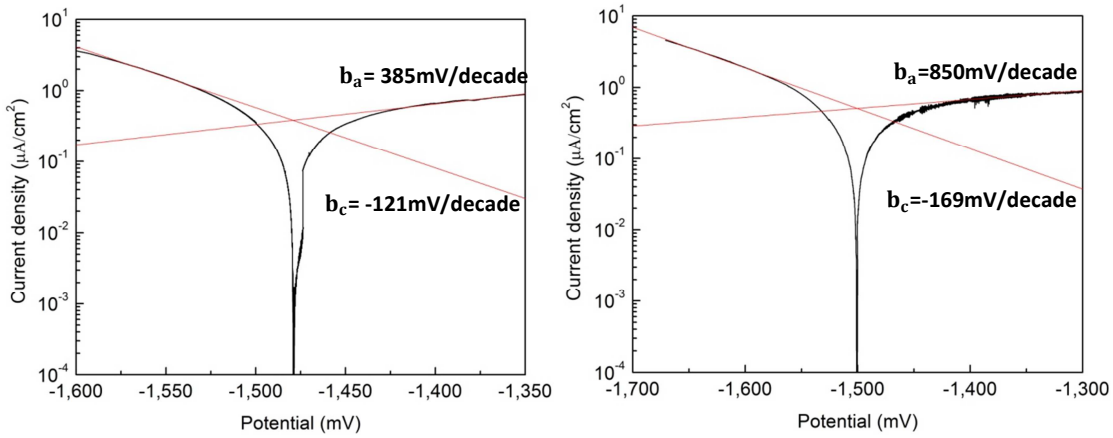

Figure 65: The Tafel slopes of aluminium in 0.005M NaCl with scan rate of: (left) 10mV/h and (right) 20mV/h.

Theoretical background mentioned that

a) For Cathodic Tafel slope:

From Volmer-Tafel mechanism of hydrogen evolution ($z = 1$) on metal surface,

$b_c = 2.3 \times \left(\frac{2RT}{zF}\right) = -118 \frac{mV}{decade}$ at 25°C.

If the electrode has an oxide film on metal surface, the Tafel slope may increase due to the influence of two potential energy barriers of the oxide film on the reduction process. The first barrier is the barrier in Helmholtz double layers. The charge carrier, H_3O^+ ions, must negotiate this barrier to reach the reaction site at the oxide/solution interface. The second barrier is the potential energy barrier within the oxide. The electron (e^-) from metal dissolution must negotiate this barrier to reach the metal/oxide interface, where the H_3O^+ and e^- subsequently neutralised each other [47, 48].

b) For Anodic Tafel slope:

From Volmer-Tafel mechanism of aluminium oxidation($z = 3$), $b_a = 40\text{mV/decade}$.

If $b_a \leq 40\text{mV/decade}$, only the uniform anodic dissolution of aluminium via hydrated Al^{3+} ions occurs [47, 48].

If b_a is much greater than 40mV/decade, it can be attributed to the presence of passive oxide film, participation of side reaction in anodic oxide film growth and penetration of chloride ions into film. Moreover, it has been indicated that the growth of oxide layer during anodic polarization also results in a high b_a [47, 48].

Tafel slopes in figure 65 and their corrosion parameters in table 6(appendix) shows that:

a) The corrosion potential of pure aluminium in 0.005M NaCl solution calculated from Tafel slope is nearly similar to that from polarization measurement.

b) b_c is in the range of expected -118mV/decade and b_a is much higher than 40mV/decade. According to the theoretical background, the deviation of b_a from Volmer-Tafel theory exhibits that there is an air-formed oxide film on surface of pure aluminium wire electrode and the oxide film is possibly growing during the anodic polarization.

c) Tafel slope from lower scan rate (10mV/h) is closer to that from scan rate of 20mV/h. This means lower scan rate seem to be more realistic.

This measurement shows that spontaneous or air-formed oxide film is formed on the surface of pure aluminium. Therefore pure aluminium always exhibits passive surface, not active surface. Moreover, no more Tafel slopes will be discussed in this research because it is commonly misused [49].

2.4) Scan rate testing: Comparison with commonly used scan rate of 600mV/h

For this measurement, polarization curve of pure aluminium wire in 0.001M NaCl solution from different scan rates are compared in order to study the effect of scan rate on corrosion parameters of pure aluminium. The two scan rates used in this measurement were widely different:

- scan rate of 10mV/h which is extremely low and not commonly used and
- scan rate of 600mV/h which is moderate and commonly used

Before starting polarization measurement, OCP of pure aluminium wire were monitored for 3h to compare the surface state of pure aluminium wire before polarization. The difference of OCP from two aluminium wires (in figure 66) is negligible. Therefore it can be assumed that these two aluminium wires have quite identical surface states before polarization measurement.

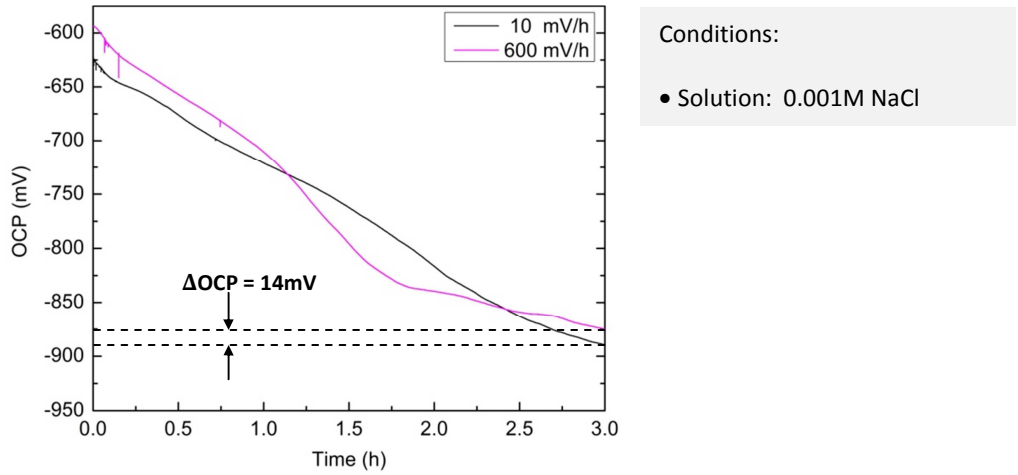

Figure 66: OCP curves of pure aluminium in NaCl solution before polarization.

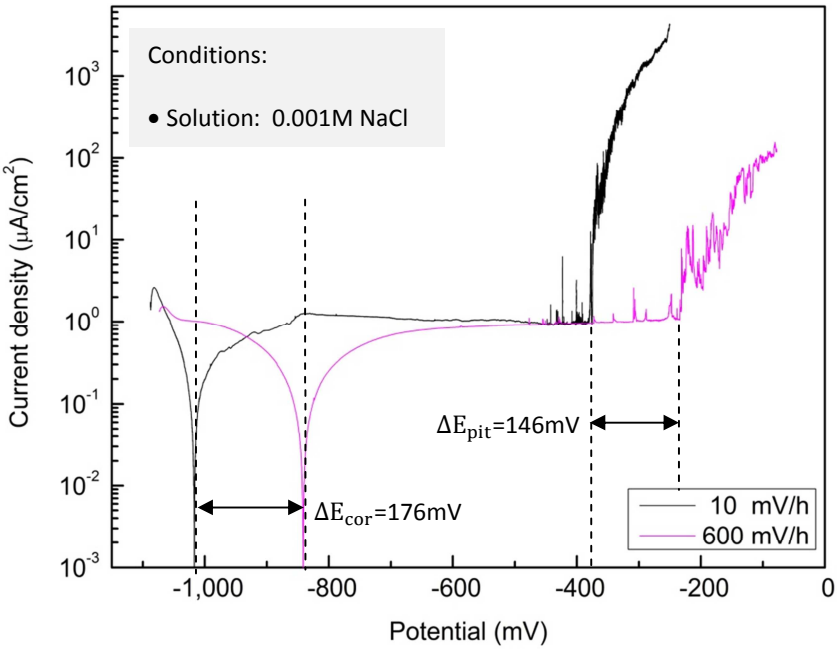

Figure 67: Polarization curves of pure aluminium in NaCl with different scan rate.

After the OCP measurement, the polarizations were conducted from 200mV below the OCP to 1,000mV above the OCP with different scan rates. The polarization curves in figure 67 show that:

a) The corrosion potential (E_{cor}) from scan rate of 10mV/h is more negative value than that from scan rate of 600mV/h, indicating the thinner of oxide film formed on pure aluminium surface during lower scan rate of 10mV/h. This can be attributed to the different time consumption during cathodic polarization. With scan rate of 10mV/h, time consumed during cathodic polarization is much longer than with scan rate of 600mV/h. Since the cathodic polarization of aluminium leads to the dissolution of oxide film on aluminium surface by the effect of hydrogen evolution process as will be mentioned later in measurement 2.7, much longer time in cathodic polarization with lower scan rate of 10mV/h results in higher thinning of oxide layer.
b) With lower scan rate of 10mV/h, potential at equilibrium state of pure aluminium after cathodic polarization (E_{cor}) shows more active value than that before cathodic polarization (OCP), confirming that longer time for cathodic polarization provides more active surface. Whereas with higher scan rate of 600mV/h, E_{cor} is nobler than OCP since the time for dissolution of oxide layer by cathodic polarization is too short and the oxide film may grow by the reduction of oxygen at low cathodic overpotential.
c) The pitting potential (E_{pit}) with scan rate of 10mV/h is at lower value than that with scan rate of 600mV/h.

In order to achieve the easier comparison of other corrosion parameters, the potential axis of polarization curve is replaced by overpotential axis. The overpotential (η) is defined as a change in potential from the corrosion potential ($\eta = E - E_{cor}$). Therefore with this overpotential axis, their corrosion potentials are correlated at 0mV. The polarization curves with over potential axis in figure 68 and their corrosion parameters in table 7(appendix) shows that

a) Passive current density (J_p) with different scan rate is nearly the same, indicating the same state of the oxide film in terms of average thickness and chemical composition.

b) Passive region range (ΔE_p) is larger by only 30mV for lower scan rate of 10mV/h, implying that susceptibility to stable pitting corrosion of pure aluminium slightly decreases with decreasing scan rate. This can be attributed to the formation of proper passive oxide film in term of uniform thickness. Since it would be mentioned later in

measurement 2.13 that in passive region, the thickness of oxide film changes greatly slowly in response to the change in the electrode potential. This means with high scan rate, time is not enough for formation of proper passive film whereas at slow scan rates, there is available time for formation the proper passive film. The better the proper passive film, the lower the susceptibility to pitting corrosion.

c) At higher scan rate of 600mV/h, metastable pitting corrosion is detected at lower overpotential than at lower scan rate of 10mV/h (see arrows). This can also be attributed to the formation of proper passive oxide film with scan rate of 10mV/h.

d) The pitting current density increases more steeply with lower scan rate of 10mV/h. This can be attributed to a longer time for polarization at potential in pitting region. It will be mentioned later in measurement 2.13 that the current density at potential higher than pitting potential strongly increases with time.

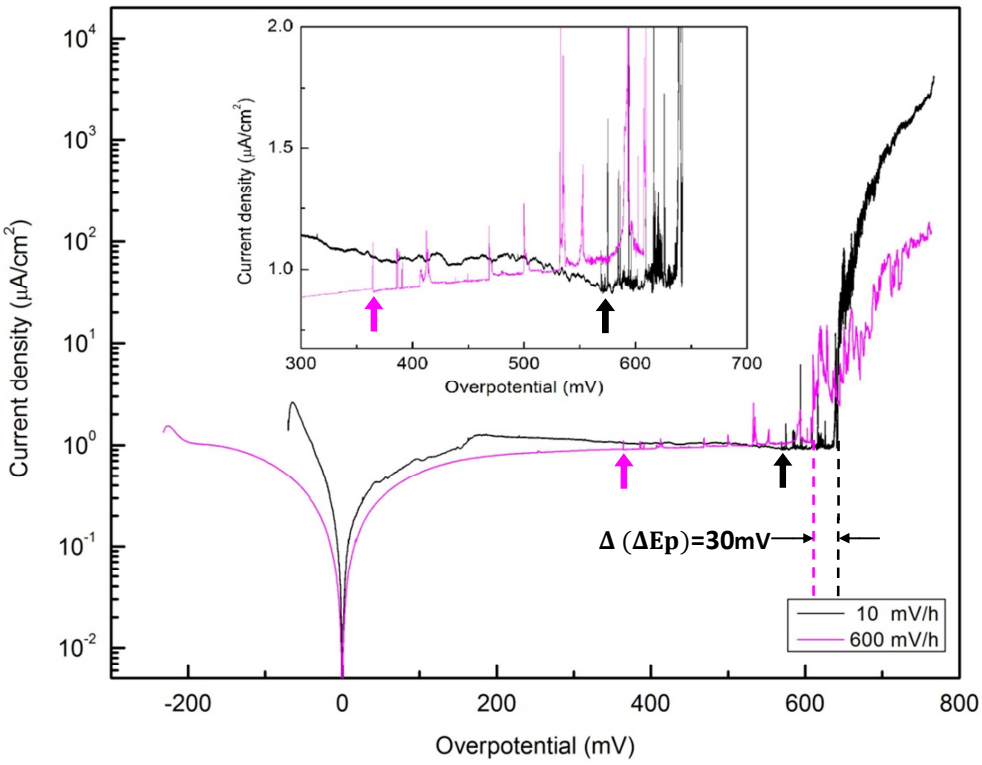

Figure 68: Overpotential-polarization curves of pure aluminium wire with different scan rates.

Therefore, it can be concluded from this measurement that the scan rate of polarization strongly shifts the polarization parameters such as corrosion potential (E_{cor}) and pitting

potential (E_{pit}). However, it only slightly affects on some of the corrosion parameters of sample under investigation such as passive region ranges (ΔE_p), which relates to pitting susceptibility of sample, and passive current density (I_p), which relates to passive behaviour of sample. Therefore in order to reduce the measurement time for later polarization measurement, the moderate scan rate of 600mV/h will be used to investigate corrosion behaviour of aluminium instead of extremely low scan rate of 10mV/h.

2.5) Long term passivation

For this measurement, long term polarization at low anodic overpotential was conducted to study the formation of oxide film on pure aluminium surface. This measurement used the set-up after measurement 2.3. The aluminium wire was polarized at anodic potential of 200mV above the OCP for 14 days without stirring and temperature control in order to study a small variation of current density.

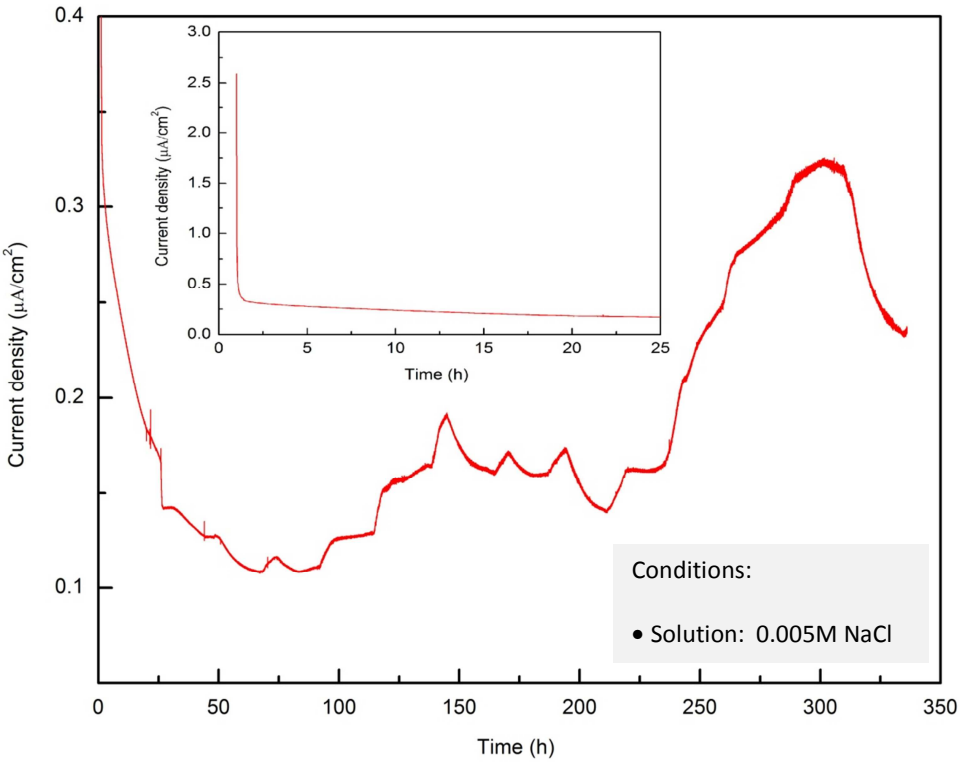

Figure 69: Anodic polarized current of pure aluminium wire at constant potential of OCP+200mV for 14 days: (small) for beginning of the polarization and (large) for full-time of polarization.

The anodic polarized current in figure 69 shows that:

a) At the beginning, anodic current density sharply decreases from 2.6 to 0.3μA/cm^2 (figure 69, small) and then the decrease rate is reduced. This indicates that the passive oxide film is fast formed at the beginning of anodic polarization and then the formation rate is dramatically decreased due to the fast thickening of oxide film.

b) After about 1 day, current slowly fluctuates in the range of only 0.1 to 0.4μA/cm^2. This slow fluctuation may be the result of the temperature change during the day.

Theoretical background for explanation of the slow fluctuation by the change in temperature: The Bulter-Volmer equation of anodic current densities is $\mathrm{i}_+ = \mathrm{i}_0 \exp\left(\frac{\mathrm{zF}}{2\mathrm{RT}}\eta\right)$, where i_o is the exchange current density, $\eta = \mathrm{E} - \mathrm{E}_0$ is overpotential and $\mathrm{z} = 3$ for anodic dissolution of aluminium [50].

If the temperature changes from T_1 to T_2, the current induced will be change from i_1 to i_2.

Therefore it is expected that $\frac{\mathrm{i}_2}{\mathrm{i}_1} = \exp\left[\frac{\mathrm{zF}\eta}{2\mathrm{R}}\left(\frac{1}{\mathrm{T}_2} - \frac{1}{\mathrm{T}_1}\right)\right]$.

If temperature changing during the day is 5K that $\mathrm{T}_1 = 293\mathrm{K}$ and $\mathrm{T}_2 = 298\mathrm{K}$, thus $\mathrm{i}_2 \approx 0.82\mathrm{i}_1$. This means if the temperature changes during the day by 5K or 5°C, the anodic current induced during anodic polarization will also be altered by about 20%.

This measurement shows that the passive oxide film is built up during anodic polarization at low overpotential in the range of 24h.

2.6) Passive behaviour : Effect of spontaneous oxide film

Starting from this measurement, the polarization measurement of pure aluminium was carried out with set-up as in figure 70. The working electrode was made of pure aluminium sheet. This pure aluminium sheet was freshly polished by a series of silicon carbide papers with abrading grit size up to 15μm. In order to avoid a prolonged exposure to atmosphere, aluminium working electrode was tested immediately after polishing, cleaning with water and dying with air process. NiO (oxidised wire) tip and platinum sheet were used as a reference and

counter electrodes. Temperature was controlled at 300 $\pm$ 3K and the solution was stirred by a magnetic stirrer and a stirring bar. In the aerated experiment, the solution was bubbled with air while in the deaerated experiment the solution was bubbled with N_2 for at least 3h before starting the measurement.

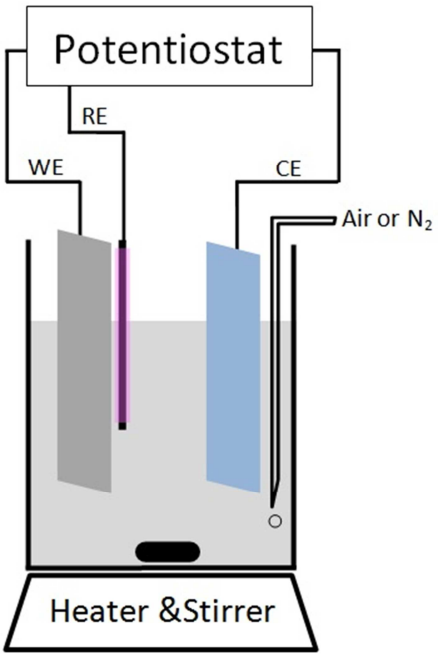

Figure 70: Measurement set-up for polarization of pure aluminium sheet.

For this measurement, the effect of spontaneous oxide film on corrosion behaviour of pure aluminium was studied. In order to obtain a spontaneous oxide film on the electrode surface, the freshly polished aluminium electrodes were left in deionised water for 20h (Passivation). This pure aluminium sheet with spontaneous oxide was then immersed in aerated 0.01M NaOH solution and held at OCP for 3h. After that, it was polarized in noble direction from 250mV below the OCP to 1,000mV above the OCP at scan rate of 600mV/h. For comparison, the polarization of pure aluminium sheet without spontaneous oxide film was also conducted.

The polarization and OCP curves in figure 71 and corrosion parameters in table 8(appendix) shows that:

a) Corrosion potential (E_{cor}) of pure aluminium with spontaneous oxide film is observed to be lower than that without spontaneous oxide film, indicating the more imperfect oxide film formed on pure aluminium surface with spontaneous oxide film.

b) The passive current density (J_p) of pure aluminium with spontaneous oxide film is higher than that without spontaneous oxide film, confirming the lower quality oxide film formed during anodic polarization of pure aluminium with spontaneous oxide film. This confirms that the spontaneous oxide film hinders the further proper formation of passive oxide film during anodic polarization in basic solution.

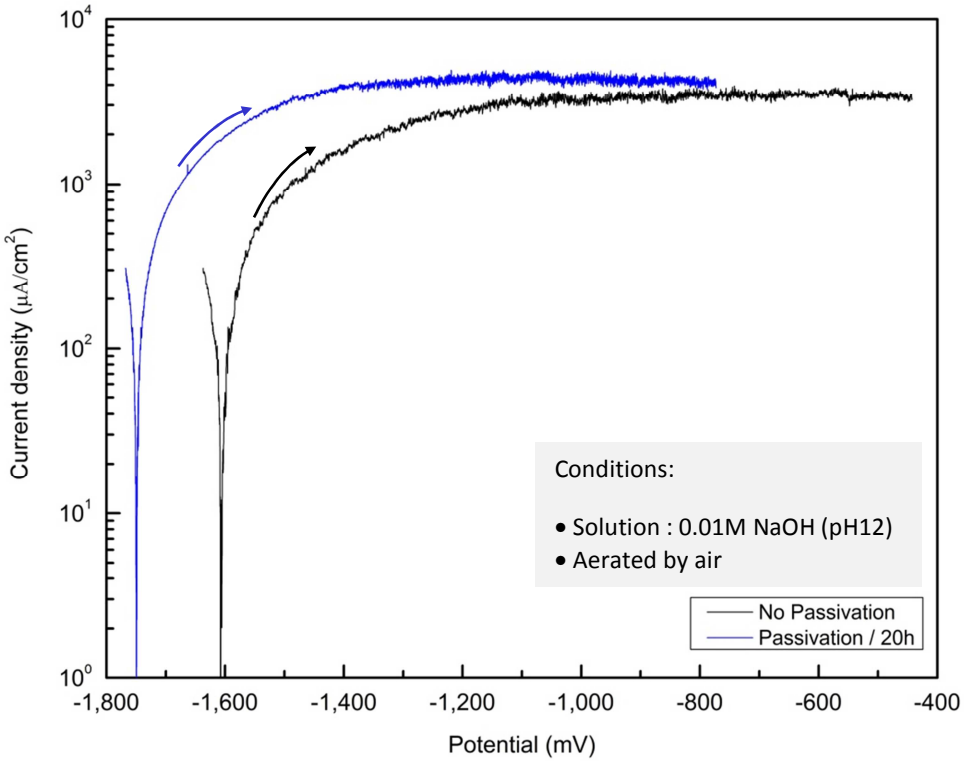

Figure 71: Polarization curves of pure aluminium in NaOH solution with and without spontaneous oxide film.

Therefore, this measurement shows that proper anodic oxide film can be formed on active surface, not spontaneous passive surface.

2.7) Passive behaviour : Different surface treatments

The objective of this measurement was to try out, if it is possible to remove any spontaneous oxide layer by constant cathodic polarization. It was mentioned in [36] that when expose aluminium in oxidising media such as water and air, spontaneous oxide layer will be

formed immediately. This spontaneous oxide layer can be eliminated from aluminium metal surface due to the effect of hydrogen evolution during cathodic polarization. During cathodic polarization, the reduction of water ($2H_2O + 2e^- \rightarrow H_2 + 2OH^-$) occurs on the oxide covered-aluminium surface. The produced hydroxide ions lead to the increase in alkalinity at the oxide/solution interface, which results in the increase of solubility of aluminium oxide [24, 26, 51]. It was also mentioned in [9] that during cathodic polarization, local pH of solution changes to higher value and the dissolution of oxide film can subsequently take place. Therefore aluminium may be no longer protected by oxide film and active surface can be reached.

For this measurement, the constant cathodic potential of 250mV below the OCP was first applied in deaerated basic solution (pH 12) for 35h before scanning polarization in order to remove any spontaneous oxide film formed prior to the measurement. After that, pure aluminium was polarized in noble direction up to 4,000mV above the OCP at scan rate of 600mV/h. For comparison the scanning polarization was also conducted on pure aluminium without prior constant cathodic polarization. With this measurement step, the effect of spontaneous oxide film on corrosion behaviour of pure aluminium was studied for comparison.

The polarization curves in figure 72 show that:

a) With prior constant cathodic polarization, *peak of current density* near corrosion potential is detected, indicating the domain of passivity. While it is not detected without prior constant cathodic polarization. It was mentioned in [50] that the peak is where the *transition of metal surface from active to passive* state takes place. The potential at this peak is called a *passivation potential*. Below this passivation potential, active dissolution of metal takes place and after reaches the passivation potential, the dissolution current drops because the metal surface is passivated by the formation of oxide film. Generally, the polarization curve of aluminium does not exhibit the domain of passivity because aluminium is naturally passive [36]. Therefore the observed peak implies that the active surface is achieved by prior constant cathodic polarization for 35h. For this research, the *peak of current density* near corrosion potential is called an *active peak*.

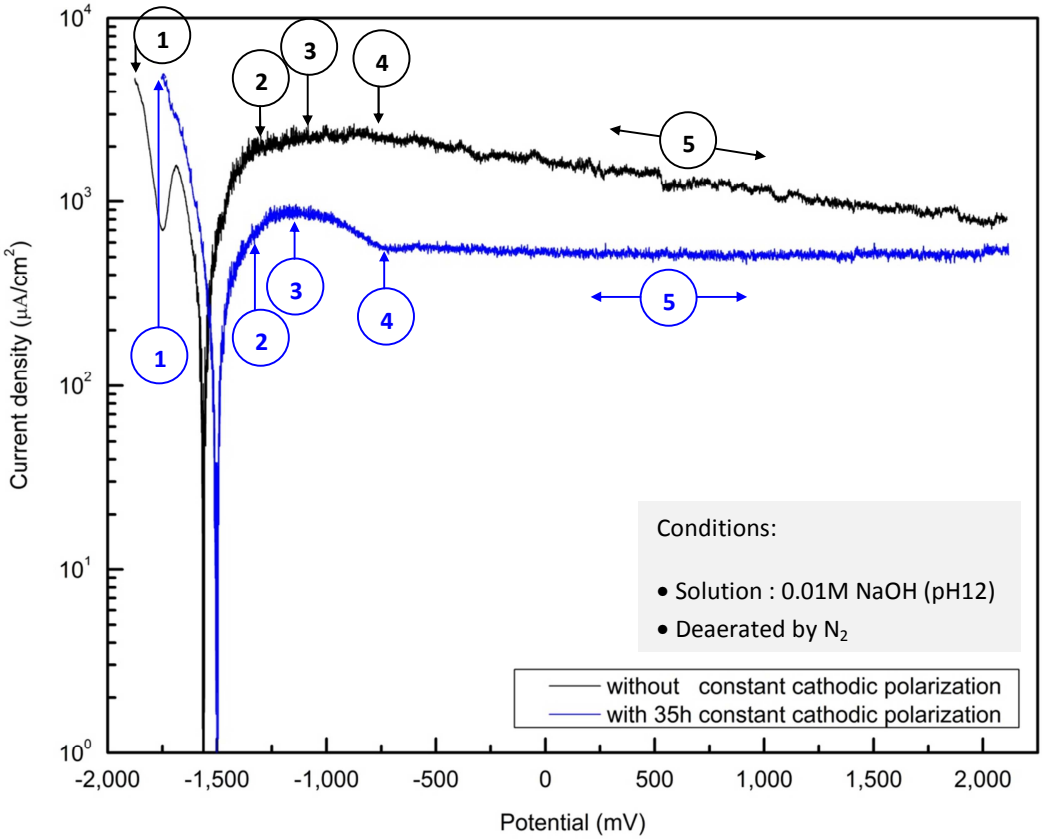

Figure 72: Polarization curves of pure aluminium with prior constant cathodic polarization.

Model for	Processing number				
	1	2	3	4	5
Without prior constant cathodic polarization	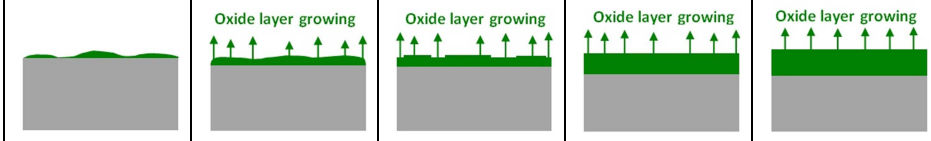				
With prior constant cathodic polarization	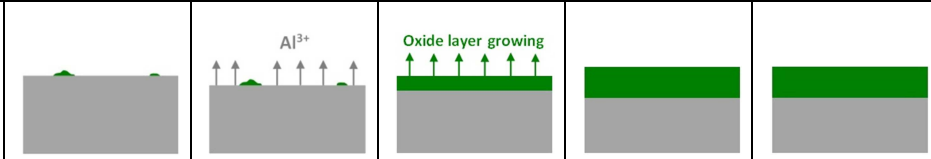				

Figure 73: Model of corrosion mechanism on pure aluminium surface during polarization measurement: Grey ( ) and green ( ) represent the aluminium and oxide, respectively. * The processing number is the number in the red circular on polarization curves of aluminium in figure 72.

b) The passive current density (J_p) of pure aluminium with prior constant cathodic polarization is lower than that without prior cathodic polarization. It indicates that during anodic polarization, the active surface of pure aluminium can form thicker passive oxide film than the surface covered with spontaneous oxide film. Moreover, the passive current density of pure aluminium with constant cathodic polarization keeps constant when potential is further increased, indicating the fast fully formed passive oxide film on initial active surface. Whereas the passive current of pure aluminium without constant cathodic polarization still decreases with increasing polarized potential, indicating the continuous growing of passive oxide film on initial spontaneous oxide surface. This confirmed the result in measurement 2.6 that the spontaneous oxide film hinders the further formation of high quality passive oxide film in basic solution.

From the information of the polarization curves in figure 72, the model of corrosion mechanism of pure aluminium is proposed in figure 73. The model for surface with prior constant cathodic polarization (blue curve in figure 72) starts with active surface (point **1**). When the potential increases from corrosion potential to point **2**, metal dissolution takes place intensively since there is no oxide surface. For the peak at point **3**, the surface state of pure aluminium changes from active to passive due to the formation of a thin anodic oxide film. When the potential further increase to point **4**, anodic current decreases due to the fast thickening of the anodic oxide film until it reaches a stable thickness on pure aluminium surface. Therefore no more thickening of oxide film is observed in region **5** (passive region). This results in a constant anodic current as the potential increases further. On the other hand, the model for surface without prior constant cathodic polarization (black curve in figure 72) starts with spontaneous passive surface (point **1**). This spontaneous passive film is inhomogeneous in thickness and hinders the active dissolution of metal. When the potential increases from corrosion potential to point **4,** transformation of this inhomogeneous to more and more homogenous thickness takes place. In region **5**, the homogenous passive film is growing with relatively slow rate. Therefore at the end of measurement, stable thickness of anodic oxide film has not yet been reached.

This measurement shows that the active aluminium surface can be achieved by constant cathodic polarization.

2.8) Passive behaviour : Time dependent activation

For this measurement, the effect of the period of time for prior constant cathodic polarization on corrosion behaviour of pure aluminium was studied. Therefore, prior to scanning polarization, different duration times of prior constant cathodic polarization at potential of 250mV below the OCP were applied.

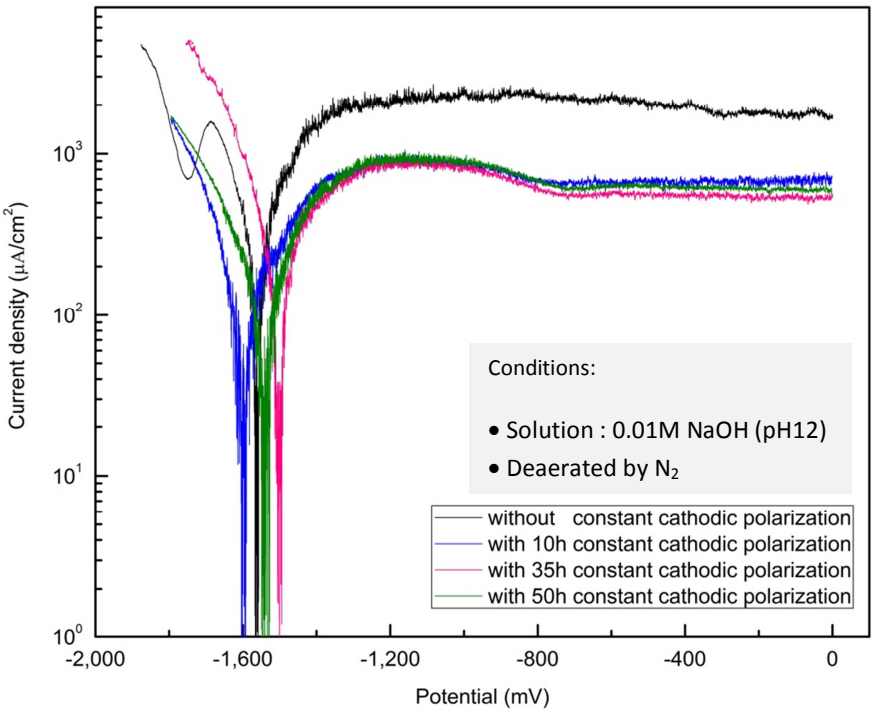

Figure 74: Polarization curves of pure aluminium with different period of time for prior constant cathodic polarization.

The polarization curves in figure 74 show that:

a) With prior constant cathodic polarization for at least 10h, an active peak is detected.

b) The different period of time for prior cathodic polarization shows no significant difference on forward polarization curves of pure aluminium.

Therefore this measurement indicates that the active surface of pure aluminium can be achieved by prior constant cathodic polarization for only 10h.

2.9) Passive behaviour : Quality of passive layer

The measurement earlier shows that the different periods of time for prior cathodic polarization show no significant effect on only forward polarization curve, whose direction is from active to noble potential. For this measurement, the effect of prior constant cathodic polarization on cyclic polarization curves of pure aluminium in basic solution was studied. Therefore the prior constant cathodic polarization at -1,800mV was firstly applied on pure aluminium in deaerated basic solution (pH12) for different periods of time before starting the cyclic polarization. The cyclic polarization was commenced at a scan rate of 600mV/h in noble direction from -1800mV up to 0mV. Then the scanning direction was reversed and potential was scanned back to -1,800mV.

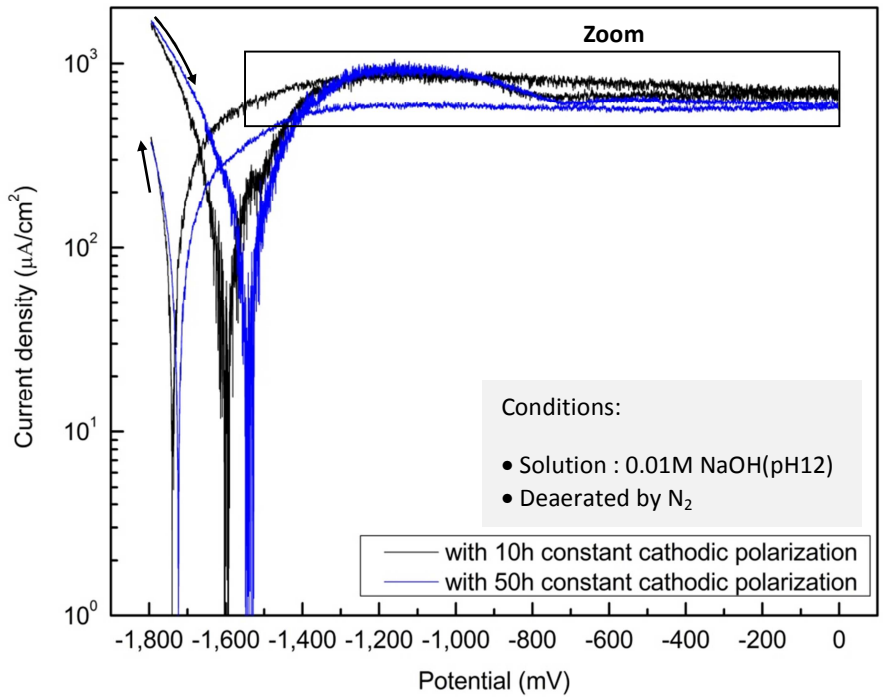

Figure 75: Cyclic polarization curves of pure aluminium with different period of time for prior constant cathodic polarization.

The polarization curves in figure 75, figure 76 and their corrosion parameters in table 9 (appendix) show that

a) Active peaks are detected with prior constant cathodic polarization for both 10h and 50h, indicating active surface of pure aluminium.

b) With shorter prior cathodic polarization (10h), passive current on the reverse curve is higher than that on forward curve and additionally increasing (figure 76). On the other hand, with longer prior cathodic polarization (50h), passive current on reverse polarization is lower than forward polarization and additionally nearly constant. This can be attributed to the ratio of active to spontaneous oxide surface. The longer constant cathodic polarization can provide the higher ratio of active surface to spontaneous oxide surface.

c) With longer prior cathodic polarization (50h), the passive current on the forward polarization slightly shifts to lower value than with shorter prior cathodic polarization (10h). This suggests that the surface with higher ratio of active to passive surface can form more homogeneous passive oxide film since spontaneous oxide film hinders the growing of a homogeneous passive oxide film.

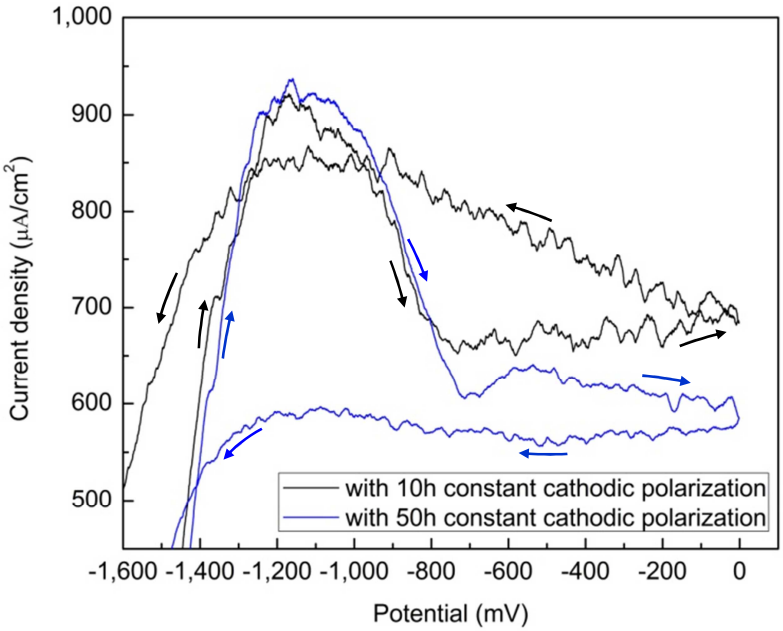

Figure 76: Zoom of smoothed-cyclic polarization curve from fig 75.

From the information of polarization curves in figure 75 and 76, the model of pure aluminium surface after prior cathodic polarization for different period of time is proposed in figure 77.

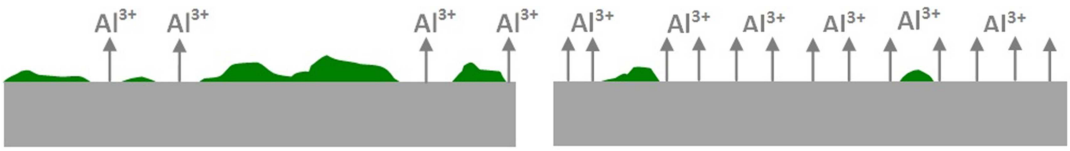

Figure 77: Model of pure aluminium after constant cathodic polarization: (left) for 10h and (right) for 50h. *Grey ( ) and green ( ) represented the aluminium metal and spontaneous oxide, respectively.

It may be concluded from this measurement that the longer the prior cathodic polarization, the more the spontaneous oxide film on pure aluminium surface is dissolved and the more and the better partial active aluminium surface is achieved. Therefore for further measurements, the prior constant cathodic polarization for 50h will be applied to aluminium before scanning polarization to get reproducible surface conditions.

2.10) Passive behaviour: Oxygen concentration in solution

For this measurement, the effect of aeration on corrosion behaviour of pure aluminium in basic solution was studied. Thus, polarization curve in aerated and deaerated solution have been compared.

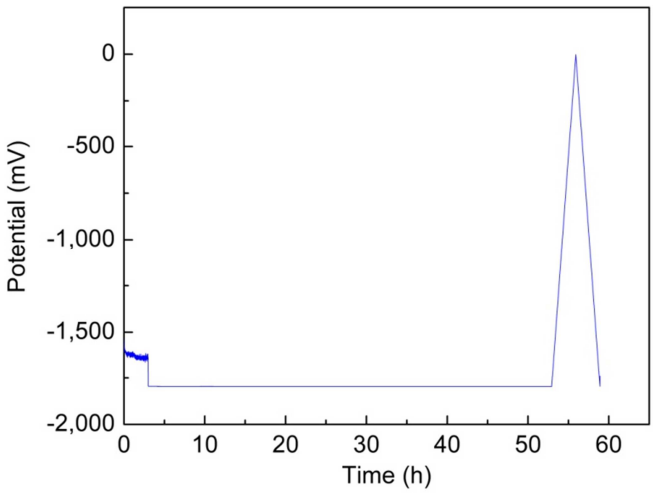

Figure 78: Measurement step for polarization of pure aluminium in basic solution (pH 12).

Starting from this measurement, steps of polarization measurement were set as in figure 78. The measurement started with OCP measurement for 3h suddenly after immersion of sample in

solution and then the prior constant cathodic polarization was applied for 50h. After about 16h, the constant current density of about 3µA/cm^2 had been reached. Finally, cyclic polarization was carried out with scan rate of 600mV/h.

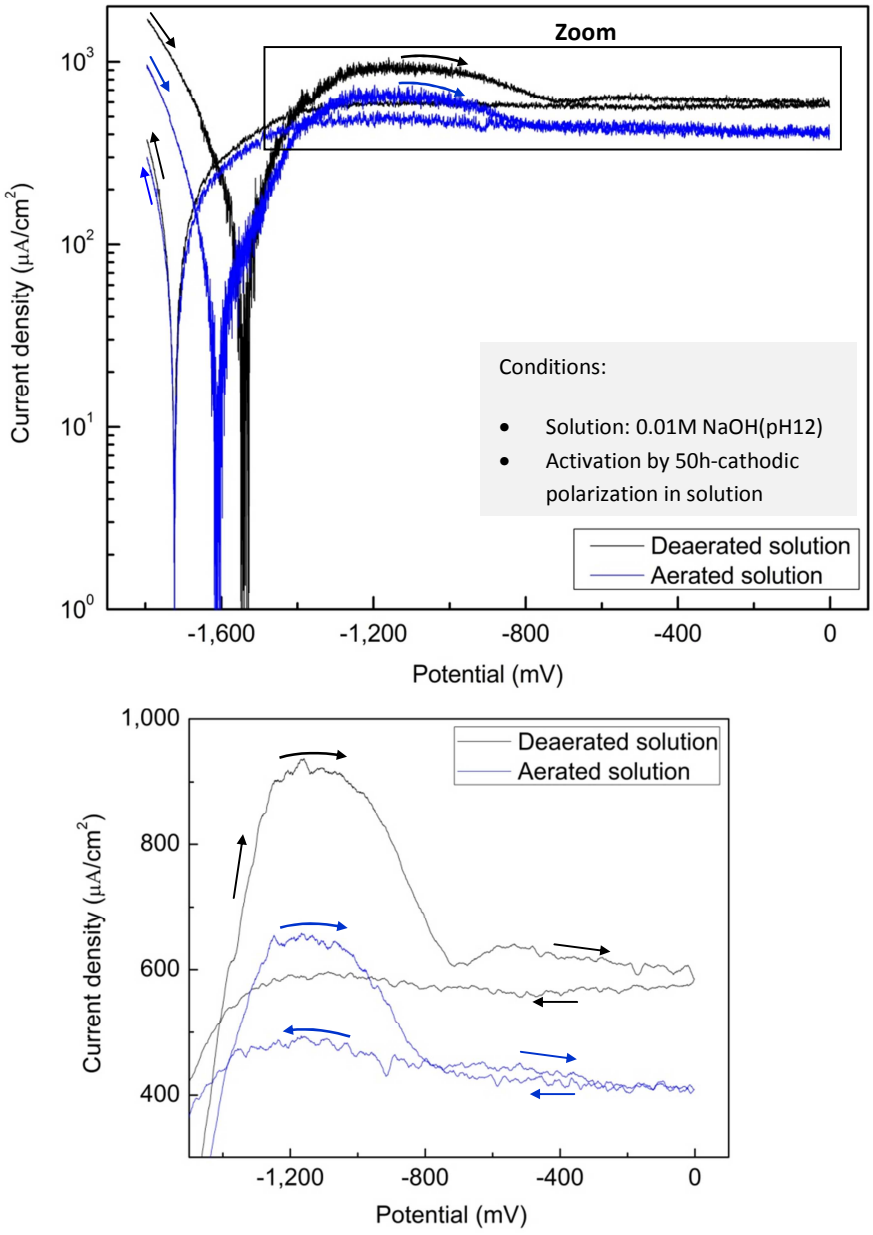

Figure 79: (Top) cyclic polarization curves of pure aluminium in basic solution with different aeration and (bottom) zoom of smoothed-cyclic polarization curves of figure on top.

The polarization curves in figure 79 and their corrosion parameters in table 10(appendix) shows that:

a) Active peaks are detected from both aeration systems, indicating that active surface can be achieved in both aerated and deaerated basic solution. However the current density at active peak or at passivation potential in deaerated basic solution is higher, reflecting that the better active surface is achieved therein. This can be attributed to low concentration of oxygen in deaerated solution.

b) Passive current density (J_p) of pure aluminium in deaerated basic solution is higher than in aerated basic solution, indicating that the formed passive oxide layer in deaerated solution is thinner than that in aerated solution. This may be due to the fact that in aerated basic solution there are available oxygen molecules for formation of a thicker oxide film.

c) The reverse anodic curves exhibit a constant current. This indicates stable oxide film in both cases.

This measurement shows that active aluminium surface can be achieved in both aerated and deaerated basic solutions. However, the deaeration with nitrogen should be applied to solution in order to achieve the better active surface.

2.11) Pitting behaviour in NaOH (pH 12)

For this measurement, pure aluminium sheets were polarized in 0.01M NaOH (pH12) with different NaCl concentrations in order to study the effect of chloride ions concentration on corrosion behaviour of pure aluminium in basic NaCl solution.

The polarization curves in figure 80 and their corrosion parameters in table 11(appendix) shows that:

a) The active peak cannot be clearly seen in basic solution containing any concentration of NaCl, showing that active aluminium surface cannot be achieved in basic solution with NaCl. This suggests that chloride ion hinders the dissolution of spontaneous oxide film during cathodic polarization.

b) The corrosion potential (E_{cor}) shows no change with increasing chloride ion concentration in basic solution. This suggests that concentration of chloride ions does not affect the surface behaviour after cathodic polarization.

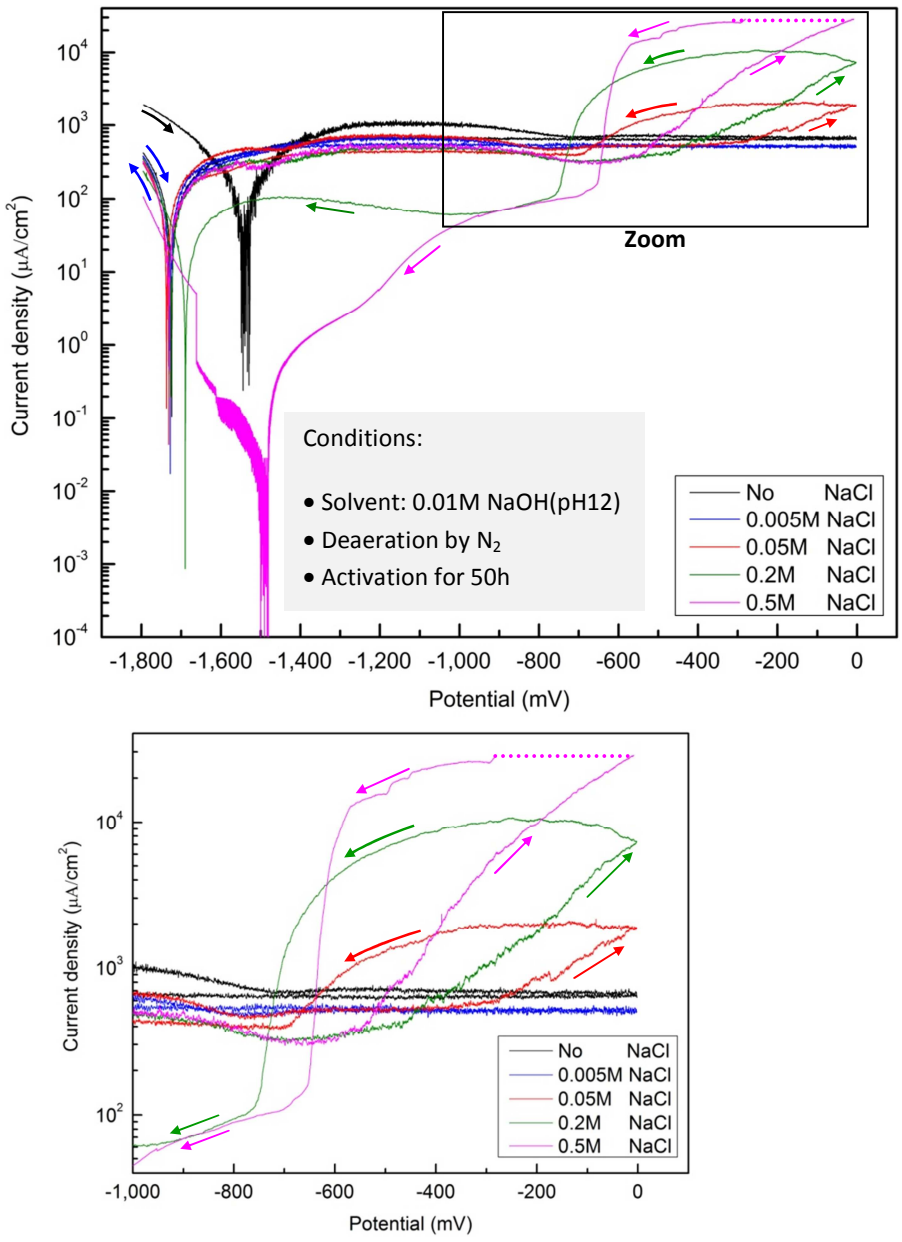

Figure 80: (Top) polarization curves of pure aluminium in deaerated basic solution (pH12) with different NaCl concentration and (bottom) zoom of the figure on top.

c) In basic solution (pH12) with low NaCl concentration (e.g., 0.005M NaCl), pitting potential has not been reached. On the other hand in basic solution with higher NaCl

concentration, stable pitting corrosion is observed on pure aluminium surface. The pitting potential (E_{pit}) shifts to more negative values with increasing chloride ion concentration in solution, see figure 81 (left). It was mentioned in [33] that the more negative the pitting potential, the easier the breakdown of the passive film and subsequent initiation of pit. Therefore the breakdown of passive film becomes easier with increasing chloride ions concentration in basic solution. Moreover, E_{pit} is observed to be a linearly inverse dependent on logarithm of chloride ions concentration in solution. This suggests that the chloride ion is responsible for the breakdown of passive oxide film and subsequently pitting initiation on surface of pure aluminium. It was mentioned in [22] that in basic salt solution the transformation of oxide/salt to form *oxo-*, *hydroxo-* and *chloro*-complexes is the cause of breakdown of the passive film and the decrease of pitting potential can be attributed to the acceleration of this transformation.

d) The passive region range (ΔE_p), see figure 81 (right), decreases with increasing chloride ions concentration, showing the increase of pitting susceptibility with increasing concentration of chloride ion.

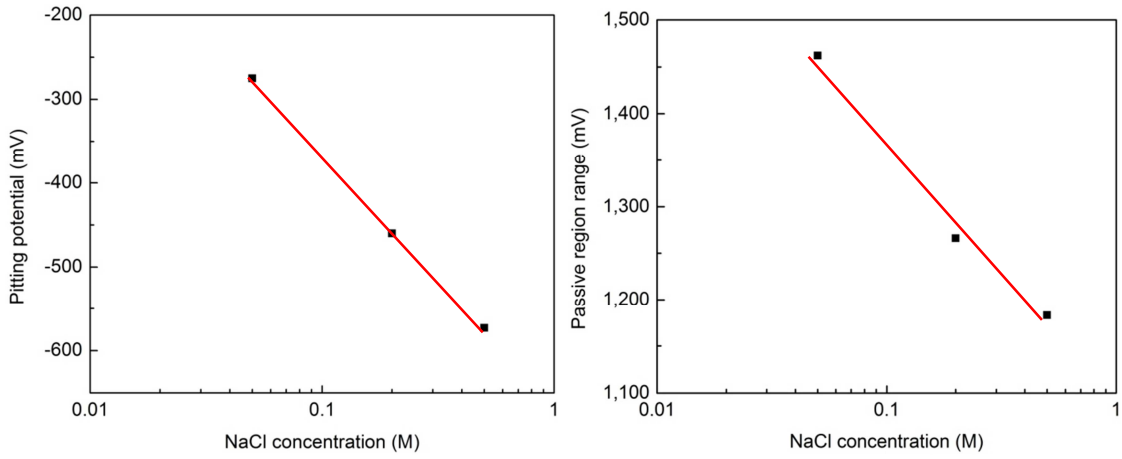

Figure 81: Pitting potential and passive region range in 0.01M NaOH (pH12) with different NaCl concentration.

e) This passive current density (J_p) is high, indicating thin passive oxide film formed on aluminium surface in basic solution.

f) The increase of chloride ions concentration also leads to an increase of maximum current in pitting region (figure 80, bottom). This suggests that the more the chloride ions in solution, the more the severity of pitting corrosion.

g) The negative hysteresis curves (clockwise), where the reverse anodic curve shifts to lower current comparing with the forward one, is observed in basic solution without any NaCl, implying the expected non-pitting behaviour. On the other hand (counter clockwise), the positive hysteresis curves, where the reverse anodic curve shifts to higher current than the forward curve, are observed in solutions with any additional concentrations of NaCl. This implies that chloride ion is able to induce the pitting corrosion even at low concentration of chloride ion in solution. Therefore in basic solution with low concentration of NaCl (0.005M), pitting corrosion will take place at higher potentials than the potential range used in this measurement.

h) The area of hysteresis loops increases with increasing chloride ions concentration in solution. It was mentioned in [52] that generally, the bigger the area of hysteresis loop, the greater the pitting susceptibility of metal. This confirms the information from passive region range that pitting susceptibility of pure aluminium increases with increasing chloride ion concentration in solution.

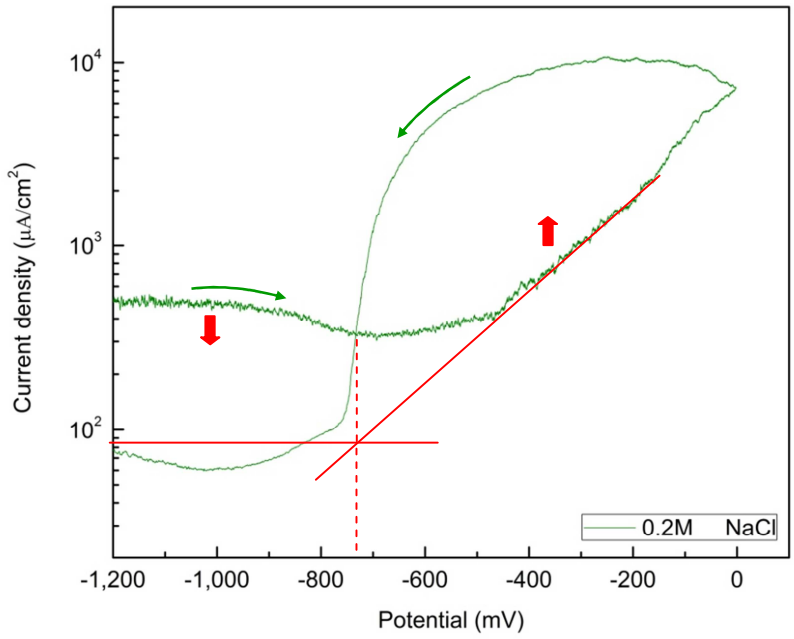

Figure 82: Evaluated pitting potential of pure aluminium in 0.01M NaOH solution with 0.2M NaCl.

The hysteresis of polarization curve is observed since the scan rate of polarization measurement is high. There is not enough time to reach the stationary state of each potential. Therefore the measured current density has not been the steady current density of the given potential. It will be mentioned later in measurement 2.13 that the steady current of potential in passive region is lower than the measured current while the steady current of potential in pitting region is higher than the measured current. Therefore the pitting potential from polarization with suitable scan rate is evaluated (figure 82). It can be seen that the evaluated pitting potential is much lower than measured pitting potential (E_{pit}) of -460mV but nearly the same as protection potential (E_{pp}) of -732mV.

From figure 82, it can be shown that for a potential lower than -732mV, no pitting corrosion takes place. According to the theoretical background, for potentials between -732 to -460mV, metastable pitting corrosion will be observed and for potentials higher than -460mV, stable pitting corrosion will take place. However, these two potentials (-460mV and -732mV) only exist due to the high scan rate of potentiodynamic cyclic polarization. For enough low scan rates, it may be assumed that these two potentials will be the same. Therefore the differences between metastable and stable pitting corrosion may not only be defined by two distinct potentials, probably.

This measurement has shown that chloride ion does not effect on passivation process but it is responsible for pitting corrosion by the breakdown of passive oxide film on pure aluminium surface.

2.12) Pitting behaviour in H_2O (pH 7)

In this measurement, the effect of chloride ion concentration in water on corrosion behaviour of pure aluminium was studied. Therefore pure aluminium was polarized in water with different NaCl concentrations was conducted and the polarization curves have been compared. In all cases, tap water has been used.

As prior constant cathodic polarization in basic solution can provide an active aluminium surface, prior constant cathodic polarization for 50h was also applied before cyclic polarization of pure aluminium in water as shown in figure 83 (top). During constant cathodic polarization at

potential of -1,600mV, the cathodic current density sharply decreases from about -700µA/cm^2 to nearly 4µA/cm^2 (figure 83, bottom). The decrease of negative current density indicates that spontaneous oxide layer is fast and mostly dissolved by hydroxide ion produced from hydrogen evolution reaction ($2H_2O + 2e^- \rightarrow H_2 + 2OH^-$) during cathodic polarization. After about 15h, current density is nearly constant at small value, indicating the constant dissolution rate of oxide film. It is predicted that active surface has been achieved. However, polarization curve shows no active peak. Therefore the small negative current density can only be referred to the state of the possible thinnest oxide film on pure aluminium surface in water with chloride ions. After constant cathodic polarization, aluminium was cyclic polarized. The potential curve shows a nonlinearity at high potential, see the pink circular in figure 83 (top). This can be attributed to a very high observed anodic current density in pitting region which exceeds the limit of the potentiostat. Thus only the forward polarization curves up to the potential of measureable current density are shown.

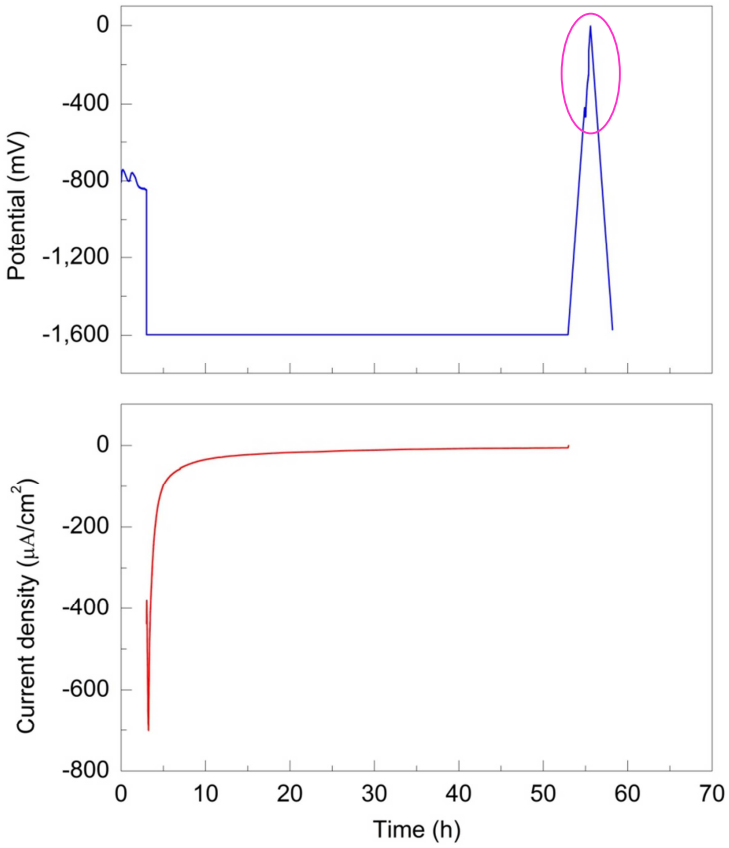

Figure 83: (Top) measurement step for polarization of pure aluminium sheet, (bottom) current density at constant cathodic polarization in tap water-solvent.

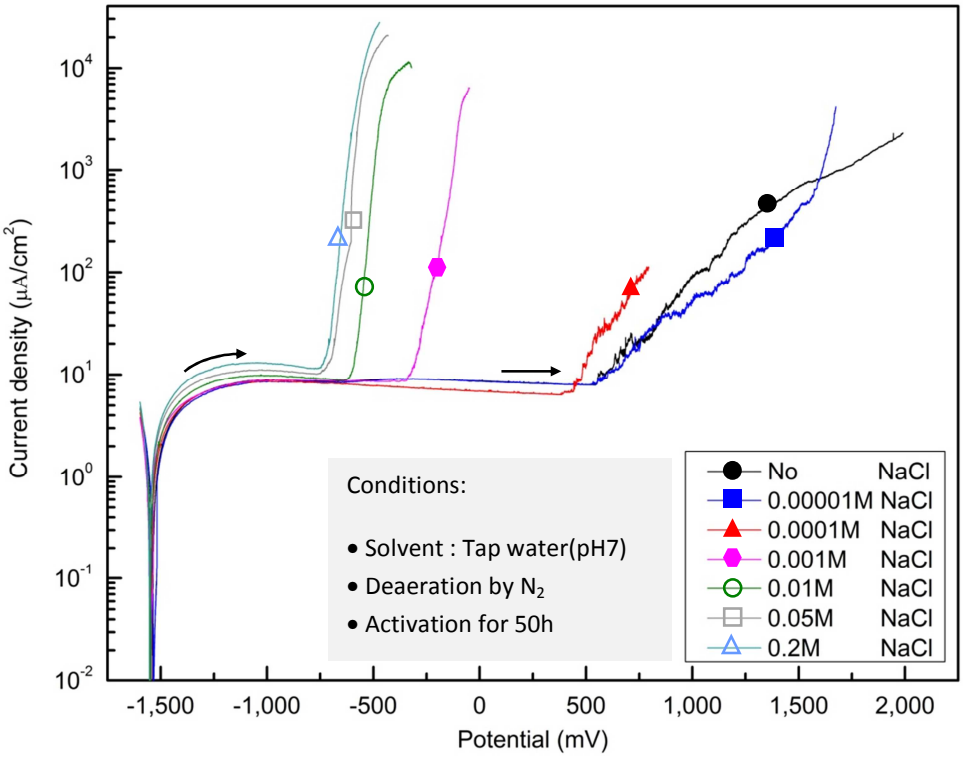

Figure 84: Polarization curves of pure aluminium in tap water with different NaCl concentration.

The polarization curves in figure 84 and corrosion parameters in table 12(appendix) shows that:

a) The active peak cannot be detected in water with and without any NaCl. This means active aluminium surface cannot be achieved in tap water even without any additional NaCl. This may be attributed to the presence of chloride ions and corrosion inhibitor in pure tap water. The chloride ion hinders the dissolution of spontaneous oxide film, and some inhibitor can form protective film on the aluminium surface.

b) Corrosion potentials (E_{cor}) of pure aluminium in water with different concentration of NaCl are nearly similar, indicating that the surface state of pure aluminium at equilibrium is independent on chloride ions concentration in solution. This suggests that chloride ion has no effect on the surface of pure aluminium at the beginning.

c) Pitting potential (E_{pit}) and passive region range (ΔE_p) decreases with increasing chloride ions concentrations, see figure 85. This indicates that pitting susceptibility of pure aluminium increases with increasing chloride ion in water. This can be attributed to the acceleration of the formation of chloride complex in neutral solution. The formation of this chloride complex is the cause of breakdown of the passive film [22].

d) Polarization curve in pure tap water and tap water with additional 0.00001M NaCl are quite similar since pure tap water already contains nearly 0.0001M chloride ions. Moreover, tap water also contains other aggressive anions such as fluoride ions [53].

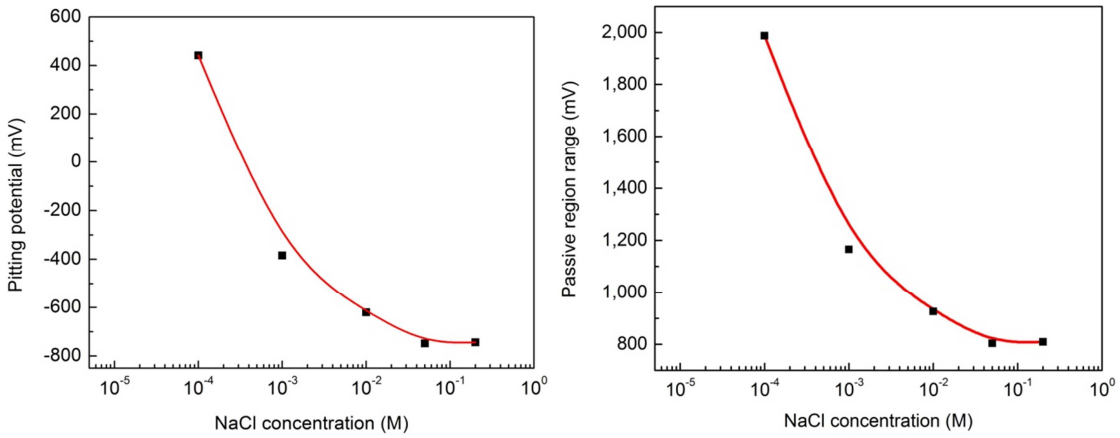

Figure 85: (Left) E_{pit} and (right) ΔE_p of pure aluminium as a function of NaCl concentration in water.

This measurement shows that pitting corrosion can occur in tap water even without any additional NaCl.

2.13) Dynamic current signal on constant anodic polarization in pitting and non-pitting regions

For this measurement, the evolution with time of corrosion of pure aluminium was studied. As corrosion was anodic reaction, the dynamic current at specific anodic polarized potential was measured. Two given anodic potentials were chosen, one potential was in the range of passive region for passivation process and another potential was in the range of the stable pitting region for pitting corrosion. Measurement started with OCP measurement for 3h, followed by a constant cathodic polarization for 50h. Then the forward polarization was conducted in noble direction with a scan rate 0f 600mV/h until reached a given anodic potential. After that the polarized potential was kept constant at that anodic potential for more than 30h, called constant anodic polarization. The electrochemical system used in this measurement was pure aluminium in deaerated water with additional 0.05M NaCl. The result from former measurement showed that corrosion potential of this system was -1,550mV and pitting

potential was about -750mV. Therefore potential of -850mV and -600mV was chosen to represent passive and stable pitting region, respectively.

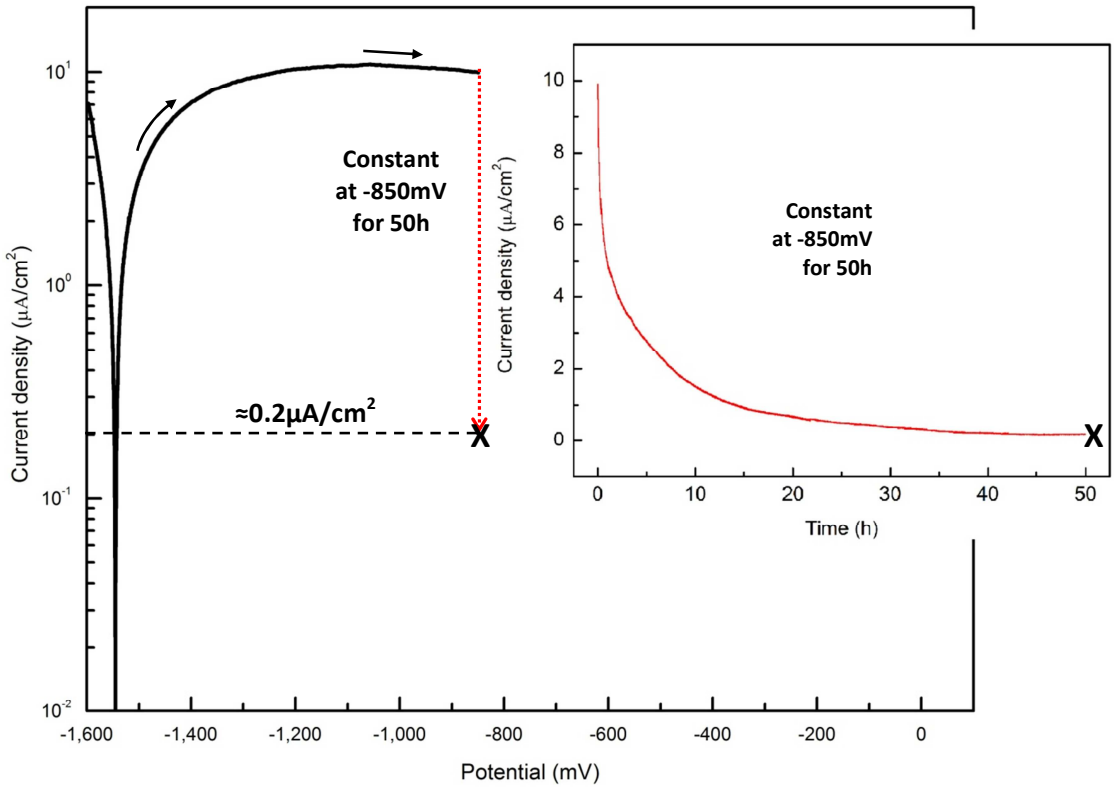

Figure 86: (Large) forward polarization curve and (small) dynamic current at constant potential of -850mV.

The results in figure 86 and 87 show that:

a) For constant polarized potential in passive region (figure 86), the current density sharply decreases from 9.9µA/cm^2 at the beginning and reaches nearly constant at 0.2µA/cm^2 after 45h. The decay of anodic current density at the beginning implies that the passivation rate or rate of aluminium oxidation reduces due to the thickening of oxide film. This exhibits that the state of the oxide film such as thickness changes slowly in response to the change in the electrode potential. Moreover, the constant anodic current detected after 45h exhibits that the pure aluminium has already reached the steady state at this potential. Therefore it can be said that passivation of pure aluminium was able to reach the steady state only after an extremely long time.

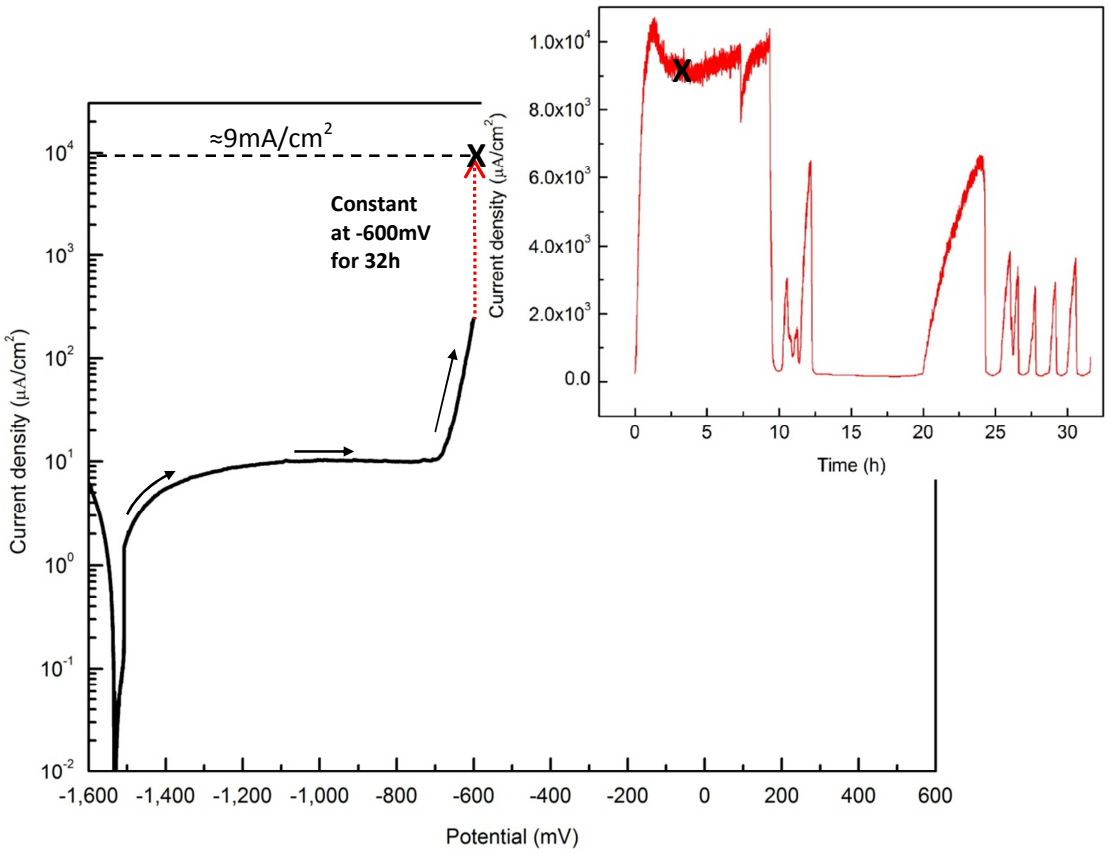

Figure 87: (Large) forward polarization curve and (small) dynamic current at constant potential of -600mV.

b) For constant polarized potential in pitting region (figure 87), current density sharply increases from nearly 200µA/cm^2 at the beginning until reaches the maximum current at nearly 10mA/cm^2 after about 1:30h. The small fluctuation at high current is also detected, possibly reflecting the continuous pit growth [28]. After nearly 10h, the current decays back to nearly 200µA/cm^2, possibly indicating simultaneous repassivation of a lot of growing pits. Moreover during 32h of measurement, current density sometimes increases with high amplitude followed by the decay back to nearly 200µA/cm^2 again. This may indicate that a lot of other pits can be simultaneously initiated and then repassivated during anodic polarization at potential in stable pitting region. Therefore it can be said that pitting corrosion of pure aluminium is not able to reach a steady state in stable pitting region.

This measurement shows that passivation rate of pure aluminium decreases with time until reaches the steady state. Whereas pitting corrosion of pure aluminium is not able to reach a steady state since new pits can be initiated all the time.

2.14) Pitting behaviour in pure tap water

As mentioned in measurement 2.12 that there are about 0.0001M chloride ions pre-existing in pure tap water and these chloride ions causes pitting corrosion on pure aluminium. Therefore in this measurement, pure deionised water with N_2 bubbling was used as the electrolyte for polarization measurement. The cyclic polarization curve and corrosion parameters of pure aluminium in pure deionised water were compared with that in pure tap water.

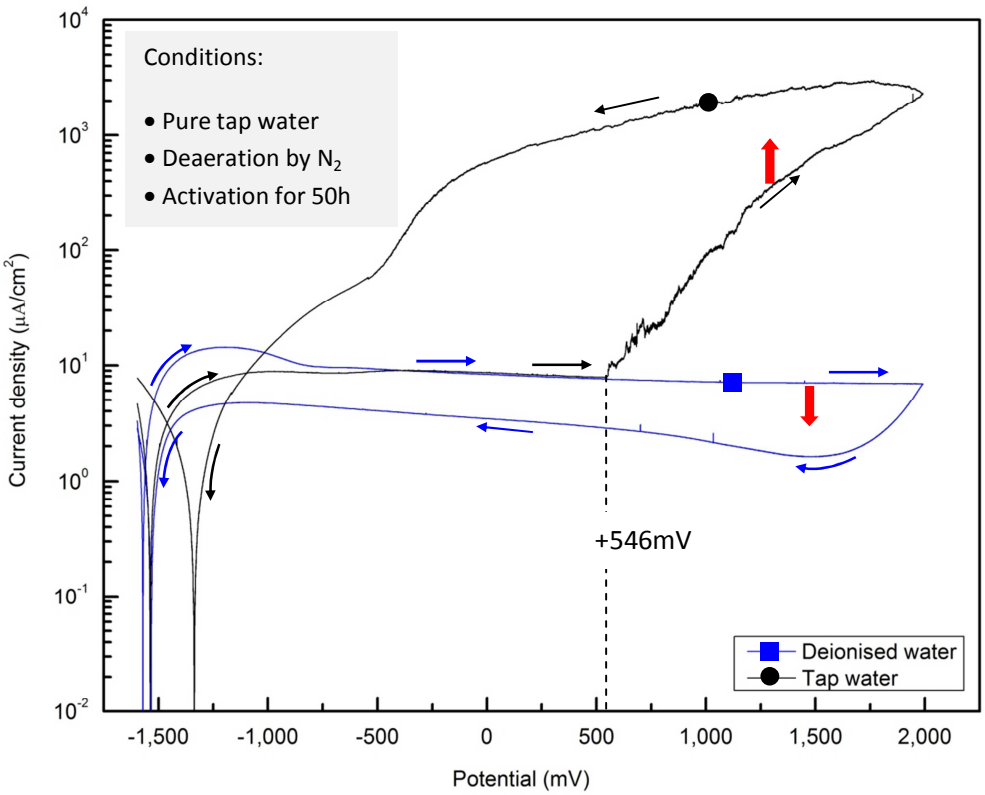

Figure 88: Cyclic polarization curves of pure aluminium sheet in pure deionised water compared with that in pure tap water. ⬆: The direction of steady current density.

The polarization curves in figure 88 and their corrosion parameters in table 13(appendix) shows that:

a) An active peak of current is detected only in pure deionised water but not in tap water. This means that unlike in pure tap water, active aluminium surface is achieved in pure deionised water owing to no chloride ions and corrosion inhibitor in pure deionised water.

b) In pure deionised water, pure aluminium shows only passive behaviour up to overpotential of 3.5V. On the other hand, pitting potential of 546mV is observed in pure tap water due to pre-existing chloride ions in pure tap water.

c) The negative hysteresis is detected in pure deionised water. As mentioned in measurement 2.13, the negative hysteresis is detected in system free from pitting corrosion since the passive current decreases with time (see the red arrow). On the other hand, the positive hysteresis is detected in pure tap water, implying that pitting corrosion is expected. The positive hysteresis is detected in systems that undergo pitting corrosion due to the fact that in pitting region the current increases with time (see the red arrow) as mentioned in measurement 2.13.

This measurement confirms that pitting corrosion occurs on pure aluminium in pure tap water due to pre-existence of chloride ion in pure tap water. Moreover active surface cannot be achieved in pure tap water but in pure deionised water because the pre-existing chloride ions and corrosion inhibitors in pure tap water hinders the activation process of pure aluminium during prior cathodic polarization.

2.15) Effect of aeration on active/passive behaviour

For this measurement the effect of aeration on corrosion behaviour of pure aluminium in pure deionised water was studied. Two polarization experiments of pure aluminium in deaerated and aerated deionised water were conducted and compared.

The cyclic polarization curves in figure 89 show that:

a) No active peak is detected for pure aluminium in aerated but in deaerated deionised water. This means active aluminium surface could not be achieved in aerated deionised

water since the high concentration of dissolved oxygen in solution facilitated the formation of oxide film on the surface of pure aluminium.

b) The corrosion potential (E_{cor}) in aerated deionised water is slightly higher by 60mV than that in deaerated solution, additionally implying that dissolved oxygen in aerated solution promotes the formation of oxide film on the surface of pure aluminium.

c) The passive current density (J_p) in deaerated solution is about 25% lower than in aerated solution. This may due to the fact that the active aluminium surface in deaerated solution can form better passive layer with uniform thickness and this result in the increase of uniform thickness of passive oxide film with increasing potential. Whereas non-uniform thickness of oxide film can be formed on the spontaneous oxide surface. Therefore it can be concluded that the initial state of pure aluminium surface exerts a great influence on the passivation mechanism.

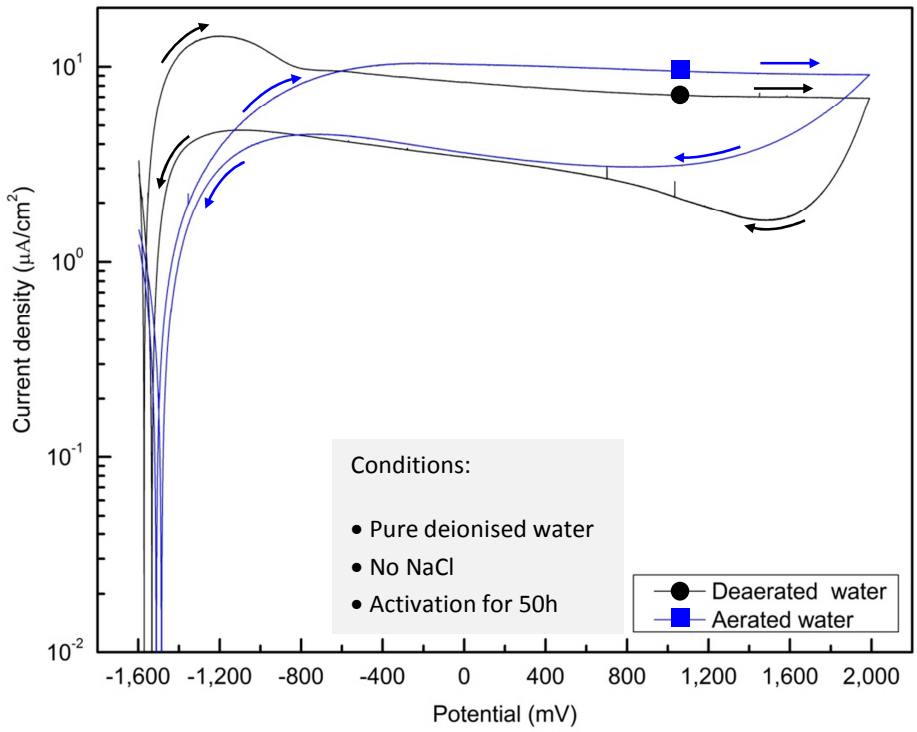

Figure 89: polarization curves of pure aluminium in deionised water with different aeration.

From the information of the polarization curves in figure 89, the model of pure aluminium surface during forward polarization is proposed in figure 90.

Aeration	Model of	
	Initial surface	Final Surface
Aerated solution	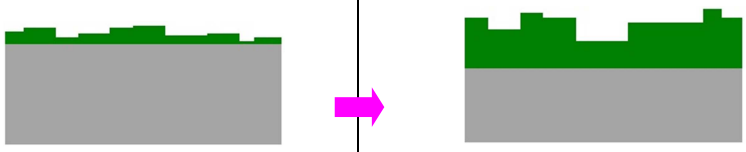	
Deaerated solution	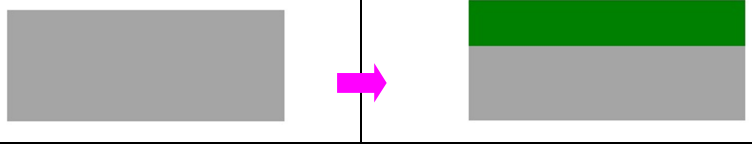	

Figure 90: Model of pure aluminium surface during forward polarization in deionised water with different aeration system. Grey (■) and green (■) represent the aluminium and oxide, respectively.

The model in aerated solution, the initial surface is covered with spontaneous oxide. This spontaneous oxide hinders the formation of proper anodic oxide film. Therefore the anodic oxide film with inhomogeneous thickness is probably formed on pure aluminium surface. On the other hand starting with active surface (in deaerated solution), anodic oxide can be form properly therefore the anodic oxide film with homogeneous thickness is reached.

This measurement shows that active aluminium surface can be achieved in deaerated but not in aerated deionised water.

2.16) Pitting behaviour in the low NaCl concentration range

For this measurement, the effect of chloride ions concentration on corrosion behaviour of pure aluminium in deionised water-solvent solution was studied. Therefore pure aluminium was polarized in deaerated deionised water containing different NaCl concentrations and then the polarization curves and corrosion parameters for different NaCl concentrations were compared.

The polarization curves in figure 91 and their corrosion parameters in table 14 (appendix) shows that:

a) NaCl concentration shows no significant effect on $\mathrm{E_{cor}} - \mathrm{forward}$. This suggests that concentration of chloride ions in solution has no effect on passivation process.

b) With NaCl concentrations of less than 0.001M, active peak is detected. This may due to the fact that chloride ion with concentrations higher than 0.001M NaCl hinders the activation process of pure aluminium during prior constant cathodic polarization.

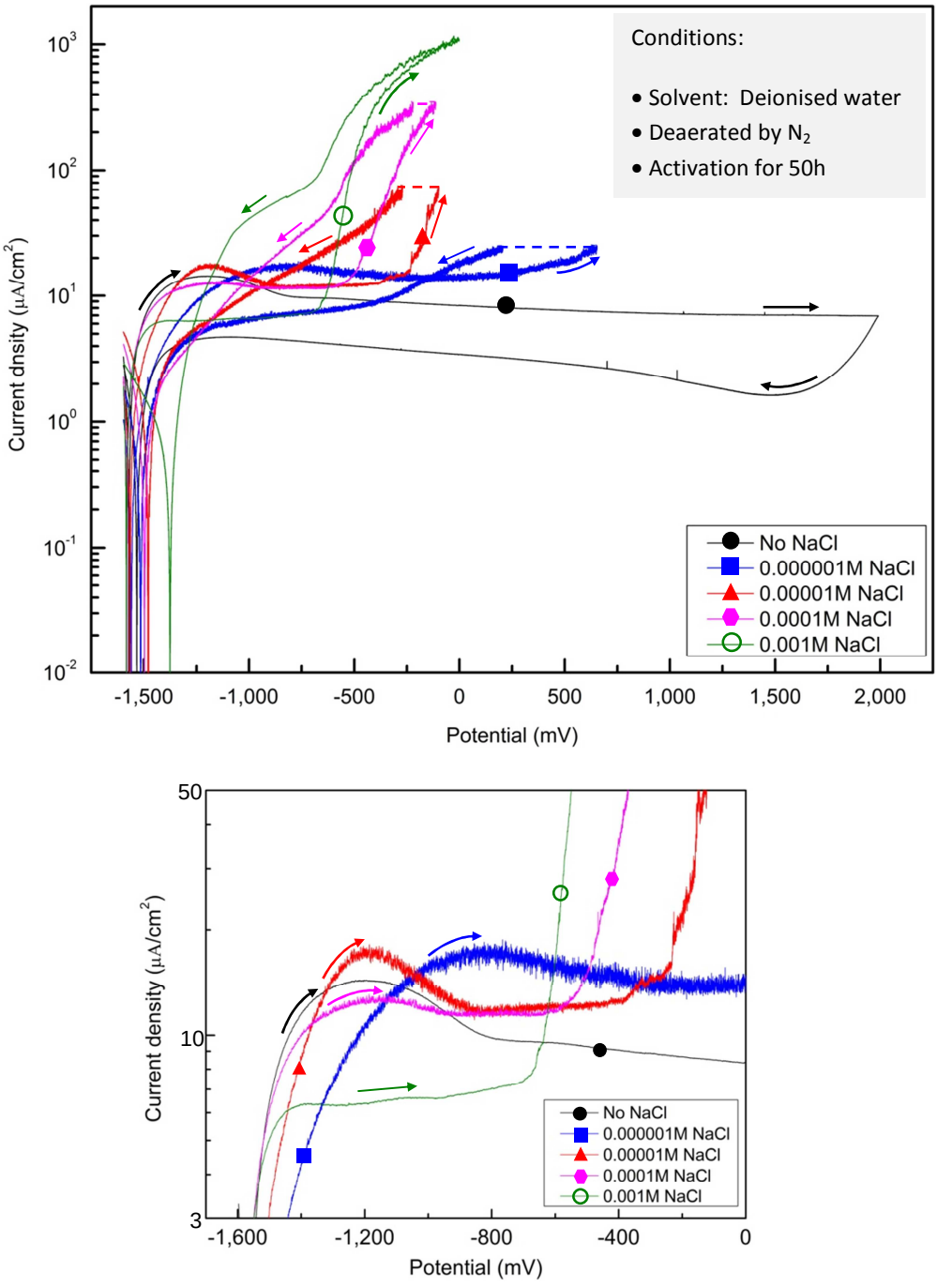

Figure 91: (Top) polarization curves of pure aluminium in deionised water-solvent with different NaCl concentrations and (bottom) zoom of figure on top.

c) Pitting corrosion (E_{pit}) is detected in deionised water with additional NaCl and the pitting potential decreases with increasing chloride ion concentration in solution. This can be attributed to the acceleration of the formation of chloride complex, which is the cause of breakdown of the passive film [22], in neutral solution. Moreover, with higher chloride ion concentration in solution, the current in pitting region increases more sharply. This may due to the increase in severity of pitting corrosion in term of the density and depth of pits with increasing chloride ions concentrations [36].

d) Passive region range (ΔE_p) decreases with increasing chloride ions concentration (figure 92, left), confirming the increase of pitting susceptibility of pure aluminium with increasing concentration of chloride ions in solution.

e) Corrosion potential shift (ΔE_{cor}), which is determined by ($E_{cor} - \text{forward}$) – ($E_{cor} - \text{reverse}$), is a positive value for solutions with all concentrations of chloride ions (figure 92, right). It is noticed in this research that the positive ΔE_{cor} is detected when pure aluminium undergo passivation followed by pitting corrosion. Moreover, with increasing chloride ions concentration, ΔE_{cor} shifts to more positive values. Since the pitting corrosion causes the damage of pure aluminium surface and the severity of pitting corrosion increases with increasing concentration of chloride ion in solution, it can be deduced that the higher the ΔE_{cor}, the higher the severity of pitting corrosion.

f) Unlike in pure deionised solution without any additional NaCl, positive hysteresis is detected in deionised solution with addition of NaCl, indicating that pitting corrosion is expected. Moreover, the area of hysteresis loops increases with increasing chloride ions concentration in solution, confirming the increase of pitting susceptibility with increasing chloride ion in solution.

g) The protection potential (E_{pp}), which is determined by the intersection of the reverse anodic polarization with forward anodic polarization curve, decreases with increasing chloride ions in solution. It was mentioned in [54] the higher protection potential reflects the better capability of passive oxide film to repair by itself (or self-repassivation). Therefore self-repassivation of pure aluminium decreases with increasing chloride ion concentration in solution due to the chloride ion hinders the repassivation processes.

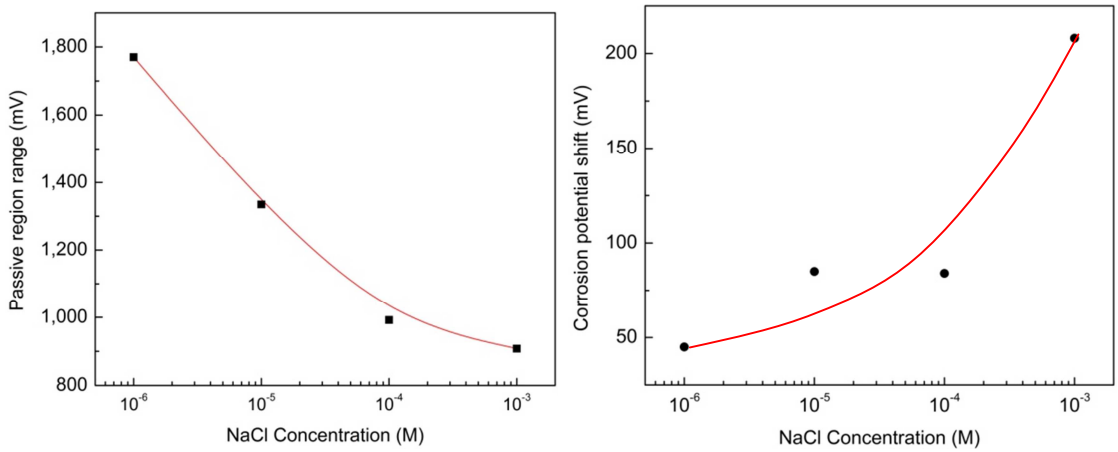

Figure 92: (Left) ΔE_p and (right) ΔE_{cor} as a function of NaCl concentration added in deionised water.

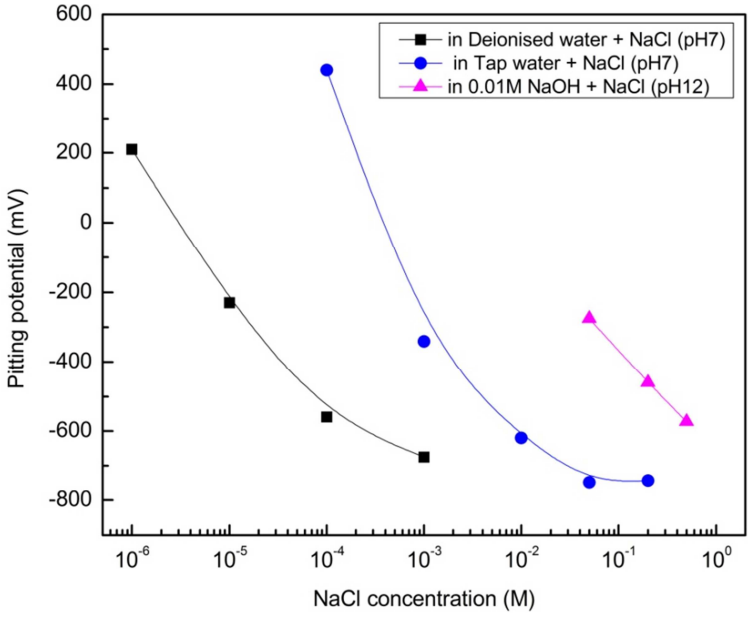

Figure 93: Pitting potential of pure aluminium as function of additional chloride ions concentration in deionised water, tap water and basic solvent solution in comparison.

The pitting potentials of pure aluminium as a function of additional NaCl concentration in deionised water, in basic solution and in tap water solvent are compared in figure 93. It shows that:

a) The pitting corrosion of pure aluminium in basic solution (pH12) is higher than in tap water and deionised water-solvent solution at every additional chloride ion

concentration in solution due to the fact that passive oxide film is really thin and continuously dissolved and formed in basic solution since the high concentration of hydroxide ions in solution facilitates the chemical dissolution of oxide layer.

b) The pitting potential in tap water is also higher than that in deionised water at every additional chloride ion concentration even there already are pre-existing chloride ions in pure tap water. This confirms that in pure tap water, there are some pitting inhibitors such as phosphate, silicate etc. [55]. Silicate and phosphate are the natural constituents in tap water and sometimes they are added as corrosion inhibitors in order to reduce the corrosion in plumbing system. It was mentioned in [56] that the phosphate (PO_4^{3-}) and silicate, which are negatively charged, will be drawn to positive charge (Al^{3+}) at anodic site and subsequently suppresses the anodic reaction by blocking the anodic oxidation site.

This measurement shows that it is not only the concentration of chloride ion in solution but also character of solvent and pH of solution influencing the pitting corrosion behaviour of pure aluminium.

2.17) Pitting behaviour in HCl

In this measurement, the effect of HCl concentration on corrosion behaviour of pure aluminium was studied. With different HCl concentrations, both, concentration of aggressive chloride ions in solution and pH of the solution were different.

The OCP evolution with time in figure 94 shows that:

a) With low HCl concentration of 0.000001M (pH 6) and 0.00001M (pH 5), the OCP evolution with time gradually shifts to nobler potential. This reflects the formation of protective passive film on pure aluminium surface due to the low solubility of aluminium oxide in nearly neutral solution.

b) With HCl concentration of 0.0001M (pH 4), the OCP evolution with time slowly shifts in cathodic direction until reaching the steady potential after about 1.2h. This indicates the

possible thinning of oxide layer on pure aluminium surface, due to the high solubility of aluminium oxide in acidic solution [9].

c) With high HCl concentration of 0.001M (pH 3), the OCP sharply increases at the beginning and then fluctuates at around -850mV. This may indicate the fast formation of imperfect passive film followed by the serious attack of pitting corrosion on pure aluminium surface in strong acidic solution [51, 52].

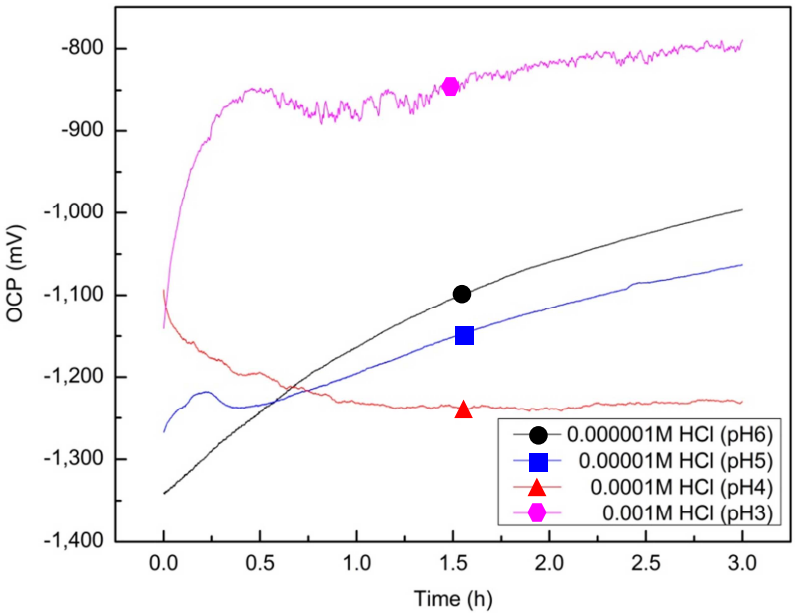

Figure 94: OCP evolution with time of pure aluminium in different concentration of HCl solution.

The polarization curves in figure 95 and their corrosion parameters in table 15(appendix) shows that:

a) No active peak of current is detected in any HCl solution, indicating that active surface could not be reached in HCl solution due to the chloride ions in solution hindering activation process.

b) In HCl solution with concentrations of 0.000001M (pH 6), 0.00001M (pH 5) and 0.0001M (pH 4), the corrosion potential ($\mathrm{E_{cor}} - \mathrm{forward}$) shifts to negative values compared with OCP. That indicates that spontaneous oxide layer is dissolved during constant cathodic polarization for 50h in nearly neutral solutions. Whereas in 0.001M HCl solution (pH 3), $\mathrm{E_{cor}} - \mathrm{forward}$ does not change from OCP value, inferring that spontaneous oxide layer is not dissolved by cathodic polarization in strong acidic solution with pH 3. It was

mentioned in [26] that during cathodic polarization in acidic solution, the hydrogen evolution by the discharge of proton ($2H^+ + 2e^- \rightarrow H_2$) took place instead of reduction of water in neutral and basic solution. No hydroxide ion was produced therefore passive oxide film cannot be dissolved in strong acidic solution.

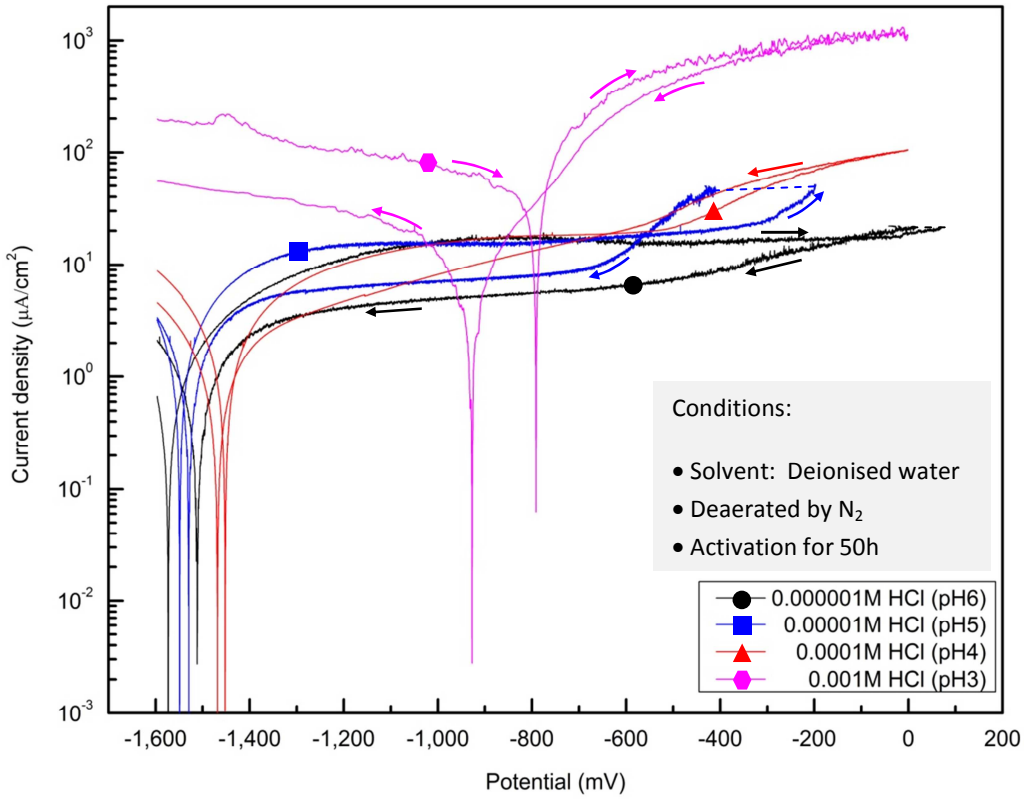

Figure 95: Polarization curves of pure aluminium in solution with different concentration of HCl.

c) In 0.001M HCl solution (pH 3), corrosion potential of pure aluminium shifts to higher potential than in other HCl solutions, implying that the thicker passive oxide film should be formed on pure aluminium surface at equilibrium state. Moreover, anodic current density in this strong HCl solution with pH 3 also shifts to much higher value than in other HCl solutions, suggesting that pitting corrosion take place at corrosion potential. Since pitting potential coincides with the corrosion potential, it can be deduced that this formed passive oxide film in strong HCl solution with pH 3 should not be perfect. According to the Pourbaix diagram in figure 6, it confirms that aluminium exhibits partial passivation or imperfect passivity in strong acid solution. When potential increases, aluminium will exhibit uniform corrosion, due to the fact that at high anodic potentials,

anodic pitting corrosion in imperfect passive film became more extensive that invades the whole surface in the way that it looks like a more or less general corrosion [51]. It was also reported in [57] that at the corrosion potential, an instable *oxyhydroxide* film with many defect was presented on the surface of pure aluminium in strong HCl solutions. Therefore, the pitting corrosion of pure aluminium in strong acid solution can spontaneously begin at the corrosion potential.

d) In HCl solution with concentration of 0.000001M (pH 6), 0.00001M (pH 5) and 0.0001M (pH 4), positive hysteresis is detected, indicating pitting corrosion. While in 0.001M HCl solution (pH 3), negative hysteresis is detected, indicating that no pitting corrosion is expected. However during anodic polarization, pure aluminium in 0.001M HCl (pH 3) undergoes serious pitting corrosion that creates more or less uniform corrosion and therefore negative hysteresis is possibly observed.

e) Pitting potential reduces with increasing HCl concentration since the increase of chloride ions in solution accelerates the formation of chloride complex, which is the cause of breakdown of passive film [22].

f) The passive region range (ΔE_p) decreases with increasing HCl concentration in solution (figure 96, left), indicating the increase of pitting susceptibility with increasing HCl concentration in solution. This can be attributed to the decrease of the stability of passive oxide film on pure aluminium in acidic solution and the increase of aggressive chloride ion in solution.

g) Corrosion potential shift (ΔE_{cor}) is positive for nearly neutral solution (pH 6 and 5) but it is negative for acidic solution (pH 3 and 4). This can possibly be attributed to the difference in the surface alteration, which is the result of different corrosion mechanisms. In nearly neutral solution, formation of oxide film followed by pitting corrosion takes place during anodic polarization. Whereas in acidic solution, the more or less uniform corrosion occurs at high anodic polarized potential. Therefore it is noticed in this research that the negative ΔE_{cor} is detected when uniform corrosion occurs.

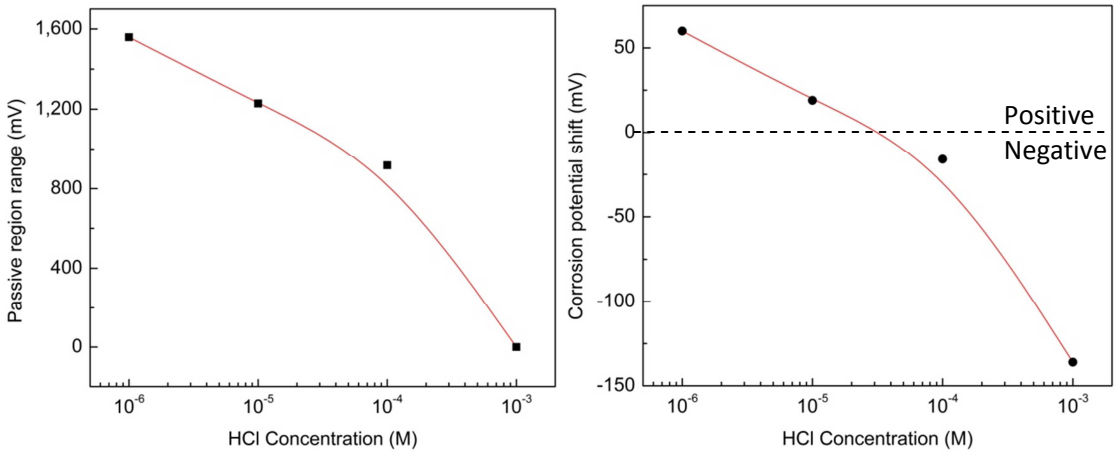

Figure 96: (left) ΔE_p and (right) ΔE_{cor} variation with concentration of HCl in solution.

This measurement shows that imperfect passive film is formed on pure aluminium surface when immersed in strong acidic solution (pH3).

2.18) Pitting behaviour : Effect of pH value and chloride concentration

The earlier measurement shows that concentration of HCl in solution has much effect on corrosion behaviour of pure aluminium. However, it doesn't show the pure effect of solution's pH on corrosion behaviour of pure aluminium since chloride ions concentration is also varied with concentration of HCl in solution. Therefore in this analysis, polarization curves of pure aluminium in solution with the same chloride ion concentration but different pH values are compared in order to understand the pure effect of solution's pH on corrosion behaviour of pure aluminium. As different concentration of chloride ions in solution, pH of NaCl is always 7 but pH of HCl is varied from 3 to 6.

The cyclic polarization curves in figure 97 show that:

a) The polarization curves of pure aluminium in the low concentration HCl solution with pH nearly neutral of 5 and 6 look quite similar to that in NaCl solution (pH 7) with the same chloride ions concentration. On the other hand in high concentration HCl solution with low pH of 3 and 4, their polarization curves look more and more different from polarization curves in NaCl solution (pH 7) with the same chloride ions concentration.

This indicates that pH of solution has effect on the corrosion behaviour of pure aluminium.

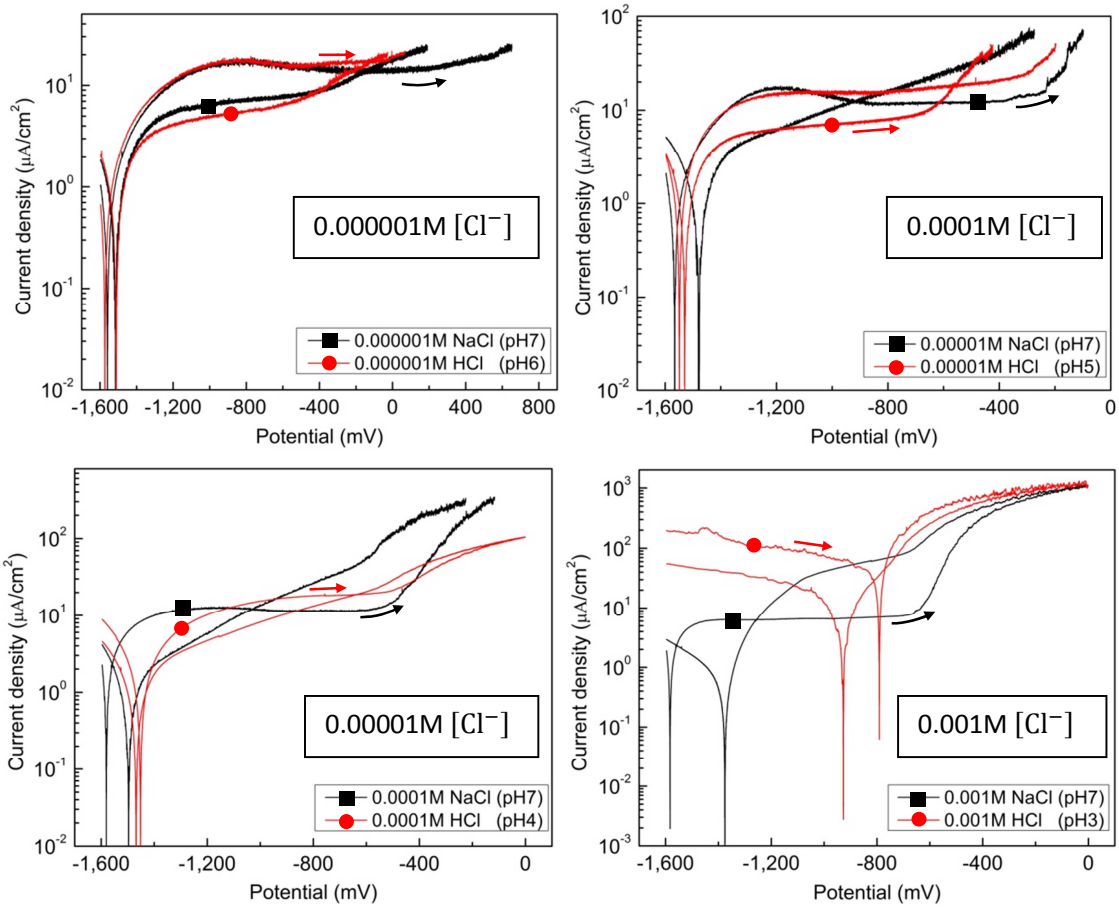

Figure 97: Cyclic polarization curves of pure aluminium in NaCl and HCl solution with the same$[Cl^-]$: (Left, top) 0.000001M, (left, bottom) 0.00001M, (right, top) 0.0001M and (right, bottom) 0.001M$[Cl^-]$.

b) In nearly neutral HCl solution with pH 6 and 5 (figure 98, left), corrosion potentials are close to that in NaCl solution with the same chloride ions concentration. Whereas in stronger acidic HCl solution with pH 4 and 3, corrosion potentials shifts to higher and higher value than that in NaCl solution with the same chloride ions concentration. This implies that the surface state of pure aluminium at equilibrium state strongly changes with pH of solution but not with chloride ions concentration in solution. Since aluminium is a valve metal, it can be deduced that pH of solution has a great effect on passive behaviour of pure aluminium.

c) In both HCl and NaCl solution (in figure 98, right), pitting potential decreases with increasing quantity of chloride ions. Although there is the same amount of chloride ions in both solutions, pitting potential in HCl is always a little bit lower than in NaCl for any concentration of chloride ions in solution. This indicates that pH of solution has no significant effect on pitting corrosion behaviour of pure aluminium.

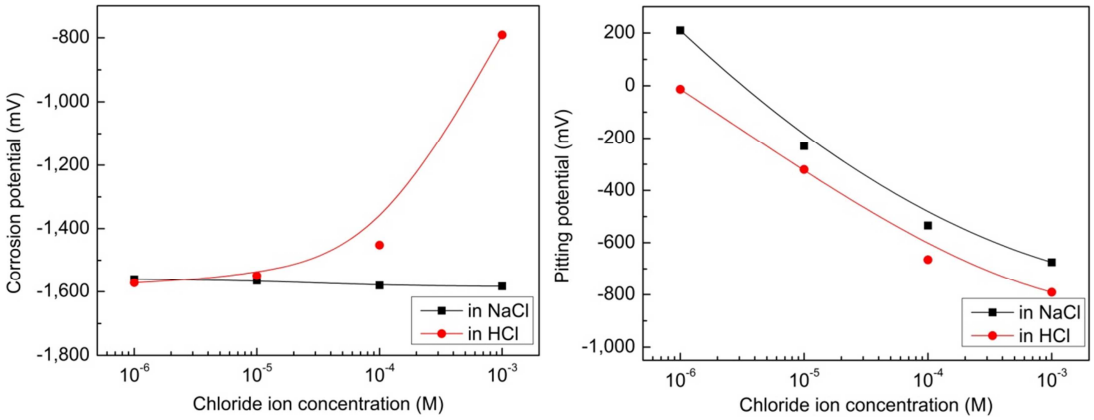

Figure 98: (Left) $\mathrm{E_{cor}}$ – forward and (right) $\mathrm{E_{pit}}$ as a function of chloride ion concentration in solution.

d) In both HCl and NaCl solutions with the same chloride ions in solution, passive region range ($\Delta \mathrm{E_p}$) decreases with increasing chloride ions concentration (figure 99, left) predominantly due to the increase of chloride ions in solution. Although there is the same amount of chloride ions in both solutions, $\Delta \mathrm{E_p}$ in HCl is always lower than in NaCl for any concentration of chloride ions in solution. Moreover, in 0.001M HCl solution (pH 3) passive region disappears totally while in 0.001M NaCl (pH 7), large passive region is still detected. This confirms that pH of solution has a strong effect on the formation of passive film of aluminium.

e) In NaCl solution, corrosion potential shift ($\Delta \mathrm{E_{cor}}$) is always positive and increases with increasing NaCl concentration, while in HCl solution it decreases from positive to negative values with increasing HCl concentration (figure 99, right). As it is mentioned earlier that positive $\Delta \mathrm{E_{cor}}$ is detected when passivation followed by pitting corrosion while the negative $\Delta \mathrm{E_{cor}}$ is detected when uniform corrosion takes place, this confirms that the pH of solution has a great effect on the type of corrosion mechanism of pure aluminium.

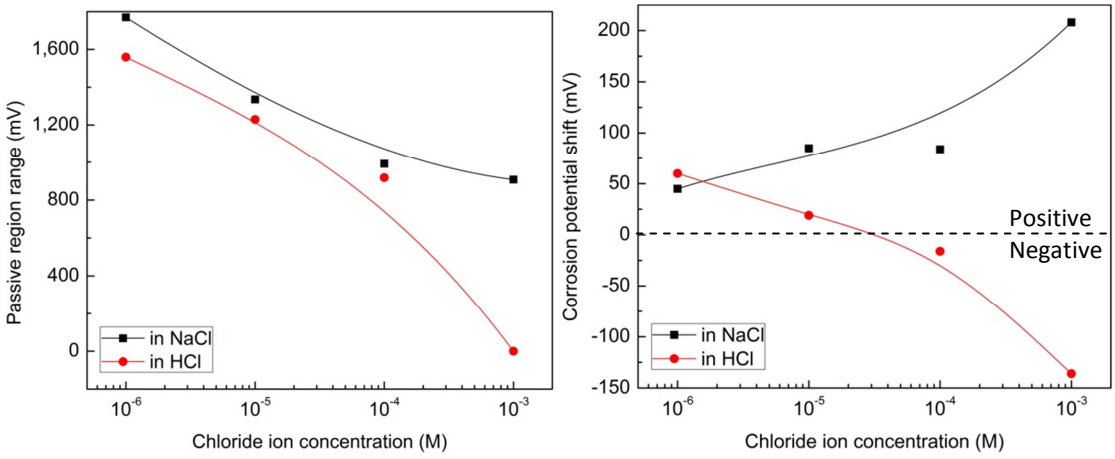

Figure 99: (Left) ΔE_p and (right) ΔE_{cor} as a function of chloride ion concentration in solution.

This measurement indicates that pH of solution has no significant effects on pitting potential but strong effects on passive behaviour of pure aluminium.

2.19) Corrosion behaviour in Nitric acid (HNO_3)

This measurement was to study the effect of nitrate ion (NO_3^-) on corrosion behaviour of pure aluminium. The source of nitrate ion was Nitric acid (HNO_3). Since HNO_3 contain H^+ which affected the pH of solution, the small concentration of only 0.00001M HNO_3 was used for this measurement. The polarization curve of pure aluminium in HNO_3 solution is compared with that in deionised water and that in HCl with the same pH value.

The polarization curves in figure 100 and their corrosion parameters in table 16(appendix) shows that:

a) No active peak of current is detected in HNO_3 solution. This means, active aluminium surface cannot be achieved in HNO_3 solution. This implies the hindrance of activation process by constant cathodic polarization by nitrate ion. It was mentioned in [58] that nitrate ions could be incorporated into the spontaneous oxide film, this possibly hindered the activation process.
b) Passive region is detected, indicating that passivation can take place on surface of pure aluminium in HNO_3 solution.

c) The passive current density (J_p) in HNO_3 is higher than that in pure deionised water, indicating the thinner oxide film formed in HNO_3 solution due to the decrease of pH of solution. While the passive current HNO_3 is the same as that in HCl, indicating same thickness of passive oxide film formed due to the same pH of solution. This confirms that the acidification of solution accelerates the uniform thinning of oxide film.

d) Negative hysteresis and no pitting potential are observed in HNO_3 solution, indicating that no pitting corrosion take place. Therefore NO_3^- does not facilitate pitting corrosion on pure aluminium. Moreover, it was also mentioned in [58] that the incorporation of nitrate ions in passive oxide film inhibited the pitting corrosion on pure aluminium in solution containing chloride ions.

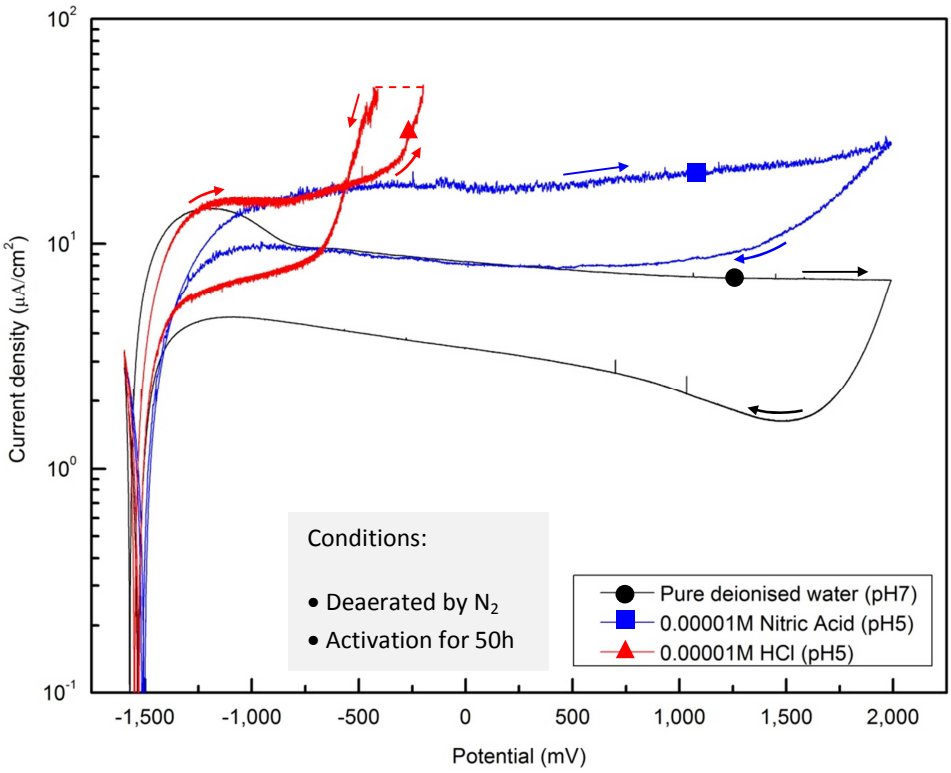

Figure 100: Cyclic polarization curves of pure aluminium in 0.00001M HNO_3.

This measurement shows that pitting corrosion does not take place on pure aluminium in nitric acid solution but only uniform corrosion.

2.20) Pitting behaviour in acidic chloride solution

In this measurement, the effect of only pH on corrosion behaviour of pure aluminium in acidic solution containing 0.001M chloride ions was studied. In order to adjust only pH of solution but still keep a constant chloride ion concentration in solution, two sources of chloride ion were used, which were NaCl and HCl. OCP and polarization curves of pure aluminium in 0.001M chloride ion-containing solution with different pH ranging from 3 to 7 were compared.

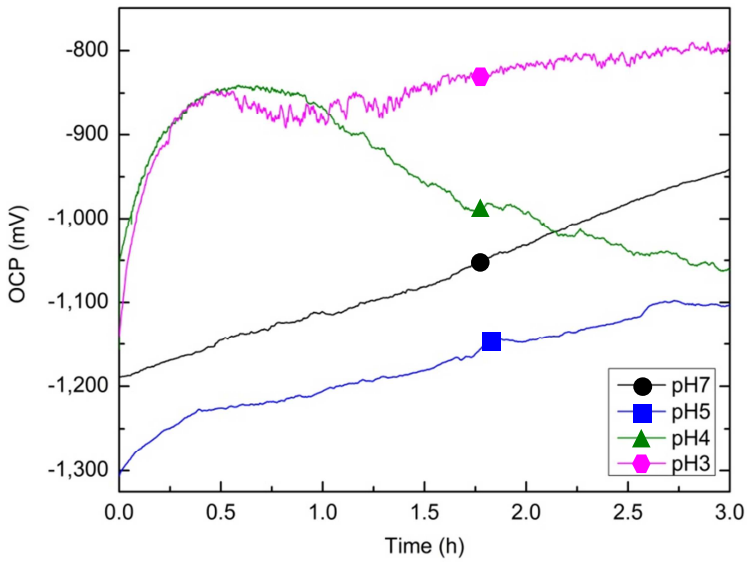

Figure 101: OCP curves of pure aluminium in 0.001M chloride solution with different pH.

According to the theoretical background, the evolution with time of OCP in figure 101 shows that:

a) In nearly neutral chloride solution with pH 5 to 7, the OCP increases with time. This indicates only passivation taking place on pure aluminium surface.

b) In chloride solution with pH 4, the OCP increases at the beginning and then decreases with time later. This indicates the formation of passive oxide layer followed by its modification like the transformation of oxide to chloride complexes [22].

c) In strong acidic chloride solution with pH 3, the increase of OCP at the beginning followed by fluctuations is detected. It can be deduced that the oxide film is fast formed at the beginning and then pitting corrosion spontaneously occurs on the surface. This

formed oxide film should be an imperfect passive film since pitting corrosion can spontaneously occur at equilibrium state.

From OCP it can be assumed that when pure aluminium immerses in nearly neutral solution with pH4 to 7, aluminium exhibits passive behaviour. On the other side, when pure aluminium immerses in strong acidic solution with low pH of 3, pure aluminium exhibits pitting corrosion at OCP.

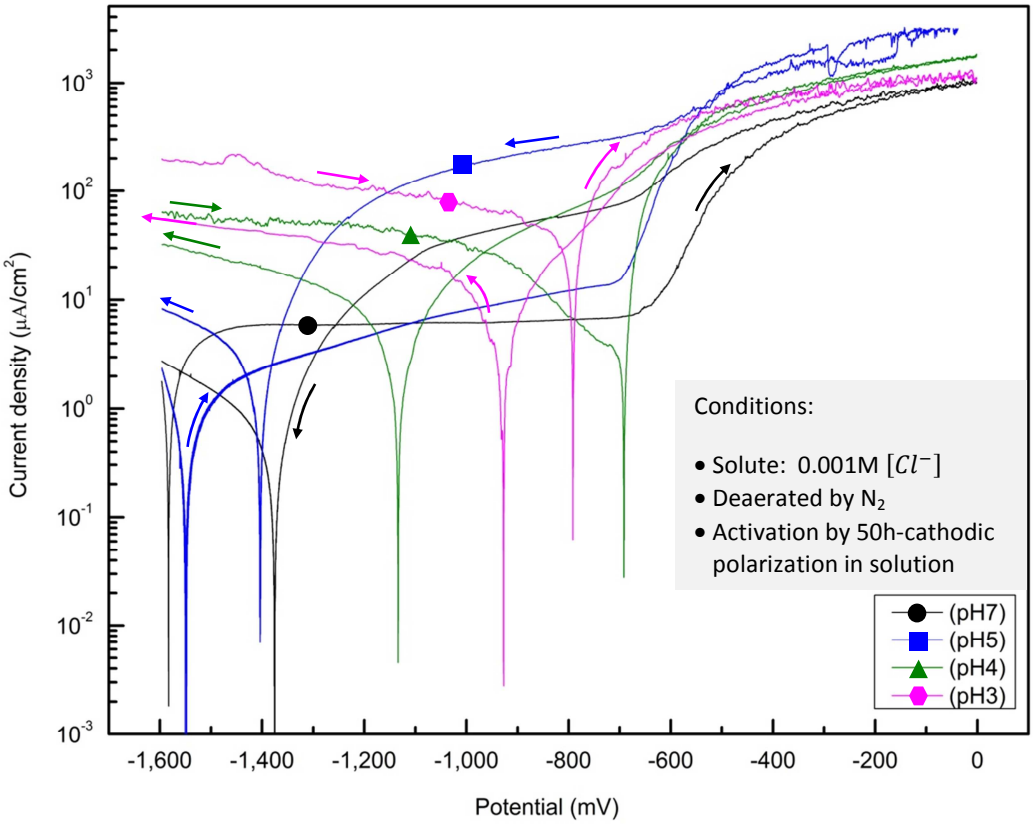

Figure 102: Polarization curves of pure aluminium in 0.001M chloride solution with different pH.

The polarization curves in figure 102 and their corrosion parameters in table 17(appendix) shows that:

a) The corrosion potential (E_{cor}) in nearly neutral chloride solution with pH 5-7 shifts to more negative potential than OCP, implying that the spontaneous oxide film is thinning during constant cathodic polarization. Whereas the corrosion potential of aluminium in acidic solution with pH 4 shifts to more positive value than OCP, implying that

spontaneous oxide film is thickening during constant cathodic polarization in this acidic solution. It was mentioned in [29] that spontaneous oxide film could grow during cathodic polarization in acidic solution. Even though the cathodic polarization prevented the oxidation of metal at the metal/oxide interface, Al^{3+} is still transported through the oxide film by a large positive overpotential across the oxide film. Therefore, the concentration of aluminium ion near metal/oxide interface consequently decreases with time. In order to sustain the electrical neutrality, the protons (H^{+}) are transferred to oxide ions near the metal/oxide interface and forms hydroxide. The converse of aluminium oxide in the inner layer of passive film to aluminium hydroxide at the metal/oxide interface by cathodic polarization reduces the cathodic overpotential. When the cathodic overpotential became zero, aluminium oxidation took place and passive film began to grow. Moreover, the partial dissolution of hydroxide film at the oxide/solution interface in acidic solution resulted in the porous structure of imperfect passive film. However in strong acidic chloride solution with pH 3, corrosion potential does not shift at all from noble OCP value possibly due to the fast and full formation of imperfect oxide in this solution during OCP measurement. Therefore in this strong acidic solution (pH 3), no more oxide film thickening during constant cathodic polarization takes place.

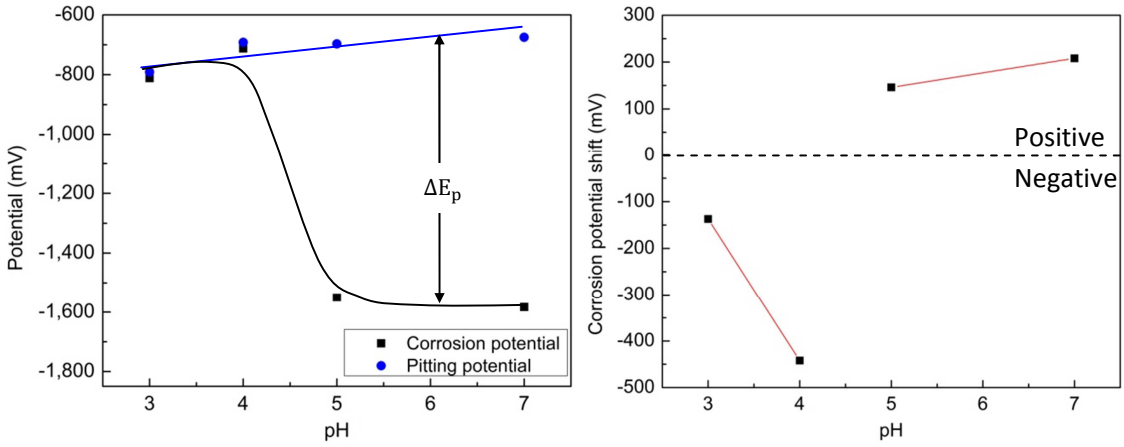

Figure 103: (Left) E_{cor} and ΔE_p as a function of pH and (right) ΔE_{cor} as a function of pH.

b) In chloride solution with pH 5 to 7, the corrosion potential is much lower than pitting potential (figure 103, left). Therefore the passive region is observed between corrosion and pitting potential. This indicates that that *pure aluminium exhibits passivation*

phenomena when it is immersed in nearly neutral chloride solution with pH 5-7. Whereas in chloride solution with pH 3 and 4, the corrosion potential is raised up to pitting potential. This rise in corrosion potential in the direction to pitting potential implies thicker of oxide films. However, this oxide film should not be perfect because pitting corrosion can spontaneously occurs at corrosion potential or equilibrium state. Therefore *the main corrosion mechanism of pure aluminium is pitting corrosion when it is immersed in strong acidic solution with pH 4 and 3*.

c) Corrosion potential, see the black line in figure 103(left), dramatically changes when pH of solution changes from nearly neutral (5-7) to acidic (3 and 4) values, implying that surface state of pure aluminium at equilibrium strongly depends on pH of solution. There is no significant change in pitting potential with pH (see the blue line in figure 103, left). This suggests that the pH of solution strongly affects the passive behaviour but not pitting corrosion of pure aluminium.

d) The passive region range (ΔE_p) decreases with decreasing pH of chloride solution from 7 to 5, indicating the increase of pitting susceptibility with decreasing pH of chloride solution. This can be attributed to the increasing number of defects in passive oxide layer with decreasing pH of the solution [22]. In chloride solution with pH 3 and 4, no passive region is detected since the imperfect passive layer is formed in acidic solution. This spontaneously leads to the pitting corrosion at OCP.

e) Positive hysteresis is observed in nearly neutral chloride solution with pH 5 to 7, suggesting that pitting corrosion is expected. On the other hand in acidic chloride solution with pH 3 to 4, negative hysteresis is observed, indicating that no pitting corrosion is expected. However, pitting corrosion at OCP is observed in acidic chloride solution with pH 3 and 4. This pitting corrosion at OCP may seriously attack the whole surface area in the way that more or less uniform corrosion takes place.

f) Corrosion potential shift (ΔE_{cor}) is positive in solution with pH 5-7, while it is negative in solution with pH 3 and 4 (figure 103, right). This confirms that in nearly neutral chloride solution with pH 5 to 7, passivation followed by pitting corrosion take place whereas in acidic chloride solution with pH 3 and 4, uniform corrosion occurs on pure aluminium surface.

g) In acidic chloride solution (pH 3 and 4), the protection potential (E_{pp}) is close to or even lower than corrosion potential (E_{cor}). This can suggest that at equilibrium state, pitting

corrosion can occur in this acidic chloride solution. Whereas in nearly neutral chloride solution (pH 5-7), E_{pp} is more positive than E_{cor}. This confirms that no pitting corrosion occur at equilibrium state in these nearly neutral solutions.

This measurement show that pitting corrosion by chloride ions attack on pure aluminium surface is accelerated at corrosion potential in strong acidic solution with pH 3 and 4 due to the formation of imperfect passive oxide film.

2.21) Pitting behaviour in basic chloride solution

In this measurement, the effect of only pH on corrosion behaviour of pure aluminium in basic solutions containing 0.001M chloride ions was studied. In order to adjust the pH of the solution, NaOH was put into 0.001M NaCl solution. The pH of solution in this measurement was ranged from 7 to 12.

From theoretical background, the OCP evolution with time in figure 104 shows that there is no significant change for all basic pH values.

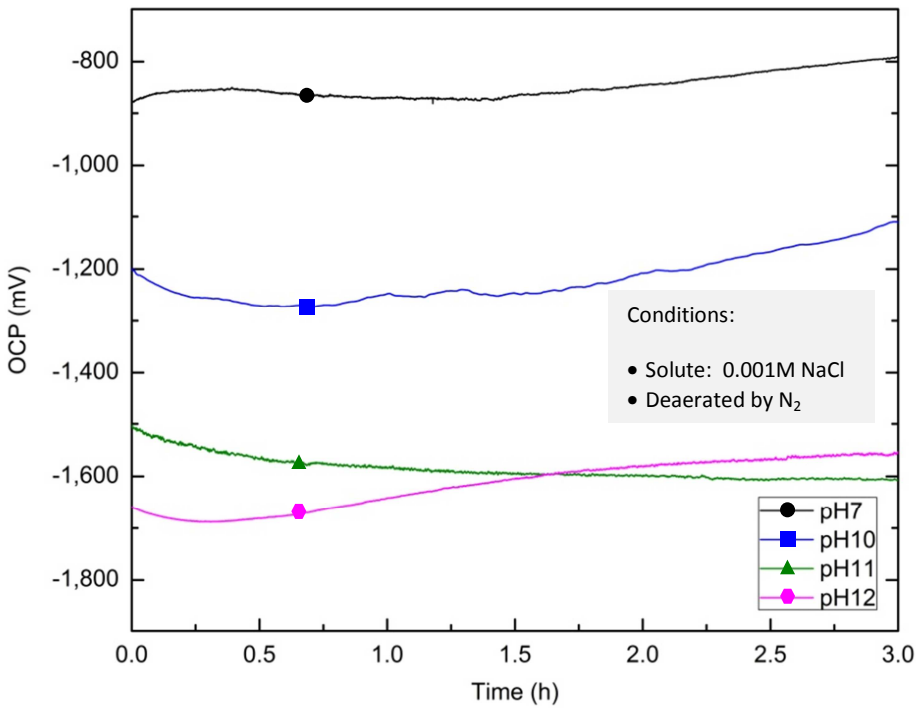

Figure 104: OCP curves of pure aluminium in basic chloride solution with different pH.

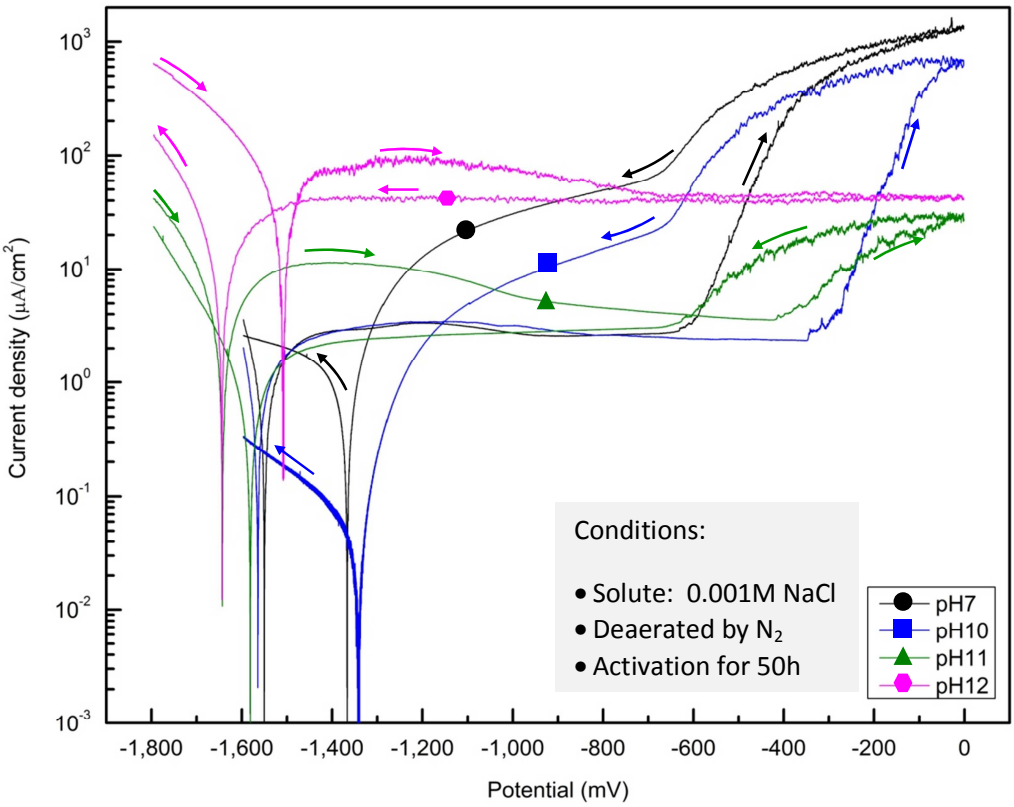

Figure 105: Polarization curves of pure aluminium in basic 0.001M NaCl solution with different pH.

The polarization curves in figure 105 and corrosion parameters in table 18(appendix) shows that:

a) Corrosion potential ($\mathrm{E_{cor}} - \mathrm{forward}$) of pure aluminium in strong basic chloride solution with pH 11and 12 shifts to more negative value than in nearly neutral chloride solution with pH 7 and 10. This indicates that in strong basic chloride solution, pure aluminium exhibits more active surface than in nearly neutral chloride solution due to the chemical dissolution of oxide film by high concentration of hydroxide ions in strong basic solution. Astonishingly, the corrosion potential in solution with pH 11 is lower than that with pH 12, indicating more active surface. This may be attributed to the lower formation rate of oxide film by $\mathrm{Al} + 3\mathrm{OH^-} \rightarrow \mathrm{Al(OH)_3} + 3\mathrm{e^-}$ due to the lower hydroxide ion in solution with pH 11.

b) The corrosion potential in nearly neutral chloride solutions (pH 7-10) greatly shifts to more negative values compared with OCP, indicating strong thinning of spontaneous

oxide film during constant cathodic polarization. The $E_{cor} - forward$ in basic chloride solution with pH 11 is only slightly lower than OCP, indicating that the spontaneous oxide layer is slightly thinned during constant cathodic polarization. On the other hand, the $E_{cor} - forward$ in strong basic chloride solution with pH 12 is slightly higher than OCP, confirms that oxide layer can be formed in strong basic solution even during constant cathodic polarization. Therefore it can be deduced that even in these basic solutions, pure aluminium metal surface is covered by passive oxide film. However corrosion current density, which is proportional to the corrosion rate, is really high in basic solution (pH 11 and 12), indicating only an extremely thin oxide film.

c) Active peaks of current are detected only in basic chloride solution (pH 11 and 12). This suggests that the active surface in chloride solution can only be achieved in only basic chloride solution. It is mentioned earlier that the chloride ion hinders the activation process by constant cathodic polarization in neutral chloride solution. However in basic chloride solution, strong chemical dissolution of oxide film by high concentration of hydroxide ion dominates over the hindrance of activation process by chloride ions.

d) Passive current density (J_p) in strong basic chloride solution with pH 12 is much higher than that in solution with other pH of 7 to 11. This very high passive current density indicates a poor corrosion resistance of pure aluminium in this strong basic chloride solution. This is possibly attributed to the formation of pseudo-passive film instead of passive film in strong basic solution since the formed passive oxide film is continuously thinned by the chemical dissolution reaction, $Al(OH)_3 + OH^- \rightarrow Al(OH)_4^-$, which is facilitated by the presence of high concentration of hydroxide ions in this solution. Whereas in the nearly neutral solution, the solubility of aluminium oxide is low so that the formed passive oxide film is more stable and protective [23, 52].

e) Pitting potential (E_{pit}) and passive region range (ΔE_p), see figure 106 (left), shifts to more positive value with increasing pH of solution. This can be attributed to the increase of hydroxide ions concentration which facilitates the chemical dissolution of passive oxide film. The formed passive oxide film continuously dissolves and forms in basic solution therefore the pitting corrosion caused by the local breakdown of oxide film is hindered.

f) Positive hysteresis is detected in chloride solution with pH 7 to 11, implying the expectation of pitting corrosion. While negative hysteresis is detected in only strong basic chloride solution with pH 12, implying that pitting is not expected in this solution up to the measured potential.

g) Corrosion potential sift (ΔE_{cor}) is positive in chloride solution with pH 7-11 (figure 106, right), confirming the formation of passive film followed by pitting corrosion taking place in these solution. Whereas negative ΔE_{cor} is observed in strong basic chloride solution with pH 12, confirming that the uniform corrosion take place in this solution up to potential of 0V

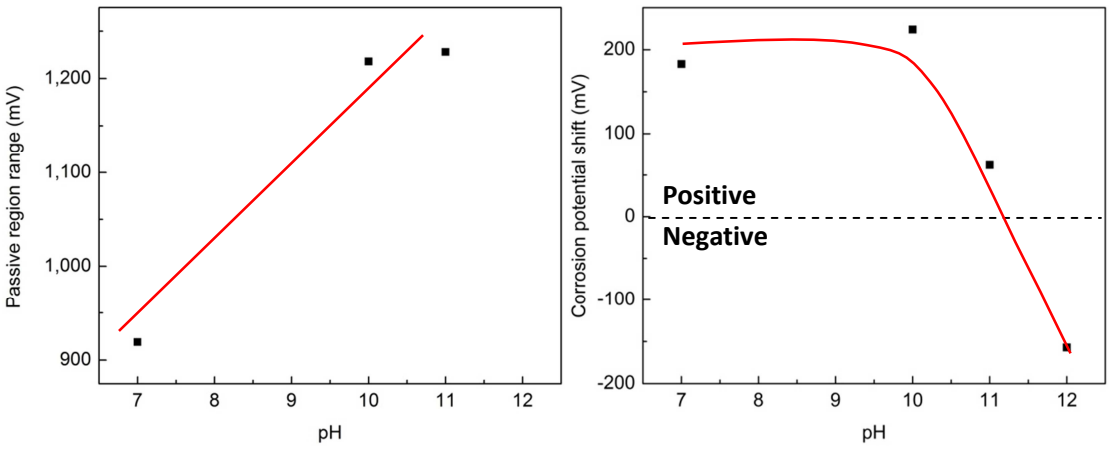

Figure 106: (Left) ΔE_p and (right) ΔE_{cor} as a function of pH.

For visualizing the different corrosion behaviour of pure aluminium between neutral and basic solutions, pictures of pure aluminium surfaces and solutions after polarization in 0.05M NaCl solution with pH 7 and 12 were taken.

The experimental pictures in figure 107 show that:

a) No visible pitting is detected after polarization of pure aluminium in basic NaCl solution (pH 12). On the other hand, pitting is visible after polarization in neutral NaCl solution (pH 7) as can be seen in figure 108. Therefore these experimental pictures confirm that there is no pitting corrosion occurring in basic NaCl solution.

b) The light reflection of pure aluminium in basic NaCl solution does change during polarization but not in neutral solution. This confirms the dissolution of oxide film in strong basic NaCl solution.

c) There are many white colloids in neutral NaCl solution, but not in the basic one. These white colloids are supposed to be $Al(OH)_3$, that is a byproduct of pitting corrosion [36].

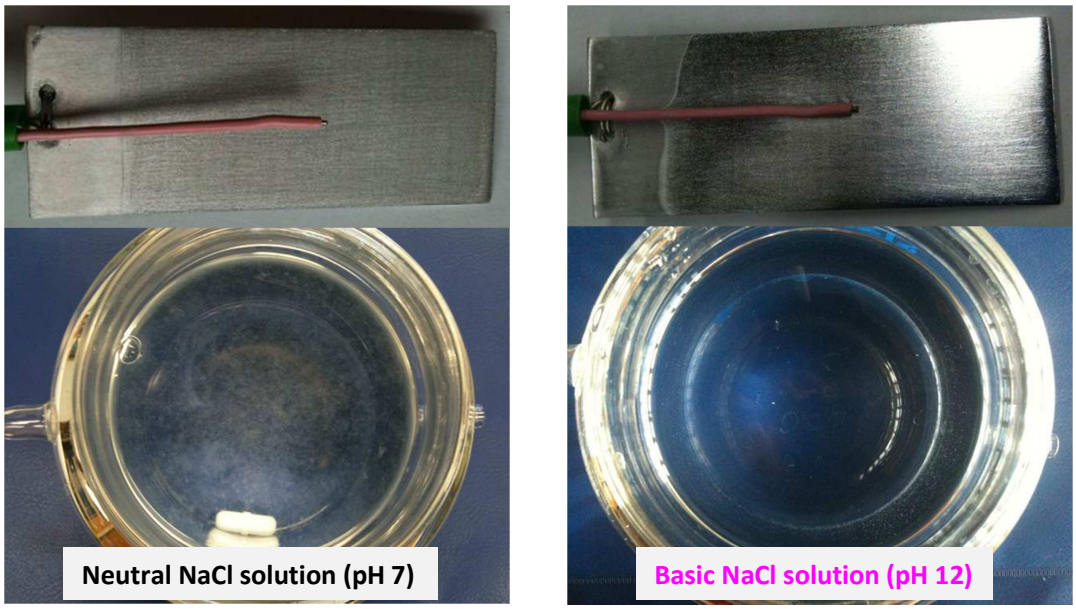

Figure 107: Pictures of pure aluminium surface and solution after polarization in: (left) neutral NaCl solution and (right) basic NaCl solution.

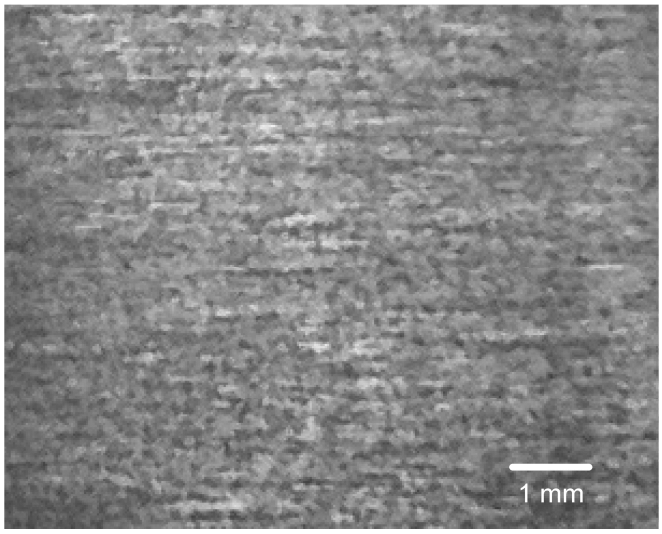

Figure 108: Zoom of pure aluminium surface after polarized in neutral solution (pH 7).

This measurement shows that in strong basic chloride solution (pH 12), pitting corrosion of pure aluminium does not take place up to the measured potential. However, uniform corrosion by the formation and chemical dissolution of the passive oxide film occurs with extremely high rate due to the formation of pseudo-passive film which is thin and continuously remove by high concentration of hydroxide ions in this solution.

2.22) Comparison of activation process in different solutions

In this analysis, the effect of solution's condition such as solute, solvent, pH and aeration on activation process of pure aluminium by constant cathodic polarization at a potential of about 250 below the OCP for 50h are discussed. The results of activation process are gathered from earlier measurements and listed in table 3. It shows that:

a) The activation process of pure aluminium by constant cathodic polarization is achieved only in deionised water and strong basic solution with pH 12. For the other solutions, the chloride ions, nitrate ions and natural corrosion inhibitors hinder the activation process. However, comparison between OCP and $\mathrm{E_{cor}}$ from the earlier measurements shows that for most of the solutions, the cathodic polarization shifts the potential at equilibrium state of pure aluminium to more active value. This means, constant cathodic polarization at least can reduce the thickness of spontaneous oxide film.

b) For pure deionised solution, the aeration of solution by air hinders the activation process since high concentration of oxygen in air facilitates the formation of oxide film.

c) For basic solution with pH 12, the active surface can be achieved in both aerated and deaerated solution. This is due to the fact that in this strong basic solution, the dissolution of oxide film is not only facilitated by electrochemical reaction of constant cathodic polarization, but also by chemical reactions by high concentration of hydroxide ions in solution. Therefore in aerated basic solution, the dissolution of oxide film dominates over the formation of oxide film, facilitated by air in this solution. Moreover in basic chloride solution with pH 12, the dissolution of oxide film also dominates over the hindrance of activation process by chloride ions if there are low chloride ion

concentrations in solution. Thus in basic chloride solution with pH 12, active surface can possibly be achieved even there is chloride ion in solution.

Conditions of solution				Activation	Remark*
Solvent	solute	pH	Aeration		
0.01M NaOH	-	12	N_2	Yes	
		12	air	Yes	
0.01M NaOH	Low NaCl	12	N_2	Yes	
	High NaCl	12	N_2	No	Chloride ion
Tap water	-	7	N_2	No	Natural-added chloride ions and corrosion inhibitors, and additional chloride ion
	NaCl	7	N_2	No	
Deionised water	-	7	N_2	Yes	
	-	7	air	No	Oxygen in air bubbling
HCl	-	3-5	N_2	No	Chloride ion
	NaCl	3-5	N_2	No	Chloride ion
NaOH	NaCl	7-10	N_2	No	Chloride ion
$HN0_3$	-	5	N_2	No	Nitrate ions (NO_3^{2-})

Table 3: Summary of the activation process of pure aluminium surface by cathodic polarization in different solution. * The ions or molecules that possibly hindered the activation.

The analysis shows that the conditions of solution strongly affects the activation process of pure aluminium surface by constant cathodic polarization and this activation process is only achieved in pure deionised water deaerated by N_2 and deaerated and aerated NaOH solution with only low concentrations of chloride ions.

2.23) Pitting behaviour: Effect of surface finish on in NaCl solution

Since it was mentioned in [31] that the corrosion behaviour of metals can be affected by its microstructure or its surface state, for this measurement, the influence of the surface finish on the corrosion behaviour of pure aluminium in deaerated chloride solutions was studied. Before starting the measurement, pure aluminium sheets were freshly polished with different silicon carbide (SiC) papers, which had different average grit sizes of abrading SiC particles from 15 to 200µm. It should be noted that for all polarization measurement other than these surface finish measurements, the surface had been final polished by the finest grit size of abrading particles (15 µm). Difference in grit size of abrading SiC particles provided different surface roughness of the sample.

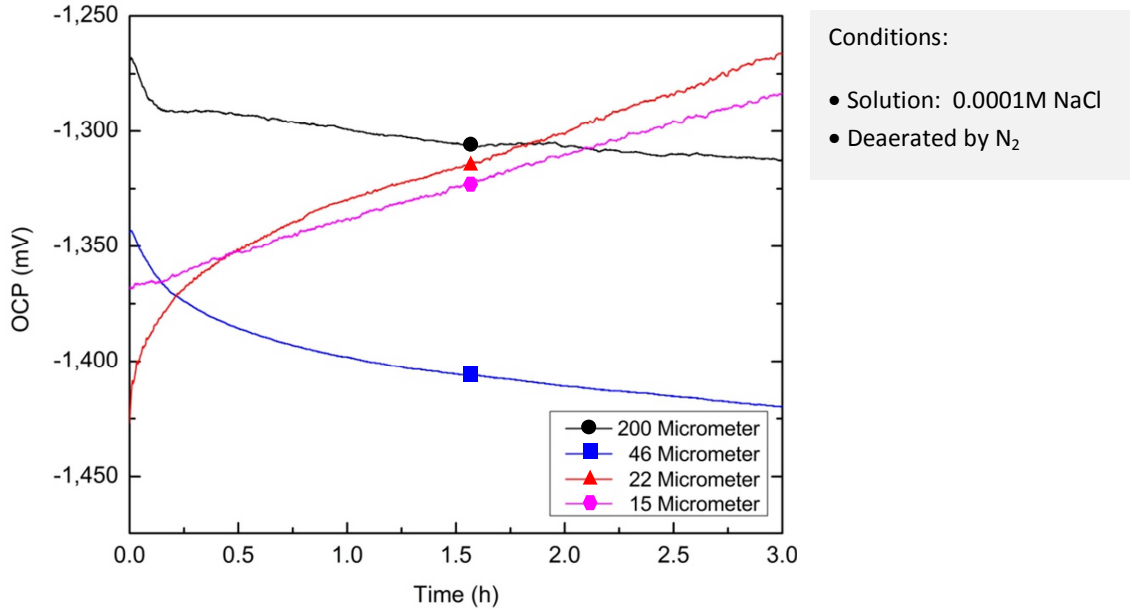

Figure 109: OCP curves of pure aluminium with different surface finishes.

According to the theoretical background, the OCP curves in figure 109 shows that:

a) For the surface polished with small grit size of abrading particles (22 and 15µm), the OCP increases with time. This relates to the formation of passive oxide layer on pure aluminium surface.

b) For the surface polished with large grit size of abrading particles (46 and 200µm), the OCP decreases with time. This indicates the attack of aluminium metal surface by chloride ions due to the high activity on the surface as a consequence of rough surface.

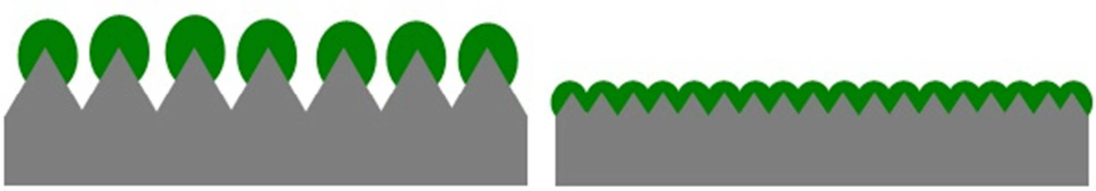

Figure 110: The model of aluminium surface, polished with different grit size of abrading particle: (left) large grit size and (right) small grit size. Grey ( ) and green ( ) represent the aluminium and oxide, respectively.

From the information of the OCP curves in figure 109, a model of pure aluminium surface is proposed in figure 110. For rough surface (see figure 110, left) prepared from the large grit sizes of abrading particles, pure aluminium surface is not fully covered with passive oxide film. The aluminium metal is partially exposed to the solution. Therefore chloride ions are able to directly attack pure aluminium metal. On the other hand for smooth surface (see figure 110, right) prepared from the small grit size of abrading particles, the aluminium surface is fully covered by passive oxide layer. There is no direct attack of chloride ions on pure aluminium metal and the passive oxide film can grow during immersion in NaCl solution. Therefore it can be deduced that surface finish influences the passivation behaviour of pure aluminium.

The polarization curves in figure 111 and their corrosion parameters in table 19(appendix) shows that:

a) Different surface finish does not produce the change in corrosion potentials, indicating the same surface state of pure aluminium before cyclic polarization started. However, the OCP evolution with time (see figure 109) before constant cathodic polarization measurement from different surface finish is quite different, indicating different surface states. This suggests that after prior constant cathodic polarization, the different surface states from different surface finish are altered to the same surface state. Therefore prior cathodic polarization is necessary for removing spontaneous oxide film and subsequently providing the same surface state before polarization for corrosion characterization of pure aluminium.

b) The pitting potential is evaluated as shown in figure 112 (left). The evaluated pitting potential decreases with increasing grit size of abrading particles (figure 112, right). This

indicates that surface finish strongly influences the pitting susceptibility of pure aluminium. The larger the grit size of abrading particle or the rougher the surface, the greater the susceptibility to pitting corrosion.

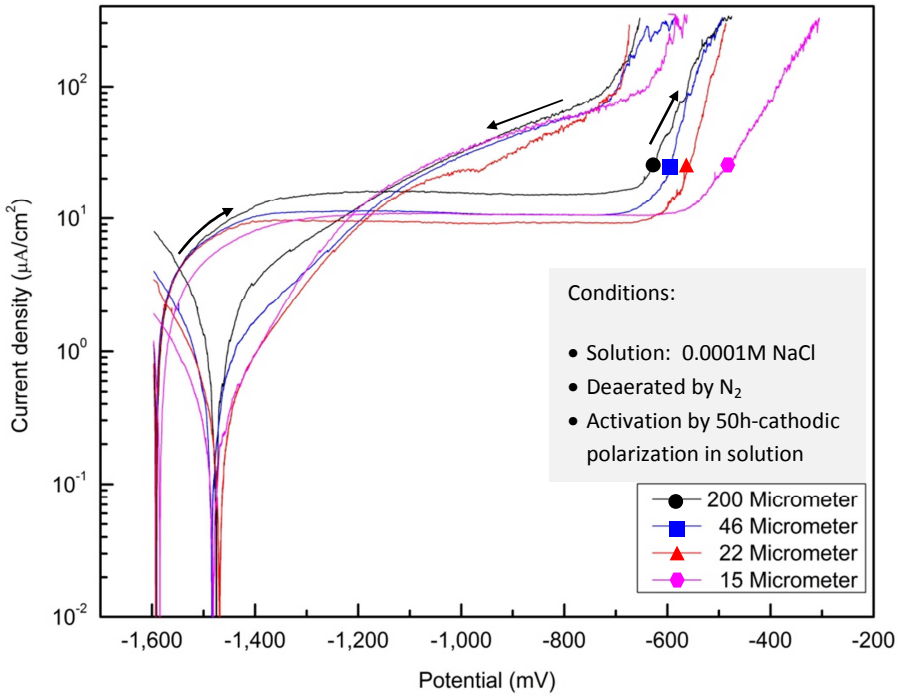

Figure 111: Polarization of pure aluminium in 0.0001M NaCl with different surface finish.

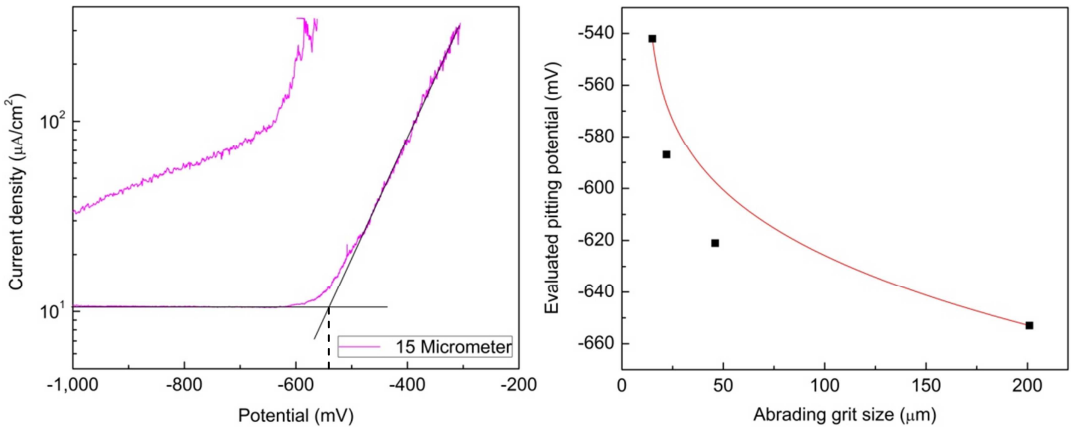

Figure 112: (Left) evaluation of pitting potential from polarization curve and (right) the evaluated pitting potential as a function of grit size of abrading SiC particle.

This measurement shows that surface finish strongly affects passive behaviour and pitting corrosion of pure aluminium.

2.24) Passive behaviour: Effect of surface finish in deionised water

For this measurement the effect of surface finish on passive behaviour of pure aluminium in pure deionised water was studied.

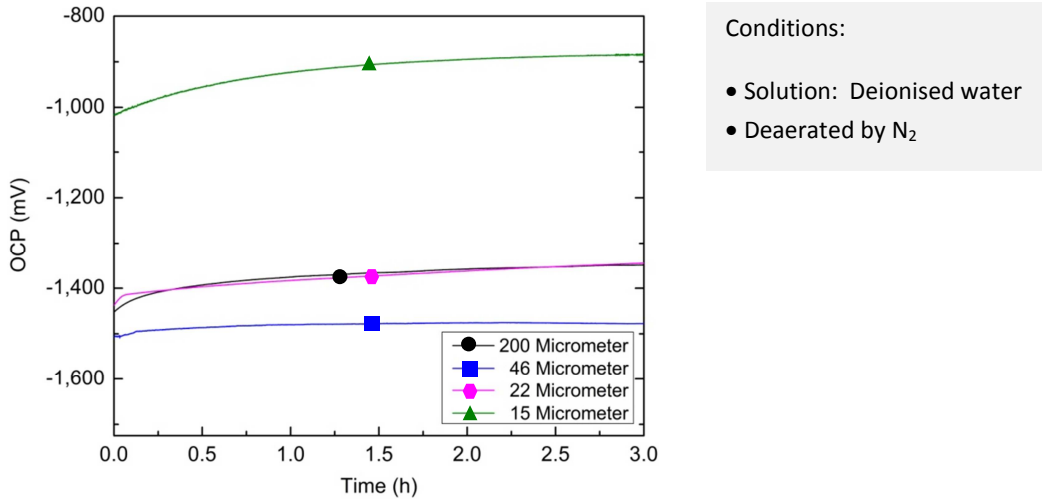

Figure 113: OCP curves of pure aluminium in deionised water with different surface finishes.

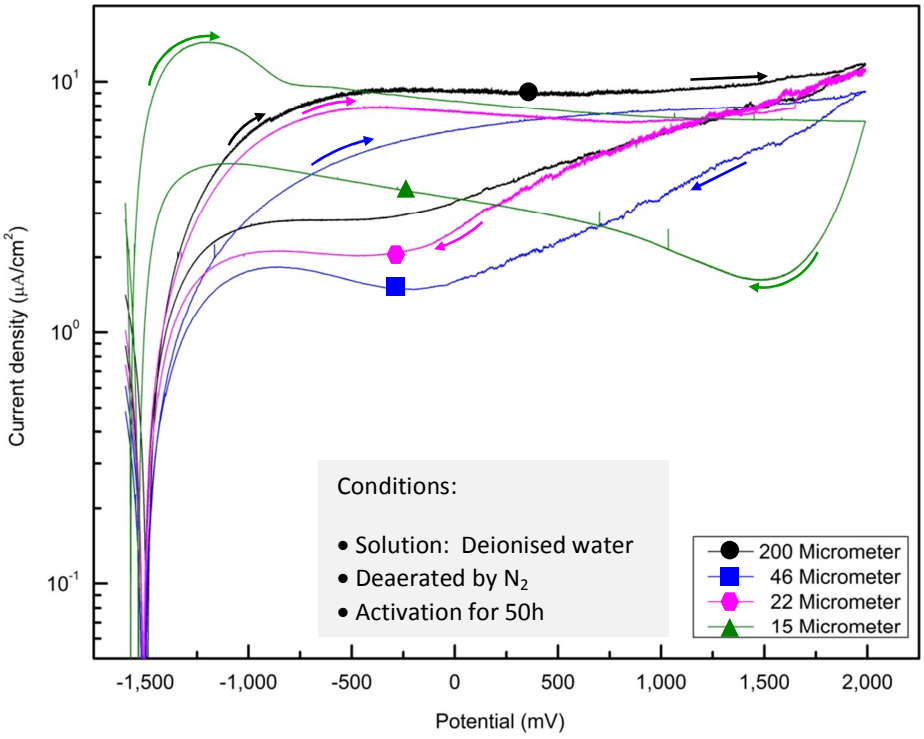

Figure 114: Polarization curves of pure aluminium in deionised water with different surface finishes.

The OCP curves in figure 113 and the polarization curves in 114 show that:

a) The OCP of smoothest surface polished with smallest abrading grit size of 15µm was much higher than the rougher surfaces prepared from bigger grit sizes (200, 46 and 22µm), indicating the more perfect passive oxide film is formed on smoothest surface.
b) For all grit sizes of abrading particles, OCP increases with time until reaching a stable value. This indicates that for all surface roughness pure aluminium is passivated in pure deionised water. Moreover the increase of OCP evolution with time of smoothest surface polished with smallest abrading grit size of 15µm was larger than the rougher surfaces.
c) Corrosion potential of smoothest surface polished with smallest abrading grit size of 15µm slightly shifts to more negative potentials (compared to OCP) than the rougher surfaces, indicating more active surface. Moreover, the active peak of current is only detected from the smoothest surface. This means active aluminium surface can only be achieved from the really smooth surface.
d) Passive current density (J_p) of smoothest surface polished with smallest abrading grit size of 15µm can reach lower value than the rougher surfaces, indicating more perfectly formed passive oxide film. Moreover, only J_p of smoothest surface decreases with increasing polarisation. This confirms, that only the active surface provides the best possible passive oxide film with uniform thickness as mentioned earlier in polarization measurement 2.7.

This measurement shows that in order to get the active surface, really smooth surface was also a necessary prerequisite beside the condition of solution, aeration system and the activation process by constant cathodic polarization.

2.25) Evolution of oxide film surface: Effect of surface finish in NaCl solution

As the result from measurement 2.23 shows that surface roughness has effect on passivation of pure aluminium in NaCl solution, the longer time of OCP measurement for 24h was conducted in this measurement in order to study the passivation behaviour of pure aluminium in NaCl solution. The surface of pure aluminium was polished with two different grit size of abrading particles which were 46 and 15µm to represent rough and smooth surface, respectively.

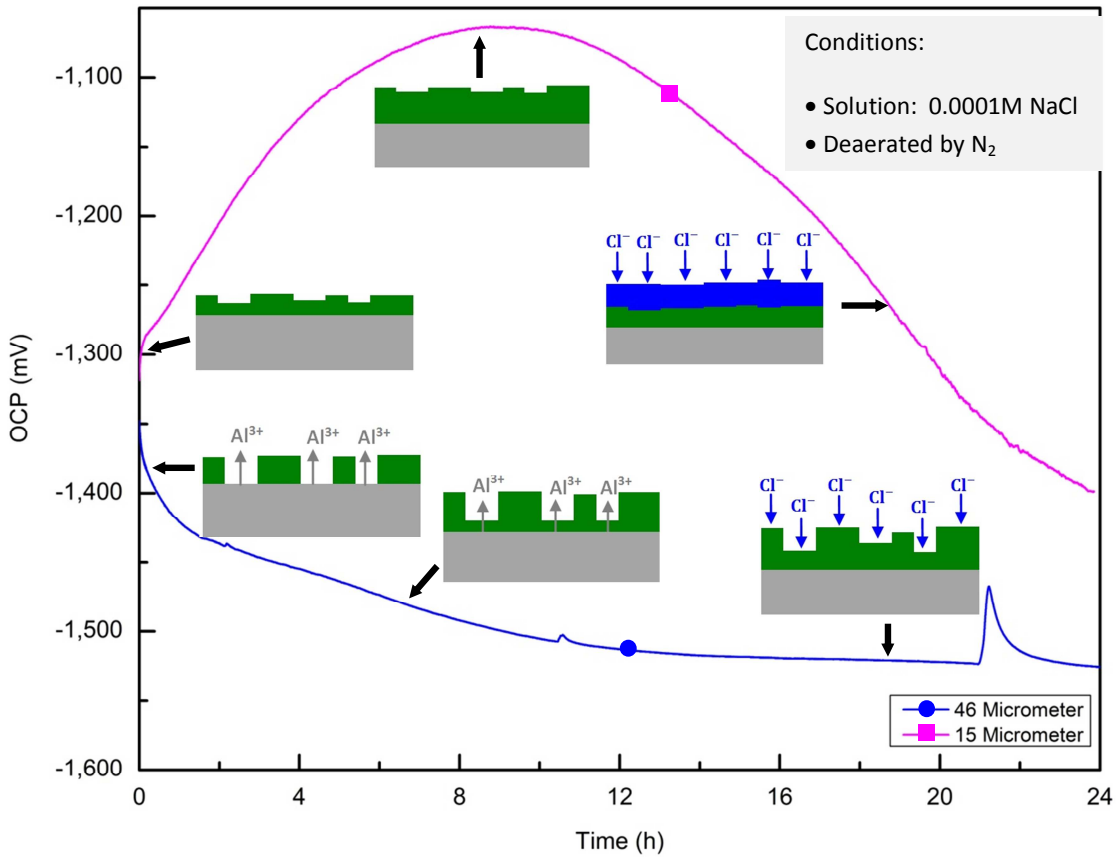

Figure 115: 24h-OCP curves of pure aluminium in 0.0001M NaCl with different surface finishes. Grey (), green () and () represent the aluminium, oxide and modified oxide, respectively.

According to the theoretical background, the OCP curves in figure 115 shows that:

a) For the rough surface polished by 46µm- abrading grit size, OCP slightly goes down until it nearly reaches stable potential. This indicates that the surface of pure aluminium is attacked by chloride ions in solution.

b) For the smooth surface polished by 15µm- abrading grit size, OCP goes up until it reaches the maximum and then goes down. This reflects that pure aluminium with smooth surface shows passivation at the beginning and then modification of the passivated surface as discussed before.

c) After 24h of OCP measurement, OCP from both rough and smooth surface still does not reach the steady value. It was mentioned in [51] that in deaerated solution, the steady state of OCP usually occurred after 4 days.

According to the information from OCP evolution with time in figure 115, the model of passive oxide film evaluating with time of pure aluminium surface is proposed and shown also in this figure. For smooth surface, passive oxide film covers all area of aluminium surface. When aluminium is immersed in chloride solution, oxide film is growing until it reaches maximum thickness. After that chloride ions incorporate in oxide film and transform oxide film into chloride complexes at the oxide/solution interface. For rough surface, area of active surface possibly exists at the beginning. When aluminium is immersed in chloride solution, aluminium metal is partially dissolved. Active dissolution of aluminium takes place, releasing aluminium ions. Then thin oxide film is formed. Since only really thin oxide film is formed at the beginning, aluminium dissolution still take place and aluminium ions can be transported out of the oxide film. Oxide film is growing and finally protects aluminium metal.

This measurement shows that the surface finish, which relates to surface roughness, strongly affects the passivation behaviour of pure aluminium in NaCl solution.

2.26) Evolution of corrosion behaviour with time of pure aluminium in NaCl solution

For this measurement, the anodic polarizations were conducted on pure aluminium that had been immersed in 0.001M NaCl for different periods of time in order to study the evolution of corrosion behaviour with time of pure aluminium in NaCl solution. Therefore prior to polarization measurement, many pure aluminium sheets were totally immersed in 0.001M NaCl for 0 day to 60days. After each period of immersion time, the measurement started with 30min of OCP measurement, followed by anodic polarization from OCP up to 1,000mV above the OCP with a scan rate of 600mV/h. Only the anodic polarization was employed for this measurement since the cathodic polarization could alter the surface of immersed pure aluminium sample.

The OCP curves in figure 116 show that:

a) For no NaCl immersion, OCP become more and more noble. This implies that pure aluminium is passivated in NaCl solution.

b) For the NaCl immersion from 1 day to 60 days, OCP become more and more active. This possibly reflects that aluminium is attacked by chloride ions due to the fact that after

immersion in NaCl solution for at least 1 day, passive layer has already been formed on the surface so that formed passive film is modified by chloride ions.

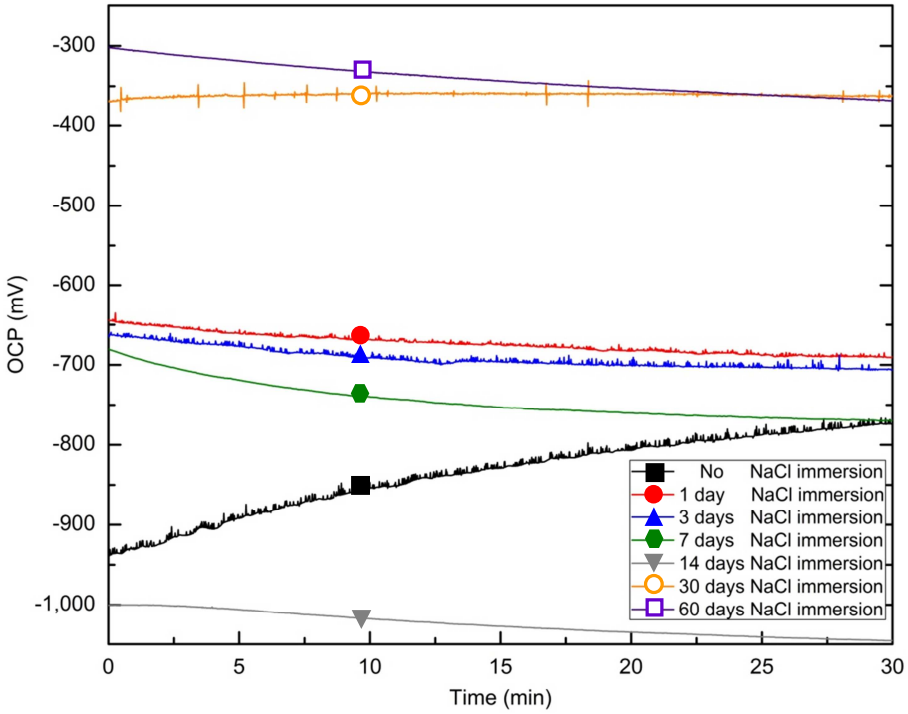

Figure 116: The OCP curves of pure aluminium sheet with different immersion times.

The anodic polarization curves in figure 117 shows that pure aluminium after immersion for any period of time exhibits passive behaviour at corrosion potential followed by pitting potential at high potentials. However for difference immersion time, pure aluminium shows different corrosion potential (E_{cor}), passive current density (J_p) and maximum pitting current density (J_{max}) as can be seen figure 118. Therefore 3 following groups of these corrosion parameters, listed in table 20(appendix), are distinguished.

I. After immersion for 0 to 7 days, corrosion potential is nearly -700mV. The passive current density is about few µA/cm^2 and the maximum pitting current density is extremely high in the range of mA/cm^2. It is predicted that during this period of immersion time, passive oxide film is spontaneously formed.

II. After immersion for 14 days, the corrosion potential shifts by nearly 300mV to more active value. Moreover, the passive current density increases but the maximum pitting current density fairly decreases in this immersion time. This can be attributed to the

thinning of spontaneous passive oxide film which is a consequence of the formation of *oxychloro complexes* in neutral NaCl solution [20].

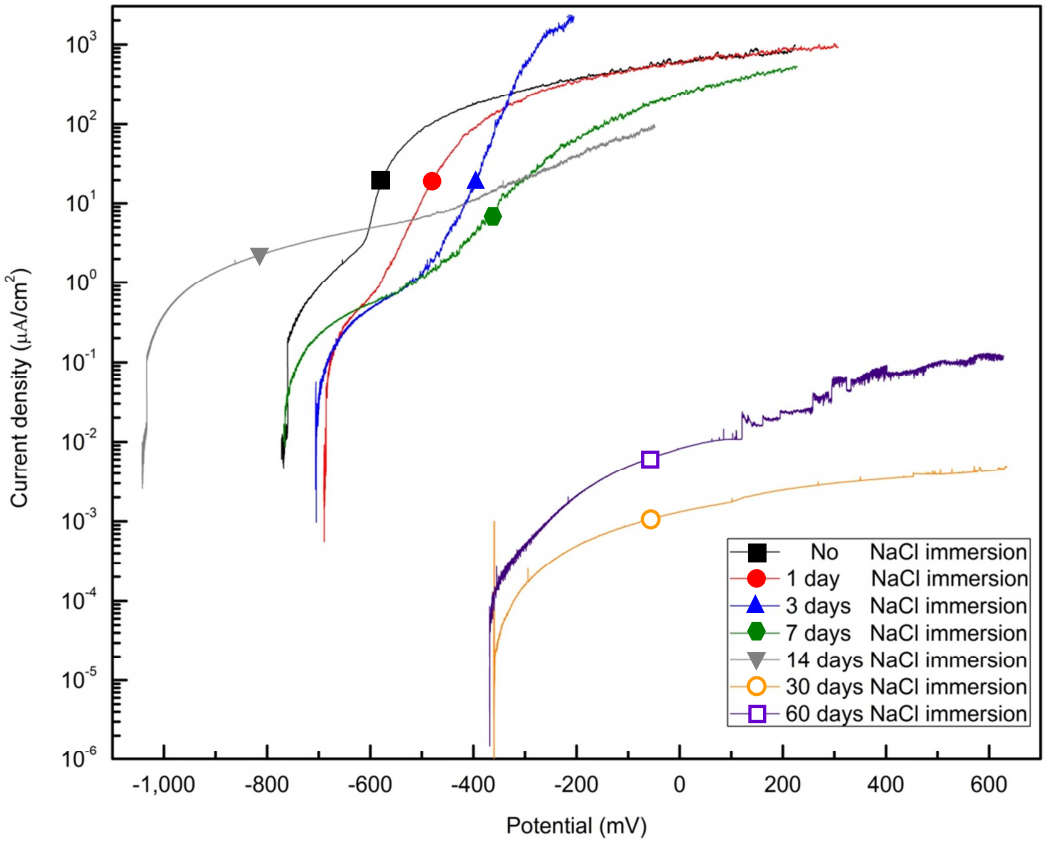

Figure 117: The anodic polarization curves of pure aluminium with different immersion time.

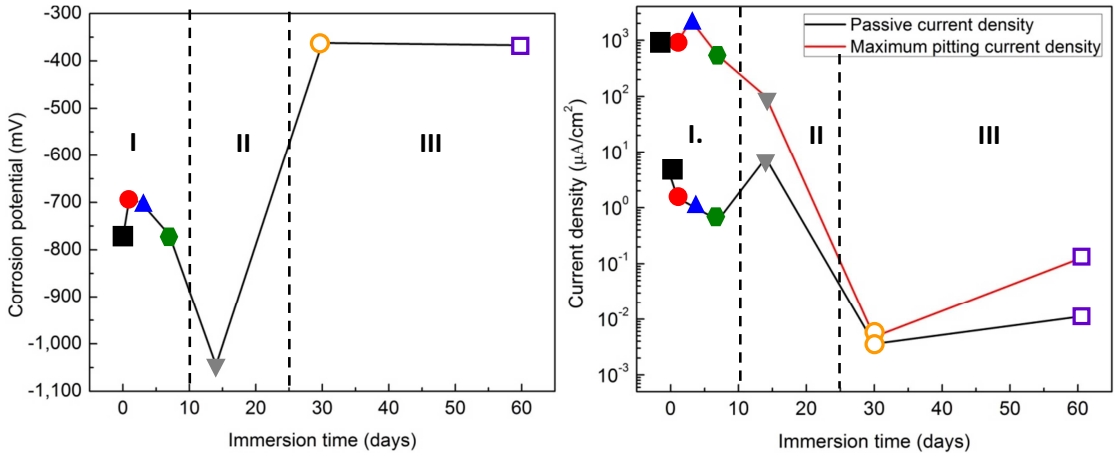

Figure 118: (Left) corrosion potential as a function of immersion time and (right) passive current density and maximum pitting current density as a function of immersion time in 0.001M NaCl.

III. After immersion time for 30 to 60 days, the corrosion potential significantly shifts by 700mV to more noble potentials. The passive and maximum pitting current densities greatly reduce to only several nA/cm^2. This indicates the greatly improved corrosion resistance of pure aluminium. This can be attributed to the fully developed passive oxide in thickness and area over the surface of pure aluminium. It was mentioned in [59] that the formation of the passive layer decreased the rate of anodic dissolution of aluminium. Therefore it can be deduced that the longer immersion time improves the self-passivation (passive) behaviour with decreasing corrosion rate of pure aluminium in low concentrated NaCl solutions. However the full development of this passive oxide film does not prevent the initiation of pits, since the pitting corrosion is still detected with a relatively low pitting current density. It was mentioned in [36] that in natural environments such as freshwater, sea water and rain water, the rate of deepening of pits reduces with time. This may be confirmed by this measurement that the improvement of self-passivation behaviour with time of pure aluminium decreases the pitting current density, which is directly proportional to pitting corrosion rate.

Therefore, this measurement shows that self-passivation (passive) behaviour of pure aluminium improves with time.

2.27) Comparing passive layer: growing in water and modified in NaCl solution

For this measurement, the effect of prior water immersion on corrosion behaviour of pure aluminium was studied. This measurement was quite similar to the measurement above. The only difference was that pure aluminium sheets were prior spontaneously passivated in deionised water for 3 days before immersing in 0.001M NaCl. The duration of immersion in 0.001M NaCl was 0 and 14 days. After each period of immersion in 0.001M NaCl solution, pure aluminium was anodic polarized in 0.001M NaCl with a scan rate of 600mV/h.

The OCP and anodic polarization curves in figure 119 shows that:

a) Without NaCl immersion, the fluctuation in OCP and anodic polarization curves exhibit pitting corrosion at corrosion potential in NaCl solution. This can be attributed to the sufficiently but imperfectly formed passive oxide film during prior water immersion for 3

days. Therefore after put pure aluminium into solution containing chloride ions, pitting corrosion instantly takes place.

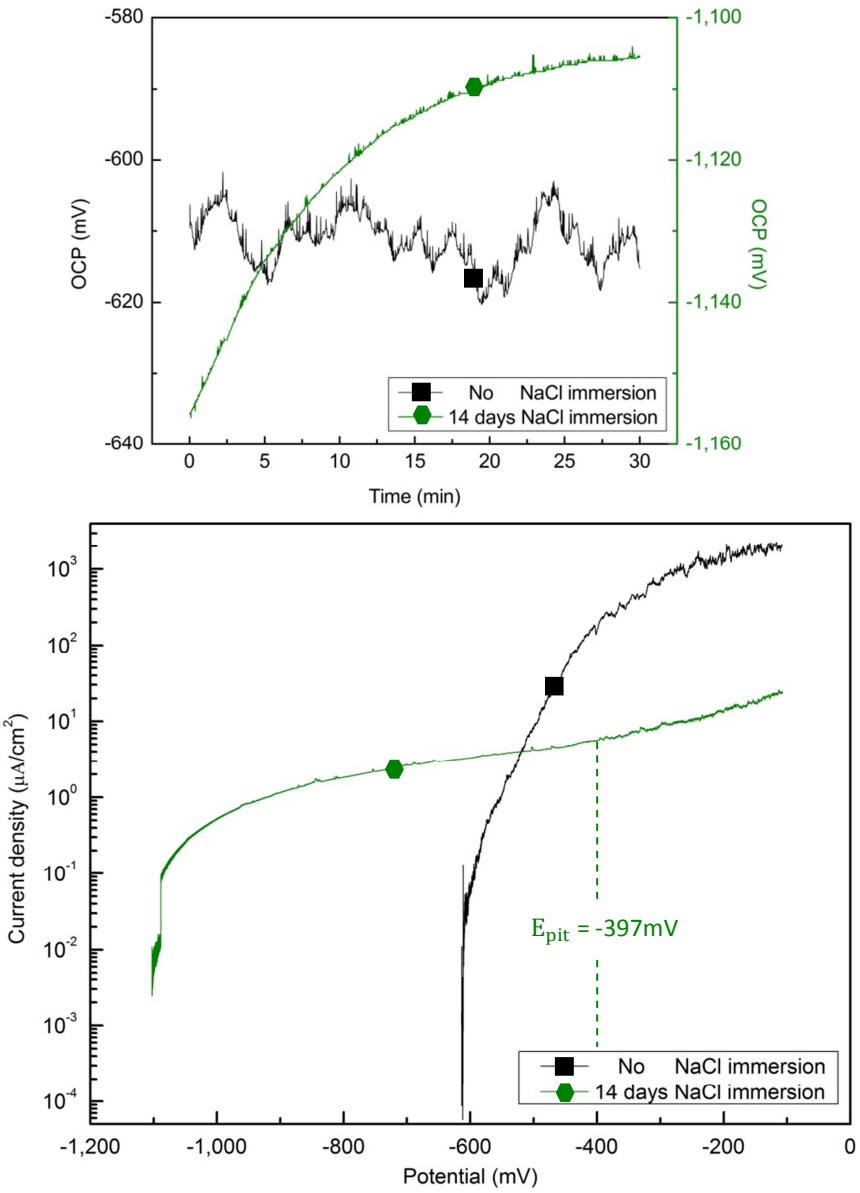

Figure 119: (Top) OCP and (bottom) anodic polarization curves of pure aluminium after immersion in 0.001M NaCl for different period of time with 3 days prior-water immersion.

b) After immersion in NaCl for 14 day, the corrosion potential and OCP value shifts to more active value. It was mentioned in [22] that the complexes containing chloride ions formed at the oxide/solution interface was more soluble than complexes formed in the absence of chloride ions and the formation of this complex containing chloride ions

causes thinning of passive oxide film. Therefore the modification of formed oxide film by chloride ion on pure aluminium surface is the cause of the decrease in corrosion potential. The low and non-fluctuating OCP become nobler with time, indicating passivation. The anodic polarization curve as well confirms the passive behaviour at corrosion potential. Therefore it can be deduced that it is not only modification but also the formation of passive oxide film taking place on pure aluminium surface during immersion in NaCl solution. Moreover, pitting corrosion with relatively low pitting current density is detected at higher potentials. This shows that the formation of passive oxide film hindered the pitting corrosion.

In order to study the effect of prior water immersion on corrosion behaviour of pure aluminium, OCP and anodic polarization curves with and without 3 days prior-water immersion are compared.

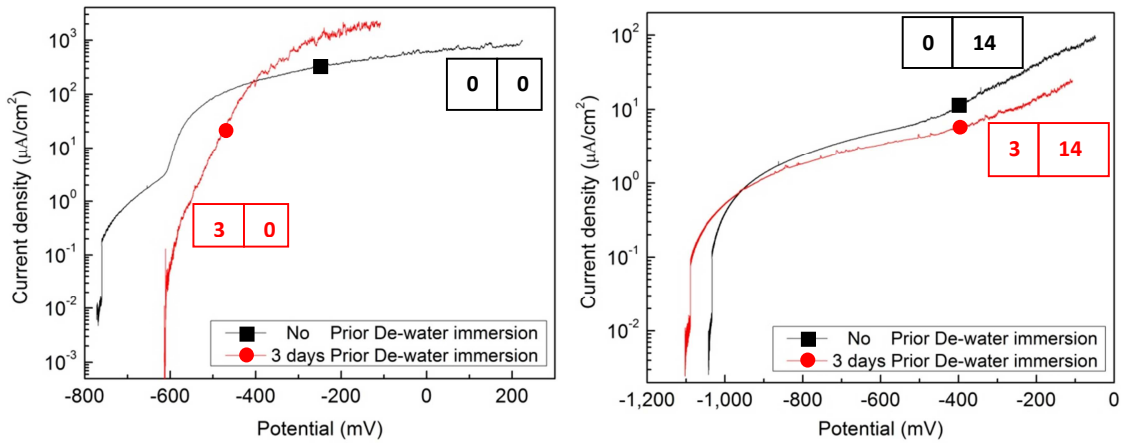

Figure 120: The anodic polarization curves of pure aluminium sheet in NaCl solution with and without 3 days prior- water immersion followed by: (left) no NaCl immersion and (right) 14 days NaCl immersion. *The boxes show the immersion days in | Water | NaCl |

The compared polarization curves in figure 120 and their corrosion parameters in table 21 (appendix) shows that:

a) For No NaCl immersion (figure 120, left), corrosion potential of pure aluminium with prior water immersion (passive surface) shifts to nobler values than without prior water immersion (nearly active surface). Moreover, pure aluminium with nearly active surface exhibits passivation while, pure aluminium with passive surface exhibits instant pitting

corrosion when put into NaCl solution. This suggests that with passive surface, pitting corrosion can be initiated instantly after immersion in NaCl solution. Therefore pure aluminium with passive surface or nearly active surface exhibits different corrosion behaviour after short time-immersion in NaCl solution.

b) After immersion in NaCl for 14 days (figure 120, right), both pure aluminium with and without prior water immersion exhibit passive behaviour and their polarization curves show no significant difference. This may be due to the formation and modification of passive oxide film during immersion in NaCl solution. For pure aluminium with prior water immersion (passive surface), the water-formed passive oxide film is firstly modified by chloride ions and the new passive oxide film is also formed and then modified during immersion of NaCl solution. While for pure aluminium without prior water immersion (nearly active surface), passive oxide film is formed and then modified during immersion of NaCl solution. Therefore pure aluminium with passive surface or nearly active surface shows the same corrosion behaviour after immersion in NaCl solution for some period of time. However, passive surface exhibits slightly lower passive current density and larger passive region range. This can be attributed to the thicker and larger passive oxide film which is the result of longer immersion time in oxidized solution including deionised water and NaCl solution. Therefore it cannot be said that spontaneous passive oxide film significantly improves corrosion resistance of pure aluminium after long term immersion in NaCl solution since the spontaneous oxide film is thinned by the effect of chloride ion.

This measurement indicates that oxide film can be spontaneously formed in both deionised water and NaCl solution and this oxide film can be modified by chloride ions in NaCl solution.

2.28) Passive behaviour of aluminium alloys in deionised water

The corrosion behaviour of pure aluminium and 3 different aluminium alloys in deionised water were studied in this measurement. The 3 aluminium alloys used in this measurement were AA2024, AA5052 and AA6061 which are named as Al-Cu alloy, Al-Mg alloy and Al-Mg-Si alloy, respectively [59]. The compositions of these alloys are already given in table 4. The aluminium alloy sheets were cut into 2x2cm square shaped specimens. Then each aluminium

samples was embedded in the epoxy resin holder allowing a total exposed surface area of 4cm^2. After that it was mechanically abraded by silicon carbide paper with abrading grit size of 46, 22 and 15µm, then cleaned with plenty of water and finally dried with air. The open circuit potential was measured first for 3h and then the constant cathodic potential of 250mV below the OCP was applied to the samples for 50h. After that the cyclic polarization was applied carried out over the potential range from 250mV below the OCP to 1,200mV above the OCP with a scan rate of 600mV/h.

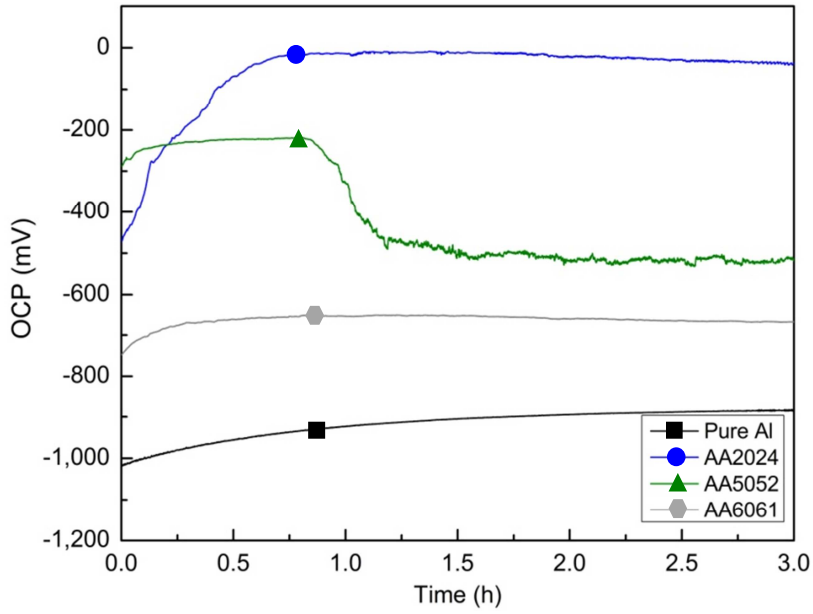

Figure 121: OCP curves of aluminium alloys in deionised water.

The OCP curves in figure 121 show that:

a) The OCP of all aluminium alloys increase with time, indicating that all aluminium alloys exhibits passive behaviour in deionised water.

b) The AA2024 shows the largest increase in OCP. This possibly implies that AA2024 has the best formation of oxide film in the sense of thickness and/or homogeneity

c) The AA5052 exhibits a drop of OCP by 200mV after nearly 50 min and then starts fluctuating with low amplitude. This may be the accidental result of a defect of its oxide layer.

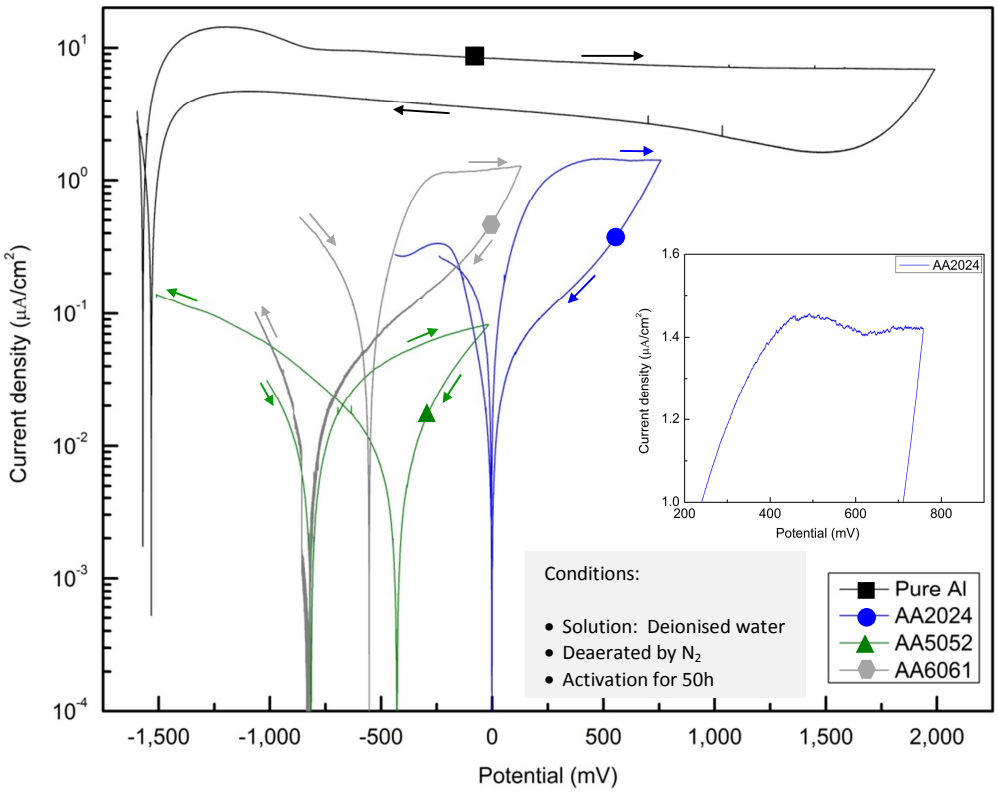

Figure 122: Cyclic polarization curves of aluminium alloys.

The polarization curves in figure 122 and their corrosion parameters in table 22(appendix) shows that:

a) The active peak is clearly detected only from pure aluminium. On the other hand, active peak of AA5052 and AA6061 cannot be observed. For AA2024, active peak can also be observed (zoom of blue line in figure 122), reflecting that AA2024 seems to be activated. This can be attributed to a cathodic reduction preferentially taking place on the intermetallic particles of aluminium alloys [30]. The intermetallic particles such as Al_3Fe of AA6061 and Al_2CuMg of AA2024 present a cathodic behaviour with respect to the surrounding matrix. During the cathodic polarization, the cathodic character of intermetallic particles induce the cathodic reduction (such as reduction of water, $H_2O + 2e^- \rightarrow H_2 + 2OH^-$) to take place intensively on them, producing the increase of local solution's pH. The local alkalisation of the solution causes the intense dissolution of oxide layer only around the intermetallic particles. After the oxide layer around the particles had been removed, the local alkalisation causes an intense attack of aluminium

metal at the intermetallic particles/matrix interface, resulting in the decrease of the contact area between the matrix and the intermetallic particle. Finally, pit is formed due to disappearance of intermetallic particle possibly by detachment action as shown in the model of figure 123 [30]. Therefore the constant cathodic polarization only produces the active surface in the vicinity of intermetallic particle.

Process No.	**1**	**2**	**3**
Process	Nearly uniform dissolution of oxide film over entire surface area	After the exposure of intermetallic particle, intense dissolution of oxide film only in its vicinity	Intense attack of aluminium metal by alkalisation at the particle/matrix interface
	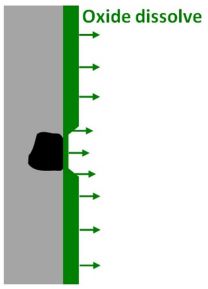	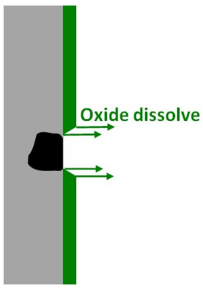	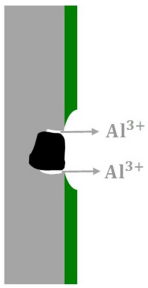
Process No.	**4**	**5**	**6**
Process	Reduction of contacting area between aluminium matrix and intermetallic particle	Disappear of intermetallic particle by detachment action	Formation of pit
			

Figure 123: Model of the surface of aluminium alloy during the constant cathodic polarization. Grey (▒), black (■) and green (■) represent the aluminium and oxide, respectively (Modified after [30]).

b) Negative hysteresis is detected from all aluminium alloys, inferring the expected behaviour in deionised water.

c) The corrosion potential and passive current density are different for different aluminium alloys (figure 124), indicating the corrosion potential and passive current density are

strongly dependent on the alloying metal of aluminium. Moreover, all aluminium alloys exhibit much lower passive current density than pure aluminium, indicating that pure aluminium is less resistant to corrosion than the aluminium alloys. This suggests that the alloying of pure aluminium with copper, magnesium and silicon lead to the rise in corrosion resistance of aluminium. Comparing the passive current densities, the corrosion resistance ranging from the highest to the lowest are AA5052, AA6061, AA2024 and Pure Al. This is corresponded with [Ref. 58] that the corrosion resistance of aluminium alloy series arranging from highest to lowest are AA5XXX, AA6XXX and AA2XXX.

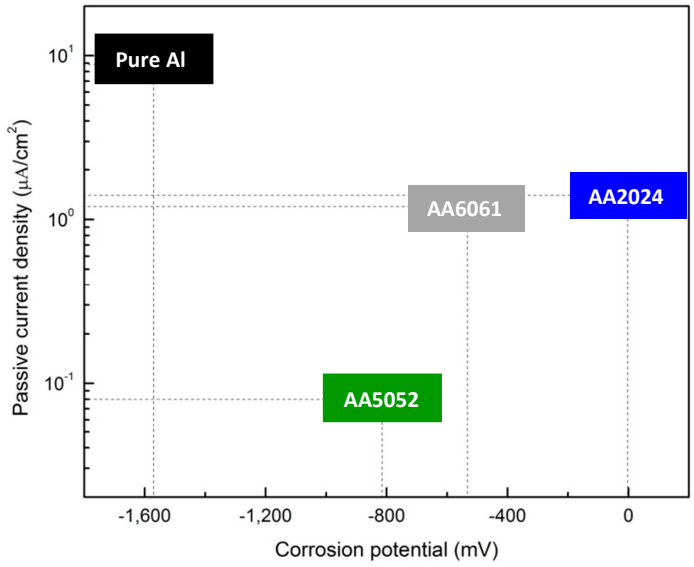

Figure 124: The relationship between corrosion potential and passive current density of the aluminium samples.

This measurement shows that aluminium alloys exhibits higher corrosion resistance than pure aluminium in deionised water.

2.29) Pitting behaviour of aluminium alloys in NaCl solution

It was mentioned in [59] that the corrosion rate of aluminium alloys in chloride ions solution was quite low, but even the alloys can be attacked by pitting corrosion in such solutions. Therefore in this measurement, three aluminium alloys were polarization in solutions with

different NaCl concentrations (0.1M, 0.01M and 0.001M), in order to study the effect of chloride ion concentrations on the corrosion behaviour of aluminium alloys. The polarization measurement started with 50h constant cathodic polarization at about 250mV below E_{cor} and then forward polarization in noble direction was conducted up to 1,000mV above E_{cor} at a scan rate of 600mV/h. It should be mentioned that the limit of current density is in the range of 10^4µA/cm^2.

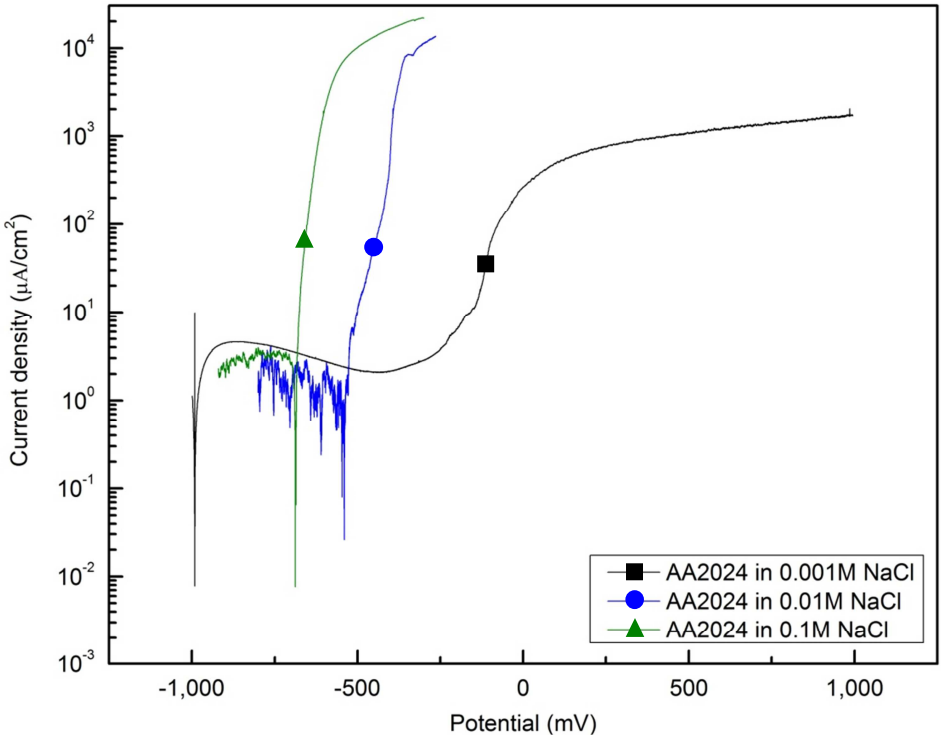

Figure 125: Polarization curves of AA2024 in solution with different NaCl concentrations.

The polarization curves of AA2024 in figure 125 and their corrosion parameters in table 23(appendix) shows that:

a) Pitting corrosion occurs in every NaCl concentration and pitting potential decreases with increasing NaCl concentration.

b) Pitting corrosion and fluctuations even in the cathodic regime are observed in 0.01 and 0.1M NaCl solutions. This possibly indicates that the pitting corrosion can take place during cathodic polarization in these solutions. On the other hand in 0.001M NaCl solution, passive behaviour followed by pitting corrosion is detected. This may reflect

that in solutions with low amount of chloride ions, the local breakdown of passive film is spontaneous healed. While in higher chloride concentrations, healing processes is prevented, therefore a passive region completely disappears [22].

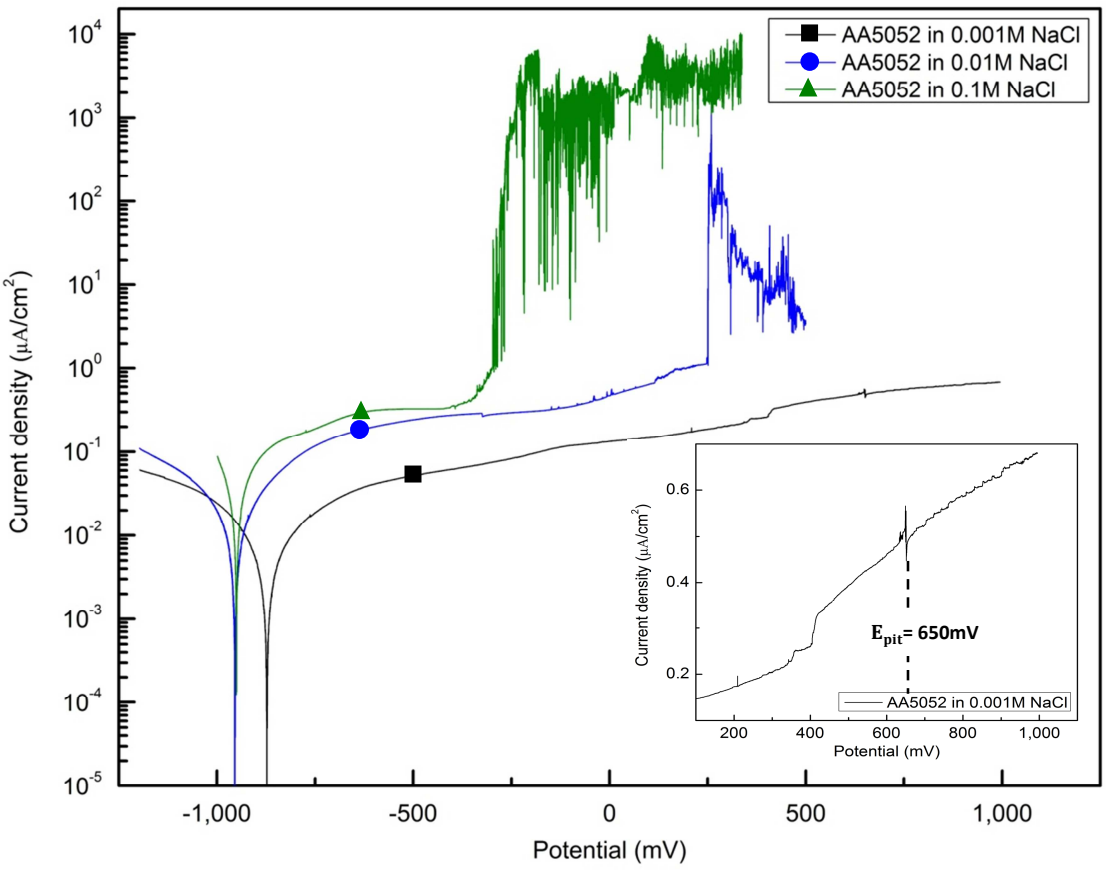

Figure 126: Polarization curves of AA5052 in solution with different NaCl concentrations.

The polarization curves of AA5052 in figure 126 and their corrosion parameters in table 23 (appendix) shows that:

a) Pitting corrosion occurs in every NaCl concentration and pitting potential decreases with increasing NaCl concentration. Moreover no pitting corrosion at E_{cor} is detected from AA5052 in any concentration of NaCl solution.

b) The passive region range decreases with increasing NaCl concentration indicating the decrease of pitting susceptibility of this alloy with increasing NaCl concentration.

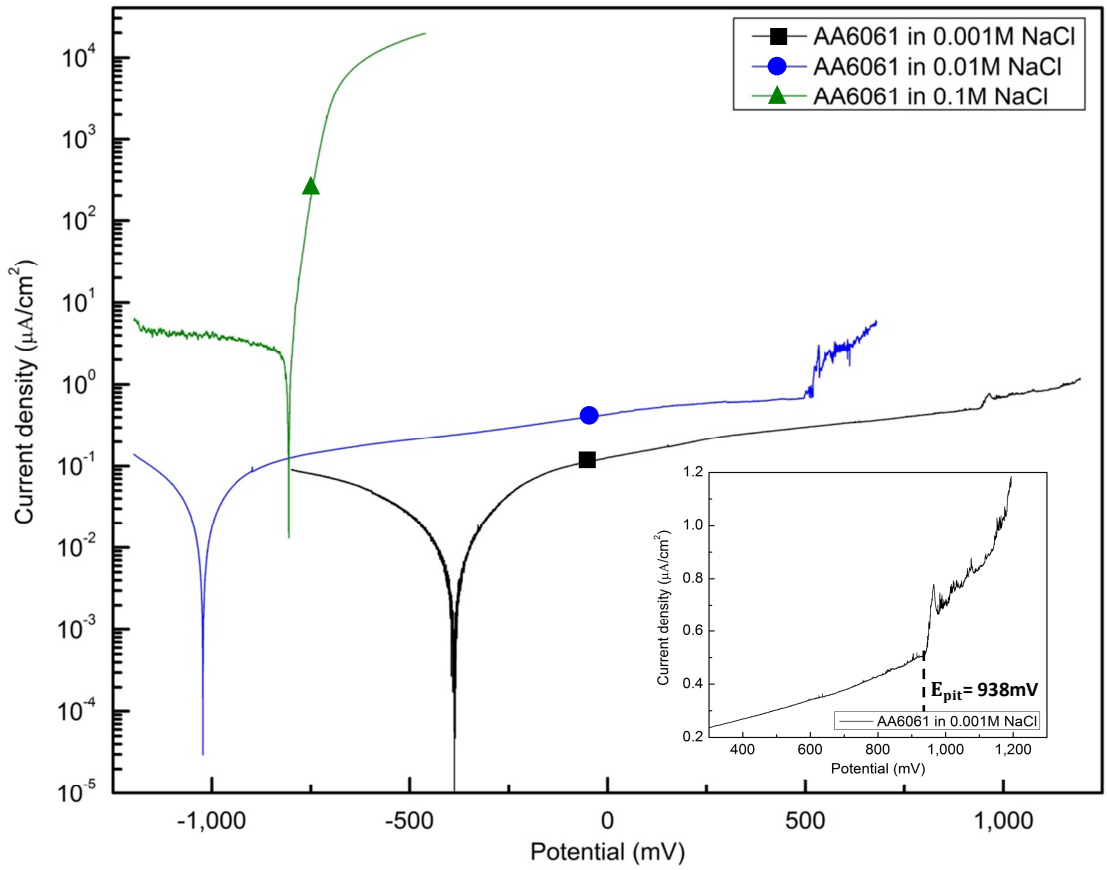

Figure 127: Polarization curves of AA6061 in different NaCl concentration.

The polarization curves of AA6061 in figure 127 and their corrosion parameters in table 23 (appendix) shows that:

a) Pitting corrosion is detected in every NaCl concentration and pitting potential decreased with increasing NaCl concentration.

b) Pitting corrosion and fluctuations in the cathodic regime are detected only at high concentration of 0.1M.

Figure 128 shows a comparison of the pitting potential of the all three aluminium alloys. It can be seen that in solution with high NaCl concentration of 0.1M NaCl, the pitting potential ranging in order from the highest to lowest are AA2024, AA5052 and AA6061. While in solution with lower NaCl concentration of 0.01M and 0.001M NaCl, the pitting potential ranging in order from the highest to the lowest are AA6061, AA2024 and AA5052. Therefore it can be concluded that it is not only the concentration of chloride ion in solution

influencing the pitting corrosion of aluminium alloys but also the type of aluminium alloys in use.

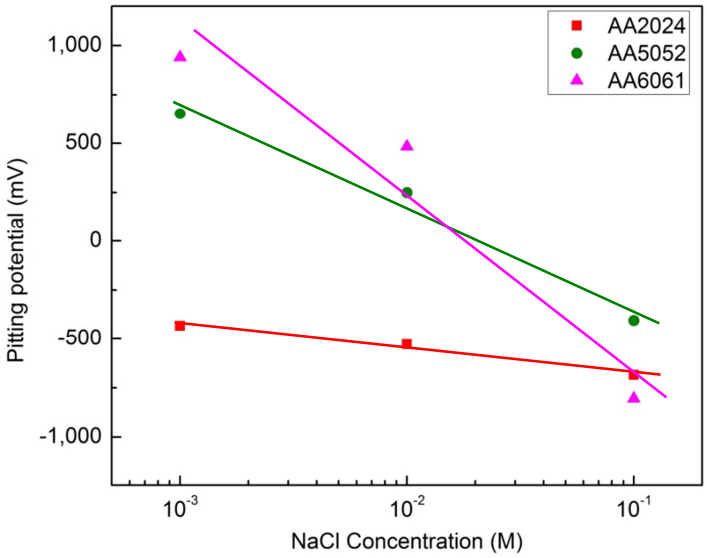

Figure 128: Pitting potential variation of aluminium alloys with NaCl concentration.

In order to study only effect of the type of aluminium alloys on corrosion of aluminium, the corrosion current density and passive region range, in table 23(appendix), of pure aluminium and aluminium alloys in 0.001M NaCl are compared. The corrosion current density is calculated by extrapolating the passive current density down to the corrosion potential.

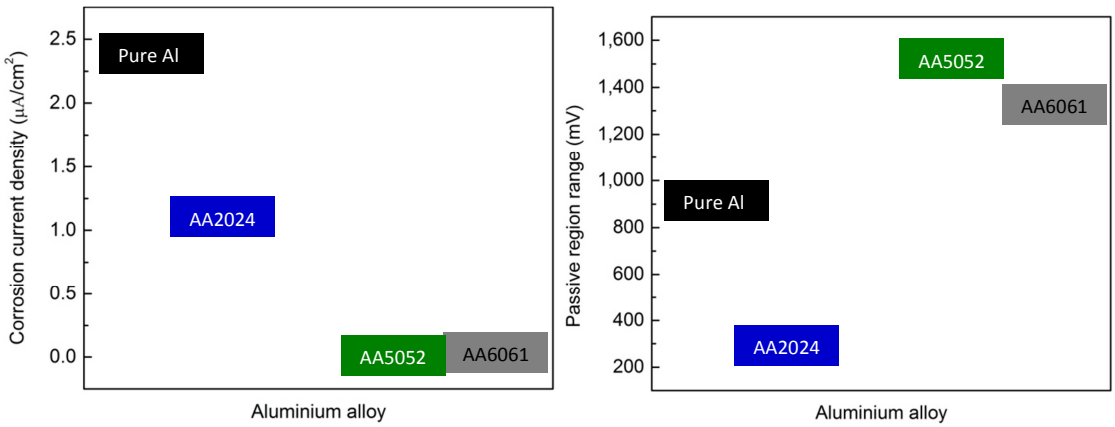

Figure 129: (Left) corrosion current density and (right) passive region range of pure aluminium and aluminium alloy in 0.001M NaCl solution.

The corrosion current densities and passive region ranges of all aluminium alloys range in figure 129 shows that

a) The corrosion rate (figure 129, left), which is proportional to corrosion current density there, ranging from the highest to lowest are Pure Al, AA2024, AA6061 and AA5052. The corrosion rate of pure aluminium is higher than that of all aluminium alloys. This suggests that alloying metals can improve the corrosion resistance of aluminium.
b) The pitting susceptibility (figure 129, right), which is proportional to the passive region range, of AA2024 is lower than that of pure aluminium whereas the pitting susceptibilities of AA5052 and AA6061 are higher than that of pure aluminium. This can be attributed to the structure of passive oxide film on the surface of aluminium alloy. It was mentioned [Ref.36] that Al-Mg alloy of 5000 series have excellent corrosion resistance because the structures of aluminium oxide and magnesium oxide was compatible. Therefore magnesium strengthened the protective oxide film by forming mixed oxide film. The strengthening of protective oxide film by magnesium may be also applied to Al-Mg-Si alloy of series 6000. On the other hand, Al-Cu alloy of 2000 series was a poor corrosion resistant due to the fact that the copper, which is nobler than aluminium, weakened the protective properties of oxide film.

This measurement shows that the corrosion behaviour and corrosion rate and of aluminium in NaCl solution strongly depend on concentration of chloride ions in solution as well as a type of aluminium alloy in use.

2.30) Electrochemical behaviour of CFRP in NaCl solution

In this measurement, the effect of NaCl concentration in solution on corrosion behaviour of CFRP was studied by polarization measurement. The CFRP specimens, used in this measurement, were made of 8 ply of unidirectional prepreg sheets of carbon/epoxy at 0˚ fibre orientation. The prepreg sheet (Sigrafil prepregs from SGL group) was nominally 0.22mm thick. During manufacturing in the heating press, a temperature of 130˚C, time of 90 min and vacuum pressure of 2.5 bars were set as curing conditions. The thickness of the cured CFRP was about 2mm. CFRP was cut into square plates of 2cmx2cm, which was the same size as aluminium samples for further comparison. Prior to polarization, the OCP measurement was carried out for

3h. Then CFRP was polarized from 1,200mV below the OCP up to 1,000mV above the OCP in noble direction with scan rate of 600mV/h.

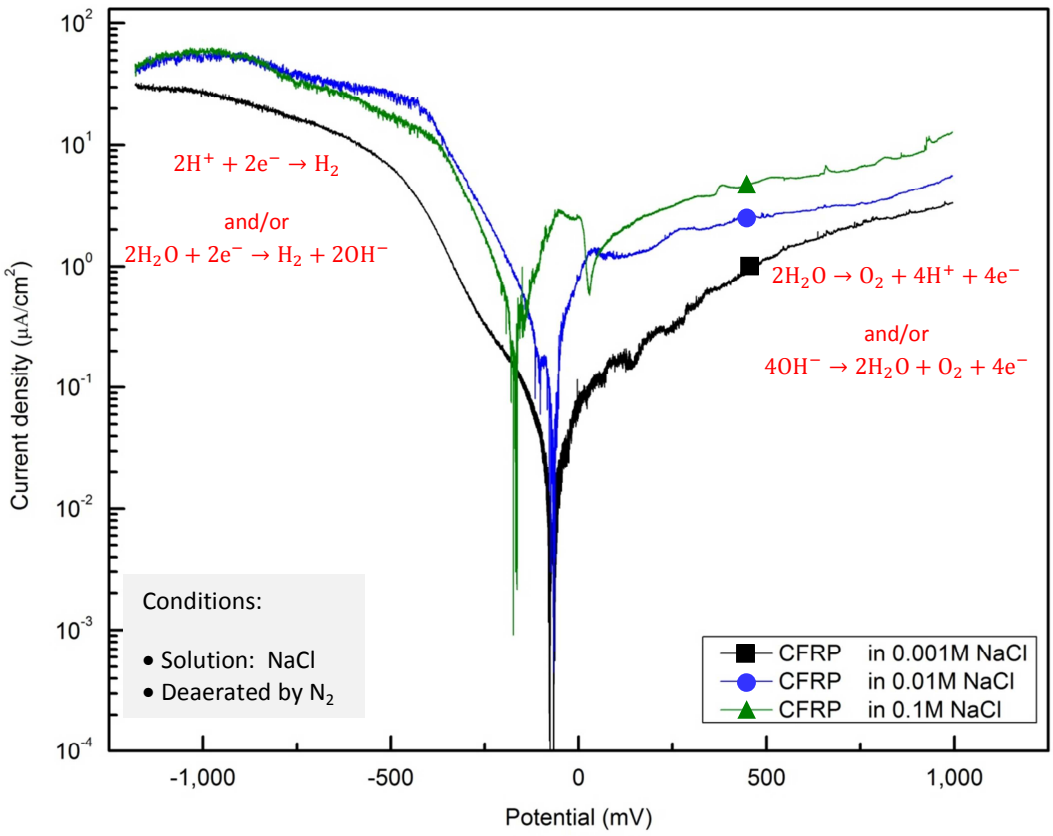

Figure 130: Polarization curves of CFRP in solution with different NaCl concentration.

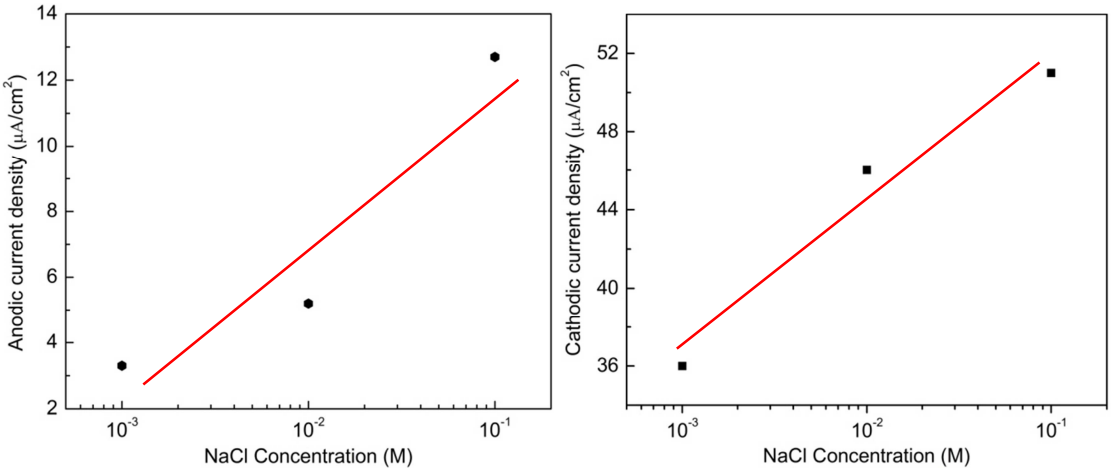

Figure 131: (Left) cathodic current density at - 1,200mV and (right) anodic current density at 1,000mV of CFRP in different NaCl concentration solution.

The polarization curves of CFRP in figure 130 shows that:

a) It is predicted that the cathodic reaction of CFRP are the reduction of hydrogen ions on carbon fibre surface ($2H^+ + 2e^- \rightarrow H_2$) in low pH solution and/or reduction of water on carbon fibre surface ($2H_2O + 2e^- \rightarrow H_2 + 2OH^-$) in high pH solution [60]. Moreover, the value of cathodic current density increases with increasing concentration of NaCl in solution (figure 131, left).
b) It is predicted that the anodic reaction of CFRP are the oxidation of water on carbon fibre surface ($2H_2O \rightarrow O_2 + 4H^+ + 4e^-$) in low pH solution and/or the oxidation of hydroxide ions on carbon fibre surface ($4OH^- \rightarrow 2H_2O + 4e^- + O_2$) in high pH solution [60]. Additionally, the anodic current density increases with increasing concentration of NaCl in solution (figure 131, right).

This measurement shows that the reaction rate of both anodic and cathodic reactions of CFRP increases with increasing chloride ions concentration in solution.

2.31) Galvanic behaviour of aluminium alloys coupled with CFRP in NaCl solution

As carbon fibre is nobler than aluminium alloys, galvanic coupling between carbon and aluminium alloy can occur when both materials are in electrical contact in the presence of an electrolyte. Therefore the uniform galvanic corrosion of aluminium alloy can occur. Additionally on aluminium alloy, which is a passive metal, localised corrosion such as pitting corrosion can possibly be initiated or encouraged as the potential of aluminium alloy increases [7]. It is possible to use the polarization curves of two materials to predict the extent of galvanic corrosion when they are coupled [38].

Therefore for this analysis, the polarization curves of aluminium alloys and CFRP for each NaCl concentration were superimposed in one graph in order to estimate the corrosion rate of aluminium alloys when coupled with CFRP. Such a graph is commonly referred as the Evans diagram [35]. The intersection of polarization curves of one aluminium alloy and CFRP in the same solution gives the predicted corrosion potential and corrosion current of the Aluminium/CFRP system. It should be mentioned that the corrosion parameters may strongly depend on the area ratio of the two materials.

In 0.001M NaCl

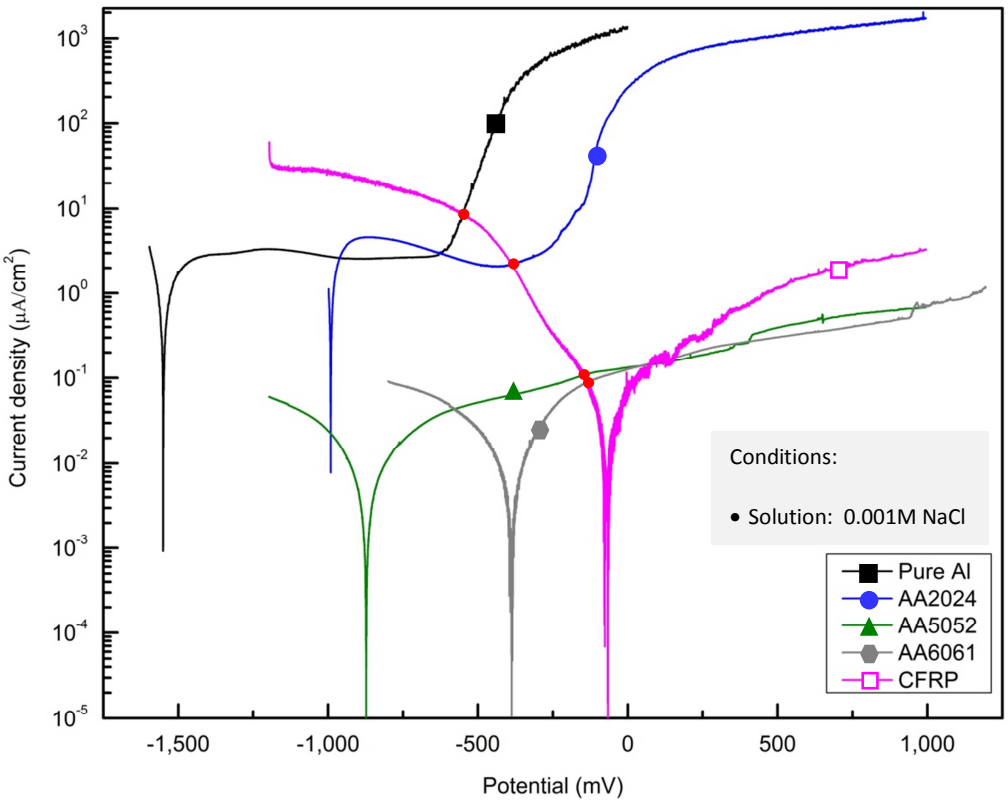

Figure 132: Evans diagrams for aluminium alloys with CFRP in deaerated 0.001M NaCl solution.

The Evans diagrams in 0.001M NaCl solution (figure 132) shows that:

a) For all aluminium alloys, the corrosion potential of CFRP is higher than that of aluminium alloys, meaning that CFRP is more "noble" than all aluminium alloys. Therefore, aluminium alloys tend to corrode faster when coupled with CFRP.

b) The anodic polarization curves of all aluminium alloys intersect the cathodic polarization curve of CFRP. This implies that when aluminium alloy is coupled with CFRP, the aluminium alloy is polarized anodically and CFRP is polarized cathodically. Aluminium alloys will become the anode of Aluminium/CFRP system and anodic corrosion will occur on aluminium alloys, while CFRP will become the cathode of the system, and reduction reaction will occur on CFRP. Therefore when aluminium coupled with CFRP, the predicted cathodic reactions are the reduction of hydrogen ion and/or reduction of water on carbon fibre surface and the predicted anodic reaction is the corrosion of aluminium.

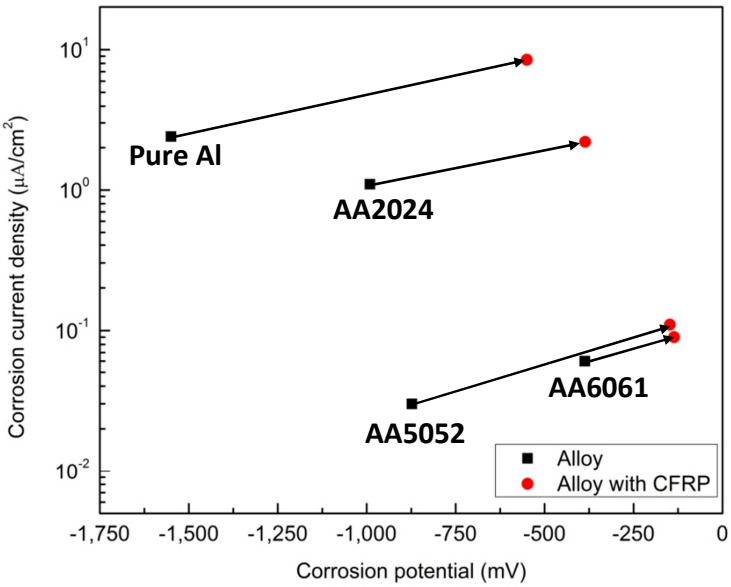

Figure 133: Shifting of corrosion potential and corrosion current density of Aluminium/CFRP systems in 0.001M NaCl.

The estimated corrosion potential and corrosion current density, which is the intersection of polarization curves of aluminium samples and CFRP, for the Aluminium/CFRP coupled systems in figure 133 and in table 24(appendix) show that:

a) For all aluminium alloys, corrosion potential of aluminium alloys shift to more noble potential when coupled with CFRP. This hints that the corrosion rate of aluminium alloys will increase when coupled with CFRP.
b) The corrosion current density of aluminium alloys will increase when coupled with CFRP, confirming the increase of corrosion rate of aluminium when coupled with CFRP.
c) The corrosion rates of aluminium alloys when coupled with CFRP ranging in order from the highest to the lowest are Pure Al, AA2024, AA5052 and AA6061. This indicated that pure aluminium will corrode much faster than other aluminium alloys when coupled with CFRP.
d) Intersections are in stable pitting region (Pure Al), in metastable pitting region (AA2024) and in passive region (AA5052 and AA6061).

For further analysis, 2 individual Evans diagrams for aluminium samples with CFRP are conducted. The individual Evans diagram of Pure Al with CFRP is plotted in figure 155 since it exhibits the highest corrosion rate in 0.001M NaCl solution.

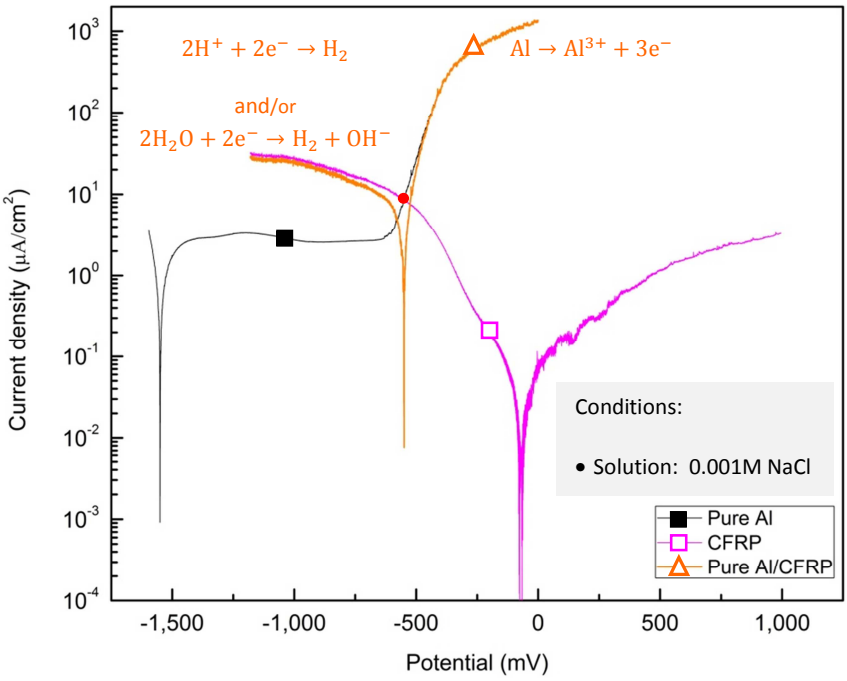

Figure 134: Evans diagram for pure aluminium with CFRP in 0.001M NaCl (pH7). * The orange line is the calculated polarization curve of Pure Al/CFRP system in 0.001M NaCl.

The Evans diagram for pure aluminium coupled with CFRP (same area ratio) in figure 134 and their corrosion parameters in table 24(appendix) shows that:

a) The corrosion potential of CFRP is much higher than that of pure aluminium in 0.001M NaCl solution. This implies that CFRP is much nobler than pure aluminium. Therefore pure aluminium tends to corrode faster when coupled with CFRP. Moreover the corrosion potential of pure aluminium will increase by 950mV when pure aluminium coupled with CFRP.

b) Anodic polarization curve of pure aluminium intersects the cathodic polarization curve of CFRP and the intersection point on polarization curve of pure aluminium is at the potential higher than the pitting potential. Therefore the predicted cathodic reaction of Pure Al/CFRP system are the reduction of hydrogen ions and/or reduction of water on the carbon fibre surface while the predicted anodic reaction is stable pitting corrosion of pure aluminium. Therefore it can be concluded that the corrosion behaviour of pure aluminium will change from passivation in the absence of CFRP to instant *stable pitting corrosion* when coupled with CFRP.

c) After coupled with CFRP, the corrosion current density of pure aluminium increases from 2.4 to 8.5µA/cm^2. This implies that when coupled with CFRP, pure aluminium will corrode 3.5 times faster than in the absence of CFRP.

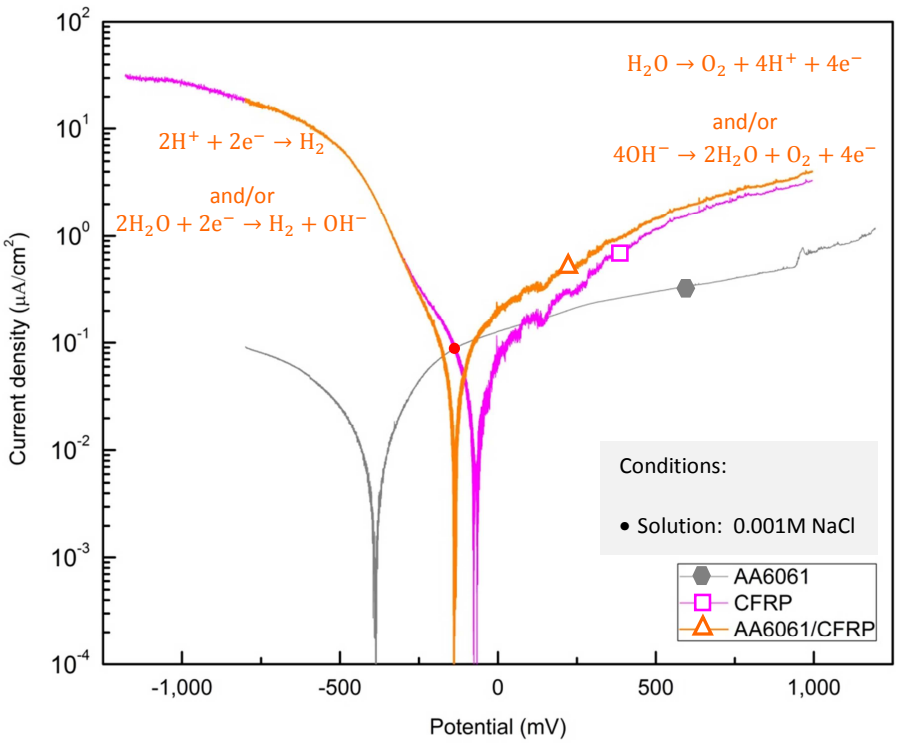

Figure 135: Evans diagram for AA6061 with CFRP in 0.001M NaCl. * The orange line is the calculated polarization curve of AA6061/CFRP in 0.001M NaCl.

Unlike the highest corrosion rate of pure Al/CFRP system, AA6061/CFRP system exhibited the lowest corrosion rate. Therefore the individual Evans diagram AA6061 with CFRP was also discussed. The Evans diagram for AA6061 with CFRP in figure 135 and their corrosion parameters in table 24(appendix) shows that:

a) The corrosion potential of CFRP is only slightly higher than that of AA6061, implying that the CFRP is also nobler than AA6061. Therefore, AA6061 tends to corrode faster when coupled with CFRP. In addition, the corrosion potential of AA6061 will increase only by 251mV when coupled with CFRP.
b) Anodic polarization curve of AA6061 intersects the cathodic polarization curve of CFRP and the intersection point on polarization curve of AA6061 is lower than the pitting potential. Therefore the predicted predominant cathodic reaction of AA6061/CFRP in

0.001M NaCl is the reduction of hydrogen ions and/or water on the carbon fibre, while the predominant anodic reaction is the passivation of aluminium alloy at low overpotentials and the oxidation of hydroxide ions and/or water at high overpotentials. It can be concluded that when coupled with CFRP in 0.001M NaCl, AA6061 will still exhibit *passive behaviour*, which is the same behaviour as AA6061 in the absence of CFRP.

c) When coupled with CFRP, the corrosion current density of AA6061 increases only from 0.06 to 0.09μA/cm^2. Therefore when coupled with CFRP, AA6061 will corrode only 1.5 times faster than in the absence of CFRP.

Comparing the calculated corrosion current densities, which are proportional to corrosion rates, of Aluminium/CFRP between pure aluminium and AA6061 shows that pure aluminium will corrode nearly 100 times faster than AA6061 when coupled with CFRP. In addition, when coupled with CFRP, AA2024 and AA5052 will still exhibits passive behaviour as in the absence of CFRP.

In 0.01M NaCl

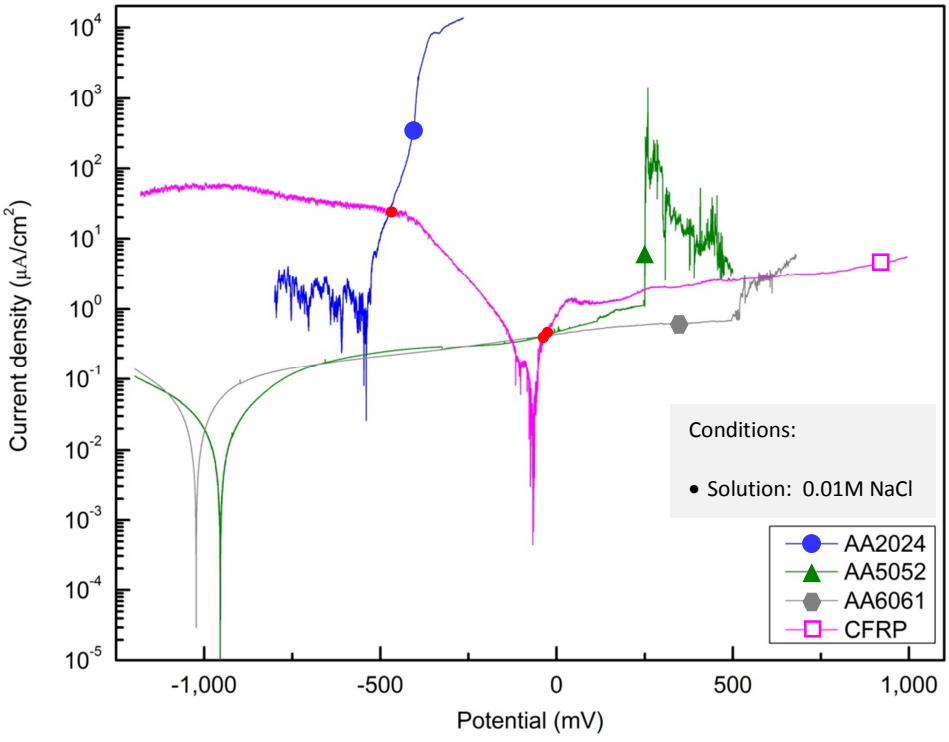

Figure 136: Evans diagrams for aluminium alloys with CFRP in deaerated 0.01M NaCl solution.

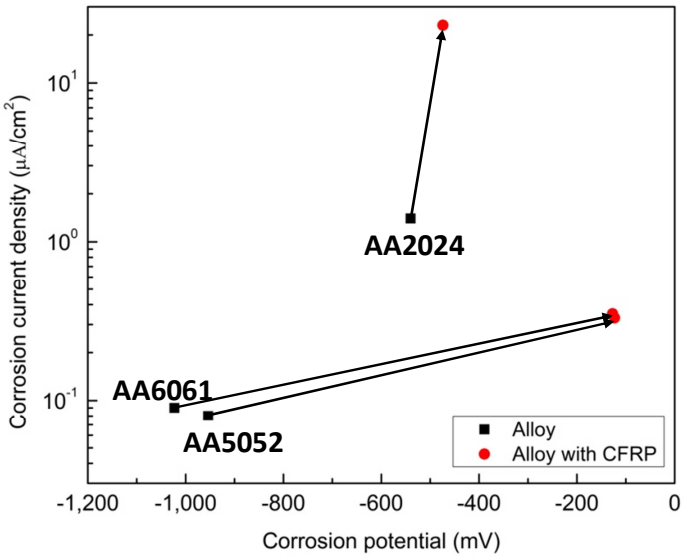

Figure 137: Shifting of corrosion potential and corrosion current density of Aluminium/CFRP systems in 0.01M NaCl.

The Evans diagrams in 0.01M NaCl in figure 136 and their corrosion parameters in table 24 (appendix) shows that:

a) The corrosion potential of CFRP is higher than that of all aluminium alloys, meaning that CFRP is more “noble” than all aluminium alloys. Therefore, aluminium alloys tend to corrode faster when coupled with CFRP in 0.01M NaCl.

b) When aluminium alloys coupled with CFRP in 0.01M NaCl solution, the corrosion potential of all aluminium alloys will shift to nobler potential and the corrosion current density will also increase (figure 137). This suggests the increase of corrosion rate of aluminium alloys when coupled with CFRP. The ranging of predicted corrosion rates of aluminium alloys when coupled with CFRP in order from the highest to the lowest are AA2024, AA6061 and AA5052. Moreover, AA2024 is corroded much faster than AA5052 and AA6061 when coupled with CFRP.

c) When coupled with CFRP, AA2024 is predicted to exhibit pitting corrosion at corrosion potential in 0.01M NaCl as is also the case in the absence of CFRP. The pitting corrosion rate of AA2024 coupled with CFRP is predicted to be about 16 times higher than that in the absence of CFRP. On the other hand when coupled with CFRP, AA5052 and AA6061 are predicted to still exhibit passive behaviour as in the absence of CFRP because the

stable pitting is not reached. The passivation rates of AA5052 and AA6061 when coupled with CFRP in 0.01M NaCl are predicted to be nearly 4 times higher than that in absence of CFRP.

In 0.1M NaCl solution

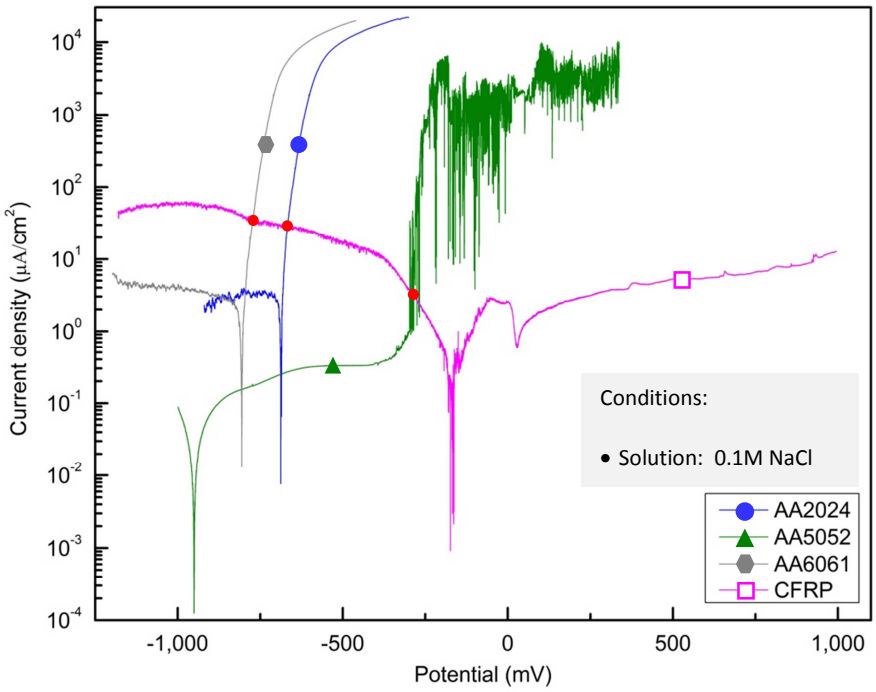

Figure 138: Evans diagrams for aluminium alloys with CFRP in deaerated 0.1M NaCl solution.

The Evans diagrams in 0.1M NaCl (figure 138) and their corrosion parameters in table 24 (appendix) shows that:

a) For all aluminium alloys, the corrosion potential of CFRP is higher than that of aluminium alloys, meaning that CFRP is more "noble" than aluminium alloy. Therefore, aluminium alloys tend to corrode faster when coupled with CFRP in 0.1M NaCl solution.

b) When aluminium alloy coupled with CFRP in 0.1M NaCl solution, the corrosion potential and corrosion current density of all aluminium alloys increase (figure 139), implying the increase of corrosion rate of aluminium alloys when coupled with CFRP. The predicted corrosion rate of aluminium alloys when coupled with CFRP ranging in order from the highest to the lowest are AA6061, AA2024 and AA5052. Moreover, AA6061 and AA2024

should corrode nearly 10 times faster than AA5052 when coupled with CFRP in 0.1M NaCl.

c) When coupled with CFRP in 0.1M NaCl, AA2024 and AA6061 are calculated to exhibit stable pitting corrosion even in the cathodic regime as is the case in absence of CFRP. The pitting corrosion rate of AA2024 and AA6061 when coupled with CFRP are predicted to be approximately 10 times higher than that in absence of CFRP.

d) When coupled with CFRP, AA5052 is predicted to instantly exhibit pitting corrosion instead of passive behaviour in the absence of CFRP. The corrosion rate of AA5052 is predicted to increases by 40 times when coupled with CFRP.

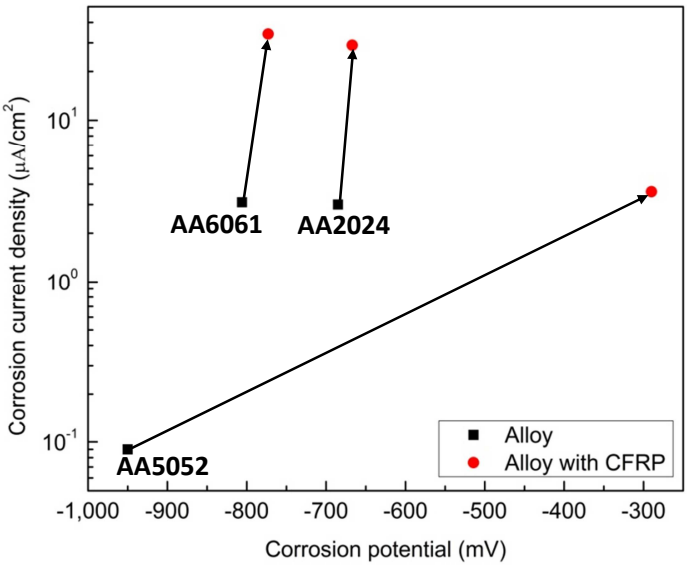

Figure 139: Shifting of corrosion potential and corrosion current density of Aluminium/CFRP systems in 0.1M NaCl.

Therefore it can be said that when coupled with CFRP in solution containing high chloride concentrations (0.1M NaCl), all 3 aluminium alloys will instantly exhibit pitting corrosion with a strong increase in stable pitting corrosion rate.

As the corrosion resistance is inverse proportional to corrosion rate (or corrosion current density), the predicted relative corrosion resistance of Aluminium/CFRP for each aluminium alloy is concluded in the table 24(appendix) and shown in figure 140. It can be seen that:

a) For all aluminium alloys, the corrosion resistance of aluminium alloys when coupled with CFRP decrease with increasing chloride ions in solution.

b) The corrosion resistance of aluminium alloys when coupled with CFRP also strongly depend on the type of aluminium alloy in use.

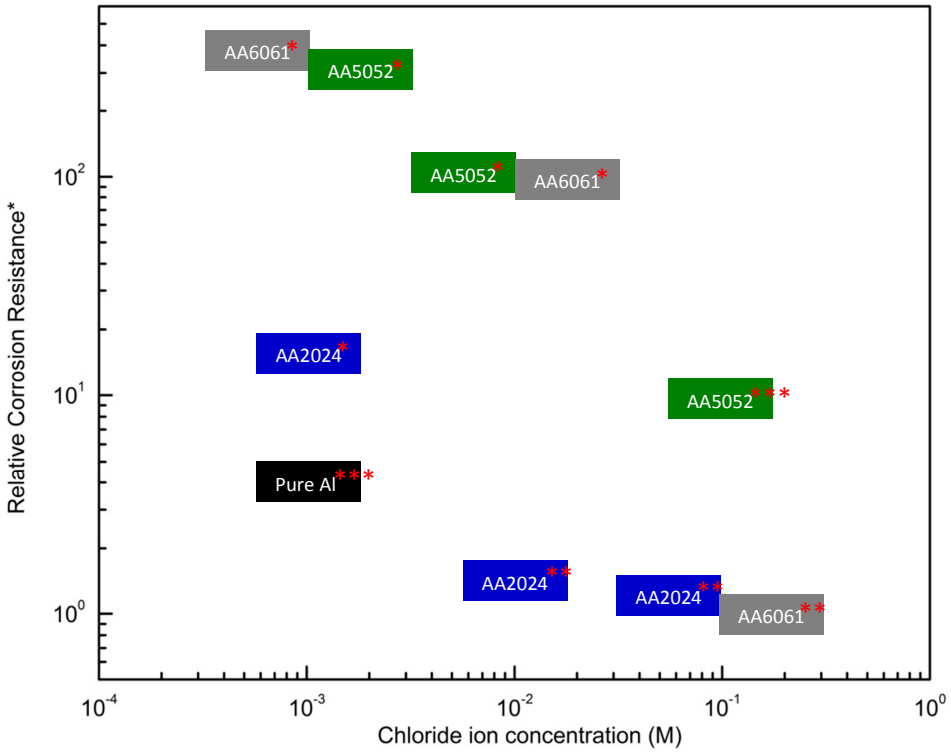

Figure 140: The predicted relative corrosion resistance of aluminium alloys when coupled with CFRP in NaCl solutions. The relative corrosion resistance is the corrosion resistance of each aluminium alloy relative to that of AA6061 when coupled with CFRP in 0.1M NaCl, which exhibited maximum corrosion rate. * represent the alloys which still exhibit passive behaviour, ** represent the alloys which still exhibit pitting behaviour with increasing rate and *** represent the alloy whose corrosion behaviour change from passive to pitting when coupled with CFRP.

This analysis shows that corrosion behaviour and corrosion rate of aluminium alloys when couple with CFRP strongly depend on type of aluminium and the solution in use.

2.32) Galvanic behaviour : Effect of surface area ratio

For this calculation, the effect of surface area ratio of CFRP to pure aluminium on corrosion behaviour of Pure Al/CFRP system is studied. Measured current of pure aluminium and CFRP with the same surface area ($4cm^2$) come from the former measurements. Then current of CFRP with different surface areas are calculated. Two surface area ratios of CFRP to pure aluminium (such as 5:1 and 1:7) are plotted on the Evans diagram. Please note, that due to different surface areas, the Evans diagram is plotted in the dimension of current instead of current density. This analysis controls the surface area of CFRP, not the surface area of carbon fibre which is the true cathode of galvanic coupling between pure aluminium and CFRP.

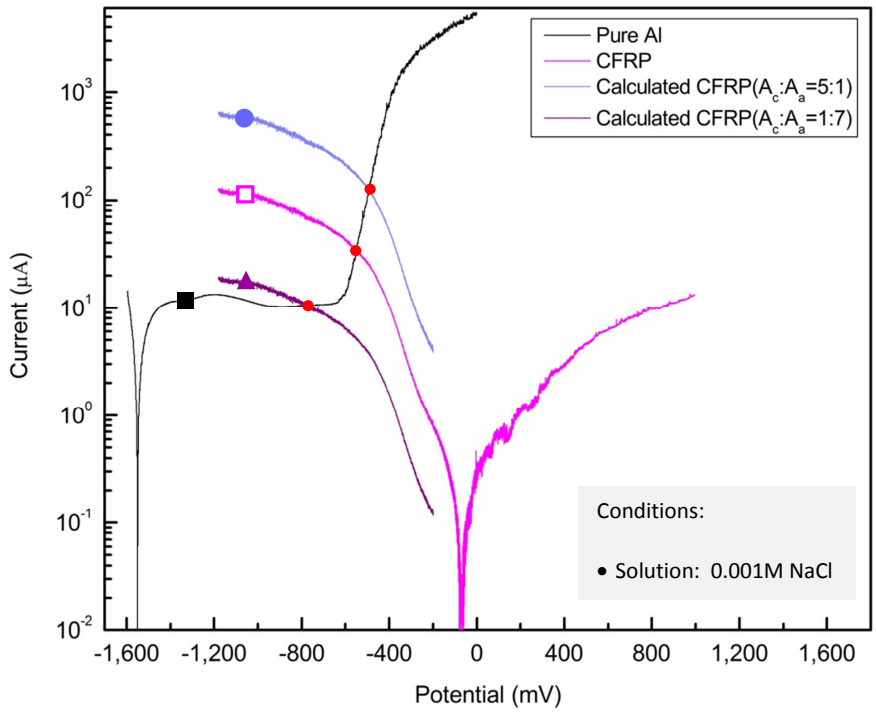

Figure 141: Evans diagram for pure aluminium with CFRP for different surface area in 0.001M NaCl solution.

The Evans diagram in figure 141 and their corrosion parameters in table 25(appendix) shows that:

a) With decreasing surface ratio of CFRP to pure aluminium from 1:1 to 1:7, the decrease of corrosion potential to potentials lower than stable pitting potential as well as the decrease of corrosion current is detected. This indicates that corrosion behaviour of

pure aluminium changes from pitting corrosion to passive behaviour with decreasing corrosion rate with this decreasing surface ratio.

b) With increase surface ratio of CFRP to pure aluminium from 1:1 to 5:1, corrosion potential and corrosion current increase. This indicates that the pure aluminium still exhibit stable pitting corrosion with increasing rate.

Therefore this calculation shows that the change of surface area ratio of CFRP to aluminium can lead to the change in corrosion rate and/or corrosion behaviour of aluminium.

2.33) Galvanic behaviour: Effect of solution's pH

For this measurement, polarization of pure aluminium and CFRP were conducted in chloride solutions with different pH (3, 7 and 11) in order to study the effect of pH's solution on corrosion behaviour of pure aluminium coupled with CFRP. All solutions contained the same concentration of 0.001M chloride ions, but pH of solutions was adjusted by HCl and NaOH.

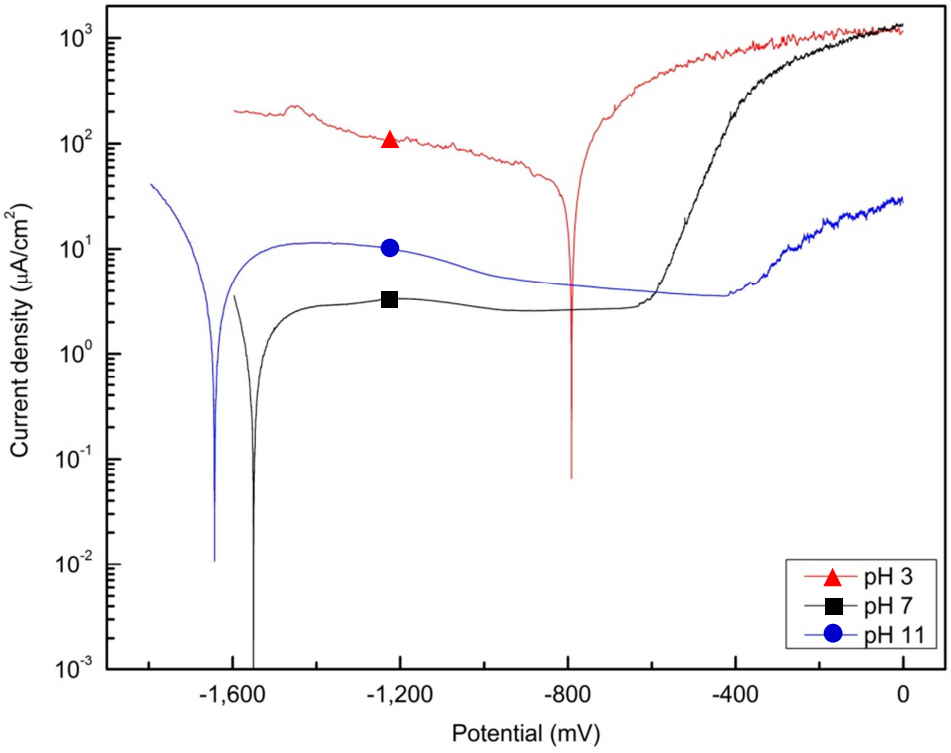

Figure 142: Polarization curves of pure aluminium in chloride solutions with different pH.

The polarization curves in figure 142 and their corrosion parameters in table 26(appendix) shows that:

a) In neutral chloride solution (pH 7) and basic chloride solution (pH 11), pure aluminium exhibits passive behaviour but in acidic chloride solution (pH 3), pure aluminium exhibits pitting corrosion at corrosion potential and even quite below.
b) Corrosion current density, which is proportional to corrosion rate, of pure aluminium in acidic and in basic chloride solution is much higher than that in neutral chloride solution. Therefore, pure aluminium corrodes more rapidly in both acidic and basic solution due to the enhanced solubility of aluminium oxide in these solutions [9]. The corrosion rates of pure aluminium in solution with different pH ranging from the highest to the lowest are pH 3, pH 11 and pH 7.
c) In acidic chloride solution (pH 3), the pitting potential of pure aluminium is lower than that in neutral chloride solution (pH 7) due to the formation of imperfect passive layer in acidic solution which results in the stable pitting corrosion at corrosion potential. On the other hand in basic chloride solution (pH 11), the pitting potential is higher than that in neutral solution due to the continuous chemical dissolution of passive oxide in this basic solution. The pitting potentials in solutions with different pH ranging from the lowest to the highest are pH 3, pH 7 and pH 11. This means pitting corrosion decreases with increasing pH of solution
d) The passive region range is smallest in acidic chloride solution and largest in basic chloride solution. This can be attributed to the type of charge on the surface. It was mentioned in [22] that in acidic chloride solution, the surface is probably positively charged while it is negatively charged in basic chloride solution. As Chloride ions are directly attached to the positively charged surface, small or no passive region can be detected in acidic chloride solutions. On the other side, protonated water can be adsorbed on the negatively charged surface in basic chloride solution so that passivation is favoured.

Therefore it can be deduced that pH of solution has a strong effect to the corrosion behaviour of pure aluminium.

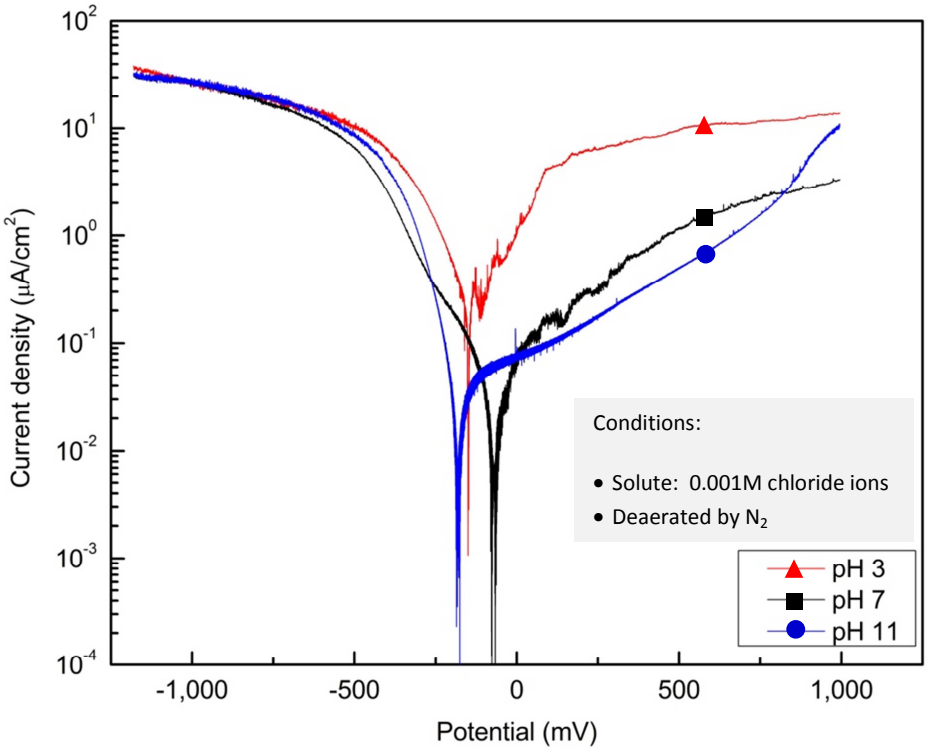

Figure 143: Polarization curves of CFRP in chloride solution with different pH.

The polarization curves of CFRP in figure 143 show that:

a) The pH of solution shows no significant effect on cathodic polarization curve of CFRP.

b) The pH of solution shows strong effect on anodic reaction of CFRP. The anodic current density of CFRP in acidic solution is nearly 10 times higher than that in basic and neutral chloride solution. It is predicted that anodic reaction of CFRP was the combination of oxidation of hydroxide ions and water. However in acidic chloride solution which contains less hydroxide ion, oxidation of hydroxide ion and water is not favoured. Oxidation of chloride ions ($2Cl^- + 2e^- \rightarrow Cl_2$) possibly takes place. This may cause an increase of anodic current density.

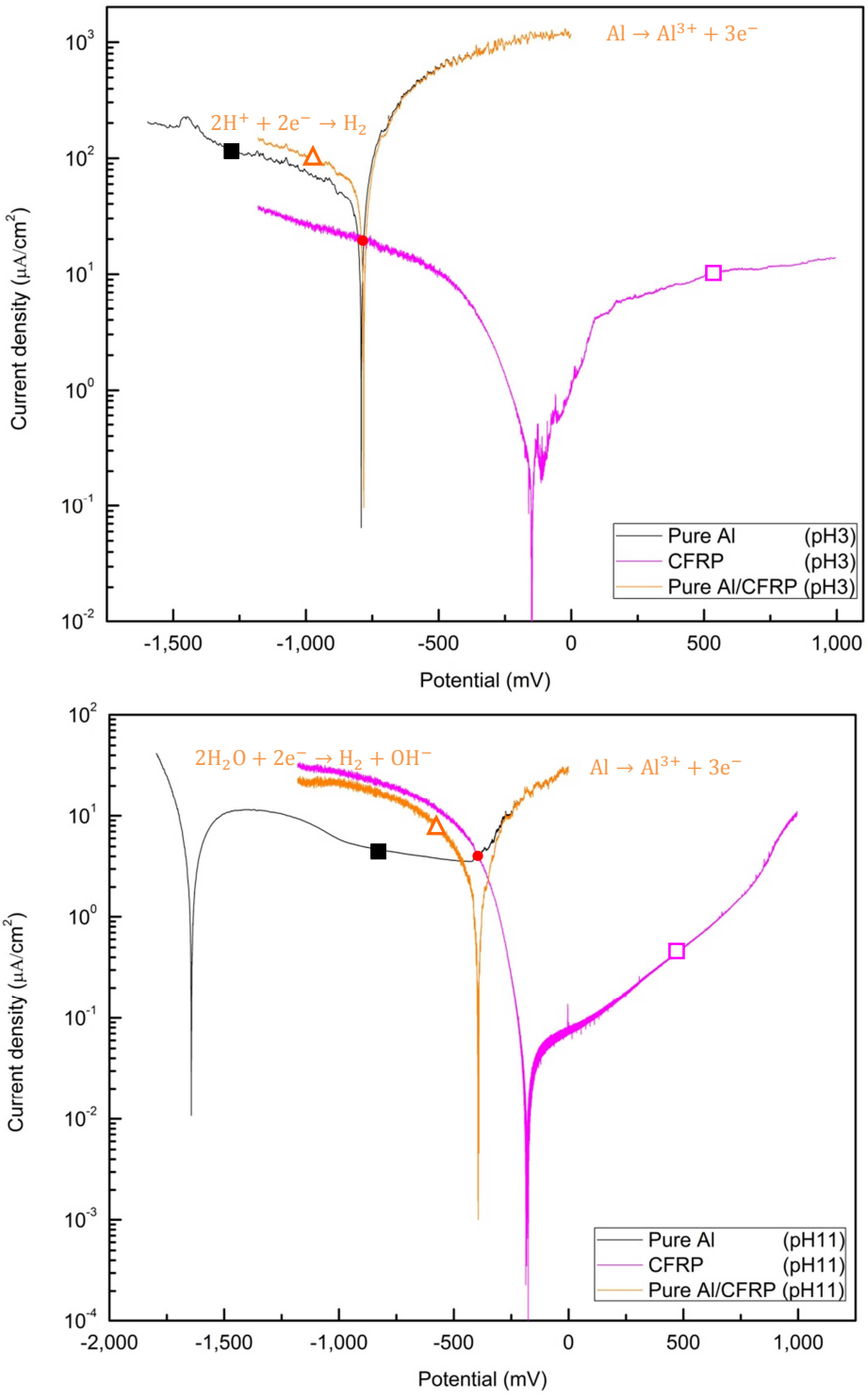

Figure 144: Evans diagram for pure aluminium with CFRP in chloride solution with (top) pH 3, and (bottom) pH 11. * The orange line is the calculated polarization curve of Pure Al/CFRP in the same solution.

The Evans diagrams for pure aluminium with CFRP in each pH solution are plotted in order to predict the effect of pH on corrosion behaviour of Pure Al/CFRP systems in chloride solution. The Evans diagram for pure aluminium with CFRP in solution with pH 3, 11 (figure 144) and pH 7 (figure 134) and their corrosion parameters in table 26(appendix) shows that:

a) For all pH solutions, corrosion potential of pure aluminium is much lower than that of CFRP. This hints that corrosion rate of pure aluminium will increase when coupled with CFRP in all solution.

b) In acidic chloride solution (pH 3), both cathodic and anodic current densities of pure aluminium are much higher than that of CFRP. Therefore the predicted polarization curves of the Pure Al/CFRP system is nearly the same as the polarization curve of pure aluminium in the absence of CFRP and the predicted anodic and cathodic reactions of Pure Al/CFRP system will take place preferentially only on pure aluminium. The predicted anodic reactions of the Pure Al/CFRP system are pitting corrosion at corrosion potential of aluminium, as in the absence of CFRP. The predicted cathodic reaction is the reduction of hydrogen ions also on pure aluminium surface. The predicted corrosion potential of pure aluminium when coupled with CFRP shifts by only 10mV to nobler value than that in the absence of CFRP. However, the calculated corrosion current density of pure aluminium astonishingly decreases from 50 to 19µA/cm^2 (see figure 145, left) when coupled with CFRP. Therefore it can be deduced that when coupled with CFRP, pure aluminium will still exhibit pitting corrosion at corrosion potential with a decreasing corrosion rate.

c) In basic chloride solution (pH11), the anodic polarization curve of pure aluminium intersects the cathodic polarization curve of CFRP and the intersection point on polarization curve of pure aluminium is at a potential higher than the pitting potential. Therefore the predicted anodic reaction of Pure Al/CFRP system is stable pitting corrosion of pure aluminium and the predicted cathodic reaction is reduction of water. The corrosion potential of pure aluminium when coupled with CFRP is calculated to increase by more than 1,000mV and its corrosion current density is calculated to slightly increase from 3.5 to 4.0µA/cm^2 (see figure 145, left). It can be deducted that the corrosion behaviour of pure aluminium will change from passive behaviour in the absence of CFRP to stable pitting corrosion when coupled with CFRP

d) Comparing the calculated corrosion current densities of Pure Al/CFRP in different pH solutions show that corrosion rate in chloride solution with different pH ranging from the highest to the lowest are pH 3, pH 7and pH 11. Therefore it can be deduced that alkalisation of solution to weak basic solution will improve the corrosion resistance of pure aluminium when coupled with CFRP, whereas the acidification of solution to strong acid solution will degrade the corrosion resistance of pure aluminium when coupled with CFRP (figure 145, right).

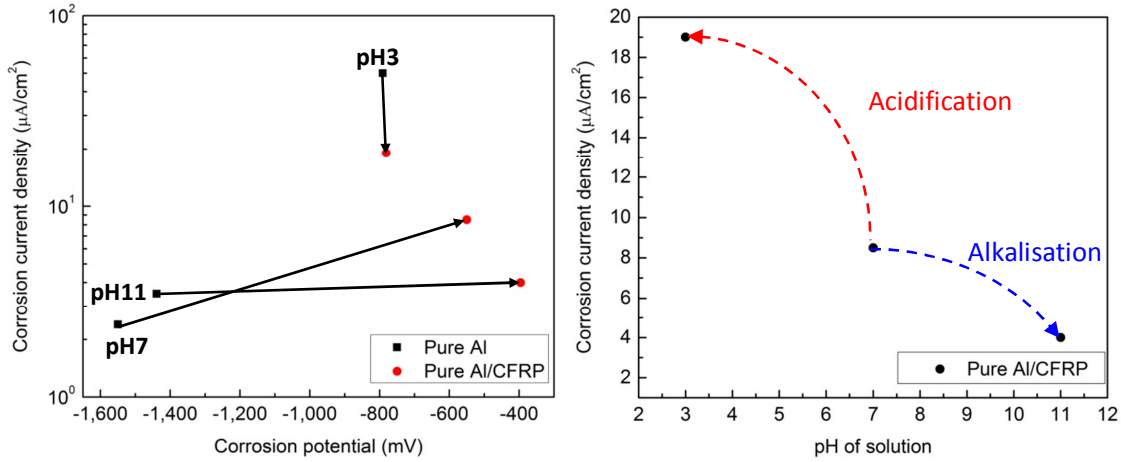

Figure 145: (Left) corrosion potentials and corrosion current densities of pure aluminium before and after coupled with CFRP in solution with different pH and (right) predicted corrosion current density of Pure Al/CFRP as a function of pH.

This measurement shows that pure aluminium is predicted to exhibit pitting corrosion instantly when coupled with CFRP in chloride solution with all pH (3, 7 or 11) for surface area ratio of 1.

3. Surface Analysis

3.1) Surface Morphology of Aluminium/CFRP adhesive joints after long time immersion

For this measurement, Aluminium/CFRP adhesive joints were fabricated by hand laying 2 layers of unidirectional carbon fibre/epoxy prepregs on both sides of aluminium alloys (Pure Al, AA2024, AA5052 and AA6061). Prior to the laying of the prepregs, the surface of aluminium sample was prepared by polishing with SiC paper using tap water as a lubricant to roughen the surface, followed by plenty of deionised water washing. Only half of the whole length of aluminium alloy was adhered with the prepreg sheets and the other half was unmodified. The orientation angle of the assembly was stacked to $[0_2/\mathrm{Al}/0_2]$. After that, the assembly was cured in heating press at 130°C for 90min. The structure of the joint was shown in the figure 146 (left and middle). After fabrication, all Aluminium/CFRP adhesive joints were completely immersed in neutral solution of 0.001M NaCl at room temperature. After 8 months of immersion, Aluminium/CFRP adhesive joints were removed from the solution. One side of CFRP was peeled off the aluminium surface and then all samples were rinsed with water, cleaned in ultrasonic bath and finally dried in an air flow. After that the surfaces of aluminium alloys were examined using a digital microscope. In order to study the effect galvanic corrosion between CFRP and aluminium samples of the Aluminium/CFRP adhesive joints, the aluminium surface area was separated into 4 main areas as can be seen from the red dashed line in figure 146(right).

Figure 146: Structure of Aluminium/CFRP adhesive joints: (left and middle) side and top views for immersion test and (right) for digital microscope after peel off one side of CFRP.

It can be seen from the image of Aluminium/CFRP adhesive joints in figure 147 that:

a) The distinct coloration is appeared and corrosion is evident on the surface of all aluminium alloys.

b) Aluminium alloys, especially AA2024, show more serious damage than pure aluminium. The more serious galvanic corrosion on aluminium alloys compared with pure

aluminium can be attributed to the formation of non-uniformed, thin and non-coherent oxide film on surface of aluminium alloys [58]. Therefore only a certain level of protection is reached on surface of aluminium alloys. The surface damages of aluminium component of Aluminium/CFRP adhesive joints ranging from the most to the least are AA2024, AA6061, AA5052 and Pure Al

Figure 147: Image of peeled off-Aluminium/CFRP adhesive joints after long immersion in 0.001M NaCl.

c) For all aluminium alloys, the surface of aluminium alloy under CFRP corroded much more intensively than the free surface of aluminium alloy. This reveals the expected galvanic coupling effect between aluminium alloys and CFRP, possibly combined with crevice corrosion.

d) For Pure Al, surface area 4 seems to be the most damaged one, revealing the galvanic coupling effect between CFRP and Pure Al. However, surface area 3 is astonishingly

intact, posibly due to a non-contact of electrolyte between CFRP and Pure Al. Therefore no kind of corrosion can take place between CFRP and Pure Al in this area.

e) For AA5052 and AA6061, the whole surface of aluminium alloy corrode. The surface area 3 and 4 are more damaged than the surface area 1 and 2. This may due to the surface area 3 and 4 has direct contact to CFRP during immersion. This reveals the effect of galvanic coupling between CFRP and AA5052, or AA6061.

f) For AA2024, the sample shows the strongest damage compared with all the aluminium alloys. On the surface area 3 and 4, seriously pitting corrosion is found with a green powdery substance formed at the interface between AA2024 and CFRP. The surface area 2 shows much less pitting corrosion. However, the surface area 1 does not show any pitting corrosion. This reveals the strong effect of galvanic coupling between CFRP and AA2024.

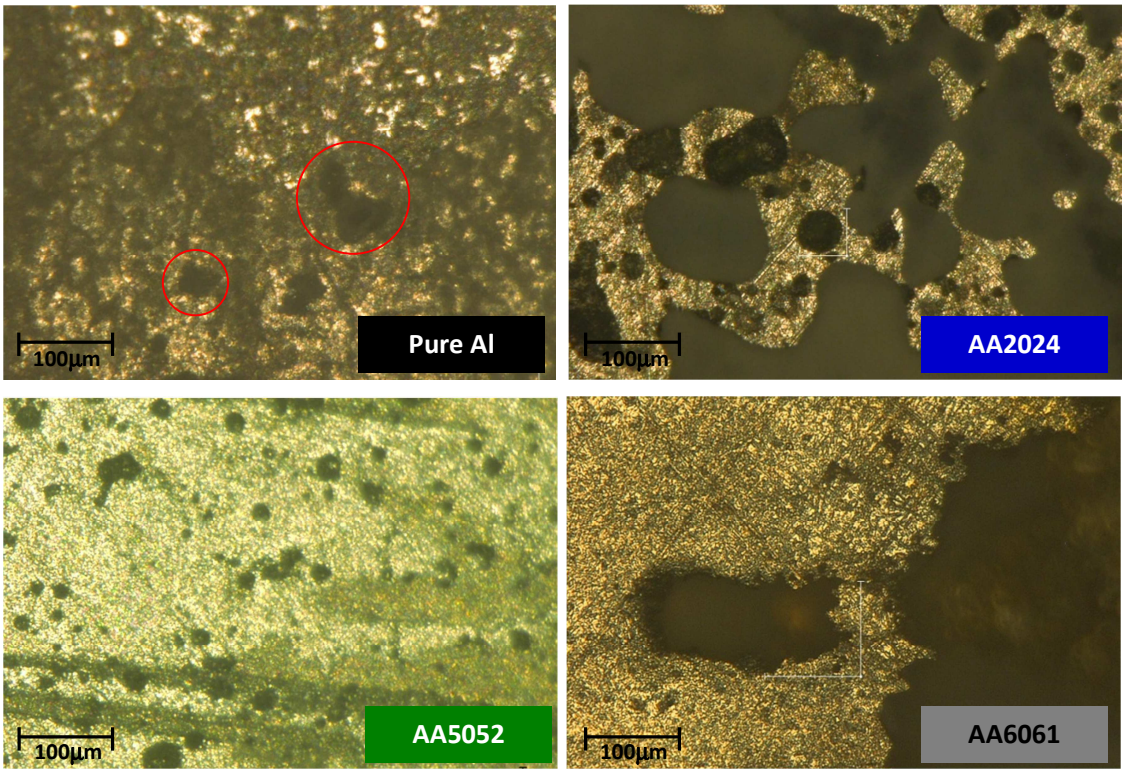

Figure 148: The surface morphology of aluminium alloys after long immersion of Aluminium/CFRP adhesive joints in 0.001M NaCl solution.

The surface morphology images in figure 148 shows that many pitting sites are detected on the surface of all aluminium alloys. Therefore it can be said that after immersion in NaCl solution, all Aluminium/CFRP adhesive joints are seriously suffered from pitting corrosion. On surface of Pure Al, AA2024 and AA5052, the numerous pits with relative small sizes in the range of 10 - 100µm are observed while on the surface of AA6061, few pits of dramatic largeness, which are possibly the overlapping of many smaller pits, are observed.

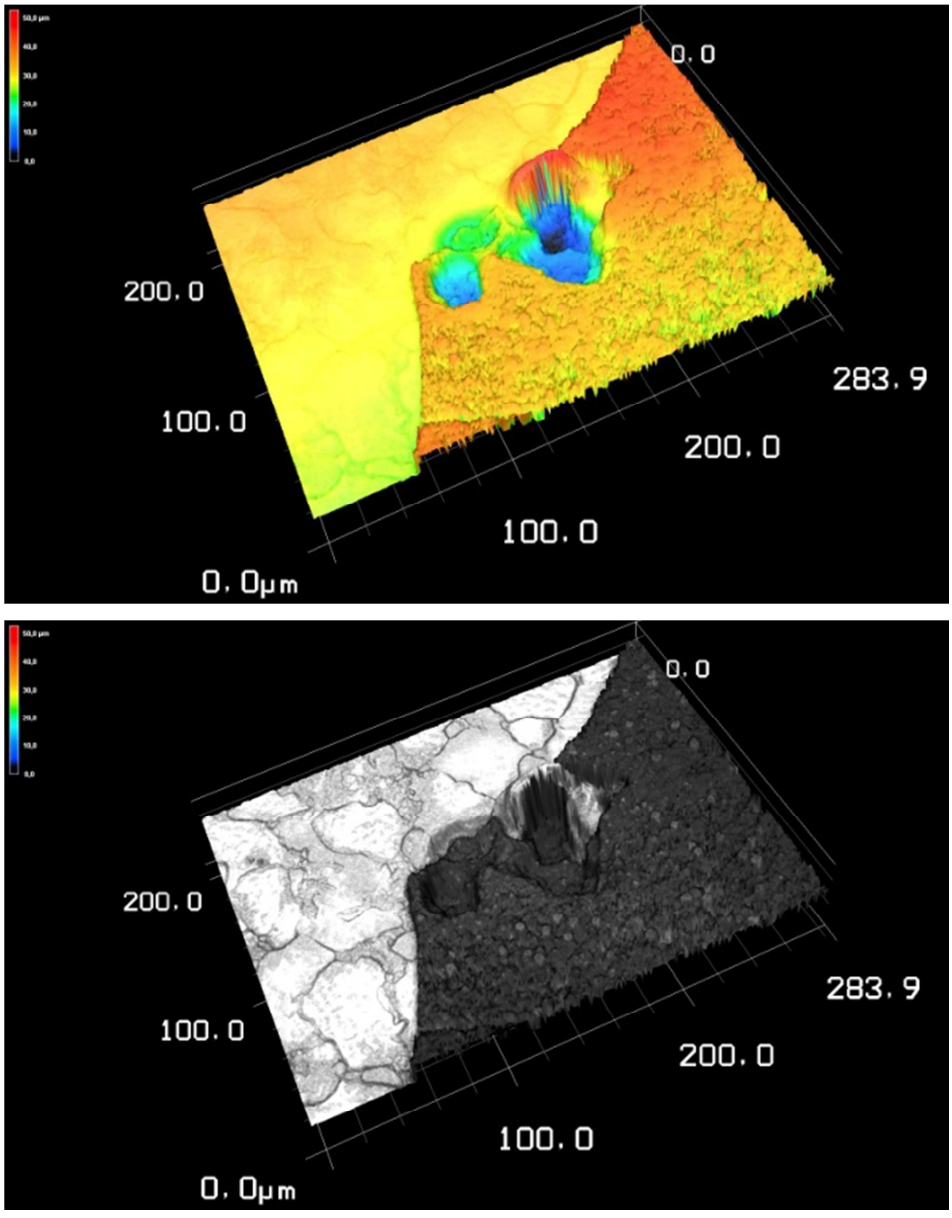

Figure 149: 3-D images of pure aluminium surface: (top) depth profile and (bottom) reflection colure.

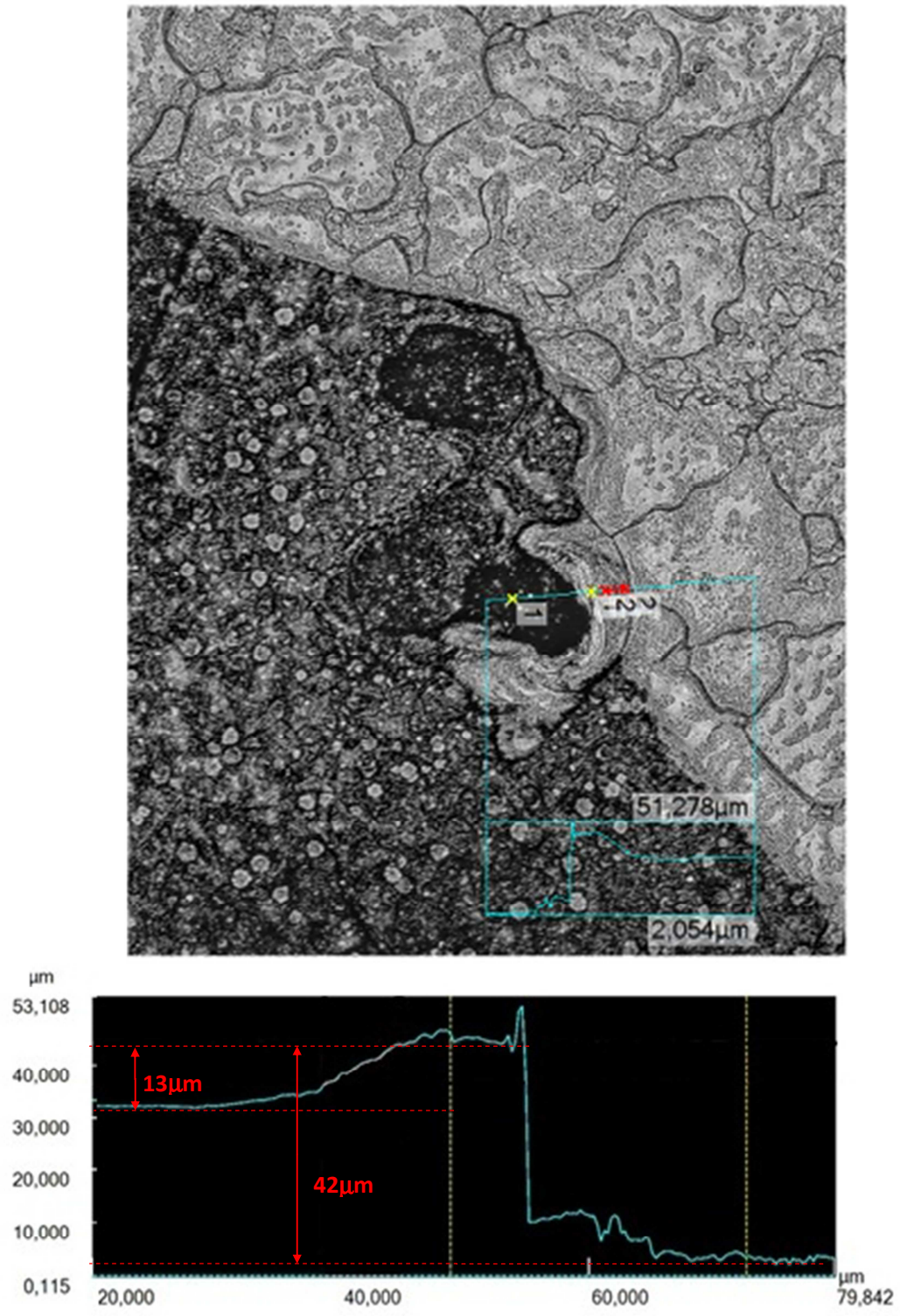

Figure 150: (Top) top view image with of small area of pure aluminium surface in the vicinity of pits and (bottom) pit depth analysis on pure aluminium surface.

The digital microscopic images are often blurred since the corrosion products, such as aluminium hydroxide film, hinders the light get onto the surface of aluminium alloys. Therefore the laser scanning microscopy was applied for better surface images. Moreover, it also can be used to analyse the depth profile of pits.

The surface morphology of peeled off-Pure Al/CFRP adhesive joint (area 1 or 2) from laser scanning microscope in figure 149-150 show that:

a) The 3-D surface images in figure 149 show that after immersion in 0.001M NaCl for 8 months, pits are initiated on the surface of pure aluminium. The surface area in the vicinity of pits is covered with corrosion product (height in the depth profile image and black area in reflection colour image). Moreover, there is a pits-free surface area (lower thickness in the depth profile image and white area in reflection colour image) that has no corrosion product covering over it.

b) Pit depth analysis in figure 150 shows that the depth of the pit is about 42µm and the film thickness of corrosion product in the vicinity of the pit's opening is about 13µm.

This measurement shows that when Aluminium/CFRP adhesive joints immersed in NaCl solution for long time, all aluminium alloys undergo galvanic corrosion between aluminium alloy and CFRP and pitting corrosion can take place on the surface.

CHAPTER **V**

DISCUSSION

The corrosion behaviour of aluminium was already studied separately by means of EN, OCP, polarization measurement and surface analysis. In this chapter, the correlations of the corrosion behaviour of aluminium from different measurement techniques are discussed.

1. The correlation between EN and polarization measurements for corrosion characterization of pure aluminium in tap water and in NaCl solution

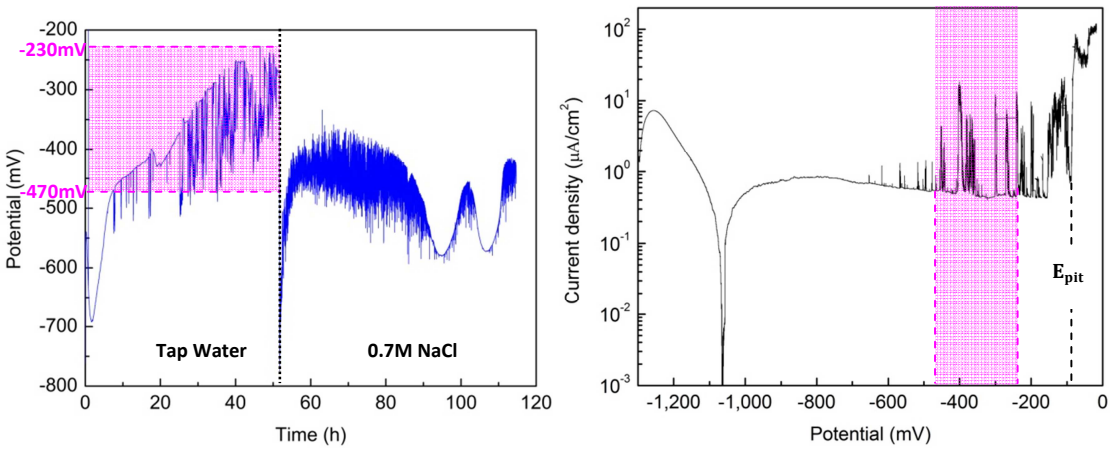

Figure 151: (Left) EN potential signal of pure aluminium in tap water, and (right) polarization curve of pure aluminium in tap water.

Potential signal from EN measurement 1.2 (figure 151, left) exhibits that passive oxide film is formed on pure aluminium in tap water at the beginning and then pitting corrosion is observed in the potential range between -470 and -230mV. When compared this potential range with polarization curve of pure aluminium in tap water from measurement 2.2, it can be seen that this potential range is lower than pitting potential of -88mV (figure 151, right). This means stable pitting corrosion cannot occur on pure aluminium in tap water, however metastable pitting corrosion can be detected on polarization curve in this potential range. Therefore the polarization curve confirms that pitting corrosion can occur on pure aluminium when immersed

in tap water and this pitting corrosion is identified as *metastable pitting corrosion*. This can also be identified by an extremely low frequency of EN signal in tap water.

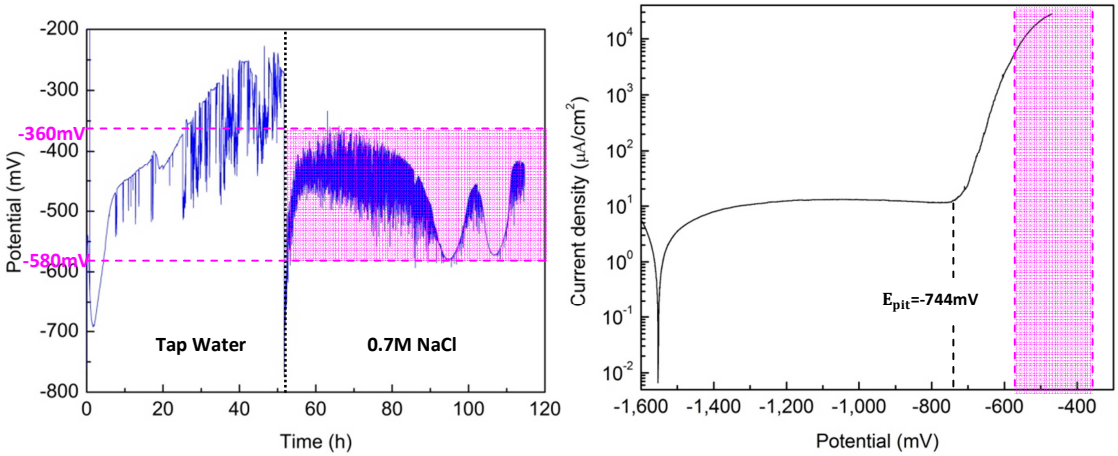

Figure 152: (Left) EN potential signal of pure aluminium in 0.7M NaCl and (right) polarization curve of pure aluminium in 0.2M NaCl.

Potential signal from EN measurement 1.2 (figure 152, left) also exhibits that pure aluminium in 0.7M NaCl solution is seriously attacked by pitting corrosion in the potential range between -580 and -360mV. Comparing this potential range with the polarization curve of pure aluminium in 0.2M NaCl solution from measurement 2.12 (figure 152, right) shows, that this potential range is higher than pitting potential of -744mV, implying that stable pitting corrosion can attack pure aluminium surface in this potential range. Even the concentration of NaCl solution used for polarization measurement is lower than that used for electrochemical noise measurement, the predicted pitting potential in 0.7M NaCl solution should be lower than that of 0.2M NaCl (-744mV) since in measurement 2.12, pitting potential is found to decrease with increasing concentration of NaCl in solution. Therefore the polarization curve confirms that when immerse in 0.7M NaCl solution, pure aluminium can be seriously attacked by *stable pitting corrosion*. This can also be identified by a higher frequency of EN signal in NaCl solution.

The correlation between EN and polarization measurements shows, that in tap water, pure aluminium undertakes metastable pitting corrosion while in solution containing high NaCl concentration of 0.7M, pure aluminium is attacked by stable pitting corrosion. The change of corrosion behaviour from metastable pitting corrosion in tap water to serious stable pitting corrosion in 0.7M NaCl solution can be attributed to the hindrance of self-healing processes or repassivation by high concentration of chloride ions in this NaCl solution. Therefore most of the pits continue to grow after they are initiated.

2. The correlation between EN and polarization measurements for corrosion characterization of aluminium alloy in NaCl solution

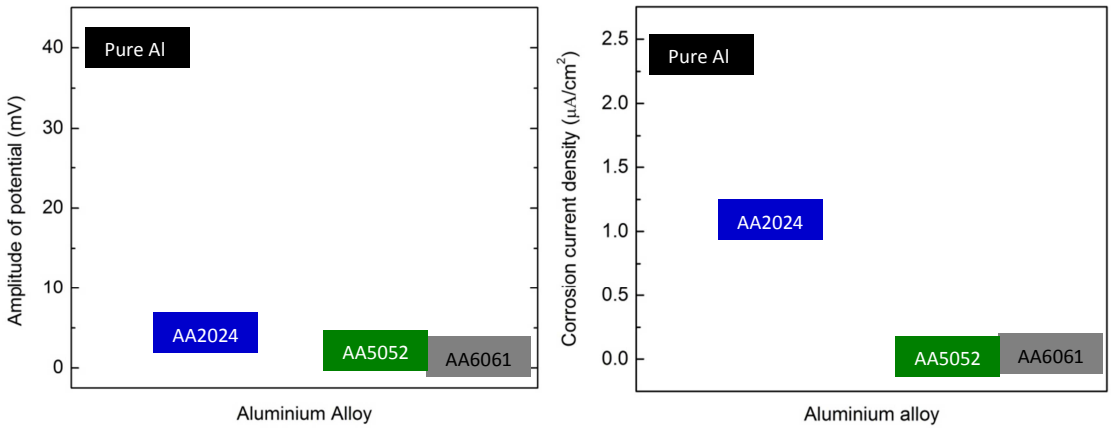

Figure 153: (Left) EN potential noise amplitude of aluminium alloys in 0.5M NaCl solution and (right) corrosion current density from polarization curve of aluminium alloys in 0.001M NaCl solution.

The electrochemical noise signal from measurement 1.7 (figure 153, left) shows that the potential fluctuation's amplitude of aluminium alloys in deaerated 0.5M NaCl solution ranging from the largest to the smallest are Pure Al, AA2024 and AA5052 and AA6061. This is also consistent with the surface damage of aluminium samples after EN measurement examined under digital microscope (measurement 1.7). While the polarization curves of pure aluminium and aluminium alloys in deaerated 0.001M NaCl solution from measurement 2.29 (figure 153, right) show, that the corrosion current density, which is direct proportional to the corrosion rate, ranging from the highest to the lowest are Pure Al, AA2024, AA6061 and AA5052. The order of the amplitude of potential fluctuation from EN measurement is nearly similar to that of corrosion rate from polarization measurement. Thus it can be deduced, that the amplitude of potential from EN measurement is direct relation to the corrosion rate from polarization measurement.

The correlation between EN and polarization measurement shows that the amplitude of potential fluctuation from EN measurement observed from one working electrode set-up can be a useful parameter to compare the corrosion rates of different metals.

3. The correlation between OCP and polarization measurements for corrosion characterization of pure aluminium when coupled with CFRP

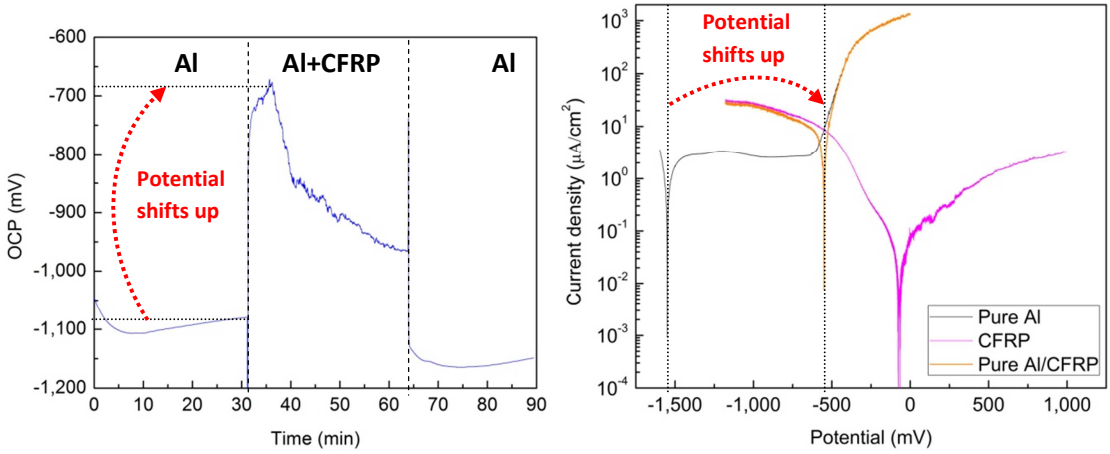

Figure 154: (Left) OCP of pure aluminium when coupled with CFRP in 0.05M NaCl and (right) Evans diagram for pure aluminium with CFRP in 0.001M NaCl.

The OCP curve from measurement 2.1 (figure 154, left) shows that OCP of pure aluminium when coupled with CFRP in 0.05M NaCl shifts up with strong fluctuating and the corrosion behaviour of pure aluminium changes from passive behaviour in the absence of CFRP to pitting corrosion when coupled with CFRP. This observed corrosion behaviour from OCP measurement is consistent with the predicted corrosion behaviour from the Evans diagram from polarization measurement 2.31 (figure 154, right) that when pure aluminium coupled with CFRP in 0.001M NaCl, corrosion potential of pure aluminium will shift up to potentials slightly higher than pitting potential of pure aluminium so that stable pitting corrosion will take place on pure aluminium surface.

Therefore, the correlation between OCP and polarization measurement confirms that when coupled with CFRP in NaCl solution, potential of pure aluminium shifts to higher values and pitting corrosion instantly attacks the surface of pure aluminium.

4. The correlation between EN and polarization measurements for corrosion characterization of pure aluminium when coupled with graphite or CFRP in NaCl solution

The potential and current signals of pure aluminium wire when coupled with graphite in 0.001M NaCl from the EN measurement 1.11 (figure 155, left) show that the predominant corrosion behaviour of pure aluminium changes from modification of passive oxide film to pitting corrosion when coupled with graphite. The Evans diagram for pure aluminium with CFRP

from polarization measurement 2.31 (figure 155, right) predicts that corrosion behaviour of pure aluminium changes from passivation in the absence of CFRP to pitting corrosion when coupled with CFRP. Since modification of passive oxide film cannot be detected by polarization measurement and passivation may also occur with relative lower rate, it can be deduced that the observed corrosion behaviour from EN measurement is consistent with predicted corrosion behaviour from polarization measurement. That means, when coupled with CFRP or graphite, corrosion behaviour of pure aluminium changes from passive behaviour of the oxide film to pitting corrosion.

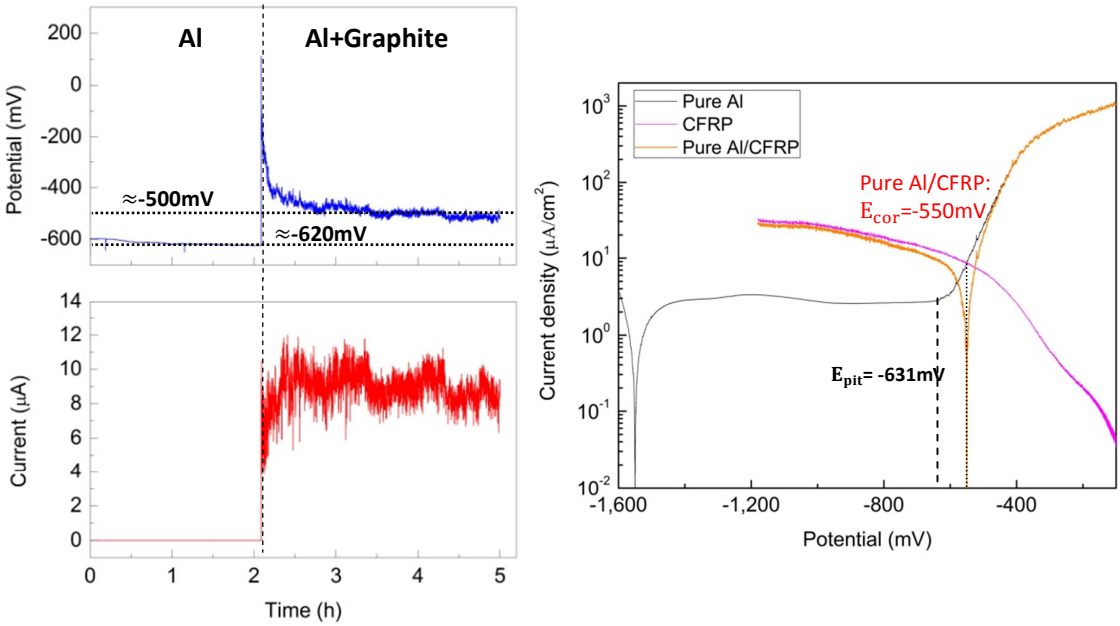

Figure 155: (Left) potential and current signals of pure aluminium wire when coupled with graphite in 0.001M NaCl and (right) Evans diagram for pure aluminium with CFRP in 0.001M NaCl.

Moreover, the EN measurement also exhibits, that, when coupled with graphite, potential of pure aluminium increases from -620mV to -500mV (figure 155, left), so that pitting potential of pure aluminium should be located between -620 to -500mV. The Evans diagram (figure 155, right) shows, that the calculated corrosion potential of pure aluminium when coupled with CFRP is about -550mV and pitting potential of pure aluminium is -631mV. The only slight differences of the absolute values when coupled with CFRP from EN and polarization measurement can be attributed to the difference in surface preparation and difference in surface area ratio of coupled materials. For EN measurement, pure aluminium wire was used as received so that pure

aluminium started with *passive surface*. Whereas for polarization measurement, the surface was polished with SiC paper and activation process by constant cathodic polarization was applied so that pure aluminium started with *active surface*. Therefore it can be deduced that the corrosion information from EN and polarization measurement are in a good agreement.

The correlation between electrochemical noise and polarization measurement confirms, that when pure aluminium coupled with CFRP or graphite, pitting corrosion can attack pure aluminium surface.

5. The correlation between EN and polarization measurements for analysis of the effect of surface area ratio of pure aluminium to graphite or CFRP on corrosion rate of pure aluminium when coupled with graphite or CFRP in NaCl solution

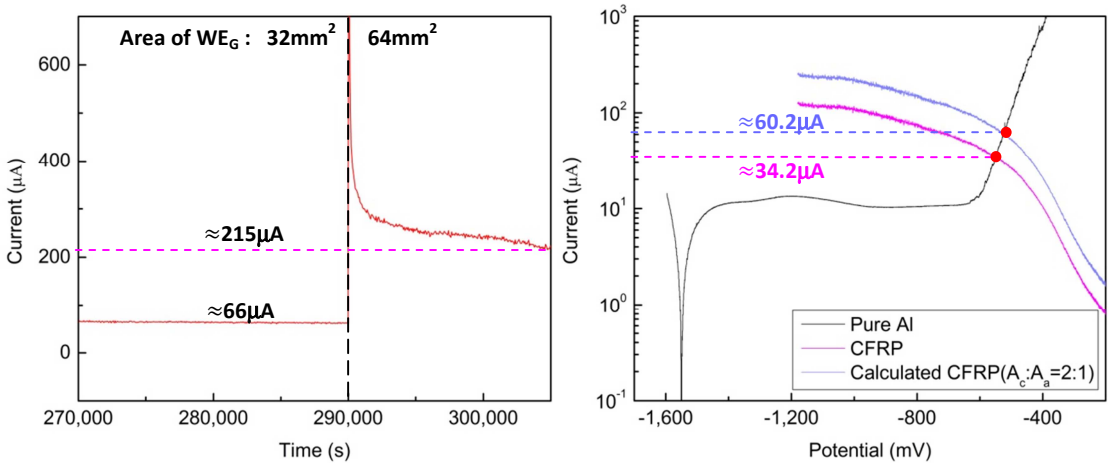

Figure 156: (Left) current signal of pure aluminium when coupled with graphite in 1M NaCl with increasing surface area of graphite and (right) Evans diagram of pure aluminium and CFRP for different surface area ratio in 0.001M NaCl.

The current signal of pure aluminium, when coupled with graphite in 1M NaCl (figure 156, left) from electrochemical noise measurement 1.12, shows that, when the surface area ratio of graphite to pure aluminium increases, pitting corrosion of pure aluminium is detected with higher corrosion rate. This is confirms by the calculation from the Evans diagram of pure aluminium with CFRP in 0.001M NaCl of polarization measurement 2.32 (figure 156, right), that the pitting corrosion is predicted to still occur on pure aluminium surface with higher corrosion rate. From Evans diagram, corrosion rate increases 1.8 times. This is only slightly different from the increase of corrosion rate (3.2 times) from EN measurement. It is mentioned that when pure aluminium coupled with graphite or CFRP, aluminium acts as anode and graphite or carbon fibre

of CFRP acts as cathode. The increase of current with increasing surface ratio of cathode to anode can be attributed to the increasing surface area of cathode for cathodic reaction to take place. With larger surface area of cathode, the electrons produced by anodic reaction can be consumed faster, possibly resulting in the increase of the rate of anodic reaction which is the corrosion of aluminium. Thus the current flowing between anode and cathode increases. Therefore it can be deduced [61] that the galvanic corrosion of pure aluminium when coupled with CFRP (or graphite) is controlled by cathodic reaction on the carbon fibre (or graphite).

The correlation between EN and polarization measurement confirms that for Pure Al/CFRP system (or Pure Al/Graphite system), the corrosion rate of pure aluminium increases with increasing surface area of CFRP (or graphite).

6. The correlation between polarization measurement and surface analysis for corrosion characterization of Aluminium/CFRP joint

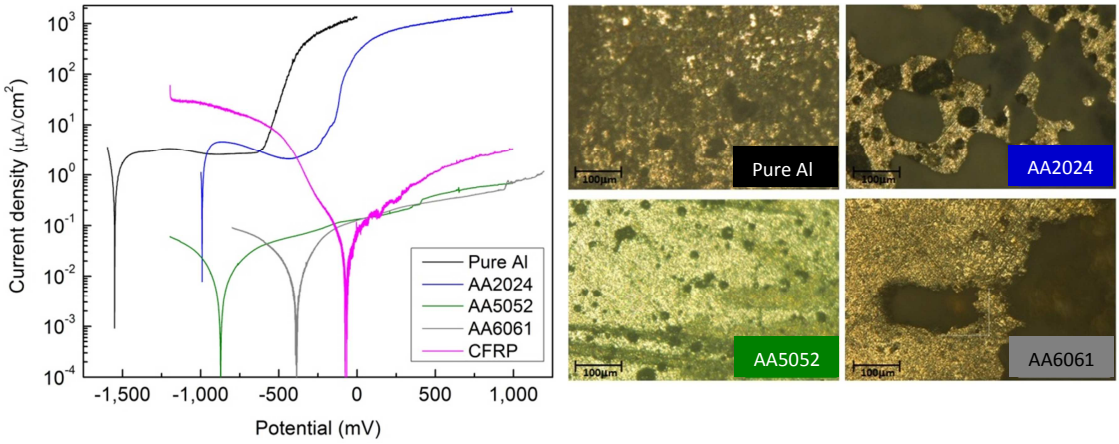

Figure 157: (Left) Evans diagram for aluminium alloys with CFRP in 0.001M NaCl and (right) surface morphology of aluminium surface after long immersion of aluminium/CFRP in 0.001M NaCl solution

The Evans diagrams for aluminium alloys with CFRP in deaerated 0.001M NaCl solution in figure 157(left) from polarization measurement 2.31 predicts that pure aluminium will exhibit pitting corrosion while aluminium alloys (AA2024, AA5052 and AA6061) will exhibit passive behaviour when coupled with CFRP. However, the surface morphology analysis of Aluminium/CFRP joints after long term immersion in 0.001M NaCl solution in figure 157(right) from surface analysis 3.1 exhibits that it is not only pure aluminium that is attacked by pitting corrosion but also all aluminium alloys. This may be attributed to the presence of intermetallic

particles in aluminium alloys. The intermetallic particles and their vicinal matrix will form micro-galvanic corrosion cells and these micro-galvanic corrosion cells accelerate the formation of *alkaline pits*. This type of pitting corrosion can occur at the potential below pitting potential and cannot be observed on the polarization curves [30]. Additionally, crevice corrosion also possibly takes place.

Therefore the correlation between polarization measurement and surface analysis shows that the alkaline pitting corrosion can take place on aluminium alloys but it cannot be observed by polarization measurement.

7. The correlation between polarization and surface analysis of Aluminium/CFRP joints

Figure 158: (Left) predicted corrosion current density of aluminium/CFRP in 0.001M NaCl, (right) Image of peeled off-aluminium/CFRP sample after immersion in 0.001M NaCl for 8 months.

The predicted corrosion current density of Aluminium/CFRP in NaCl solution (figure 158, left) from polarization mesurement 2.31 shows, that predicted corrosion rates of aluminium alloys when coupled with CFRP ranging from the highest to lowest are Pure Al, AA2024, AA5052 and AA6061. This contradicts the image of Aluminium/CFRP adhesive joints after immersion in NaCl for 8 months (figure 158, right) from surface analysis 3.1, that the surface damage of aluminium alloys ranges from the highest to the lowest are AA2024, AA6061, AA5052 and Pure Al. It can be seen, that the polarization measurement predicted that pure aluminium showed higher corrosion rate than all aluminium alloys, while surface analysis of the Aluminium/CFRP joint after long term immersion in NaCl solution reveals less surface damage of pure aluminium compared with all other aluminium alloys when coupled with CFRP. This can be attibuted to the

improvement of self-passivation (passive) behaviour of pure aluminium as already mentioned in anodic polarization measurement 2.26.

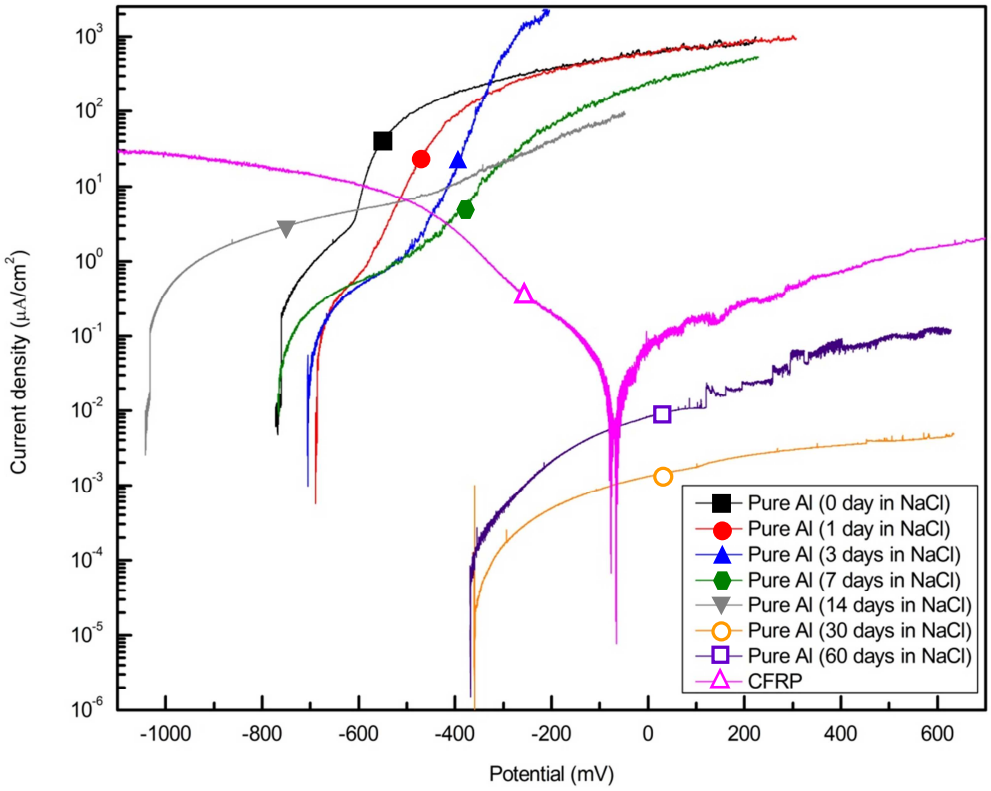

Figure 159: The Evans diagram for pure aluminium with CFRP for pure aluminium with different immersion time in 0.001M NaCl solution.

The anodic polarization curves of pure aluminium with different immersion times in 0.001M NaCl are superimposed with polarization curve of CFRP in the same solution (figure 159), in order to predict the corrosion behaviour and corrosion parameters in table 27(appendix) of Pure Al/CFRP joint after immersion in solution for different periods of time. It shows that:

a) During immersion time of 0-7 days, the predicted corrosion potential of Pure Al/CFRP joint is higher than pitting potential of pure aluminium therefore pure aluminium will exhibit pitting corrosion when coupled with CFRP in that time range
b) During immersion time of 30 - 60 days the predicted corrosion potential of Pure Al/CFRP joint is lower than pitting potential of pure aluminium therefore pure aluminium will exhibit passive behaviour when coupled with CFRP for time ranges larger than 30 days.

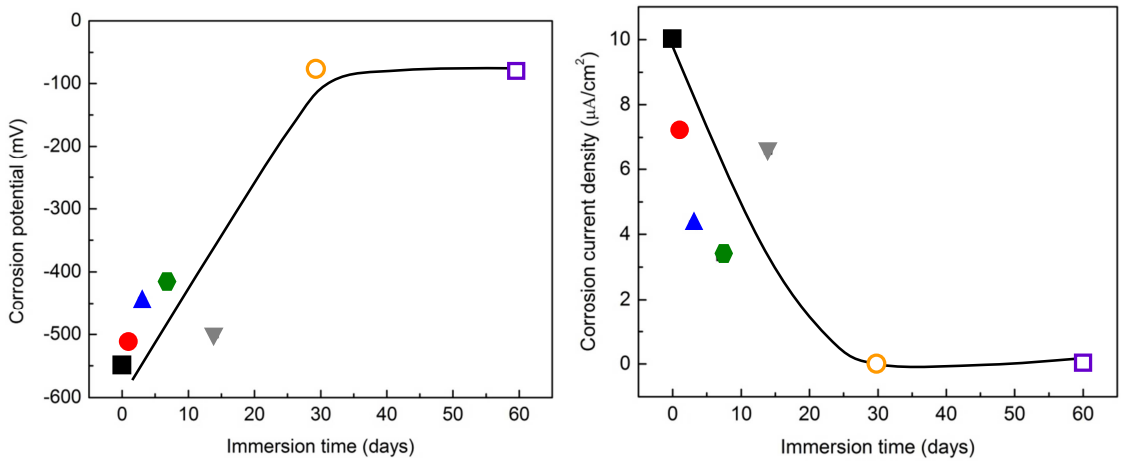

Figure 160: (Left) the predicted corrosion potential and (right) the predicted corrosion current density as a funtion of immersion time.

The predicted corrosion potential and corrosion current density of Pure Al/CFRP joint as a function of time in figure 160 shows that:

a) The predicted corrosion potential of Pure Al/CFRP (figure 160,left) increases with time until reaches a constant value at noble potentials at 30 days of immersion. This can be attributed to the development of passive film on the surface of pure aluminium. The passive oxide film is gradually developed with time until it is fully developed in thickness and area.

b) The predicted corrosion current density of Pure Al/CFRP (figure 160,right) decreases with time until it reaches an extremely low value. This indicates the decrease of corrosion rate with time because the gradual development of passive oxide film prevent pure aluminium from furthur corrosion.

It is also mentioned in [36] that during the first months in salt solution, pure aluminium will suffer dense pitting corrosion however after an initiation period of a few months, these pits will not deepen. Therefore it may be said that when pure aluminium was coupled with CFRP and then exposed in NaCl solution for 8 months, the galvanic corrosion can initially attack on the surface of pure aluminium at very high intensity. However, the accumulation of corrosion product, which is a uniformed aluminium hydroxide film, on the surface may slow down or even stop corrosion of pure aluminium. Unlike homogeneous structure of pure aluminium, the formed micro-galvanic corrosion cells between the intermetallic particles and the vicinal matrix may prevent the improvement of self-passivation (passive) behaviour on heterogonous structure of aluminium alloys. Therefore the galvanic corrosion can continuously take place.

The correlation between polarization and surface morphology analysis of Aluminium/CFRP joints shows, that corrosion rate of Pure Al/CFRP in 0.001M NaCl solution slows down with time due to the improvement of self-passivation behaviour of pure aluminium while the presence of intermetallic particles in aluminium alloys prevent the improvement of self-passivation behaviour to occur on aluminium alloys.

CHAPTER **VI**

CONCLUSION

1. Electrochemical noise(EN) can be a powerful technique to detect the corrosion of aluminium in solution:
   a. One working electrode set-up can be used to study the corrosion behaviour of metal in solution.

      It is found that pure aluminium is attacked by metastable pitting corrosion in tap water but by stable pitting corrosion in NaCl solutions. The amplitudes of potential and current fluctuations as well as their frequencies strongly depend on concentration of chloride ions, surface area ratio and immersion time in the solution. Moreover, amplitude of potential fluctuation is found to be directly proportional to the corrosion rate of aluminium alloys. The corrosion rate of aluminium alloys ranging from the highest to lowest are pure aluminium, AA2024, AA5052 and AA6061.
   b. In order to study corrosion of galvanic coupling system, the two working electrode set-up must be used:

      It is found that, when aluminium is coupled with graphite in deionised water, the potential of pure aluminium increases and pure aluminium still exhibit passive behaviour as in the uncoupled situation but with higher passive current density. In NaCl solution, corrosion behaviour of pure aluminium changes from formation and modification of spontaneous oxide film to serious pitting corrosion when coupled with graphite. Moreover, the rate of pitting corrosion of pure aluminium when coupled with graphite increases with increasing surface area ratio of graphite to pure aluminium.
2. OCP and Polarization measurements show, that the corrosion of aluminium depends on:
   a. Experimental set-up such as scanning rate and activation process by constant cathodic polarization: It is found that the observed pitting susceptibility slightly decreases with increasing scan rate from 10mV/h to 600mV/h. The active surface of pure aluminium can provide thicker and better passive oxide films with uniform thickness.

b. Environmental conditions such as type of solution, chloride ions concentration in solution, pH of solution and aeration system: Tap water solvent with additional NaCl exhibits lower pitting susceptibility than deionised solvent since tap water inherently contains pitting inhibitors. Pitting potential decreases with increasing chloride ions concentration in solution. Corrosion behaviour of pure aluminium change with pH of solution such as in neutral solution (pH7) pure aluminium exhibits passive behaviour due to the formation of stable passive film, in acidic solution (pH3) pure aluminium exhibits pitting corrosion at corrosion potential due to the formation of imperfect passive film and in basic solution (pH 12) pure aluminium exhibits uniform corrosion with high rate due to the formation of pseudo-passive film. Deaeration by nitrogen can provide better active surface of pure aluminium than in aerated solution by air since oxygen in air facilitates the formation of less homogeneous passive oxide film.

c. Surface preparation of aluminium such as surface roughness: The pitting susceptibility increases with increasing surface roughness. The active surface can only be achieved on pure aluminium surface prepared from smallest abrading grit size of 15μmm meaning smoothest surface.

d. Type of aluminium in use: Active surface of aluminium alloys cannot be achieved due to the presence of intermetallic particles on the surface of aluminium alloys. The corrosion rate of pure aluminium is higher than that of all other aluminium alloys. The alloy 2024 exhibits higher pitting susceptibility than pure aluminium while AA5052 and AA6061 exhibits lower pitting susceptibility than pure aluminium since the alloying metals have an effect on the structure of passive oxide film.

3. Evans diagrams by superimposing the polarization curves of aluminium with CFRP in the same solution can be used to predict the corrosion of Aluminium/CFRP joints. Since carbon in CFRP is nobler than aluminium, the aluminium will be polarized anodically and CFRP will be polarized cathodically when aluminium coupled with CFRP. Aluminium will become the anode of Aluminium/CFRP system and anodic corrosion occurs on aluminium. The potential of aluminium will shift to higher potentials, this result in the increase of its corrosion rate. Moreover, the corrosion behaviour of aluminium, which is valve metal, may change from passivation to pitting corrosion when coupled with CFRP in NaCl solution. The corrosion behaviour and corrosion rate of Aluminium/CFRP joints strongly depend on type of

aluminium in use, concentration of chloride ions in solution, pH of solution and surface area ratio of CFRP to aluminium.

a. The corrosion behaviour of pure aluminium changes from passivation to pitting corrosion when coupled with CFRP in 0.001M NaCl. Whereas aluminium alloys (AA2024, AA5052 and AA6061) when coupled with CFRP in 0.001M NaCl still exhibits passivation as in the uncoupled situation (surface area ratio=1).
b. The corrosion rate of Aluminium/CFRP joints in 0.001M NaCl ranging from highest to lowest are Pure Al/CFRP, AA2024/CFRP, AA5052/CFRP and AA6061/CFRP (surface area ratio=1).
c. The corrosion rate of Aluminium/CFRP joints increases with increasing chloride ion concentration in solution. In addition, it is also possible that the corrosion behaviour of Aluminium/CFRP joints will change from passivation to pitting corrosion with increasing concentration of chloride ions in solution.
d. Alkalisation of NaCl solution to weak basic solution (pH 11) can improve the corrosion resistance of Pure Al/CFRP, whereas the acidification of solution to strong acid solution (pH3) degrades the corrosion resistance of Pure Al/CFRP.
e. The corrosion rate of Pure Al/CFRP increases with increasing surface area ratio of CFRP to aluminium.

4. Surface morphology analysis of Aluminium/CFRP joints with long term immersion in 0.001M NaCl solution revealed that all Aluminium/CFRP joints suffers from galvanic corrosion between aluminium and CFRP.
   a. Unlike the prediction from Evans diagram that only pure aluminium is attacked by pitting corrosion when coupled with CFRP, the surface morphology analysis exhibits that aluminium alloys are also attacked by pitting corrosion when coupled with CFRP. This can be attributed to the formation of *alkaline pits* on the surface of aluminium alloys.
   b. Unlike the prediction from Evans diagram that corrosion rate of pure aluminium is higher than all other aluminium alloys when coupled with CFRP, the surface morphology analysis of Aluminium/CFRP joints exhibits, that when coupled with CFRP, aluminium alloys are more seriously damaged by pitting corrosion than pure aluminium when coupled with CFRP. This can be attributed to the improvement of self-passivation behaviour with time of pure aluminium.

Appendix

Measurement table

Table 1-4 are in the text

Sample	E_i* (mV)	E_f** (mV)	$E_f - E_i$ (mV)	Amplitude of potential fluctuations (mV)
Pure Al	-288	-370	-82	40.1
AA2024	-350	-242	+108	4.6
AA5052	-668	-742	-74	2.4
AA6061	-648	-763	-115	1.6

Table 5: The potential noise parameters of aluminium samples in 0.5M NaCl, *E_i is initial open circuit potential and **E_f is final open circuit potential

Solution	Scan rate	From measurement		From Tafel mechanism			
		E_{cor} (mV)	E_{pit} (mV)	E_{cor} (mV)	I_{cor} (pA)	b_c (mV/decade)	b_a (mV/decade)
Tap water	10mV/h	-1,118	-67	-1,144	0.27	-	-
	20mV/h	-1,064	-88	-1,081	0.37	-	-
0.005M NaCl	10mV/h	-1,479	-	-1,479	0.41	-121	385
	20mV/h	-1,494	-	-1,498	0.50	-169	850

Table 6: Corrosion parameters of pure aluminium wire

Scan rate	OCP	E_{cor} (mV)	E_{cor} - OCP (mV)	E_{pit} (mV)	E_{cor} (mV)
10mV/h	-889	-1,017	-128 *(more active)*	-380	637
600mV/h	-875	-841	+34*(nobler)*	-234	607
Difference	*14*	*176*		*146*	*30*

Table 7: Corrosion parameters of pure aluminium wire in 0.001M NaCl solution with different scan rate

Oxidation time	OCP in de-water (mV)	OCP in NaOH (mV)	E_{cor} (mV)	J_s* ($\mu A/cm^2$)
No	-540	-1,390	1,607	3,177
20h	NO	-1,520	-1,750	4,098
Difference		*130*	*143*	*921*

Table 8: Corrosion parameters of pure aluminium sheet in 0.01M NaOH solution with spontaneous oxidation in deionised water, *J_s is the stable current

Cathodic Polarization time (h)	OCP (mV)	E_{cor}-forward (mV)	E_{cor}-reverse (mV)	E_{pit} (mV)	J_{max} ($\mu A/cm^2$)
10	-1,310	-1,595	-1,740	No	1,016
50	-1,200	-1,540	-1,724	No	1,024
Difference	*110*	*55*	*16*		*8*

Table 9: Corrosion parameters of pure aluminium in 0.01M NaOH with different prior constant cathodic polarization time

Aeration	OCP (mV)	E_{cor} − forward (mV)	E_{cor} − reverse (mV)	E_{pit} (mV)	E_{pp} (mV)	J_{max} ($\mu A/cm^2$)
N_2	-1,573	-1,610	-1,724	No	-1,406	750
Air	-1,200	-1,540	-1,724	No	-1,382	1,024
Difference	*273*	*70*	*0*		*24*	*274*

Table 10: Corrosion parameters of pure aluminium in 0.01M NaOH with different aerations

$[Cl^-]$ (M)	OCP (mV)	E_{cor}-forward (mV)	E_{pit} (mV)	ΔE_p (mV)	Max. J ($\mu A/cm^2$)	E_{pp} (mV)
0	-1,724	-1,540	-	-	-	-1,408
0.005	-1,727	-1,730	-	-	-	-862
0.05	-1,731	-1,737	-275	1,462	2,056	-666
0.2	-1,690	-1,726	-460	1,266	10,448	-732
0.5	-1,490	-1,730	-547	1,183	limit	-644

Table 11: Corrosion parameters of pure aluminium sheet in deaerated basic solution (pH12) with different NaCl concentrations, * Max. J is the maximum current density after pitting starts

Additional NaCl (M)	OCP (mV)	E_{cor} (mV)	E_{pit} (mV)	ΔE_p (mV)
0	-695	-1,538	+546	2,084
0.00001	-726	-1,535	+530	2,065
0.0001	-1,068	-1,545	+442	1,987
0.001	-1,175	-1,550	-384	1,166
0.01	-982	-1,546	-620	926
0.05	-815	-1,551	-748	803
0.2	-850	-1,553	-744	809

Table 12: Corrosion parameters pure aluminium in tap water with different NaCl concentrations

Solution	bubbling	pH	$E_{cor} - forward$ (mV)	$E_{cor} - reverse$ (mV)	E_{pit} (mV)
pure deionised water	N_2	7	-1,571	-1,533	NO
Pure tap water	N_2	7	-1,538	-1,336	+546

Table 13: Corrosion parameters of pure aluminium in pure deionised and pure tap water

NaCl concentration	$E_{cor} - forward$ (mV)	$E_{cor} - reverse$ (mV)	ΔE_{cor} (mV)	E_{pit} (mV)	ΔE_p (mV)
NO	-1,571	-1,533	38	NO	-
0.000001M NaCl	-1,560	-1,515	45	+210	1,770
0.00001M NaCl	-1,565	-1,480	85	-230	1,335
0.0001M NaCl	-1,580	-1,496	84	-588	992
0.001M NaCl	-1,583	-1,375	208	-675	908

Table 14: Corrosion parameters of pure aluminium in deionised water with different NaCl concentrations

Solution	pH	OCP (mV)	$E_{cor} - forward$ (mV)	$E_{cor} - reverse$ (mV)	ΔE_{cor} (mV)	E_{pit} (mV)	ΔE_p (mV)
0.000001M HCl	6	-997	-1,572	-1,512	60	-13	1,559
0.00001M HCl	5	-1,060	-1,549	-1,530	19	-320	1,229
0.0001M HCl	4	-1,230	-1,452	-1,468	-16	-534	918
0.001M HCl	3	-790	-791	-927	-136	-791	0

Table 15: Corrosion parameters of pure aluminium solutions with different HCl concentrations

Solution	pH	$E_{cor} - forward$ (mV)	$E_{cor} - reverse$ (mV)	ΔE_{cor} (mV)	ΔE_p (mV)
Pure Deionised water	7	-1,571	-1,533	38	>3,500
De-water +0.00001M HNO_3	5	-1,502	-1,512	-10	>3,500
De-water +0.00001M HCl	5	-1,549	-1,530	19	-320

Table 16: Corrosion parameters of pure aluminium sheet in deaerated HNO_3

Electrolyte	pH	OCP (mV)	$E_{cor} - forward$ (mV)	$E_{cor} - reverse$ (mV)	ΔE_{cor} (mV)	E_{pit} (mV)	ΔE_p (mV)
0.001M NaCl	7	-940	-1,583	-1,375	208	-675	908
0.00001M HCl + 0.001M NaCl	5	-1,102	-1550	-1,404	146	-697	583
0.0001M HCl + 0.0009M NaCl	4	-1,061	-692*	-1,134	-442	-692*	0
0.001M HCl	3	-790	-791*	-927	-137	-791*	0

Table 17: Corrosion parameters of pure aluminium sheet in acidic solutions of 0.001M Chloride ions with different pH. * Pitting corrosion at corrosion potential where $E_{pit} = E_{cor} - forward$

Electrolytes	pH	OCP (mV)	$E_{cor} - forward$ (mV)	$E_{cor} - reverse$ (mV)	ΔE_{cor} (mV)	E_{pit} (mV)	ΔE_p (mV)
No NaOH + 0.001M NaCl	7	-792	-1,550	-1,367	183	-631	919
0.0001M NaOH + 0.001M NaCl	10	-1,110	-1,564	-1,340	224	-346	1,218
0.001M NaOH + 0.001M NaCl	11	-1,603	-1,643	-1,581	62	-415	1,228
0.01M NaOH + 0.001M NaCl	12	-1,554	-1,507	-1,644	-157	-	>1507

Table 18: Corrosion parameters of pure aluminium in basic NaCl solution with different pH

Size of abrading SiC particle (μm)	$E_{cor} - forward$ (mV)	$E_{cor} - reverse$ (mV)	E_{pit} (mV)	Evaluated E_{pit} (mV)
201	-1,590	-1,475	-725	-653
46	-1,593	-1,482	-724	-621
22	-1,592	-1,469	-668	-587
15	-1,585	-1,482	-623	-542

Table 19: Corrosion parameters of pure aluminium in deaerated 0.0001M NaCl with different surface finish.

Immersion time (days)	E_{cor} (mV)	Maximum J_p ($\mu A/cm^2$)	E_{pit} (mV)	ΔE_p (mV)	Max. J ($\mu A/cm^2$)
0	-773	3.5	-609	164	985
1	-690	1.5	-556	134	934
3	-705	1.1	-512	193	2,252
7	-769	0.6	-581	188	532
14	-1,045	7.7	-480	565	99
30	-362	0.0036	452	814	0.0048
60	-367	0.011	120	487	0.12

Table 20: The corrosion parameters of pure aluminium sheet after long term immersion in 0.001M NaCl

Immersion time in De-water	Immersion time in 0.01M NaCl	E_{cor} (mV)	Max. J_p ($\mu A/cm^2$)	E_{pit} (mV)	ΔE_p (mV)	Max. J ($\mu A/cm^2$)
No	No	-773	3.5	-609	164	985
	14 days	-1,045	7.7	-480	565	99
3 days	No	-612*	-	-612*	0	2,120
	14 days	-1,102	4.4	-397	705	107

Table 21: The corrosion parameters of pure aluminium sheet after long term immersion in 0.001M NaCl with prior water immersion for 3 days, * Pitting corrosion at corrosion potential when is detected where $E_{cor} = E_{pit}$

Aluminium sample	OCP (mV)	$E_{cor} - forward$ (mV)	$E_{cor} - reverse$ (mV)	ΔE_{cor} (mV)	J_p ($\mu A/cm^2$)
Pure Al	-885	-1,571	-1,533	38	8.8
AA2024	-38	-3	-1	2	1.4
AA5052	-470	-815	-428	387	0.08
AA6061	-688	-533	-830	-297	1.2

Table 22: Corrosion parameters of aluminium alloys in deionised water

Aluminium sample	Solution	OCP (mV)	E_{cor} (mV)	J_{cor} ($\mu A/cm^2$)	E_{pit} (mV)	ΔE_p (mV)
Pure Al	0.001M NaCl	-792	-1,550	2.4	-631	919
AA2024	0.001M NaCl	-432	-991	1.1	-148	284
	0.01M NaCl	-650	-540	1.4	-540*	-*
	0.1M NaCl	-578	-685	3.0	-685*	-*
AA5052	0.001M NaCl	-568	-873	0.03	+650	1,523
	0.01M NaCl	-84	-954	0.08	+248	1,202
	0.1M NaCl	-296	-950	0.09	-408	542
AA6061	0.001M NaCl	+19	-387	0.05	+938	1,325
	0.01M NaCl	-130	-1,023	0.09	+497	1,520
	0.1M NaCl	-708	-806	3.1	-806*	-*

Table 23: Corrosion parameters of aluminium samples in deaerated NaCl solution, * Pitting corrosion at corrosion potential is detected where $E_{pit} = E_{cor}$

Solution	System	Predicted E_{cor} (mV)	Predicted J_{cor} ($\mu A/cm^2$)	Relative Corrosion rate*
0.001M NaCl	Pure Al with CFRP	-550	8.5	4
	AA2024 with CFRP	-386	2.2	15.4
	AA5052 with CFRP	-148	0.11	309
	AA6061 with CFRP	-136	0.09	377
0.01M NaCl	AA2024 with CFRP	-474	23	1.4
	AA5052 with CFRP	-123	0.33	103
	AA6061 with CFRP	-127	0.35	97.1
0.1M NaCl	AA2024 with CFRP	-667	29	1.17
	AA5052 with CFRP	-290	3.6	9.44
	AA6061 with CFRP	-773	34	1.00

Table 24: The predicted corrosion parameters of aluminium alloys when coupled with CFRP in different NaCl solution, * Relative corrosion resistance is the relative of corrosion resistance to that of AA6061 in 0.1M NaCl which exhibits the maximum corrosion rate

Surface area proportion of CFRP to aluminium	Predicted E_{cor} (mV)	Predicted J_{cor} ($\mu A/cm^2$)
1:1	-550	34.2
5:1	-490	125
2:1	-524	60.2
1:7	-780	10.8

Table 25: The calculated corrosion parameters of pure aluminium when coupled with CFRP in chloride ions solution with different surface area ratio of CFRP to pure aluminium

Solution	pH	Only pure Al			Only CFRP	Al/CFRP system	
		E_{cor} (mV)	E_{pit} (mV)	J_{cor} ($\mu A/cm^2$)	E_{cor} (mV)	E_{cor} (mV)	J_{cor} ($\mu A/cm^2$)
0.001M HCl	3	-791*	-791*	50	-148	-781	19
0.001M NaCl	7	-1,550	-631	2.4	-67	-550	8.5
0.001M NaOH +0.001M NaCl	11	-1,439	-415	3.5	-176	-396	4.0

Table 26: The predicted corrosion parameter of pure aluminium when coupled with CFRP in chloride ions solution with different pH

Immersion time of pure aluminium in 0.001M NaCl solution (days)	**E_{cor} (mV)**	**J_{cor} ($\mu A/cm^2$)**
0	-550	10
1	-513	7.1
3	-446	4.3
7	-418	3.3
14	-500	6.6
30	-77	$9.7x10^{-4}$
60	-81	$5.5x10^{-3}$

Table 27: The predicted corrosion parameters of pure aluminium when coupled with CFRP in 0.001M NaCl for different period of immersion time of pure aluminium in solution

REFERENCE

[1] Lee, K.S., Im, K.H., & Yang, I.Y. (2010). Experimental evolution of crashworthiness for lightweight composite structural member. *Thin Solid Films*, 518 , 5637-5641.

[2] Asundi, A., & Choi, A.Y.N. (1997). Fiber Metal Laminates: An advanced material for future aircraft. *Journal of Materials Processing Technology, 63,* 384-394.

[3] Vogelesang, L.B., & Vlot, A. (2000). Development of fibre metal laminates for advanced aerospace structures. *Journal of Material Processing Technology, 103,* 1-5.

[4] Bambach M.R. (2010). Axial capacity and crushing behaviour of metal-fiber square tubes-steel, stainless steel and aluminium with CFRP. *Composites: Part B, 41*, 550-559.

[5] Mutasher, S.A., Sahari, B.B., Hamouda, A.M.S., & Sapuan, S.M. (2007). Experimental Study of Bending Fatigue Characteistics of a Hybrid Aluminium/Composite Drive Shaft. *Journal of Composite Materials, 41*, 2267-2287.

[6] Doyle, G., & Pethrick, R.A. (2009). Environmental effects on the ageing of epoxy adhesive joints. *International Journal of Adhesion & Adhesives, 29,* 77-90.

[7] Tucker, W.C., Brown, R., & Russell, L. (1990). Corrosion between a Graphite/Polymer Composite and Metals. *Journal of Composite Materials, 24,* 92-103.

[8] Schnerch, D., Stanford, K., Sumner, E., & Rizkalla, S. (2005). Bond behavior of CFRP strengthened steel bridges and structures. *Proceeding of International Symposium on band Behaviour of FRP in Structures*.

[9] Lampeas, N., & Koutsoukos, P.G. (1994). The importance of the solution pH in electrochemical studies of aluminium num in aqueous media containing chloride. *Corrosion Science, 36* (6), 1011-1025.

[10] Branzoi, F., Branzoi, V., Popa, M.V. & Golgovici, F. (2000). The influence of different aggressive anions on the electrochemical behaviour of aluminium in sodium nitrate aqueous solutions. *Material and Corrosion, 51,* 635-641.

[11] Gheem, E.V., Vereecken, J., & Pen, C.L. (2002). Influence of different anions on the behaviour of aluminium in aqueous solutions. *Journal of Applied Electrochemistry, 32,* 1193-1200.

[12] Halliday, S.T., Banks, W.M. & Tethrick, R.A., (1999). Influence of humidity on the durability of adhesively bonded aluminium composite structures. *Proc Instn Mech Engrs, 213,* 27-35.

[13] Zhang, T., Shao, Y., Meng, G., & Wang, F. (2007). Electrochemical noise analysis of corrosion of AZ91D magnesium alloy in alkaline chloride solution. *Electrochimica Acta, 53,* 561-568.

[14] Lafront, A.M., Zhang, W., Jin, S., Tremblay, R., Dube, D., & Ghali, E. (2005). Pitting corrosion of AZ91D and AJ62x magnesium alloys in alkaline chloride medium using electrochemical techniques. *Electrochimical Acta, 51,* 489-501.

[15] Breslin, C.B., & Rudd, A.L. (2000). Activation of pure Al in an indium-containing electrolyte-an electrochemical noise and impedance study. *Corrosion Science, 42,* 1023-1039.

[16] Sasaki, K., & Isaacs, H.S. (2004). Origins of electrochemical noise during pitting corrosion of aluminium. *Journal of the Electrochemical Society, 151,* 124-133.

[17] Sasaki, K., Levy, P.W., & Isaacs, H.S. (2002). Electrochemical noise during pitting corrosion of aluminium in chloride environments. *Electrochemical and Solid-state Letters, 5* (8), 25-27.

[18] Cheng, Y.L., Zhang, Z., Cao, F.H., Li, J.F., Zhang, J.Q., Wang, J.M., & Cao, C.N. (2003). Study of the potential electrochemical noise during corrosion process of aluminium alloys 2024, 7075 and pure aluminium. *Material and Corrosion, 54,* 601-608.

[19] Arrieta, I., Saques, A., & Joseph, B. (2004). Surface area dependence of electrochemical potential noise of aluminium alloys in chloride media. *Corrosion 2004.*

[20] Gouveia-Caridade, C., Pereira, M.I.S., & Brett, C.M.A. (2004). Electrochemical noise and impedance study of aluminium in weakly acid chloride solution. *Electrochimica Acta, 49,* 785-793.

[21] Klapper, H.S., Goellner, J., & Heyn, A. (2010). The influence of the cathodic process on the interpretation of electrochemical noise signal arising from pitting corrosion of stainless steel. *Corrosion Science, 52,* 1362-1372.

[22] Mazhar, A.A., Arab, S.T., & Noor, E.A. (2001). The role of chloride ions and pH in the corrosion and pitting of Al-Si alloys. *Journal of Applied Electrochemistry, 31,* 1131-1140.

[23] Zhang, J., Klasky, M., & Letellier, B.C. (2009). The aluminium chemistry and corrosion in alkaline solutions. *Journal of Nuclear Materials, 384,* 175-189.

[24] Emregul, K.C., & Aksut, A.A. (2000). The behaviour of aluminium in alkaline media. *Corrosion Science, 42,* 2051-2067.

[25] Vijh, A.K. (1968). Electrolytic hydrogen evolution reaction on aluminium, oxide-covered electrodes. *The journal of Physical Chemistry, 73* (3), 506-513.

[26] Moon, S.-M., & Pyun, S.-I. (1997). The corrosion of pure aluminium during cathodic polarization in aqueous solutions. *Corrosion Science, 39* (2), 339-408.

[27] Moon, S.-M., & Pyun, S.-I. (1998). Growth mechanism of anodic oxide films on pure aluminium in aqueous acidic and alkaline solutions. *J Solid State Electrochem, 2,* 156-161.

[28] Munoz, A.G., & Bessone, J.B. (1999). Pitting of aluminium in non-aqueous chloride media. *Corrosion Science, 41,* 1447-1463.

[29] Lin, C.F., & Hebert, K.R. (1994). Changes produced by cathodic polarization in the electrical conduction behaviour of surface films on aluminium. *J. Electrochem. Soc., 141* (1), 104-110.

[30] Aballe, A., Bethencourt, M., Botana, F.J., Cano, M.J., & Marcos, M. (2001). Localzed alkaline corrosion of alloy AA5083 in neutral 3.5% NaCl solution. *Corrosion Science, 43,* 1657-1674.

[31] Aballe, A., Bethencourt, M., Botana, F.J., Marcos, M., & Sanchez-Amaya, J.M. (2004). Influence of the degree of polishing of alloy AA5083 on its behaviour against localised alkaline corrosion. *Corrosion Science, 46,* 1909-1920.

[32] Lacroix, L., Blance, C., Pebere, N., Thompson, G.E., Tribollet, B., & Vivier, V. (2012). Simulating the galvanic coupling between S-Al_2CuMg phase particles and the matrix of 2024 aerospace aluminium alloy. *Corrosion Science, 64,* 213-221.

[33] Ahmed, Z., Ul-Hamid, A., &Abdul-Aleem, B.J. (2001). The corrosion behaviour of scandium alloyed Al 5052 in neutral sodium chloride solution. *Corrosion Science, 43,* 1227-1243.

[34] Su, T.L., Wang, S.S., Tsao, L.C., Chang. S.Y., Chuang, T.H. & Yeh, M.S. (2002). Corrosion behaviours of Al-Si-Cu-based filler metals and 6061-T6 Brazements. *Journal of Materials Engineering and Performance, 11* (2), 187-193.

[35] Tavakkolizadeh, M., & Saadatmanesh, H. (2001). Galvanic corrosion of carbon and steel in aggressive environments. *Journal of composites for construction, 5* (3), 200-210.

[36] Vargel, C. (2004). *Corrosion of Aluminium*. Paris: Elsevier.
[37] Kaesche, H. (2003). *Corrosion of metals: physicochemical principles and current problems.* Berlin: Springer.
[38] Bard, A.J., Stratmann, M., & Frankel, G.S. (2003). *Encyclopedia of Electrochemistry, Volume 4, Corrosion and Oxide Films.* Michigan: Wiley.
[39] Ren, J., & Zuo, Y. (2005). The growth mechanism of pits in NaCl solution under anodic films on aluminium. *Surface & Coating Technology, 191,* 311-316.
[40] Sukiman, N.L., Zhou, X., Birbilis, N., & Hughes, A.E. (2012). Durability and Corrosion of Aluminium and Its Alloys: Overview, Property Space, Techniques and Developments, Aluminium Alloys - New Trends in Fabrication and Applications. Available from: http://www.intechopen.com/books/aluminium-alloys-new-trends-in-fabrication-and-applications/durability-and-corrosion-of-aluminium-and-its-alloys-overview-property-space-techniques-and-developm.
[41] Corrosion control-Galvanic tables. Retrieved 14:30, November 14, 2014, http://l-36.com/corrosion.php.
[42] Enos, D.G., & Scribner, L. (1997). *The potentiodynamic polarization scan: Technical report 33*.
[43] Cottis, R.A. (2006). Sources of electrochemical noise in corroding systems. *Russian Journal of Electrochemistry, 42* (5), 497-505.
[44] Speckert, L., & Burstein, G.T. (2011). Combined anodic/cathodic transient currents within nucleating pits on Al-Fe alloy surfaces. *Corrosion Science, 53,* 534-539.
[45] Meng, G., Wei, L., Zhang, T., Shao, Y., Wang, F., Dong, C., & Li, X. (2009). Effect of microcrystallization on pitting corrosion of pure aluminium. *Corrosion Science, 51,* 2151-2157.
[46] Larson, T.E. (1975). Corrosion by domestic waters. Illinois state water survey, Urbana, Bulletin 59.
[47] Metikos-Hukovic, M., Babic, R., Grubac, Z., & Brinic, S. (1994). Inhibition of the hydrogen evolution reaction on aluminium covered by "spontaneous" oxide. Journal *of applied electrochemistry, 24,* 325-331.
[48] Abd El-Wahab, E.A., Marei, A.H., Khalifa, O.R., & Mohamed, H.A. (2010). Corrosion behaviour of aluminium electrode in absence and in presence of sodium chloride at differet pH solutions using Toludine as inhibitor. *Journal of American Science, 6* (8), 476-486.
[49] Kear, G., & Walsh, F.C. (2005). The characteristics of a true Tafel slope. *Corrosion and Material, 30* (6), 1-4.
[50] Marcus, P., & Maurice, V. (2013). Passivity of metals alloys. Material science technology. Paris: Weiley.
[51] Gimenez, Ph., Rameau, J.J., & Reboul, M.C. (1981).Experimental pH potential diagram of aluminium for sea water. *National Association of Corrosion Engineers, 37* (12), 673-682.
[52] Zaid, B., Saidi, D., Benzaid, A., & Hadji, S. Effects of pH and chloride concentration on pitting corrosion of AA6061. *Corrosion Science, 50,* 1841-1847.
[53] Augsburger trinkwasser-analysewerte. Retrieved 13:00, May 20, 2013, http://www.sw-augsburg.de/downloads/Wasseranalyse_Internetversion.pdf
[54] Hu, J., Tian, K., & Chu, W.Y. (2005). Electrochemical corrosion behaviour of $Al_{18}B_4O_{33}$w/Al composite. *Journal of materials science, 40,* 5147-5151.
[55] Phosphatdosierung-muss das sein?. Retrieved April 17, 2014, https://www.sw-augsburg.de/downloads/Phosphatdosierung.pdf

[56] Sarver, E., & Edwards, M. (2012). Inhibition of copper pitting corrosion in aggressive potable waters. *International journal of corrosion*, 1-16.

[57] Branzoi, V., Golgovici, F., & Branzoi, F. (2002). Aluminum corrosion in hydrochloric acid solutions and the effect of some organic inhibitors. *Materials chemistry and physics, 78*, 122-131.

[58] Pyun, S.-I., & Moon, S.-M. (1999). The inhibition mechanism of pitting corrosion of pure aluminium by nitrate and sulphate ions in neutral chloride solution. Journal of solid state electrochemistry, 3 (6), 331-336.

[59] Ezuber, H., El-Houd, A., & El-Shawesh, F. (2008). A study on the corrosion behaviour of aluminium alloys in seawater. Materials and Design, 29, 801-805.

[60] Electrolysis of water, (2014, September 25), In Wikipedia The Free Encyclopedia. http://en.wikipedia.org/wiki/Electrolysis_of_water

[61] Bellucci, F. (1992). Galvanic corrosion between non-metallic composites and metals II: Effect of area ratio and environmental degradation*. Corrosion, 48* (4), 281-291.

ACKNOWLEDGEMENT

First of all I would like to thank Prof. Dr. Siegfried Horn for giving me a wonderful opportunity to do my dissertation in his group. He also gives me some valuable information and advice.

Secondly, I would like to thank Prof. Dr. Armin Reller for reviewing my dissertation.

I also would like to express my special thank to my advisor Dr. Matthias Klemm. I couldn't have done it without him. His enduring patience and infinite understanding helps me come through all the problems I met. I also want to thank him for patiently revising my dissertation.

Special thanks also go to all people in the EPII group for all their helps and good friendship through the duration of my studies.

I further want to thank Yelena Axyonova for her supporting result.

Furthermore, I want to thank my Thai government of scholarship that supports me for studying in Germany.

I also want to thank my beloved family for all their love toward me.

The last but not the least, I want to mention my husband Yu Zhang, give him very special thanks for the love and support he gave me and, above all, for enduring me when I was in a bad temper.

Curriculum Vitae

Personal information

Name	:	Oruethai Jaiboon
Date of birth	:	01 October 1983
Nationality	:	Thai
Gender	:	Female
Martial status	:	Married

Education

2002 – 2006 Bachelor's degree in Physics Khon Kaen University, Khon Kaen, Thailand.

Title: Effect of electric field on wave functions and energy states of a single electron in quantum well.

2008 – 2010 Master's degree in Advanced Materials Science, University of Augsburg Technical University of Munich and Ludwig Maximillian University of Munich, Germany.

Title: Analysis of carbon fibre-epoxy matrix interphase using phase-imaging mode of AFM.

2010 – Present Start of Ph.D. in Physics, University of Augsburg, Augsburg, Germany.

Title: Characterization of Aluminium and its Alloys by means of analysis of passive, pitting and galvanic behaviour in contact with CFRP by electrochemical noise and polarization methods.